QUANTUM LIQUIDS AND QUANTUM CRYSTALS

Some questions in the theory of a superfluid Fermi liquid with triplet pairing in a magnetic field

A. N. Tarasov*

Institute of Theoretical Physics, Kharkov Physicotechnical Institute National Science Center, ul. Akademicheskaya 1, 61108 Kharkov, Ukraine

(Submitted March 16, 2000; revised May 11, 2000)
Fiz. Nizk. Temp. **26**, 1059–1066 (November 2000)

General expressions are obtained in explicit form for the anomalous and normal distribution functions of quasiparticles in nonunitary phases of a superfluid paramagnetic Fermi liquid consisting of electrically neutral fermions with triplet pairing (the pairs have spin $s=1$ and an arbitrary odd value of the orbital angular momentum l) in a uniform static magnetic field. A generalized Fermi-liquid approach is used which takes into account the exchange Fermi-liquid interaction but does not specify the form of the energy functional of the superfluid Fermi liquid. The results are valid at any temperature in the interval $0 \leqslant T \leqslant T_c$, where T_c is the temperature of the phase transition from the normal to the superfluid state. When an explicit form of the energy functional is specified, the general formulas for the distribution function can be used to describe the various nonunitary phases of a superfluid Fermi liquid of the ^{3}He type in a high magnetic field. In particular, for ^{3}He-A_1, ^{3}He-A_2, and the nonunitary two-dimensional phase of ^{3}He in a high magnetic field at $0 \leqslant T \leqslant T_c$, an energy functional quadratic in the distribution function is used to find a system of coupled equations for the order parameter and the effective magnetic field and to obtain an expression is obtained for the nonlinear magnetic susceptibility. © *2000 American Institute of Physics.* [S1063-777X(00)00111-0]

1. INTRODUCTION

This paper is a continuation and generalization of our previous paper[1] and is devoted to a theoretical study of a superfluid Fermi liquid (SFL) with triplet pairing (the pairs have spin $s=1$ and arbitrary odd orbital angular momentum l) in a uniform static magnetic field at temperatures $0 \leqslant T \leqslant T_c$ (T_c is the temperature of the phase transition from the normal to the superfluid state in zero magnetic field). We assume (as in Ref. 1) that the SFL consists of electrically neutral fermions possessing a magnetic moment. Examples of such a SFL are the superfluid phases of ^{3}He and the superfluid state of the neutron liquid inside a neutron star. In Ref. 1 these SFLs are described in a Landau Fermi-liquid approach, which was generalized to superfluid systems in Refs. 2–4 (see also the references cited therein).

Let us briefly recall that in Ref. 1, in a generalized approach taking into account the effects of an external magnetic field **H** and the exchange Fermi-liquid interaction in the SFL, the energy of the SFL was introduced in the form of a functional $E(f,g,g^+;H)$, which is a functional not only of the normal matrix distribution function $f_{12} \equiv \mathrm{Tr}\,\rho a_2^+ a_1$ but also of the anomalous matrix distribution functions $g_{12} \equiv \mathrm{Tr}\,\rho a_2 a_1$ and $g_{12}^+ \equiv \mathrm{Tr}\,\rho a_2^+ a_1^+$ of the quasiparticles of the SFL in a magnetic field **H** (ρ is the density matrix, a_1^+ and a_1 are the creation and annihilation operators for Fermi quasiparticles in the states $1 \equiv \mathbf{p}_1, s_1$, where $\mathbf{p}_1$ is the momentum and s_1 is the spin projection on the quantization axis). As in Ref. 1, we assume that the energy functional (EF) is invariant with respect to phase transformations. In addition, we shall assume that the interaction energy functional of the SFL is invariant with respect to rotations in both coordinate (orbital) and spin space. Strictly speaking, the relativistic (spin–orbit) interactions should therefore be excluded from consideration, since they break this rotational invariance of the energy functional. However, if one specializes to the superfluid phases of ^{3}He, this relativistic interaction is a weak magnetic-dipole interaction between the nuclei of the ^{3}He atoms, which have a magnetic dipole moment μ_n. Although this interaction does play an important role[5–8] in ^{3}He, it is six orders smaller than the main Fermi-liquid interaction and can therefore be taken into account using perturbation theory (see, e.g., Ch. 6 of Ref. 8), assuming that the Cooper pairs are characterized, as before, by a definite spin $s=1$ and an orbital angular momentum l (which here can take on any odd value, in accordance with the Pauli exclusion principle). If one is considering the case of high magnetic field ($H \gg 30$ G for ^{3}He),[7,8] then the weak magnetic dipole interaction can be neglected. Thus, although the explicit form of the EF for the SFL will not be used in Sec. 2, the aforementioned invariance properties of the EF are assumed.

A study of the effects of superfluidity of a system of nucleons with triplet p pairing in heavy nuclei, where it is necessary to take the strong spin–orbit interaction into account, has been done by another method in Ref. 9 (see also Ref. 10, a review of superfluidity in neutron stars, in which triplet pairing of the nucleons can also occur in a certain interval of densities of the star; see the references cited in Refs. 9 and 10).

We also note that heavy-fermion superconductors (see, e.g., Ref. 11 and the reviews in Refs. 12–14), in which triplet Cooper pairing is apparently realized, bear some similarity to the superfluid phases of ^{3}He, although there are also substantial differences, chief among which are the presence of the crystal lattice, a rather strong spin–orbit interaction, and an electric change on the fermions. Because of these differences, the results of the present study must not be directly applied to the consideration of superfluid systems with heavy fermions.

In Ref. 1 we developed a method for finding expressions for the distribution functions (DFs) of quasiparticles of a SFL with triplet pairing in a magnetic field and established the general structure of these expressions (but not their explicit form in the general case); see Eqs. (I.31) and (I.32) [by which we denote Eqs. (31) and (32) of Ref. 1]. The explicit form of these DFs was written out in Ref. 1 only for a few particular cases (but for arbitrary odd values of l), viz., for the unitary phases of SFLs with a real order parameter $\Delta_\alpha(\mathbf{p})=\Delta^*_\alpha(\mathbf{p})$, such as ^{3}He-$B$ and the two-dimensional (2D) phase of ^{3}He [see Eqs. (I.37) and (I.40)], and also for nonunitary phases of the type ^{3}He$-A_2$, ^{3}He-A_1, and the nonunitary 2D phase of ^{3}He (see Eqs. (I.46)–(I.48). These nonunitary phases of ^{3}He in a magnetic field have been considered only in the case of p pairing, e.g., in Refs. 15 and 16, and, furthermore,in Ref. 15 the Fermi-liquid interactions were not taken into account, while in Ref. 16 the exchange Fermi-liquid interaction was taken into account on the basis of formulas (I.46)–(I.48) (this case is also considered in Sec. 3 as an illustration of the use of the general theory).

The main goal of this paper is to obtain an explicit form for the normal and anomalous DFs of quasiparticles in arbitrary nonunitary and unitary phases of a SFL with triplet pairing in a rather high magnetic field of arbitrary orientation at temperatures $0\leqslant T\leqslant T_c$. For this we shall use for the DFs the general formulas (I.31) and (I.32) obtained in Ref. 1.

2. GENERALIZED FORMULAS FOR THE DISTRIBUTION FUNCTIONS OF QUASIPARTICLES OF A SUPERFLUID FERMI LIQUID WITH TRIPLET PAIRING IN A MAGNETIC FIELD

Let us write the definitions needed for understanding the final results, and let us make some refinements to some of the formulas from Ref. 1. As in Ref. 1, we introduce in place of the matrices f_{12} and g_{12} the corresponding normal DFs $f_0(\mathbf{p})$ and $f_\alpha(\mathbf{p})$ and anomalous DFs $g_0(\mathbf{p})$ and $g_\alpha(\mathbf{p})$ for the quasiparticles of a SFL in the spatially uniform case:

$$f_{12}=f_{s_1s_2}(\mathbf{p}_1)\,\delta_{\mathbf{p}_1\mathbf{p}_2}$$
$$=[f_0(\mathbf{p}_1)\,\delta_{s_1s_2}+f_\alpha(\mathbf{p}_1)(\sigma_\alpha)_{s_1s_2}]\,\delta_{\mathbf{p}_1\mathbf{p}_2}, \quad (1)$$

$$g_{12}=g_{s_1s_2}(\mathbf{p}_1)\,\delta_{\mathbf{p}_1,-\mathbf{p}_2}=[g_0(\mathbf{p}_1)(\sigma_2)_{s_1s_2}$$
$$+g_\alpha(\mathbf{p}_1)i(\sigma_\alpha\sigma_2)_{s_1s_2}]\,\delta_{\mathbf{p}_1,-\mathbf{p}_2} \quad (2)$$

(σ_α are the Pauli matrices; $\alpha=1,2,3$), where, since $g_{12}=-g_{21}$ for fermions, we have $g_0(\mathbf{p})=g_0(-\mathbf{p})$ and $g_\alpha(\mathbf{p})=-g_\alpha(-\mathbf{p})$. We assume that in the thermodynamic equilibrium state the superfluid component of the SFL is at rest, i.e., its velocity $v_s=0$ (see Refs. 2–4 for a more detailed discussion of the condition of spatial uniformity in a SFL).

According to formulas (I.12)–(I.14), we have

$$\xi_{12}(f;H)=\varepsilon_{12}(f;H)-(\mathbf{v}_n\mathbf{p}_1+\mu)\,\delta_{12},$$

where

$$\varepsilon_{12}(f;H)=\frac{\partial E(f,g,g^+;H)}{\partial f_{21}}=\varepsilon_{\mathbf{p}_1\mathbf{p}_2}(f)\,\delta_{s_1s_2}$$
$$+(\xi_\beta(f;H))_{\mathbf{p}_1\mathbf{p}_2}(\sigma_\beta)_{s_1s_2}.$$

In the spatially uniform case it follows from this, in accordance with (1), that

$$\xi_{12}=\xi_{s_1s_2}(\mathbf{p}_1)\,\delta_{\mathbf{p}_1\mathbf{p}_2}=[\xi_0(\mathbf{p}_1)\,\delta_{s_1s_2}+\xi_\beta(\mathbf{p}_1)(\sigma_\beta)_{s_1s_2}]\,\delta_{\mathbf{p}_1\mathbf{p}_2},$$

where

$$\xi_0(\mathbf{p})=\varepsilon(\mathbf{p})-(\mathbf{v}_n\mathbf{p}+\mu), \quad (3)$$

$$\xi_\beta(\mathbf{p})=\varepsilon_\beta(\mathbf{p})-\mu_nH_\beta\equiv-\mu_n(H_{\text{eff}}(\mathbf{p}))_\beta$$

(as in Eq. (I.17) we assume that $\xi_\beta(\mathbf{p})=\xi_\beta(-\mathbf{p})$). Here $\mathbf{v}_n$ is the velocity of the normal component of the SFL, μ is the chemical potential, μ_n is the magnetic moment of the fermion, $\varepsilon(\mathbf{p})=\varepsilon(p)$ is the kinetic energy of a quasiparticle, including the nonexchange normal Fermi-liquid interaction amplitudes, $\varepsilon_\beta(\mathbf{p})$ are functions that take into account the Landau normal exchange interaction amplitudes, and $\mathbf{H}_{\text{eff}}(\mathbf{p})$ is the effective magnetic field inside the SFL (in Ref. 17 the functions $\xi_\beta(\mathbf{p})$ were not taken into account).

We assume that within the SFL there is an interaction that leads to triplet pairing of the fermions (but no interaction leading to singlet pairing). Therefore, the matrix Δ_{12}, which is the order parameter for the SFL, can be written in the spatially uniform case as

$$\Delta_{12}=2\,\frac{\partial E(f,g,g^+;H)}{\partial g^+_{21}}=i\Delta_\alpha(\mathbf{p}_1)(\sigma_\alpha\sigma_2)_{s_1s_2}\delta_{\mathbf{p}_1,-\mathbf{p}_2},$$

$$\Delta_\alpha(-\mathbf{p})=-\Delta_\alpha(\mathbf{p}) \quad (4)$$

(the function $\Delta_\alpha(\mathbf{p})$ depends on the particular choice of energy functional $E(f,g,g^+;H)$).

Let us now generalize formula (I.25) for the matrix n_{12}. Formulas (I.25) and (I.27) are valid for unitary and nonunitary phases of SFLs of the ^{3}He type in a magnetic field in the limit when $|\xi\cdot\mathbf{\Delta}|$ is small.

In particular, for a unitary phase of a SFL of the ^{3}He-B type, for which $\Delta_\alpha(\mathbf{p})=\Delta^*_\alpha(\mathbf{p})$, the system of equations (I.34), (I.36) for the functions $\Delta_\alpha(\mathbf{p})$ and $\xi_\alpha(\mathbf{p})$, with allowance for formulas (I.37) and (I.40) for the quasiparticle DF in the linear approximation in the small quantity $|\xi\cdot\mathbf{\Delta}|$ agrees with the corresponding system of equations from Ref. 18, where only the p pairing in ^{3}He-B was taken into account and it was assumed that $v_n=0$ and $v_s=0$.

For nonunitary phases the quantity $|\xi\cdot\mathbf{\Delta}|=0$ in the particular case that $\xi_\alpha=\xi l_\alpha$ (for any values of ξ), where $\mathbf{l}(\mathbf{p})$ is a real unit vector of the form [see (I.22)]

$$\mathbf{l}(\mathbf{p})\equiv\frac{i}{\eta(\mathbf{p})}[\Delta(\mathbf{p})\times\Delta^*(\mathbf{p})],$$

(the quantity $\eta(\mathbf{p})\equiv|\mathbf{\Delta}(\mathbf{p})\times\mathbf{\Delta}^*(\mathbf{p})|$ is nonzero for nonunitary states of a SFL with triplet pairing). In this case formulas (I.46)–(I.48) are valid for the DFs, which, together with

equations (I.34)–(I.36), allow us to describe the nonunitary phases of the type ^{3}He-A_2 and ^{3}He-A_1 and the nonunitary 2D phase of ^{3}He (see Ref. 16).

In the general case, for arbitrarily high magnetic fields (but within the limits of applicability of the Fermi-liquid theory, i.e., for $|\mu_n|H \ll \mu$), when no restrictions are placed on the value of $|\xi\cdot\mathbf{\Delta}|$, the expression for the matrix n_{12} [see the original definition (I.10)] under conditions of spatial uniformity has the same structure as in (I.25), i.e.,

$$n_{12}=\delta_{\mathbf{p}_1\mathbf{p}_2}[N^0_{\mathbf{p}_1}\delta_{s_1s_2}+N^{\parallel}_{\mathbf{p}_1}\hat{h}_\nu(\mathbf{p}_1)(\sigma_\nu)_{s_1s_2}], \tag{5}$$

where

$$N^0_{\mathbf{p}}\equiv\frac{1}{2}[N^{(+)}_{\mathbf{p}}+N^{(-)}_{\mathbf{p}}], \quad N^{\parallel}_{\mathbf{p}}\equiv\frac{1}{2}[N^{(+)}_{\mathbf{p}}-N^{(-)}_{\mathbf{p}}]. \tag{6}$$

However, there is a difference in the definition of the functions $N_p^{(\pm)}$ and $\hat{h}_\alpha(\mathbf{p})$, which now in the general case take the forms

$$N^{(\pm)}_{\mathbf{p}}(\Sigma)\equiv\left\{\exp\left[\frac{1}{T}\left(\frac{\xi_0(\mathbf{p})-\xi_0(-\mathbf{p})}{2}+\Sigma(\mathbf{p})\pm\underline{\Sigma}(\mathbf{p})\right)\right]+1\right\}^{-1}, \tag{7}$$

$$\hat{h}_\alpha(\mathbf{p})\equiv\frac{h_\alpha(\mathbf{p})}{\underline{\Sigma}(\mathbf{p})}, \quad (\hat{\mathbf{h}}^2\equiv 1), \tag{8}$$

where $h_\alpha(\mathbf{p})$ as before has the definition (I.28) in terms of the functions defined in Ref. 1. That is, formulas (7) and (8) contain $\Sigma(\mathbf{p})\equiv\Sigma_{2,1}(\mathbf{p})$ in place of $|\mathbf{h}_{1,2}(\mathbf{p})|$. Formula (7) also contains the functions $\underline{\Sigma}(\mathbf{p})\equiv\underline{\Sigma}_{1,2}(\mathbf{p})$, which have the form [see (I.23)]:

$$\underline{\Sigma}_{1,2}(\mathbf{p})=\frac{1}{2}[E_+(\mathbf{p})\pm E_-(\mathbf{p})]. \tag{9}$$

Here the functions $E_\pm(\mathbf{p})$, which are the energies of the quasiparticles in the SFL (with spin projections parallel and antiparallel to the magnetic field), in the general case retain their previous form (I.24), i.e.,

$$E^2_\pm(\mathbf{p})\equiv\alpha(\mathbf{p})\pm\sqrt{\beta^2(\mathbf{p})+\gamma^2(\mathbf{p})}, \tag{10}$$

where

$$\begin{aligned}&\alpha(\mathbf{p})\equiv|\Delta(\mathbf{p})|^2+z^2(\mathbf{p})+\xi^2(\mathbf{p}),\\ &\beta_\alpha(\mathbf{p})\equiv\eta(\mathbf{p})l_\alpha(\mathbf{p})+2z(\mathbf{p})\xi_\alpha(\mathbf{p}),\\ &\gamma(\mathbf{p})\equiv 2|\xi(\mathbf{p})\cdot\Delta(\mathbf{p})|,\end{aligned} \tag{11}$$

and $z(\mathbf{p})\equiv[\xi_0(\mathbf{p})+\xi_0(-\mathbf{p})]/2\equiv\varepsilon(p)-\mu$.

We emphasize that for magnetic fields of arbitrary value ($|\mu_n|H\ll\mu$) and direction, the general form of formulas (I.31) and (I.32) for the DFs of the quasiparticles in a SFL remains unchanged, but one must use for the functions $\hat{h}_\alpha(\mathbf{p})$ the generalized expression (8) obtained above.

After making these observations, let us write out the general explicit expressions we have obtained for the quasiparticle DF of a SFL in a magnetic field $\mathbf{H}$ which is spatially uniform and constant in time. For $\eta\neq 0$, $v_n\neq 0$ (but with $v_s=0$) and $(\xi\cdot\mathbf{\Delta})\neq 0$, $(\xi\cdot\mathbf{l})\neq 0$, $(\xi\cdot[\mathbf{l}\times\mathbf{\Delta}])\neq 0$, we obtain from (I.31) the following expression for the anomalous DF at $0\leqslant T\leqslant T_c$:

$$\begin{aligned}g_\alpha(\mathbf{p})=\frac{1}{2R}\Bigg\{\Bigg[(1-N^0_{\mathbf{p}}-N^0_{-\mathbf{p}})\frac{1}{\Sigma}+(N^{\parallel}_{\mathbf{p}}+N^{\parallel}_{-\mathbf{p}})\frac{1}{\underline{\Sigma}}\Bigg]\\ \times\left(\frac{i}{2}[\beta\times\Delta]_\alpha+\xi_\alpha(\xi\cdot\Delta)\right)-\Delta_\alpha[(1-N^0_{\mathbf{p}}-N^0_{-\mathbf{p}})\\ \times\Sigma+(N^{\parallel}_{\mathbf{p}}+N^{\parallel}_{-\mathbf{p}})\underline{\Sigma}]\Bigg\},\end{aligned} \tag{12}$$

$$g_0(\mathbf{p})=(N^{\parallel}_{\mathbf{p}}-N^{\parallel}_{-\mathbf{p}})\frac{i(\xi\cdot\Delta)}{2\Sigma_1\Sigma_2}. \tag{13}$$

For the normal DFs $f_0(\mathbf{p})$ and $f_\alpha(\mathbf{p})$ it follows from (I.32) that

$$\begin{aligned}f_0(\mathbf{p})=\frac{1}{2}(1+N^0_{\mathbf{p}}-N^0_{-\mathbf{p}})+\frac{1}{2R}\Bigg\{\Bigg[(1-N^0_{\mathbf{p}}-N^0_{-\mathbf{p}})\frac{1}{\Sigma}\\ +(N^{\parallel}_{\mathbf{p}}+N^{\parallel}_{-\mathbf{p}})\frac{1}{\underline{\Sigma}}\Bigg]\frac{1}{2}(\beta\cdot\xi)-z[(1-N^0_{\mathbf{p}}-N^0_{-\mathbf{p}})\\ \times\Sigma+(N^{\parallel}_{\mathbf{p}}+N^{\parallel}_{-\mathbf{p}})\underline{\Sigma}]\Bigg\},\end{aligned} \tag{14}$$

$$\begin{aligned}f_\alpha(\mathbf{p})=\frac{1}{2R}\Bigg\{\Bigg[(1-M^0_{\mathbf{p}}-N^0_{-\mathbf{p}})\frac{1}{\Sigma}+(N^{\parallel}_{\mathbf{p}}+N^{\parallel}_{-\mathbf{p}})\frac{1}{\underline{\Sigma}}\Bigg]\\ \times\left(z\frac{\beta_\alpha}{2}+\mathrm{Re}\,\Delta_\alpha(\xi\cdot\Delta^*)\right)-\xi_\alpha[(1-N^0_{\mathbf{p}}-N^0_{-\mathbf{p}})\\ \times\Sigma+(N^{\parallel}_{\mathbf{p}}+N^{\parallel}_{-\mathbf{p}})\underline{\Sigma}]\Bigg\}+(N^{\parallel}_{\mathbf{p}}-N^{\parallel}_{-\mathbf{p}})\frac{\beta_\alpha}{4\Sigma_1\Sigma_2}.\end{aligned} \tag{15}$$

Expressions (12)–(15) contain functions $N^0_{\pm\mathbf{p}}(\Sigma_{1,2})$ and $N^{\parallel}_{\pm\mathbf{p}}(\Sigma_{1,2})$ of the form (6), (7), and the argument $\mathbf{p}$ has been dropped from the remaining functions for the sake of brevity. We have also introduced the functions $R\equiv R_{1,2}(\mathbf{p})$:

$$R_{1,2}(\mathbf{p})=\pm E_+(\mathbf{p})E_-(\mathbf{p})=\pm\sqrt{\alpha^2(\mathbf{p})-\beta^2(\mathbf{p})-\gamma^2(\mathbf{p})}, \tag{16}$$

from which the subscripts 1,2 (as in the case of the functions $\Sigma(\mathbf{p})\equiv\Sigma_{1,2}(\mathbf{p})$ and $\underline{\Sigma}(\mathbf{p})\equiv\underline{\Sigma}_{2,1}(\mathbf{p})$) have been dropped in formulas (12)–(15).

In deriving Eqs. (12)–(15) from (I.31) and (I.32) we have used the following relations [see Eqs. (9)–(11)]:

$$\underline{\Sigma}^2=\Sigma^2-R, \quad \Sigma_1^2+\Sigma_2^2=\alpha, \quad (\Sigma_1\Sigma_2)^2=\frac{\beta^2+\gamma^2}{4}. \tag{17}$$

We also note that expressions (12)–(15) are symmetric with respect to interchange of the indices $1\leftrightarrow 2$.

When definitions (11) are taken into account, formulas (12)–(15) imply formulas (I.37) and (I.40) for the quasiparticle DF [with allowance for the refinement made below Eq. (8)]. These results from Ref. 1 are valid in the particular case of unitary phases of SFLs of the type ^{3}He-B and the 2D phase of ^{3}He, for which $\Delta_\alpha=\Delta^*_\alpha$ (with l an arbitrary odd integer). In addition, Eqs. (12)–(15) also immediately imply expressions for the quasiparticle DF of a unitary phase of the type ^{3}He-A, for which, if only the p pairing is taken into account, $\Delta_\alpha(\mathbf{p})$ has the form (see Ref. 8):

$$\Delta_\alpha^{(A)}(\mathbf{p})=\Delta_0\hat{d}_\alpha\Psi(\hat{\mathbf{p}}),\quad \hat{\mathbf{d}}=\hat{\mathbf{d}}^*,\quad \hat{\mathbf{d}}^2=1,\quad \hat{\mathbf{p}}\equiv\frac{\mathbf{p}}{p},$$

where

$$\Delta_0=\Delta_0(T)\quad\text{and}\quad \Psi(\hat{\mathbf{p}})\equiv\sin\vartheta_{\mathbf{p}}e^{i\varphi_{\mathbf{p}}}=\sqrt{8\pi/3}Y_{1,1}(\vartheta_{\mathbf{p}},\varphi_{\mathbf{p}}).$$

That is, it is obvious that $\Delta_\alpha^{(A)}(\mathbf{p})\neq\Delta_\alpha^{(A)*}(\mathbf{p})$, but $\eta^{(A)}(\mathbf{p})=0$.

Equations (12)–(15) also imply expressions (I.46)–(I.48) of Ref. 1 for the DFs $g_\alpha(\mathbf{p})$, $f_0(\mathbf{p})$, and $f_\alpha(\mathbf{p})$ for $\xi=\xi\mathbf{l}$ ($g_0(\mathbf{p})=0$) for nonunitary phases of the type ^{3}He-A_2, ^{3}He-A_1, and the nonunitary 2D phase (see also Ref. 16 and Sec. 3 below). In addition, formulas (12)–(15) are also valid for the nonunitary B phase of a SFL in a magnetic field (in the case of ^{3}He this is the B_2 phase, in the terminology of Ref. 8), a phase which was not considered in Ref. 1.

Expressions (12)–(15) for the quasiparticle DFs of SFLs can be put in a more explicit form by taking into account that the definitions (6) and (7) of the functions $N^0_{\pm\mathbf{p}}(\Sigma)$ and $N^{\|}_{\pm\mathbf{p}}(\Sigma)$ and Eqs. (9) and (10) for the functions $\Sigma_{1,2}(\mathbf{p})$ and $E_\pm(\mathbf{p})$ imply the relations

$$\frac{1}{2R}[(1-N^0_{\mathbf{p}}(\Sigma)-N^0_{-\mathbf{p}}(\Sigma))\Sigma+(N^{\|}_{\mathbf{p}}(\Sigma)+N^{\|}_{-\mathbf{p}}(\Sigma))\underline{\Sigma}]=\frac{1}{2}[\Phi_+(\mathbf{p},\mathbf{v}_n)+\Phi_-(\mathbf{p},\mathbf{v}_n)],\tag{18}$$

where

$$\Phi_\pm(\mathbf{p},\mathbf{v}_n)\equiv\frac{1}{4E_\pm}\left[\tanh\left(\frac{E_\pm+\mathbf{p}\cdot\mathbf{v}_n}{2T}\right)+\tanh\left(\frac{E_\pm-\mathbf{p}\cdot\mathbf{v}_n}{2T}\right)\right],$$

$$\frac{1}{2R}\left[(1-N^0_{\mathbf{p}}(\Sigma)-N^0_{-\mathbf{p}}(\Sigma))\frac{1}{\Sigma}+(N^{\|}_{\mathbf{p}}(\Sigma)+N^{\|}_{-\mathbf{p}}(\Sigma))\frac{1}{\underline{\Sigma}}\right]=\frac{2}{(E_+^2-E^2)}[\Phi_-(\mathbf{p},\mathbf{v}_n)-\Phi_+(\mathbf{p},\mathbf{v}_n)].\tag{19}$$

These expressions, which do not depend on the choice of the function $\Sigma_1(\mathbf{p})$ or $\Sigma_2(\mathbf{p})$, appear in Eqs. (12), (14), and (15). Equation (14) also contains the difference

$$N^0_{\mathbf{p}}(\Sigma_1)-N^0_{-\mathbf{p}}(\Sigma_1)=N^0_{\mathbf{p}}(\Sigma_2)-N^0_{-\mathbf{p}}(\Sigma_2)=\Psi_+(\mathbf{p},\mathbf{v}_n)+\Psi_-(\mathbf{p},\mathbf{v}_n),\tag{20}$$

where

$$\Psi_\pm(\mathbf{p},\mathbf{v}_n)\equiv\frac{1}{4}\left[\tanh\left(\frac{E_\pm+\mathbf{p}\cdot\mathbf{v}_n}{2T}\right)-\tanh\left(\frac{E_\pm-\mathbf{p}\cdot\mathbf{v}_n}{2T}\right)\right].$$

Finally, Eqs. (13) and (15) contain the following difference of functions:

$$N^{\|}_{\mathbf{p}}(\Sigma_1)-N^{\|}_{-\mathbf{p}}(\Sigma_1)=N^{\|}_{\mathbf{p}}(\Sigma_2)-N^{\|}_{-\mathbf{p}}(\Sigma_2)=\Psi_+(\mathbf{p},\mathbf{v})-\Psi_-(\mathbf{p},\mathbf{v}_n).\tag{21}$$

Relations (20) and (21) contain formulas (I.49) (for $v_n\neq0$, $v_s=0$) to the case of arbitrary nonunitary phases of a SFL with triplet pairing in a magnetic field (in the general case $(\xi\cdot\mathbf{\Delta})\neq0$, $(\xi\cdot\mathbf{l})\neq0$, $(\xi\cdot[\mathbf{l}\times\mathbf{\Delta}])\neq0$, unlike the case $\xi=\xi\mathbf{l}$, for which formulas (I.49) were written).

We note that, according to Eqs. (13) and (21), the DF $g_0(\mathbf{p})\neq0$ for $(\xi\cdot\mathbf{\Delta})\neq0$ and $(\mathbf{p}\cdot\mathbf{v}_n)\neq0$. This can apparently be interpreted as the induction of correlations of the singlet type in a moving SFL with triplet pairing in a magnetic field (recall that we assumed in Eq. (4) that the SFL does not contain an anomalous interaction amplitude that would lead to singlet pairing of fermions).

We stress that in the derivation of formulas (12)–(15) we have specified the structure of the energy functional $E(f,g,g^+;H)$ but have only assumed that it has certain invariance properties (see Introduction). Therefore, the expressions (12)–(15) obtained above, when (18)–(21) and the definitions (10) and (11) are taken into account, solve the stated problem of finding the explicit form of the anomalous $g_\alpha(\mathbf{p})$, $g_0(\mathbf{p})$ and normal $f_0(\mathbf{p})$, $f_\alpha(\mathbf{p})$ DFs of the quasiparticles in the general case for arbitrary nonunitary ($\eta\neq0$) phases of a SFL (with $v_n\neq0$ but $v_s=0$) with triplet pairing (with $s=1$ and l an arbitrary odd integer) in a static uniform magnetic field with allowance for the Landau Fermi-liquid exchange interaction. Here the temperature can take any value in the interval $0\leqslant T\leqslant T_c$.

Knowing the explicit form of the quasiparticle DFs for a specific choice of structure of the energy functional $E(f,g,g^+;H)$, we can obtain a system of coupled equations for the order parameter $\Delta_\alpha(\mathbf{p})$ (4), the effective magnetic field $\mathbf{H}_{\text{eff}}(\mathbf{p})$, and the quasiparticle energy $\xi_0(\mathbf{p})$ (3) for the different phases of the SFL. In addition, by taking into account expression (15) for the DF $f_\alpha(\mathbf{p})$ and also formulas (18), (19), and (21), we can find the magnetization M_α and the magnetic susceptibility $\chi_{\alpha\beta}$ for these phases of the SFL by using the formula

$$M_\alpha=\frac{2\mu_n}{V}\sum_{\mathbf{p}}f_\alpha(\mathbf{p})=\chi_{\alpha\beta}H_\beta\tag{22}$$

(V is the volume occupied by the SFL).

3. ^{3}He-A_1, ^{3}He-A_2, AND THE NONUNITARY TWO-DIMENSIONAL PHASE OF ^{3}He IN A MAGNETIC FIELD

As an example of the application of the general theory set forth above, let us consider the nonunitary ($\eta\neq0$) phases of the type ^{3}He-A_2, ^{3}He-A_1, and the nonunitary 2D phase of ^{3}He. For ^{3}He-A_2 the order parameter has the form[8]

$$\Delta_\alpha^{(A_2)}(\mathbf{p})=(\Delta_+\hat{d}_\alpha+i\Delta_-\hat{e}_\alpha)\Psi(\hat{\mathbf{p}}),\tag{23}$$

$$\Psi(\hat{\mathbf{p}})\equiv(\hat{m}_j+i\hat{n}_j)\hat{p}_j,$$

where $\hat{\mathbf{d}}$ and $\hat{\mathbf{e}}$ are mutually orthogonal real vectors in spin space, $\hat{\mathbf{d}}\cdot\hat{\mathbf{e}}=0$, $\hat{\mathbf{d}}^2=\hat{\mathbf{e}}^2=1$, $\hat{\mathbf{m}}$ and $\hat{\mathbf{n}}$ are real, mutually orthogonal real unit vectors in orbital space, $\hat{\mathbf{m}}\cdot\hat{\mathbf{n}}=0$, $\hat{\mathbf{m}}^2=\hat{\mathbf{n}}^2=1$ (the orbital function $\Psi(\hat{\mathbf{p}})$ has the same form for ^{3}He-A_2, ^{3}He-A_1, and ^{3}He-A), and $\Delta_\pm(T)\equiv(\Delta_{\uparrow\uparrow}(T)\pm\Delta_{\downarrow\downarrow}(T))/2$. In the nonunitary ^{3}He-A_1 phase $\Delta_{\downarrow\downarrow}=0$, while in the unitary phase ^{3}He-A, which exists in the limit of zero magnetic field, $\Delta_{\uparrow\uparrow}=\Delta_{\downarrow\downarrow}\equiv\Delta_0$. For the nonunitary 2D phase of ^{3}He the order parameter has the form[8]

$$\Delta_\alpha^{(2D)}(\mathbf{p})=\frac{e^{i\phi}}{2}[\Delta_{\uparrow\uparrow}(\hat{d}_\alpha+i\hat{e}_\alpha)\Psi^*(\hat{\mathbf{p}})+\Delta_{\downarrow\downarrow}(\hat{d}_\alpha-i\hat{e}_\alpha)\Psi(\hat{\mathbf{p}})],\tag{24}$$

while in the unitary 2D phase one has $\Delta_{\uparrow\uparrow}=\Delta_{\downarrow\downarrow}\equiv\Delta_\perp$.

We choose the energy functional $E_{\rm int}(f,g)$ of the interaction to be quadratic in the quasiparticle DFs of the SFL, specifically (see Ref. 1):

$$E(f,g,g^+;H)=E_0(f;H)+E_{\rm int}(f,g),$$

$$E_{\rm int}(f,g)=\frac{1}{2V}\sum_{\mathbf{p}_1\mathbf{p}_2}[f_0(\mathbf{p}_1)F_1(\mathbf{p}_1,\mathbf{p}_2)f_0(\mathbf{p}_2)+f_\alpha(\mathbf{p}_1)F_2(\mathbf{p}_1,\mathbf{p}_2)f_\alpha(\mathbf{p}_2)]+\frac{1}{V}\sum_{\mathbf{p}_1\mathbf{p}_2}g^*_\alpha(\mathbf{p}_1)L_t(\mathbf{p}_1,\mathbf{p}_2)g_\alpha(\mathbf{p}_2), \tag{25}$$

where $E_0(f;H)$ is the EF of noninteracting fermions in a magnetic field [see (I.2)]. In the case of ^{3}He the normal interaction functions F_1 and F_2 (introduced by Landau) depend only on the angle θ between p_1 and p_2, and we therefore expand them in a series in Legendre polynomials,

$$F_{1,2}(\theta)=\sum_{l=0}^{\infty}(2l+1)F^{(l)}_{1,2}P_l(\cos\theta) \tag{26}$$

in which we shall henceforth keep only one of the Landau exchange amplitudes, $F_2^{(0)}$, assuming for simplicity that $F_2^{(l)}=0$ for $l\geqslant 2$. Further, in the anomalous interaction function $L_t(\mathbf{p}_1,\mathbf{p}_2)$ we shall take into account only the p pairing between ^{3}He atoms, i.e.,

$$L_t(\mathbf{p}_1,\mathbf{p}_2)=-3(\hat{\mathbf{p}}_1\cdot\hat{\mathbf{p}}_2)L^{(1)},\quad L^{(1)}>0 \tag{27}$$

(the minus sign corresponds to their mutual attraction).

In the case of a quadratic energy functional $E_{\rm int}(f,g)$ in (25), $\Delta_\alpha(\mathbf{p})$ and $\mathbf{H}_{\rm eff}(\mathbf{p})$ are described by Eqs. (I.34) and (I.36), which, when Eqs. (12)–(15), (23), (24), (26), and (27) are taken into account, acquire the following form[16] (in the limit $V\to\infty$) for the nonunitary (and unitary) ^{3}He phases considered here for $\xi=\xi\mathbf{l}$ and $\mathbf{v}_n=0$, $\mathbf{v}_s=0$:

$$\Delta_{\uparrow\uparrow}=\frac{3}{8}L^{(1)}J_+(\xi,T)\Delta_{\uparrow\uparrow},\qquad \Delta_{\downarrow\downarrow}=\frac{3}{8}L^{(1)}J_-(\xi,T)\Delta_{\downarrow\downarrow}. \tag{28}$$

The functions $J_\pm(\xi,T)$ are given by the formulas

$$J_\pm(\xi,T)=\int_0^{\varepsilon_c}d\varepsilon\ \nu(\varepsilon)\int_0^1 dx(1-x^2)\frac{\tanh(E_\pm(\varepsilon,x^2)/2T)}{E_\pm(\varepsilon,x^2)},$$

$$E_\pm=\sqrt{(\Delta_+\pm\Delta_-)^2(1-x^2)+(z+\xi)^2},\quad z\equiv\varepsilon-\mu \tag{29}$$

[see Eqs. (10) and (11)], where ε_c is the ''cutoff'' energy (which is introduced on physical considerations to ensure convergence of the integrals, $T_c\ll z_c\ll\mu$),[19] and $\nu(\varepsilon)$ is the density of states in the vicinity of the Fermi surface. We note that in the case of ^{3}He-A_1 only the first of Eqs. (28) is valid, since $\Delta_{\downarrow\downarrow}=0$. For $\mathbf{H}_{\rm eff}(\mathbf{p})$ we obtain the equation

$$\xi_\alpha=\xi l_\alpha=\frac{-\mu_n H_\alpha}{1+F_2^{(0)}\mathcal{F}(\xi,T)/4}, \tag{30}$$

where

$$\mathcal{F}(\xi,T)=\frac{1}{4\xi}\int_0^1 dx\int_0^\infty d\varepsilon\ \nu(\varepsilon)\phi(\varepsilon-\mu,x^2;\xi,T),$$

$$\phi(z,x^2;\xi,T)\equiv\frac{z+\xi}{E_+}\tanh\left(\frac{E_+}{2T}\right)-\frac{z-\xi}{E_-}\tanh\left(\frac{E_-}{2T}\right). \tag{31}$$

In Eqs. (28) and (30) we have taken into account the explicit form of the functions (18)–(21) for $v_n=0$.

From Eqs. (22) and (30) we obtain a unified formula for the nonlinear magnetic susceptibility of the superfluid phases ^{3}He-A_2, ^{3}He-A_1, and the nonunitary 2D phase of ^{3}He:

$$\chi_{zz}(\xi,T)=\mu_n^2\frac{\mathcal{F}(\xi,T)}{1+F_2^{(0)}\mathcal{F}(\xi,T)/4} \tag{32}$$

(here the axis $\mathbf{z}\|\mathbf{H}$).

The system of equations (28), (30) and the formula (32) for χ_{zz} obtained above are valid at temperatures $0\leqslant T\leqslant T_c$ and generalize the results of Ref. 15, where the Fermi-liquid interactions were not taken into account, to the nonunitary phases of ^{3}He considered in the present study [see Eqs. (23) and (24)].

In an analogous way one can consider the case of the nonunitary B_2 phase of ^{3}He in a high magnetic field, with the order parameter (see Ref. 8):

$$\Delta^{(B_2)}_\alpha(\mathbf{p})=\frac{e^{i\phi}}{2}[\Delta_{\uparrow\uparrow}(\hat{d}_\alpha+i\hat{e}_\alpha)\Psi^*(\hat{\mathbf{p}})+\Delta_{\downarrow\downarrow}(\hat{d}_\alpha-i\hat{e}_\alpha)\Psi(\hat{\mathbf{p}})+\Delta_{\uparrow\downarrow}[\hat{\mathbf{d}},\hat{\mathbf{e}}]_\alpha[\hat{\mathbf{m}},\hat{\mathbf{n}}]_j\hat{p}_j] \tag{33}$$

(for the unitary ^{3}He-B phase in a high magnetic field one has $\Delta_{\uparrow\uparrow}=\Delta_{\downarrow\downarrow}\equiv\Delta_\perp$, $\Delta_{\uparrow\downarrow}\equiv\Delta_\|$).

CONCLUSION

The present study can provide a theoretical basis for describing specific nonunitary phases of SFLs with triplet pairing in a magnetic field and for finding such physical quantities for these phases as the magnetic susceptibility, thermodynamic potential, and the thermodynamic functions, which can be found with the use of the general formulas (12)–(15) for the quasiparticle DFs of the SFL. We again emphasize that the specific structure of the energy functional $E_{\rm int}(f,g)$ is not restricted to the form (25) but can be chosen in another form (e.g., substantially nonquadratic in the DFs f and g) that conforms to the necessary invariance properties (see Introduction).

We also note that near T_c ($T_c-T\ll T_c$) one can use Eqs. (12)–(15) and (18)–(21) and equations of the type (I.34)–(I.36) to obtain the Ginzburg–Landau equations for a SFL with triplet pairing for $H\neq 0$, $v_n\neq 0$ with allowance for the terms nonlinear in powers of the order parameter Δ (see also Refs. 19 and 20 and the references cited therein).

In this connection let us mention several papers of other authors. Specifically, the unitary phase ^{3}He-B in a sufficiently high magnetic field ($\Delta_\perp\neq\Delta_\|$) and at low pressures (when one can neglect the strong-coupling effects in the ^{3}He) has been investigated theoretically by other approaches to the weak-coupling theory in Refs. 18 and 21 (for more details see Ref. 8 and the Introduction to Ref. 1), where, among

other things, the nonlinear magnetic susceptibility of ^{3}He-B was found with allowance for the Landau Fermi-liquid exchange amplitudes F_0^a and F_2^a. A phase transition between the A and B phases of ^{3}He in a magnetic field has also been investigated in the weak-coupling theory in Refs. 22 and 23. In an experimental study of the behavior of the ^{3}He phases in high magnetic fields, it was conjectured that new superfluid phases of ^{3}He can exist between the A_2 and B phases[24] and between the A_1 and A_2 phases of ^{3}He (see Ref. 25 and the references cited therein).

These conjectures as to the existence of new phases in superfluid ^{3}He in a magnetic field require further study; in our view, they confirm the necessity of using a general (unified) approach to the description of the different phases of SFLs (and not only of ^{3}He, see Introduction) with triplet pairing in a magnetic field. Such an approach has been the subject of this paper.

The author thanks S. V. Peletminskiĭ for interest in this study and a discussion of the results.

*E-mail: antarasov@kipt.kharkov.ua

[1] A. N. Tarasov, Fiz. Nizk. Temp. **24**, 429 (1998) [Low Temp. Phys. **24**, 324 (1998)].
[2] V. V. Krasil'nikov, S. V. Peletminskii, and A. A. Yatsenko, Physica A **162**, 513 (1990).
[3] A. I. Akhiezer, V. V. Krasil'nikov, S. V. Peletminskiĭ, and A. A. Yatsenko, Usp. Fiz. Nauk **163**, 1 (1993) [Phys. Usp. **36**, 35 (1993)].
[4] A. I. Akhiezer, V. V. Krasil'nikov, S. V. Peletminskii, and A. A. Yatsenko, Phys. Rep. **245**, 1 (1994).
[5] A. J. Leggett, Rev. Mod. Phys. **47**, 331 (1975).
[6] I. M. Khalatnikov (Ed.), *Superfluid Helium-3* (Collection of Articles) [in Russian], Mir, Moscow (1977).
[7] V. P. Mineev, Usp. Fiz. Nauk **139**, 303 (1983) [Sov. Phys. Usp. **26**, 160 (1983)].
[8] D. Vollhardt and P. Wölfle, *The Superfluid Phases of Helium-3*, Taylor and Francis, London (1990).
[9] V. I. Fal'ko and I. S. Shapiro, Zh. Éksp. Teor Fiz. **91**, 1194 (1986) [Sov. Phys. JETP **64**, 706 (1986)].
[10] D. M. Sedrakyan and K. M. Shakhabasyan, Usp. Fiz. Nauk **161**, 3 (1991) [Sov. Phys. Usp. **34**, 555 (1991)].
[11] G. E. Volovik and L. P. Gor'kov, Zh. Éksp. Teor Fiz. **88**, 1412 (1985) [Sov. Phys. JETP **61**, 843 (1985)].
[12] N. E. Alekseevskiĭ and D. I. Khomskiĭ, Usp. Fiz. Nauk **147**, 767 (1985) [Sov. Phys. Usp. **28**, 1136 (1985)].
[13] V. V. Moshchalkov and N. B. Brandt, Usp. Fiz. Nauk **149**, 585 (1986) [Sov. Phys. Usp. **29**, 725 (1986)].
[14] M. Sigrist and K. Ueda, Rev. Mod. Phys. **63**, 239 (1991).
[15] Y. Hasegawa, Prog. Theor. Phys. **63**, 1040 (1980).
[16] A. N. Tarasov, J. Mol. Liquids **87** (2000) (in press).
[17] A. A. Isaev and S. V. Peletminskiĭ, Ukr. Fiz. Zh. **37**, 952 (1992).
[18] N. Schopohl, J. Low Temp. Phys. **49**, 347 (1982).
[19] A. N. Tarasov, Fiz. Nizk. Temp. **21**, 24 (1995) [Low Temp. Phys. **21**, 17 (1995)].
[20] A. N. Tarasov, Fiz. Nizk. Temp. **23**, 243 (1997) [Low Temp. Phys. **23**, 117 (1997)].
[21] R. S. Fishman and J. A. Sauls, Phys. Rev. B **33**, 6068 (1986).
[22] M. Ashida and K. Nagai, Prog. Theor. Phys. **74**, 949 (1985).
[23] H. Furusawa, H. Shimahara, and K. Nagai, Physica B **194–196**, 801 (1994).
[24] J. M. Kyynäräinen, J. P. Pekola, A. J. Manninen, and K. Torizuka, Phys. Rev. Lett. **64**, 1027 (1990).
[25] G. Frossati, S. A. J. Wiegers, T. Tata, R. Jochemsen, P. G. van de Haar, and L. P. Roobol, Czech. J. Phys. **40**, 909 (1990).

Translated by Steve Torstveit

SUPERCONDUCTIVITY, INCLUDING HIGH-TEMPERATURE SUPERCONDUCTIVITY

Flux quantization in stationary and nonstationary states in long Josephson junctions

K. N. Yugay,* N. V. Blinov, and I. V. Shirokov

Omsk State University, Omsk, 644077, Russia
(Submitted September 17, 1999; revised June 15, 2000)
Fiz. Nizk. Temp. **26**, 1067–1072 (November 2000)

Dynamical chaos and the stability of states in long Josephson junctions are investigated from the standpoint of flux quantization. It is shown that the stationary Meissner and fluxon states having integer numbers of fluxons are stable. Stationary antifluxon states also having integer numbers of flux quanta and all other states with half-integer numbers of flux quanta are unstable. Transitions between all states — Meissner states and states having integer and half-integer numbers of flux quanta — take place in the nonstationary case, and all these states are dynamically equivalent, but the number of flux quanta is an irregular time-dependent function for the chaotic states and a regular one for the regular states. © *2000 American Institute of Physics.* [S1063-777X(00)00211-5]

INTRODUCTION

Long Josephson junctions (LJJs) are of great interest first of all from the standpoint of making SQUIDs based on them. However, LJJs are of interest also as a simple and at the same time deep physical and mathematical model of nonlinear phenomena. Dynamical chaos in LJJs is a subject of intensive research[1–19] and may be a source of dynamic noise.

It is well known that the number of solutions of the nonlinear stationary Ferrell–Prange equation for the conventional Josephson phase variable (which is just the phase difference of the wave functions of a superconducting condensate at the junction) describing stationary states in a LJJ at given boundary conditions depends on the value of the external magnetic field H_0, bias current β, and the total length L of the junction. It is clear that only one solution may be realized in a concrete junction at given values of H_0, β, and L. Clearly this state must be one of the solutions of the Ferrell–Prange equation. Stationary states of a LJJ which are solutions of the Ferrell–Prange equation have been investigated, for example, in Ref. 20. The question is, how does the selection of this solution happen? What is the selection of this solution affected by? The problem of the selection of the solutions of the Ferrell–Prange equation is usually treated in the framework of a thermodynamic approach.[20] Within such approach one assumes that only the solution corresponding to the global minimum of the Gibbs thermodynamic potential is realized under the concrete physical conditions. In our previous work[21] we have proposed another approach, based on the fact that the Ferrell–Prange equation is the stationary limit of the time-dependent sine-Gordon equation describing the dynamics of a LJJ. Thus, we applied the sine-Gordon equation with dissipation to find a dynamical criterion of stability of a state. Using this criterion, we have shown that not all solutions of the Ferrell–Prange boundary-value problem are stable; some of them are metastable.

We have also shown[22] that in a LJJ with dissipation the selection of the specific asymptotic solution (including a nonstationary one) can be affected by the form of the initial rapidly damped perturbation, independently of whether the initial state is chaotic or not. In other words, a rapidly damped small perturbation influences the asymptotic states substantially even if the initial state is chaotic. This characteristic of the LJJs we have called a memory effect. This effect makes dynamical chaos strangely different from statistical chaos (in the case of statistical chaos a loss of information happens during the relaxation time).

In the presence of both an external magnetic field and a dc bias current, three clusters of states can exist: stationary, regular, and chaotic. With changing parameters of the initial perturbation, the system realizes transitions between these three clusters of asymptotic states.[22] In Ref. 23 we showed that the β–H_0 parametric plane of a LJJ is divided by bifurcation lines into a series of regions with different numbers of solutions of the Ferrell–Prange equation, and a chaos strip arises along the bifurcation line that separates the region with two stationary states from the region with no stationary states. The number of stationary states decreases in the presence of a bias current, but even at $\beta=0$ some of the solutions are stable and others unstable. In this work we will try to investigate these stable and unstable states in detail. We will analyze the problem from the standpoint of flux quantization. We will show that the stationary states have only zero, integer, and half-integer numbers of flux quanta, and the states with a half-integer number of flux quanta are always unstable. The states with an integer number of flux quanta are the fluxon and antifluxon states; the fluxon states are stable and the antifluxon, unstable. Among the states with zero flux quanta only the Meissner states are stable, while the others are unstable. We will formulate a criterion by which one can determine the stability of the states from the standpoint of flux quantization. We will also show that the number of flux quanta is an irregular time-dependent function for the chaotic states and that in nonstationary – regular and chaotic

– regimes the allowed states with integer and half-integer numbers of flux quanta are in a certain sense equivalent.

1. FLUX QUANTIZATION FOR STATIONARY STATES

In contradistinction to our previous work,[23] here we have studied the stationary states of a LJJ in detail and devoted attention mainly to flux quantization in these states. We have solved numerically the boundary Ferrell–Prange problem:

$$\varphi_{xx}(x)=\sin\varphi(x)-\beta, \tag{1}$$

$$\varphi_x(x)|_{x=0}=\varphi_x(x)|_{x=L}=H_0. \tag{2}$$

Here $\varphi(x)$ is the Josephson phase variable, β is the dc bias current density normalized to the critical current density j_c of the junction, x is the distance along the junction normalized to the Josephson penetration length λ_J, H_0 is the external static magnetic field perpendicular to the junction and normalized to $\tilde{H}=\Phi_0/(2\pi\lambda_J d)$, Φ_0 is the flux quantum; $d=2\lambda_L+b$, λ_L is the London penetration length, b is the thickness of the dielectric barrier, and L is the total length of the junction normalized to λ_J.

Equation (1) with boundary condition (2) has been solved numerically for different values of H_0, β, and L. The distribution of the magnetic field $H(x)=\varphi_x(x)$ and the current density $j(x)=\varphi_{xx}(x)$ in the junction have been calculated.

We have also calculated the Gibbs thermodynamic potential for an each state using the following equation:

$$G=\int_0^L\left[\frac{1}{2}\varphi_x^2(x)+1-\cos\varphi(x)-\beta\varphi(x)-H_0\varphi_x(x)\right]dx, \tag{3}$$

where G is the Gibbs thermodynamic potential per unit length of the junction, normalized to the value $\tilde{G}=\Phi_0^2/(16\pi^3\lambda_J d)$. It should be noted that all solutions of the Ferrell–Prange equation are extremals of the functional in Eq. (3). Furthermore, it is easy to show (see, for example, Ref. 24) that these extremal values correspond to minima of the thermodynamic potential G.

As an illustration, the results of the calculations for $H_0=1.9$, $L=10$, and $\beta=0.06$ and 0.08, respectively, are listed in Tables I and II.

TABLE I. Stability, transitions, number of flux quanta, and type of state. $H_0=1.9$, $L=10$, $\beta=0.06$.

Number of state	Stability	G	Transitions $k\to l$	Number of flux quanta	Type of stable states
1	unstable	−12.849	1→7	2	2-antifluxon
2	unstable	−12.912	2→9	1.5	
3	unstable	−7.592	3→5	1	1-antifluxon
4	unstable	−7.594	4→5	0.5	
5	stable	−7.829	5→5	0	Meissner
6	unstable	−7.828	6→5	0.5	
7	stable	−13.652	7→7	1	1-fluxon
8	unstable	−13.368	8→7	1.5	
9	stable	−17.556	9→9	2	2-fluxon
10	unstable	−17.272	10→9	2.5	

TABLE II. Stability, transitions, number of flux quanta, and type of state. $H_0=1.9$, $L=10$, $\beta=0.08$.

Number of state	Stability	G	Transitions $k\to l$	Number of flux quanta	Type of stable states
1	unstable	−14.747	1→3	2	2-antifluxon
2	unstable	−14.771	2→3	1.5	
3	stable	−20.328	3→3	2	2-fluxon
4	unstable	−20.177	4→3	2.5	

We now calculate the flux in a LJJ. In the case of an infinitely long junction the following condition holds for the stationary states: $\varphi(x)|_{x\to-\infty}=0$, $\varphi(x)|_{x\to+\infty}=2\pi$, and the total flux is[25,26]

$$\Phi=\frac{1}{2\pi}\int_{-\infty}^{+\infty}\varphi_x(x)dx=n \quad (n=1,2,3,\ldots). \tag{4}$$

Here the flux Φ is normalized to the flux quantum Φ_0. In the case of a junction of finite length the situation changes drastically, because the boundary effects must be taken into account. In this case a shielding current always flows at the edge of the junction, and the total flux must be calculated in another way excluding boundary effects. Because the shielding current cannot be associated with flux quantization in a junction, we have to exclude boundary effects from the flux calculation. Then we can write the required flux as follows:

$$\Phi=\frac{1}{2\pi}\int_{x_1}^{x_2}\varphi_x(x)dx=\frac{1}{2\pi}[\varphi(x_2)-\varphi(x_1)], \tag{5}$$

where x_1 and x_2 are the nearest points to the left and right edges, respectively, at which $j(x)\equiv\varphi_{xx}(x)=0$. At these points $j_x>0$ for the fluxon states and $j_x<0$ for the antifluxon states. Formula (4) is a special case of (5) because $j(x_1=-\infty)=j(x_2=+\infty)=0$.

Using the definition of the points x_1 and x_2, we find that three types of states exist, in which

$$\begin{aligned}&1)\ \Phi=0,\\ &2)\ \Phi=n, \quad n=1,2,3,\ldots,\\ &3)\ \Phi=n/2\pm\arcsin\beta/\pi, \quad n=1,2,3,\ldots.\end{aligned} \tag{6}$$

These will be called the allowed states. The value $\Phi=0$ corresponds to the Meissner and quasi-Meissner states, $\Phi=n$ $(n=1,2,3,\ldots)$ to the fluxon and antifluxon states, and $\Phi=n/2\pm\arcsin\beta/\pi$ $(n=1,2,3,\ldots)$ to all the other states.

A comparison of the case of zero bias current with the case $\beta\neq0$ makes it possible to say that the dc bias current lifts the degeneracy of the states with half-integer numbers of flux quanta. The splitting value of the flux is equal to $2\arcsin\beta/\pi$, and at $\beta=0.06$ and 0.08 (Tables I and II) it is equal to 0.038 and 0.050, respectively.

We determine the stability of the stationary states as follows. First we solve numerically the equation for time-dependent perturbations of the stationary state (this equation can be easily found from the sine-Gordon equation as a result of linearization[21]). Then we determine the stability or instability of the stationary state with respect to small perturbations by calculating the Lyapunov exponent.[22] As we can

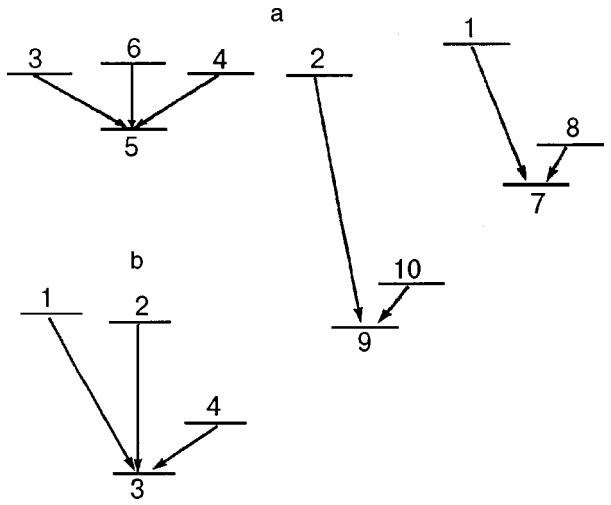

FIG. 1. The schemes of transitions between states at $H_0=1.9$ and $L=10$ for $\beta=0.06$ (a) and $\beta=0.08$ (b).

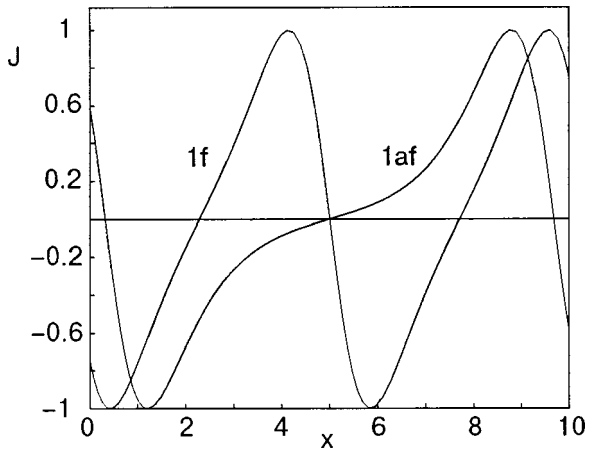

FIG. 2. Distribution of the current in one-fluxon (1f) and one-antifluxon (1af) states. $H_0=1.9$, $\beta=0$, $L=10$.

see from Tables I and II, the antifluxon states and states with half-integer numbers of flux quanta are unstable. These states decompose into some stable states (Meissner states or states with an integer number of flux quanta). To find the final stable state l to which the metastable state k passes (the transition $k\rightarrow l$), we used the solution of the Ferrell–Prange equation corresponding to the state k as an initial state for the nonstationary sine-Gordon equation.

As is seen from the calculated results listed in Tables I and II, the transition $k\rightarrow l$ is always accompanied by the inequality $G_k>G_l$ $(k\neq l)$, where G_k and G_l are the Gibbs thermodynamic potentials of states k and l, respectively. If the state k is stable, then $k=l$ $(G_k=G_l)$. One of the unexpected results is that the metastable, i.e., unstable, state has a Gibbs thermodynamic potential that is not necessarily greater than that for some stable states. In Fig. 1 the schemes of the transitions between states are shown at $H_0=1.9$, $L=10$, and $\beta=0.06$ (Fig. 1a) and 0.08 (Fig. 1b). The horizontal lines correspond to fixed values of the Gibbs thermodynamic potential of the states for the given parameters H_0, L, and β. It is seen from Fig. 1 that $G_{10}<G_5$ and $G_{10}<G_7$ — states 5 and 7 are stable.

Our calculations show that the number of stable states decreases with increasing β. For example, four stable states exist at $H_0=1.9$, $L=10$, and $\beta=0$: the Meissner (M), one-fluxon (1f), two-fluxon (2f), and three-fluxon (3f) states; we have 3 stable states (M, 1f, and 2f) at $\beta=0.06$, two states (1f and 2f) at $\beta=0.07$, and one state (2f) at $\beta=0.08$. There are no stationary states at $\beta=0.15$. The stable states with $G_l>G_{l_0}$, where G_{l_0} corresponds to the global minimum, fall into the state with G_{l_0} as β increases.

The character of the stationary states changes together with the number of states when the external magnetic field H_0 is varied with the other parameters held fixed. For example, for $\beta=0$ and $L=10$ the number of stable states at $H_0=1.4$ equals three (M, 1f, and 2f), at $H_0=0.6$ there are two stable states (M and 1f), and at $H_0=0.05$ only one stable stationary state (M) exists; at $H_0=2.0$ there are again three stable states (1f, 2f, and 3f), and there are two stable states at $H_0=2.1$ (2f and 3f), $H_0=2.2$ (3f and 4f), and $H_0=2.9$ (4f and 5f).

Figure 2 shows the one-fluxon (1f) and one-antifluxon (1af) states at $H_0=1.9$, $\beta=0$, and $L=10$. Tables I and II list the numbers of flux quanta for the stationary states. The calculations allow one to draw the following conclusions: 1) the stationary states at a given set of parameters can have a number of flux quanta equal to zero, a half integer, or an integer; 2) all the fluxon and antifluxon states have a positive integer number of flux quanta, according to the criterion (5) formulated above. All fluxon states are stable and all antifluxon states are unstable; 3) all states with a half-integer number of fluxons are always unstable; 4) in the Meissner states one always has $x_1=x_2$ and $n=0$. This state is stable. Besides the stable Meissner states, unstable states with $n=0$ exist; one of them is a quasi-Meissner state with $x_1=x_2$. In Fig. 3 the Meissner and quasi-Meissner states are shown for $H_0=1.2$, $\beta=0$, and $L=10$. All the quasi-Meissner states in Fig. 4 fall into some stable states.

All states with half-integer numbers of flux quanta and the antifluxon states are nonphysical because they disintegrate and therefore cannot be realized in real systems. As to the quasi-Meissner states, all of them arise in the capacity of some intermediate states and ultimately disintegrate.

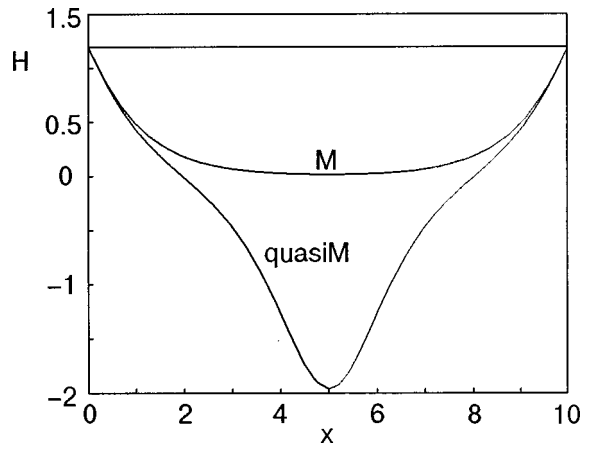

FIG. 3. Meissner and quasi-Meissner states at $H_0=1.2$, $\beta=0$, $L=10$.

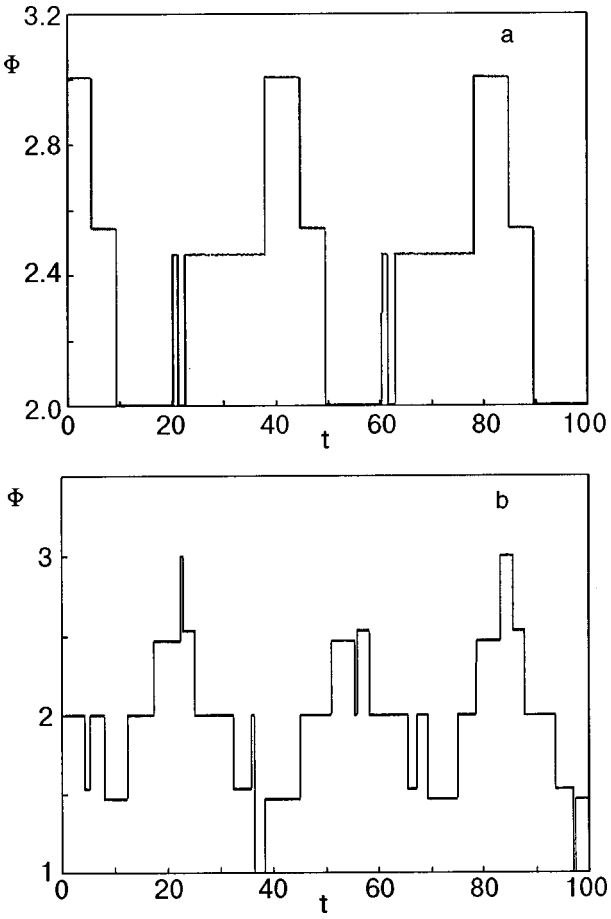

FIG. 4. Dependence of the flux Φ on time in the regular regime at $H_0=1.9$, $\beta=0.1$, $\gamma=0.26$, $L=10$ (a) and in the chaotic regime at $H_0=1.9$, $\beta=0.125$, $\gamma=0.1$, $L=10$ (b).

The number of fluxon and antifluxon states decreases at $\beta>0$. For example, there are four fluxon and antifluxon states at $H_0=1.9$, $L=10$, and $\beta=0.06$ (instead of the five at $\beta=0$), and at $\beta=0.08$ there are only two (one of them is a two-fluxon state and the other a two-antifluxon state).

Thus not all states having integer numbers of flux quanta are stable — only the fluxon states are. The criterion (5) formulated above may also serve as a simple criterion of stability of the solution of the Ferrell–Prange equation.

2. FLUX QUANTIZATION AND CHAOS

As is noted above, the number of stationary states decreases as the dc bias current increases, while at the same time the number of nonstationary states increases. In the general case, three clusters of states — stationary, regular, and chaotic — exist in a LJJ.[21] In the present Section we will consider the nonstationary regular and chaotic states from the standpoint of flux quantization.

The nonstationary states can be found by numerical integration of the nonstationary sine-Gordon equation

$$\varphi_{tt}(x,t)+2\gamma\varphi_t(x,t)-\varphi_{xx}(x,t)=-\sin\varphi(x,t)+\beta \qquad (7)$$

with the following boundary conditions:

$$\varphi_x(x,t)|_{x=0}=\varphi_x(x,t)|_{x=L}=H_0, \qquad (8)$$

where t is the time normalized to the inverse of the Josephson plasma frequency ω_J, $\omega_J=(2\pi c j_c/(C\Phi_0))^{1/2}$, C is the junction capacitance per unit area, γ is the dissipative coefficient per unit area, $\gamma=\Phi_0\omega_J/4\pi cRj_c$, and R is the resistance of the junction per unit area. Of course, the solutions of the Ferrell–Prange equations (1), (2) coincide with the asymptotic solutions of the sine-Gordon equations (7), (8). All solutions of the Ferrell–Prange equation, i.e., the stationary solutions, appear from any initial state during the evolution governed by the sine-Gordon equations (7), (8), but these solutions are not equivalent: some of them are stable and others unstable (metastable).

As in the case of the stationary states of junctions of finite length, in the nonstationary case the shielding currents flowing at the junction edges must be taken into account, and we again define the points x_1 and x_2. In this case: (i) the locations of these points will depend on time, $x_1=x_1(t)$ and $x_2=x_2(t)$, and (ii) we must find these points using the conditions of vanishing of the total — superconducting and quasiparticle — current in the junction, i.e., $j(x_1)=j(x_2)=0$, where $j(x_1)=[\varphi_{tt}(x)+2\gamma\varphi_t(x)-\varphi_{xx}(x)|_{x=x_1}$. We have the same for $j(x_2)$. This condition determines the allowed states, in which

$$\begin{aligned} &1)\ \Phi=0,\\ &2)\ \Phi=n(t), \quad n=1,2,3,\ldots,\\ &3)\ \Phi=n(t)/2\pm\arcsin\beta/\pi, \quad n=1,2,3,\ldots\ . \end{aligned} \qquad (9)$$

Here n is a discrete function of time in the sense that it performs jumps between constant values. Of course, the flux Φ behaves in the same manner. In contrast to the stationary states [see Eq. (6)], the flux $\Phi(t)$ takes different values for all the series 1)–3) in Eq. (9), spending a certain time in each of them. Besides, the points x_1 and x_2 move along the junction, and the character of this motion is different for regular and chaotic states.

Figures 4a and 4b show the dependence of $\Phi(t)$ for the two regimes — regular at $H_0=1.9$, $\beta=0.1$, $L=10$ (Fig. 4a) and chaotic at $H_0=1.9$, $\beta=0.125$, $L=10$ (Fig. 4b). The character of these regimes was determined by calculation of the Lyapunov exponent λ (see Ref. 22): $\lambda=0$ in regular regimes, and $\lambda>0$ in chaotic ones. The dependence of the flux in the regular regime, for example, has a regular character, and the evolution of the flux consists of regular transitions from one allowed state to another. Of course, the dependences of $x_1(t)$ and $x_2(t)$ have the same character. In contrast, in the chaotic regime, $x_1(t)$ and $x_2(t)$ are irregular time-dependent functions. The function $\Phi(t)$, as is clearly seen in Fig. 4b, exhibits jumps between allowed states as it did in the regular case, only now the response time in a fixed state changes irregularly. We note also that there is not any explicit preference for the states with integer numbers of flux quanta in comparison with the states with half-integer numbers of flux quanta, in either the regular or the chaotic regimes.

Thus, whereas in the stationary regime the states with integer numbers of flux quanta (fluxon states) are preferred in the sense that they are stable, in the nonstationary regimes — regular and chaotic — the allowed states with integer and half-integer numbers of flux quanta are in a certain sense equivalent.

CONCLUSIONS

We have considered the problem of the stability of states and the chaotic dynamics in LJJs from the standpoint of flux quantization. We have shown that only the stationary states with integer and half-integer numbers of flux quanta are realized, and among them only the Meissner and fluxon states are stable, while the quasi-Meissner and antifluxon states are unstable even though they have also an integer number of flux quanta. All the other states with a half-integer number of flux quanta are always unstable. Thus the stable states are states in which the flux is always quantized.

The states with a half-integer number of flux quanta are doubly degenerate. A dc bias current lifts this degeneracy. Among the stationary states, only those fluxon states with an integer number of flux quanta and the Meissner state have preference; they are the allowed ones.

All the allowed states with integer and half-integer numbers of flux quanta are equivalent in a certain sense in the nonstationary case, and the system passes from one allowed state to another; the response time in the states is chaotic in the chaotic states and regular in the regular states. In other words, in nonstationary states — both regular and chaotic — there are half-integer quantum numbers in addition to the integer quantum numbers.

*E-mail: yugay@phys.omsu.omskreg.ru

[1] M. Cirillo and N. F. Pedersen, Phys. Lett. A **90**, 150 (1982).
[2] N. F. Pedersen and A. Davidson, Appl. Phys. Lett. **39**, 830 (1981).
[3] P. S. Lomdahl, O. H. Soerensen, and P. L. Christiansen, Phys. Rev. B **25**, 5737 (1982).
[4] R. L. Kautz, IEEE Trans. Magn. **19**, 465 (1983).
[5] A. H. MacDonald and M. Plischke, Phys. Rev. B **27**, 201 (1983).
[6] M. P. Soerensen, N. Arley, P. L. Christiansen, R. D. Parmentier, and O. Skovgaard, Phys. Lett. **51**, 1919 (1983).
[7] A. R. Bishop, K. Fesser, P. S. Lomdahl, and S. E. Trullinger, Physica D **7**, 259 (1983).
[8] J. C. Eilbeck, P. S. Lomdahl, O. H. Olsen, and M. R. Samuelsen, J. Appl. Phys. **57**, 861 (1985).
[9] B. S. Han, B. Lee, O. G. Symko, W. J. Yeh, and D. J. Zheng, IEEE Trans. Magn. **25**, 1396 (1989).
[10] W. J. Yeh, O. G. Symko, and D. J. Zheng, Phys. Rev. B **42**, 4080 (1990).
[11] G. F. Eriksen and J. B. Hansen, Phys. Rev. B **41**, 4189 (1990).
[12] X. Yao, J. Z. Wu, and C. S. Ting, Phys. Rev. B **42**, 244 (1990).
[13] L. E. Guerrero and M. Ostavio, Physica B **165–166**, 11657 (1990).
[14] I. H. Dalsgaard, A. Larsen, and J. Mygind, Physica B **165–166**, 1661 (1990).
[15] S. Rajasekar and M. Lakshmanan, Physica A **167**, 793 (1990).
[16] S. Rajasekar and M. Lakshmanan, Phys. Lett. A **147**, 264 (1990).
[17] N. Gronbech-Jensen, P. S. Lomdahl, and M. R. Samuelsen, Phys. Rev. B **43**, 1279 (1991).
[18] N. Gronbech-Jensen, Phys. Rev. B **45**, 7315 (1992).
[19] J. McDonald and J. R. Clem, Phys. Rev. B **56**, 14723 (1997).
[20] C. S. Owen and D. J. Scalapino, Phys. Rev. **164**, 538 (1967).
[21] K. N. Yugay, N. V. Blinov, and I. V. Shirokov, Phys. Rev. B **49**, 12036 (1994).
[22] K. N. Yugay, N. V. Blinov, and I. V. Shirokov, Phys. Rev. B **51**, 12737 (1995).
[23] K. N. Yugay, N. V. Blinov, and I. V. Shirokov, Fiz. Nizk. Temp. **25**, 712 (1999) [Low Temp. Phys. **25**, 530 (1999)].
[24] I. M. Gelfand and S. V. Fomin, *Calculus of Variations* [in Russian], Fizmatgiz, Moscow (1961).
[25] A. Barone and G. Paterno, *Physics and Applications of the Josephson Effect*, Wiley-Interscience, New York (1982).
[26] K. K. Likharev, *Introduction to Dynamics of Josephson Junctions* [in Russian], Nauka, Moscow (1985).

This article was published in English in the original Russian journal. Reproduced here with stylistic changes by the Translation Consultant.

LOW-TEMPERATURE MAGNETISM

Josephson properties of transparent tunnel junctions

Yu. V. Shlapak,* A. L. Kasatkin, and É. M. Rudenko

Institute of Metal Physics, National Academy of Sciences of Ukraine, Bul'v. Vernadskogo 36, 03680 Kiev-142, Ukraine

(Submitted December 24, 1999; revised June 13, 2000)
Fiz. Nizk. Temp. **26**, 1073–1076 (November 2000)

With allowance for possible deviations of the current–phase relation from the usual sinusoidal dependence, a modified Ferrell–Prange equation is used to examine the steady-state electrodynamics of transparent Josephson junctions in an external magnetic field. It is shown that in this case the penetration of a weak magnetic field into a transparent Josephson junction is generally nonexponential, and the field H_{c1} at which vortices arise in transparent junctions and the dependence of the critical current on the magnetic field in them are calculated. © *2000 American Institute of Physics.* [S1063-777X(00)00311-X]

The electrodynamics of superconducting Josephson junctions is ordinarily based on the well-known Josephson relation between the superconducting current j_S flowing through the junction and the phase difference φ of the order parameter on the two sides of the junction, $j_S(\varphi)=j_c\sin\varphi$. This form of $j_S(\varphi)$ presupposes the presence of a rather weak coupling between the massive superconducting (S) ''banks'' of the junction, e.g., a low transparency of the tunnel barrier (I) in the case of an S–I–S tunnel junction or a rather wide interlayer of normal metal (N) for junctions of the S–N–S type.[1–3]

Recently, however, the junctions realized at grain boundaries in high-T_c superconductors (e.g., YBCO and BiSCCO bicrystals)[4] have been attracting a great deal of interest from the standpoint of their prospective use as Josephson elements. In the case of small-angle grain boundaries such junctions are generally characterized by a rather high transparency to electrons. In that case, as has been shown in a number of theoretical papers,[2,6–11] the current–phase relation $j_S(\varphi)$ in the Josephson effect can differ substantially from sinusoidal.

In the present paper we shall assume that $j_S(\varphi)$ has the form[9]

$$\frac{j_S(\varphi)}{j_c}=f(\varphi)=\frac{\sin\varphi}{\sqrt{1-D\sin^2(\varphi/2)}}\tanh\left(A(T)\sqrt{1-D\sin^2(\varphi/2)}\right), \tag{1}$$

where D is the transparency of the barrier, and $A(T)=\Delta(T)/(2k_BT)$.

We write the Ferrell–Prange equation[5]

$$\frac{d^2\varphi}{dx^2}=\frac{1}{\lambda_j^2}f(\varphi) \tag{2}$$

(where $f(\varphi)=j_S(\varphi)/j_c$) in the form

$$\frac{x\sqrt{2}}{\lambda_j}=\int_{\varphi_0}^{\varphi}\frac{d\varphi'}{\sqrt{F(\varphi)}};\quad F(\varphi)=\int f(\varphi)d\varphi. \tag{3}$$

The derivation of Eq. (2) presupposes that the condition $\lambda_j\gg\lambda$ holds (λ_j and λ are the Josephson and London penetration depths, respectively). According to Ref. 12, this condition holds for $j_c\ll j_d/\kappa$, where j_c is the critical current density of the junction, j_d is the pairing current density, and κ is the Ginzburg–Landau parameter. Taking into account that $j_c\sim j_dD$ (Ref. 12), we obtain a restriction on the value of the transparency D in order for Eq. (2) to remain valid: $D\ll\kappa^{-1}$.

For small values of the transparency, $0<D\ll\kappa^{-1}$

$$F(\varphi)\underset{D\ll1}{\approx}F(\varphi_0)+2\tanh(A(T))\sin^2\frac{\varphi}{2}\times\left[1-\frac{DA(T)}{2\sinh(2A(T))}\sin^2\frac{\varphi}{2}\right]. \tag{4}$$

For $D\ll1$, one can use (4) to find the following solution for equation (2):

$$\frac{x\sqrt{\tanh(A(T))}}{\lambda_j(D)}\underset{D\ll1}{\approx}\left[\ln\left(\tan\frac{\varphi}{4}\right)-\frac{DA(T)}{4\sinh(2A(T))}\cos\frac{\varphi}{2}\right]_{\varphi_0}^{\varphi}, \tag{5}$$

which describes the behavior of a Josephson junction in an external magnetic field parallel to the junction and higher than the characteristic transition field H_{c1}. The second term on the right-hand side in (5) shows the change in the distribution of the jump in phase of the order parameter upon a small increase in the transparency of the junction.

Equation (5) has the approximate solution

$$\varphi(x)\underset{D\ll1}{\approx}4\arctan\left(\exp\left(x'+\frac{DA(T)}{2\sinh(2A(T))}\frac{1}{1+x'^2}\right)\right)+2\pi n;$$

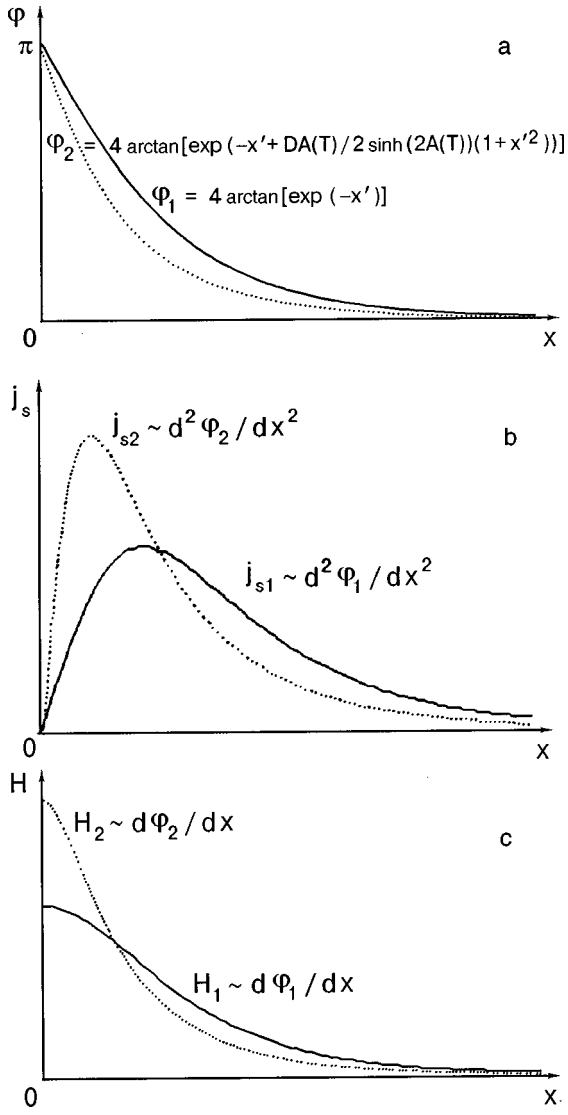

FIG. 1. Distribution of the phase difference (a), supercurrent (b), and magnetic field (c). The solid curve corresponds to $D=0$, the dotted curve to small D.

$$x'=\frac{x\sqrt{\tanh(A(T))}}{\lambda_j(D)}. \tag{6}$$

The behavior of the functions $\varphi(x)$, $d\varphi(x)/dx\sim H(x)$, and $d^2\varphi(x)/dx^2\sim j_S$ is shown in Fig. 1.

In the case of very weak external fields $H_0\ll\Phi_0/(2\pi\lambda_j d)$, where $\Phi_0=hc/2e$ is the magnetic flux quantum, one can use Eq. (5) to find the coordinate dependence of the field in the junction. In this case the currents through the junction are weak, and so the phase difference φ is small, and we find from (5) that

$$\varphi \underset{\substack{D\ll 1\\ \varphi\ll 1}}{\approx} \varphi_0\exp(-x')\left[1-\frac{DA(T)}{16\sinh(2A(T))}\varphi_0^2\exp(-2x')\right];$$

$$x'=\frac{x\sqrt{\tanh(A(T))}}{\lambda_j(D)}. \tag{7}$$

It is seen from this expression that increasing the transparency alters the character of the coordinate dependence of the phase, and the penetration depth decreases as a function of the transparency D more slowly than $\lambda_j(D)\sim j_c^{-1/2}(D)\sim D^{-1/2}$.

To find the critical field of the transition H_{c1} it is necessary to examine the total free energy per unit length of the junction along the magnetic field, which for a single vortex is given by a functional of the function $\varphi(x)$:

$$W_0=\int_{-\lambda}^{\lambda}(w_j+w_H)dx, \tag{8}$$

where

$$w_j=\frac{\Phi_0 j_c}{2\pi c}\int_{\varphi_0}^{\varphi}f(\varphi)d\varphi, \quad w_H=\frac{\lambda_j^2\Phi_0 j_c}{4\pi c}\left(\frac{d\varphi}{dx}\right)^2.$$

A vortex can penetrate in the junction starting at an external field H_{c1}, at which the quantity $\int(\mathbf{B}\cdot\mathbf{H}/4\pi)dV=\Phi_0 H_{c1}/4\pi$ becomes equal to W_0, i.e.,

$$H_{c1}(D)=\frac{4\pi}{\Phi_0}W_0=H_{c1}^{(0)}(D)\frac{1}{4\lambda_j}\int_{-\lambda_j}^{\lambda_j}dx\int f(\varphi)d\varphi, \tag{9}$$

where $H_{c1}^{(0)}(D)$ is given by the expression $H_{c1}=2\Phi_0/(\pi^2 d\lambda_j)$.

For $D\ll 1$ we obtain from (9) with allowance for (4)

$$H_{c1}(D)\underset{D\ll 1}{=}H_{c1}^{(0)}(D)\tanh(A(T))\left(1-\frac{DA(T)}{2\sinh(2A(T))}\right),$$
$$H_{c1}(D)\sim D^{1/2}(1-\alpha D), \tag{10}$$

where $\alpha=A(T)/(2\sinh 2A(T))<1/4$.

As is seen from the above relation, as the transparency of the barrier is increased slightly, the critical field for the entry of the first vortex into the interlayer between superconductors increases more slowly than $H_{c1}^{(0)}(D)$.

Let us consider the change in $j_c(H)$ due to the nonsinusoidal dependence of $j(\varphi)$ (1).

Let us assume that the dimension L of the junction is small compared to λ_j, so that we can neglect the self-magnetic field of the supercurrent flowing through the junction in comparison with the external field H_0.[2] Under these conditions the field inside the junction can be assumed constant and equal to H_0. We shall assume that the field H_0 is directed along the z axis (the plane of the junction is $0xz$); then the vector potential is $A_y=H_z(y)x=H_0x$.

The average current density through the junction (i.e., the quantity measured in an experiment) is given by

$$\bar{j}=\frac{1}{L}\int_{-L/2}^{L/2}j(\varphi(x))dx, \tag{11}$$

$$\varphi(x)=\theta+\frac{2e}{\hbar c}\int A_y\,dy=\theta+\frac{2e}{\hbar c}H_0 d_H x.$$

For the current–phase relation (1) we obtain

$$\bar{j}=j_c\frac{1}{2}\frac{4}{DA(T)}\frac{1}{t}\ln\left(\frac{\cosh(A(T)\sqrt{1-D\sin^2(\theta/2-t/2)})}{\cosh(A(T)\sqrt{1-D\sin^2(\theta/2+t/2)})}\right), \tag{12}$$

where $t=\pi\Phi/F_0$, and θ is a quantity that is adjusted as the total current is varied at a fixed magnetic field in such a way that the current $j(\theta,H)$ has the maximum possible value.

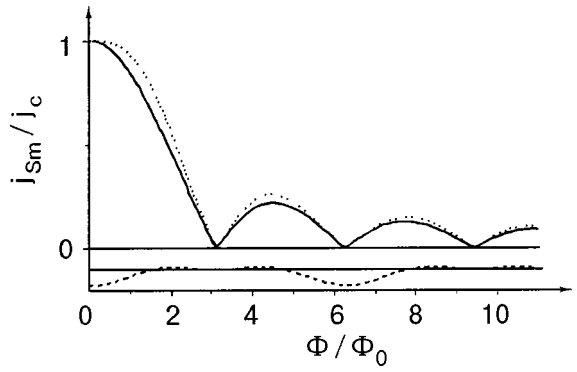

FIG. 2. Dependence of the critical current of the transition on the value of an external magnetic field parallel to the plane of the junction. The solid curve corresponds to $D=0$, the dotted curve to small D; the dashed curve near the x axis is a quantity proportional to the change in the curve upon a small increase in the transparency.

At small D we find, using (4), that

$$\overline{j} \underset{D\ll 1}{\approx} j_c \tanh(A(T))\sin\theta \times \left|\frac{\sin t}{t}\right|\left(1+\frac{2A(T)}{\sinh(2A(T))}\frac{D}{4}(1-\cos t\cos\theta)\right). \tag{13}$$

Taking into account that $j'_\theta=0$ for $j_{\max}$ at small D ($D \ll k_BT/\Delta(T)$), we obtain

$$j_c(H)\equiv\overline{j}_{\max} \underset{D\ll 1}{\approx} j_c\left|\frac{\sin t}{t}\right|\tanh(A(T)) \times\left(1+\frac{DA(T)}{\sinh(2A(T))}-2\left(\frac{DA(T)}{\sinh(2A(T))}\right)^2 \times\cos t(1+\cos t)\right). \tag{14}$$

Relation (14) is plotted in Fig. 2. The curves are normalized to $j_c(D)$.

Thus in the present paper we have investigated the changes in the Josephson properties of transparent junctions when the current–phase relation deviates from the usual sinusoidal law. We have obtained the corrections to the value of the field H_{c1} for the entry of a vortex into a transparent junction, for the the penetration depth of the magnetic field into the junction, and for the dependence of the critical current on the magnetic field.

*E-mail: shat@d24.imp.kiev.ua

[1] A. Barone and G. Paterno, *Physics and Applications of the Josephson Effect* [Wiley, New York (1982); Mir, Moscow (1984)].
[2] K. K. Likharev, *Introduction to the Dynamics of Josephson Junctions* [in Russian], Nauka, Moscow (1985).
[3] M. Tinkham, *Introduction to Superconductivity* [McGraw-Hill, New York (1975); Atomizdat, Moscow (1980)].
[4] J. Manhart, Z. Phys. B: Condens. Matter **101**, 175 (1996).
[5] R. Ferrell and R. Prange, Phys. Rev. Lett. **10**, 479 (1963).
[6] I. O. Kulik and A. N. Omel'yanchuk, Fiz. Nizk. Temp. **3**, 945 (1977) [Sov. J. Low Temp. Phys. **3**, 459 (1977)].
[7] A. V. Svidzinskiĭ, *Spatially Nonuniform Problems in the Theory of Superconductivity* [in Russian], Naukova Dumka, Kiev (1973), s. 228.
[8] F. Sols, Phys. Rev. B **49**, 15913 (1994).
[9] A. F. Volkov, Zh. Éksp. Teor. Fiz. **66**, 758 (1974) [Sov. Phys. JETP **39**, 366 (1974)].
[10] W. Habercorn, H. Knauer, and J. Richter, Phys. Status Solidi **47**, K161 (1978).
[11] C. B. Beenaker Jr., Phys. Rev. Lett. **66**, 3056 (1991).
[12] A. Gurevich, Phys. Rev. B **46**, 3187 (1992).
[13] P. G. de Gennes, *Superconductivity of Metals and Alloys* [Benjamin, New York (1966); Mir, Moscow (1968)].

Translated by Steve Torstveit

Effect of a nonmagnetic impurity on the superconducting transition temperature in layered structures with a non-phonon-mediated pairing mechanism

M. E. Palistrant and F. G. Kochorbé

*Institute of Applied Physics, Academy of Sciences of Moldova, ul. Akademicheskaya 5, 2028 Kishinev, Molodova**

(Submitted March 21, 2000; revised June 26, 2000)
Fiz. Nizk. Temp. **26**, 1077–1090 (November 2000)

The effect of nonmagnetic impurities on the superconducting transition temperature T_c in superconductors with a non-phonon-mediated (nonphononic) mechanism of superconductivity is investigated. Two features inherent to high-T_c superconductors are taken into account: the overlap of the energy bands, and the variable density of charge carriers. The cases of *s* and $d_{x^2-y^2}$ symmetry of the order parameter are considered. It is demonstrated that the Anderson theorem is violated in the case of *s* symmetry of the order parameters, both on account of interband scattering of electrons on impurities and on account of intraband scattering due to the electron–hole asymmetry in systems with a nonphononic mechanism of superconductivity. Analytical expressions are obtained for the value of T_c in the regions of small and large impurity concentrations, and numerical solutions of a self-consistent system of equations are found. The influences on T_c due to various mechanisms (the change in the chemical potential and in the intraband and interband relaxation times at an impurity) are analyzed for the types of symmetry indicated above. It is shown that a number of the features inherent to high-T_c superconductors can be explained, including, in particular, the possibility of complete suppression of superconductivity by a nonmagnetic impurity and the possibility of attaining high values of T_c upon doping of an insulator. It is also shown that as the interband scattering on the impurity potential increases, there is a change in the dependence of T_c on the impurity concentration. Qualitative agreement is obtained between the proposed theory and the experimental data on the dependence of T_c on the concentration of Zn, Al, and Ga impurities in yttrium and lanthanum ceramics. © *2000 American Institute of Physics.* [S1063-777X(00)00411-4]

1. INTRODUCTION

The influence of nonmagnetic impurities (Zn, Al, Ga) on the superconducting transition temperature is one of the most important topics in research on high-T_c superconducting materials today. This topic has been the subject of many experimental studies[1–8] (see also the review in Ref. 9).

The solution of this problem can shed light on the mechanism of high-T_c superconductivity. The point is that different nonmagnetic impurities have different effects on the critical temperature T_c of cuprate compounds. The substitution of Al or Ga atoms for Cu has a weakly destructive effect on the superconductivity.[1]

When the copper atoms are replaced by zinc, on the other hand, the zinc behaves as a magnetic impurity, suppressing the superconductivity.[2–4] However, experimental studies[10] show that zinc doping of the compound $YBa_2Cu_3O_7$ does not lead to magnetic breaking of electron pairs. Consequently, the Abrikosov–Gor'kov theory[11] on the effect of a paramagnetic impurity on superconductivity cannot be used to explain the suppression of superconductivity in such a system.

According to the Anderson theorem,[12] a nonmagnetic impurity does not affect the superconducting transition temperature T_c of an isotropic superconductor. However, high-T_c superconducting materials are anisotropic systems, and their various peculiarities can lead to a dependence of T_c on the concentration of nonmagnetic impurities. For example, studies[13–15] based on a two-band model have been able to explain the rather rapid lowering of T_c with increasing concentration of a nonmagnetic impurity owing to the intraband channel for the scattering of electrons on nonmagnetic impurities. However, in that model, on the assumption of a phonon-mediated mechanism of superconductivity, there is no critical concentration of the impurity, i.e., a nonmagnetic impurity cannot suppress the superconductivity completely.

In Ref. 16 the effect of a nonmagnetic impurity on the superconductivity was investigated for the case of *s* pairing in a single-band system with an anisotropic electron–electron interaction, and also for a superconductor with an order parameter of symmetry $d_{x^2-y^2}$. In the case of an anisotropic *s* pairing the value of T_c is lowered as the impurity concentration increases. However, as in the case of two-band superconductors,[13–15] there is no critical concentration of the impurity ($T_c \neq 0$). In the case of $d_{x^2-y^2}$ symmetry of the order parameter, T_c falls as the impurity concentration increases, and suppression of the superconductivity is possible. The curve of T_c as a function of the impurity concentration has negative curvature (is convex upward).

In Ref. 17 the effect of a nonmagnetic impurity on a superconducting state with *s* pairing was investigated on the basis of the so-called pair tunneling mechanism proposed in Ref. 18. It was found that in this case the lowering of the superconducting transition temperature T_c with increasing impurity concentration could occur at a faster rate than for

the anisotropic model.[16] However, the character of the dependence of T_c on the impurity concentration was analogous to that found in Ref. 14 on the basis of the two-band model.[19,20]

The theoretical papers cited above made use of the standard Abrikosov–Gor'kov theory when taking into account the influence of the randomly distributed impurity in the superconductor. There are some papers in which an attempt has been made to go beyond this approach (see, e.g., Refs. 21 and 22). It was stated in Ref. 21 that a correct description of high-T_c cuprates (with a short coherence length) can be obtained by taking into account the spatial variation of the order parameter, which is strongly suppressed near an impurity. In the case of $d_{x^2-y^2}$ symmetry of the order parameter a weaker suppression of the superconductivity was obtained than in the Abrikosov–Gor'kov approach.[17,23] In Ref. 22 the various phase transitions in two-dimensional disordered systems containing an impurity was investigated on the basis of a one-band model with *s* symmetry of the order parameter; the density of charge carriers in this model is equal to the concentration of the randomly distributed impurities. It was shown that the phase states (insulator, metal, superconductor) are determined by the values of the charge carrier density and the impurity scattering parameter.

In the case of a nonphononic mechanism of superconductivity, the value of T_c and the other characteristics of pure one-band and multiband superconductors depend on the position of the chemical potential (on the density of charge carriers).[24–29]

The present paper is devoted to a study of the superconducting transition in two-band superconductors containing a nonmagnetic impurity in the case of a nonphononic mechanism of superconductivity.

The two-band model in different variants is widely used to describe the properties of high-T_c superconductors (HTSCs); see, e.g., the reviews[14,30] and also Refs. 31 and 32, etc. In the present paper we consider a version of the two-band model with a nonmagnetic impurity, which incorporates the main features inherent to high-T_c superconducting materials, viz., the layered structure and the variable density of charge carriers. We proceed from the Hamiltonian of a two-band system, making use of the equivalence of treating multilayer and multiband systems and the possibility of reducing a multilayer system to a multiband system.[33–35] For this it is sufficient to carry out some canonical transformations. As a result, the constants of the intraband and interband interactions of the electrons are expressed in terms of the constants of the intralayer and interlayer interactions.[35] Thus the model considers a layered structure and takes into account the presence of intralayer and interlayer electron–electron interactions and also the corresponding kinds of scattering of electrons on the impurities. The two-band model is applicable to both phonon-mediated and nonphononic mechanisms of superconductivity. Even in the most unfavorable case, when all the constants of the intraband and interband electron–electron interactions are repulsive, it is still possible to have high-T_c superconductivity.[25] We note that the presence of overlap of the energy bands at the Fermi surface is a reliably established fact and has been confirmed by numerous band calculations (see, e.g., Refs. 36 and 37).

In the present paper we attempt to construct a theory of impure two-band superconductors with energy gaps, corresponding to *s* pairing, and of superconductors having order parameters with the $d_{x^2-y^2}$ symmetry observed in HTSCs. We study the change in T_c with increasing impurity concentration due to two mechanisms: the change in the chemical potential with increasing impurity concentration, and the scattering of electrons on impurity atoms (intraband and interband). The lowering of T_c with increasing impurity concentration in the metallic phase is studied to the point of complete suppression of the superconductivity ($T_c \to 0$) as the chemical potential goes beyond the range of the effective electron–electron interaction in the case of *s* symmetry of the order parameter. We also establish that in the case of $d_{x^2-y^2}$ symmetry of the order parameter the superconductivity is rapidly suppressed as the impurity concentration is increased.

High-T_c superconducting materials are highly anisotropic and can be treated as quasi-two-dimensional systems.

In purely two-dimensional systems an important role is played by fluctuations of the phase of the order parameters, which radically alter the superconductivity scenario.[38,39]

In quasi-two-dimensional systems, as the three-dimensionality parameter increases, ordinary superconductivity arises at not-too-low concentrations of the charge carriers.[40]

These circumstances allow us to use the mean field approximation in studying the superconducting properties of such systems at carrier densities in the region indicated above, where we assume that it will give a qualitative description of the behavior of the thermodynamic characteristics in a HTSC.

This paper is constructed as follows. In Sec. 2 we present the Hamiltonian of the system and the Green functions averaged over the randomly distributed impurities. In Sec. 3 we obtain the basic equations and expressions for T_c for superconductors with *s* and $d_{x^2-y^2}$ symmetry of the order parameters. In Sec. 4 we carry out a numerical calculation and discuss the results. The results are compared with the experimental data on HTSC materials.

2. MODEL AND BASIC EQUATIONS

The Hamiltonian of a two-band system with impurities which are randomly distributed at points $\mathbf{r}_j$ is written

$$H=\sum_{n\mathbf{k}\sigma}\varepsilon_n(\mathbf{k})a^+_{n\mathbf{k}\sigma}a_{n\mathbf{k}\sigma}$$
$$-\frac{1}{V}\sum_{nn'}\sum_{\mathbf{k}\mathbf{k}'}V_{nn'}(\mathbf{k}\mathbf{k}')a^+_{n\mathbf{k}\uparrow}a^+_{n-\mathbf{k}\downarrow}a_{n'-\mathbf{k}'\downarrow}a_{n'\mathbf{k}'\uparrow}$$
$$+\frac{1}{V}\sum_{nn'}\sum_{\mathbf{k}\mathbf{k}'\sigma}u(\mathbf{k}-\mathbf{k}')\rho(\mathbf{k}-\mathbf{k}')\chi(n\mathbf{k},n'\mathbf{k}')a^+_{n\mathbf{k}\sigma}a_{n'\mathbf{k}'\sigma}, \tag{1}$$

where

$$\varepsilon_n(\mathbf{k})=\xi_n(\mathbf{k})-\mu;\quad \xi_n(\mathbf{k})=\zeta_n+\frac{k_x^2+k_y^2}{2m_n}; \tag{2}$$

$$\chi(n\mathbf{k},n'\mathbf{k}')=\int_{V_0} u^*_{n\mathbf{k}}(\mathbf{r})u_{m\mathbf{k}'}(\mathbf{r})d\mathbf{r};\quad \rho(\mathbf{k})=\sum_j e^{\mathbf{kr}}; \tag{3}$$

V_{mn} are the intraband ($m=n$) and interband ($m\neq n$) interaction constants, V is the volume of the system, V_0 is the unit cell volume, $u_{n\mathbf{k}}(\mathbf{r})$ is the modeling factor of the Bloch functions, $u(\mathbf{k})$ is the Fourier transform of the impurity potential, μ is the chemical potential, and $n,m=1,2$.

Hamiltonian (1) is a generalization of the BCS model to the case of overlap of the energy bands and a nonphononic mechanism of superconductivity. The overlap of the energy band leads to a summation over the band index n and gives rise to an interband $V_{nn'}$ ($n\neq n'$) electron–electron interaction in addition to the intraband interaction V_{nn}. The mechanism of the superconductivity is determined by the signs of the electron–electron interaction constants $V_{nn'}$ and by the region of energy values in which superconducting pairing is possible ($V_{nn'}\neq 0$).[24–26] In the case of a nonphononic mechanism of superconductivity in systems with a lowered charge carrier density, this energy region in which $V_{nn'}\neq 0$ is determined by the dispersion relation (2): $-\mu<\varepsilon_n(k)<\zeta_{cn}-\mu$ (ζ_{cn} is the cutoff energy, which is of the order of the electron energy).

Using perturbation theory[41] (treating the interaction with impurities in (1) as a perturbation), we obtain the following expressions for the normal and anomalous Green functions, respectively, averaged over the positions of the randomly distributed impurities:

$$\overline{G}_n(\mathbf{p},\omega)=-\frac{i\tilde{\omega}_n+\tilde{\varepsilon}_n}{\tilde{\omega}_n^2+\tilde{\varepsilon}_n^2+\tilde{\Delta}_n^2};\quad \overline{F}_n(\mathbf{p},\omega)=\frac{\tilde{\Delta}_n}{\tilde{\omega}_n^2+\tilde{\varepsilon}_n^2+\tilde{\Delta}_n^2}, \tag{4}$$

where

$$\tilde{\omega}_n=\omega+\mathrm{Im}\,M_n(\omega)$$

$$=\omega+\sum_l \frac{1}{2\tau_{nl}}\frac{1}{2\pi}\int_0^{2\pi}d\varphi_l\frac{\tilde{\omega}_l f_l(\omega)}{(\tilde{\omega}_l^2+\tilde{\Delta}_l^2)^{1/2}}; \tag{5}$$

$$\tilde{\Delta}_n=\overline{\Delta}_n+\sum_l \frac{1}{2\tau_{nl}}\frac{1}{2\pi}\int_0^{2\pi}d\varphi_l\frac{\tilde{\Delta}_l f_l(\omega)}{(\tilde{\omega}_l^2+\tilde{\Delta}_l^2)^{1/2}};$$

$$\tilde{\varepsilon}_n=\varepsilon_n+\mathrm{Re}\,M_n(\omega); \tag{6}$$

$$\mathrm{Re}\,M_n(\omega)=-\sum_l \frac{1}{4\tau_{nl}}\frac{1}{2\pi}\int_0^{2\pi}d\varphi_l\ln\frac{D_{cl}^2+\tilde{\omega}_l^2+\tilde{\Delta}_l^2}{D_l^2+\tilde{\omega}_l^2+\tilde{\Delta}_l^2}.$$

Here M_n is the mass operator; τ_{nm} is the relaxation time of the intraband and interband scattering on the impurity potential;

$$f_l(\omega)=\frac{1}{\pi}\left[\arctan\frac{D_{cl}}{(\tilde{\omega}_l^2+\tilde{\Delta}_l^2)^{1/2}}+\arctan\frac{D_l}{(\tilde{\omega}_l^2+\tilde{\Delta}_l^2)^{1/2}}\right]; \tag{7}$$

$$D_{cl}=\zeta'_{cl}-\mu;\quad D_l=\mu-\zeta'_l;\quad \zeta'_{cl}=\zeta_{cl}+\mathrm{Re}\,M_n(0),$$

$$\zeta'_l=\zeta_l+\mathrm{Re}\,M_n(0). \tag{8}$$

We assume a nonphononic mechanism of superconductivity. Accordingly, in the formulas given above the integration over energy is done using dispersion relation (2), assuming that the cutoff energy ζ_{cl} of the integrals is of the order of the electron energy.

The system of equations for the order parameter $\overline{\Delta}_n$ ($n=1,2$) can be reduced to the form

$$\overline{\Delta}_n=\sum_l V_{nl}N_l\frac{1}{2\pi}\int_0^{2\pi}d\varphi_l\overline{\Delta}_l\int_{-D_l}^{D_{cl}}d\tilde{\varepsilon}_l$$

$$\times\frac{\tanh\beta(\tilde{\varepsilon}_l^2+\overline{\Delta}_l^{-2})^{1/2}/2}{2(\tilde{\varepsilon}_l^2+\overline{\Delta}_l^2)^{1/2}}+\sum_l V_{nl}N_l\frac{1}{2\pi}\int_0^{2\pi}d\varphi_l\frac{2\pi}{\beta}$$

$$\times\sum_{\omega>0}\left[\frac{\mathrm{sgn}\,\tilde{\Delta}_l f_l(\omega)}{(u_l^2+1)^{1/2}}-\frac{\overline{\Delta}_l f_l^0(\omega)}{(\omega^2+\overline{\Delta}_l^2)^{1/2}}\right]. \tag{9}$$

Here $f_l^0=f_l|_{\tilde{\omega}=\omega,\ \tilde{\Delta}=\overline{\Delta}}$; N_n is the energy of electron states at the nth band of the Fermi surface, and $u_l=\tilde{\omega}_l/\tilde{\Delta}_l$. The order parameter $\overline{\Delta}_n$ is determined self-consistently from Eqs. (5)–(9).

3. SUPERCONDUCTING TRANSITION TEMPERATURE

3.1. The case of *s* symmetry of the order parameter

Assuming in Eq. (9) that $\Delta_l=\mathrm{const}$, we perform the integration over the angle variables. At temperatures in the critical region ($T\sim T_c$, $\Delta_n\to 0$) we have $u_l\gg 1$. Using the calculational technique proposed in Refs. 15 and 42, we can determine the u_l and obtain a system of equations for $\overline{\Delta}_n$ in the regions of small and large impurity concentrations. From the solvability condition for this system of equations we obtain an equation for the superconducting transition temperature T_c:

$$a\tilde{\xi}_{c1}\tilde{\xi}_{c2}\gamma_1\gamma_2-\tilde{\xi}_{c1}\gamma_1[N_1V_{11}+\overline{N}_1aF(\rho'_c)]-\tilde{\xi}_{c2}\gamma_2$$
$$\times[N_2V_{22}+\overline{N}_1aF(\rho'_c)]+1+[\overline{N}_1(N_2V_{22}-N_2V_{12})$$
$$+\overline{N}_2(N_1V_{11}-N_1V_{21})]F(\rho'_c)=0, \tag{10}$$

where

$$a=N_1N_2(V_{11}V_{22}-V_{12}V_{21});\quad \overline{N}_i=\frac{N_if_1f_2}{N_1f_1+N_2f_2}, \tag{11}$$

$$\tilde{\xi}_l=\int_{-D_l}^{D_{cl}}d\tilde{\varepsilon}_l\frac{\tanh\beta\tilde{\varepsilon}_l/2}{2\tilde{\varepsilon}_l}=\frac{2\pi}{\beta}\sum_{\omega>0}\frac{f_l^0(\omega)}{\omega},$$

$$F(\rho'_c)=\Psi\left(\frac{1}{2}+\frac{\rho'_c}{2}\right)-\Psi\left(\frac{1}{2}\right) \tag{12}$$

$$=\left\{\begin{array}{ll}\dfrac{\pi^2}{4}\rho'_c & \text{for } \rho'_c\ll 1\\ \ln 2\,\gamma\rho'_c & \text{for } \rho'_c\gg 1\end{array}\right.;\ \rho'_c\equiv\rho'\Bigg|_{T=T_c},$$

Ψ is the logarithmic derivative of the Γ function, and

$$\rho'_c=f_2\rho_1+f_1\rho_2;\quad \rho_1=\frac{1}{2\tau_{12}\pi T_c};$$

$$\rho_2=\frac{1}{2\tau_{21}\pi T_c};\quad \gamma_l=f_l/f_l^0. \tag{13}$$

The solutions of equation (10) depend on the values of the chemical potential (charge carrier density). In analytical investigations we will consider certain intervals of the chemical potential in which the conditions $|D_{cn}|/T_c, |D_n|/T_c \gg 1$ hold, and also the points $D_n=0$ and $D_{cn}=0$ ($n=1,2$).

Then, in the regions of small and large values of the parameters ρ_n ($\rho_n \ll 1$ and $\rho_n \gg 1$, respectively), the equation for T_c can be approximated by the expression

$$\ln\frac{T_c}{\overline{T}_{c0}} = -\alpha\left\{\Psi\left(\frac{1}{2}+\frac{f_2}{4\tau_{12}\pi T_c}+\frac{f_1}{4\tau_{21}\pi T_c}\right)-\Psi\left(\frac{1}{2}\right)\right\}, \tag{14}$$

or

$$T_c = \overline{T}_{c0} - \alpha\frac{\pi}{8\tau_{12}}\left(f_2+\frac{\tau_{12}}{\tau_{21}}f_1\right) \quad \text{for } \rho_n \ll 1, \tag{15}$$

$$T_c = \overline{T}_{c0}^{1/(1-\alpha)}\left[\frac{\gamma}{\pi\tau_{12}}\left(f_2+\frac{\tau_{12}}{\tau_{21}}f_1\right)\right]^{\alpha/(\alpha-1)} \quad \text{for } \rho_n \gg 1, \tag{16}$$

$$\overline{T}_{c0} = \frac{2\gamma}{\pi}E\exp\left\{-\frac{N_1V_{11}\gamma_1+N_2V_{22}\gamma_2}{2\gamma_1\gamma_2 a}+\frac{(b_0^2-4\gamma_1\gamma_2 a c_0)^{1/2}}{2\gamma_1\gamma_2 a}\right\}, \tag{17}$$

where

$$b_0 = N_1V_{11}\gamma_1+N_2V_{22}\gamma_2-\gamma_1\gamma_2 aQ,$$

$$c_0 = 1-N_2V_{22}\gamma_2 Q,$$

$$\alpha = \frac{1}{2}\left\{\frac{\overline{N}_1\gamma_1+\overline{N}_2\gamma_2}{\gamma_1\gamma_2}-\frac{b_0(\overline{N}_1\gamma_1+\overline{N}_2\gamma_2)/\gamma_1\gamma_2-2\overline{N}_1(N_2V_{22}-N_2V_{12})-2\overline{N}_2(N_1V_{11}-N_1V_{21})}{(b_0^2-4\gamma_1\gamma_2 a c_0)^{1/2}}\right\}. \tag{18}$$

Those quantities appearing in these expressions which have a substantial dependence on the value of the chemical potential and also on the impurity concentration are given below. Let us give analytical expressions for them at the points $\mu=\zeta_2'$, $\mu=\zeta_{c1}'$, and in the overlap region of the energy bands, $\zeta_2'<\mu<\zeta_{c1}'$:

1) for $\mu=\zeta_2'$ we have

$$E=(D_1D_{c1})^{1/4}D_{c2}^{1/2}, \quad Q=\ln\frac{D_{c2}}{(D_1D_{c1})^{1/2}}, \tag{19}$$

2) $\zeta_2'<\mu<\zeta_{c1}'$

$$E=(D_1D_{c1}D_2D_{c2})^{1/4}, \quad Q=\ln\left(\frac{D_2D_{c2}}{D_1D_{c1}}\right)^{1/2}, \tag{20}$$

3) $\mu=\zeta_{c1}'$

$$E=(D_2D_{c2})^{1/4}D_1^{1/2}, \quad Q=\ln\frac{D_1}{(D_2D_{c2})^{1/2}}. \tag{21}$$

In the regions $\mu<\zeta_2'$ and $\mu>\zeta_{c1}'$ the expression for the superconducting transition temperature depends on the impurity concentration only through this dependence of the chemical potential and its renormalization due to the scattering of electrons on impurities. For $\mu>\zeta_{c2}'$ the temperature $T_c\to 0$. For $D_1=D_{c1}=D_2=D_{c2}=\omega_D$, the analytical values (15) and (16) agree with previous results[13] and correspond to values of the superconducting transition temperature for ordinary two-band superconductors with low and high impurity concentrations, respectively. Here T_c turns out to depend on the impurity concentration by a power law (in the region of high impurity concentrations), and, consequently, for such a system there cannot be a critical concentration at which T_c goes to zero.

In the case of a nonphononic mechanism of superconductivity the expression (16) for T_c contains both explicit and implicit dependence on the impurity concentration. The explicit dependence is contained in the second factor, which falls off with increasing concentration by a power law and cannot lead to a value $T_c=0$. The first factor in (16), $\overline{T}_{c0}^{1/(1-\alpha)}$, characterizes the implicit dependence on the impurity concentration through the renormalization of the chemical potential. Here a situation can arise in which $\overline{T}_{c0}=0$ on account of the chemical potential going beyond the range of the effective electron–electron interaction. This leads to vanishing of the superconductivity ($T_c=0$).

We also note that it follows from Eq. (14) that the Anderson theorem[12] is violated as a consequence of the overlap of the energy bands at the Fermi surface and because of the electron–hole asymmetry.

3.2. The case of $d_{x^2-y^2}$ symmetry of the order parameter

Let us consider a quasi-two-dimensional electron system with a cylindrical Fermi surface and an effective electron–electron interaction

$$V_{nm}(kk') = V_{nm}\cos 2\varphi_n \cos 2\varphi_m, \tag{22}$$

where φ_n is the polar angle in the (x,y) plane for the nth band of the Fermi surface.

Such a dependence of the pair potential leads to order parameters $\Delta_n=\Delta_n^0\cos 2\varphi_n$, corresponding to $d_{x^2-y^2}$ symmetry. In this case the order parameter is determined by the system of equations

$$\overline{\Delta}_n=\sum_l V_{nl}N_l\cos 2\varphi_n\frac{1}{2\pi}\int_0^{2\pi}d\varphi_l\cos 2\varphi_l\int_{-D_l}^{D_{cl}}d\tilde{\varepsilon}_l \times\frac{\tanh\beta(\tilde{\varepsilon}_l^2+\overline{\Delta}_l^2)^{1/2}/2}{2(\tilde{\varepsilon}_l^2+\overline{\Delta}_l^2)^{1/2}}+\frac{2\pi}{\beta}\sum_{l,\omega<0}V_{nl}N_l\cos 2\varphi_n\frac{1}{2\pi} \times\int_0^{2\pi}d\varphi_l|\cos 2\varphi_l|\left(\frac{f_l(\omega)}{(u_l^2+1)^{1/2}}-\frac{\overline{\Delta}_l f_l^0(\omega)}{(\omega^2+\overline{\Delta}_l^2)^{1/2}}\right), \quad (23)$$

$$u_n-\sum_l\frac{1}{2\tau_{nl}\overline{\Delta}_l}\frac{1}{2\pi}\int_0^{2\pi}d\varphi_l\,\mathrm{sgn}\,\tilde{\Delta}_l\frac{(u_l-u_n)f_l(\omega)}{(u_l^2+1)^{1/2}}=\frac{\omega}{\overline{\Delta}_n}. \quad (24)$$

At temperatures in the region near T_c ($u_m\gg 1$), in the case of $d_{x^2-y^2}$ symmetry of the order parameter we obtain after integrating over the angle variables

$$\overline{\Delta}_n^0=\sum_l V_{nl}N_l\tilde{\zeta}_l\gamma_l\overline{\Delta}_l^0+\frac{2\pi}{\beta} \times\sum_{l,\omega>0}V_{nl}N_l\left\{f_l(\omega)\left[\frac{1}{2u_l^0}-\frac{3}{16u_l^{03}}-\frac{u_l^{0\prime}}{2u_l^{02}}\right]-\frac{\overline{\Delta}_l^0 f_l^0(\omega)}{\omega}\right\}, \quad (25)$$

where

$$u_n^0=\frac{\omega}{\overline{\Delta}_n^0}-\sum_l\frac{1}{2\tau_{nl}\overline{\Delta}_l^0}f_l,\quad u_n^{0\prime}=-\frac{1}{2\pi}\sum_l\frac{1}{8\tau_{nl}}\frac{1}{\overline{\Delta}_l^0 u_l^{02}}.$$

On the basis of (24) and (25) we obtain an equation for determining the superconducting transition temperature:

$$a(\gamma_1\tilde{\zeta}_1-f_1F_1)(\gamma_2\tilde{\zeta}_2-f_2F_2)-N_1V_{11}(\gamma_1\tilde{\zeta}_1-f_1F_1) -N_2V_{22}(\gamma_2\tilde{\zeta}_2-f_2F_2)+1=0, \quad (26)$$

where

$$F_n=\Psi\left(\frac{1}{2}+\frac{f_1}{4\tau_{n1}\pi T_c}+\frac{f_2}{4\tau_{n2}\pi T_c}\right)-\Psi\left(\frac{1}{2}\right).$$

In the region of overlap of the energy bands $\zeta_2'<\mu<\zeta_{c1}'$ ($|D_{cn}|/T_c\gg 1$, $|D_n|/T_c\gg 1$), Eq. (26) can be reduced to

$$\ln\frac{T_{c0}}{T_c}=\frac{F_1+F_2}{2}+\frac{(b_0^2-4a\gamma_1\gamma_2c_0)^{1/2}-(b^2-4a\gamma_1\gamma_2c)^{1/2}}{2a\gamma_1\gamma_2}. \quad (27)$$

The quantities b_0 and c_0 are defined in (18), and b and c differ from b_0 and c_0 by the replacement

$$Q\to Q+F_1-F_2,$$

where Q is given by formulas (19)–(21).

For the case of low impurity concentrations ($1/\tau_{nm}T_c\ll 1$) we obtain

$$T_c=T_{c0}-\frac{\pi}{4}\left[\frac{f_1}{4\tau_{11}}+\frac{f_2}{4\tau_{12}}+\frac{f_1}{4\tau_{21}}+\frac{f_2}{4\tau_{22}} +\left(\frac{f_1}{4\tau_{11}}+\frac{f_2}{4\tau_{12}}-\frac{f_1}{4\tau_{21}}-\frac{f_2}{4\tau_{22}}\right)\frac{b_0-2N_2V_{22}f_2}{(b_0^2-4a\gamma_1\gamma_2c_0)^{1/2}}\right]. \quad (28)$$

For the case of high impurity concentrations ($1/\tau_{nm}T_c\gg 1$) we have

$$T_c^2=\frac{c_0-b_0\ln l_1\sqrt{D_1D_{c1}}+N_2V_{22}f_2\ln(l_1/l_2)+a\gamma_1\gamma_2\ln l_1\sqrt{D_1D_{c1}}\ln l_2\sqrt{D_2D_{c2}}}{-b_0(\pi^2/6)l_1^2+[a\gamma_1\gamma_2\ln(l_1/l_2)-2N_2V_{22}f_2]R_-+a\gamma_1\gamma_2R_+\ln l_1l_2D_1D_{c1}}, \quad (29)$$

where

$$R_\pm=\frac{\pi^2}{12}(l_2^2\pm l_1^2);\quad \frac{1}{l_n}=\frac{f_1}{2\tau_{n1}}+\frac{f_2}{2\tau_{n2}}. \quad (30)$$

Formulas (28) and (29) contain explicit dependence on the impurity concentration (through τ_{nm}) and also implicit dependence due to the renormalization of the chemical potential.

We see from expression (29) that T_c goes to zero at a certain critical impurity concentration $n_i=n_{ic}$ determined from the condition

$$c_0-b_0\ln l_1\sqrt{D_1D_{c1}}+N_2V_{22}f_2\ln\frac{l_1}{l_2} +a\gamma_1\gamma_2\ln l_1\sqrt{D_1D_{c1}}\ln l_2\sqrt{D_2D_{c2}}=0. \quad (31)$$

We write the solution of (31) in the form

$$n_{ic}=\frac{\pi T_{c0}}{2\gamma}\sqrt{l_1'l_2'}(\sqrt{l_1'/l_2'})^{\delta}, \quad (32)$$

where

$$T_{c0}=\frac{2\gamma}{\pi}\sqrt{D_1D_{c1}}\exp\left(-\frac{b_0}{2a\gamma_1\gamma_2}+\frac{(b_0^2-4a\gamma_1\gamma_2c_0)^{1/2}}{2a\gamma_1\gamma_2}\right),$$

$$\delta=\frac{N_1V_{11}f_1-N_2V_{22}f_2+a\gamma_1\gamma_2Q}{[(N_1V_{11}f_1-N_2V_{22}f_2+a\gamma_1\gamma_2Q)^2+4N_2V_{12}N_1V_{21}f_1f_2]^{1/2}},$$

$$l_n'=l_nn_i. \quad (33)$$

Formulas (28) and (29) for $N_2=0$ ($a=N_2V_{22}=0$) correspond to the one-band case and have the form

$$T_c=T_{c0}-\frac{\pi}{8}\frac{f_1}{\tau_{11}}\quad\text{for}\quad\frac{1}{\tau_{11}T_c}\ll 1, \quad (34)$$

$$T_c^2=\frac{N_1V_{11}f_1\ln(\sqrt{D_1D_{c1}}/f_1)2\tau_{11}-1}{N_1V_{11}f_1(\pi^2/6)(4\tau_{11}^2/f_1^2)}\quad\text{for}\quad\frac{1}{\tau_{11}T_c}\gg 1.$$

For the critical impurity concentration in this case we have

$$n_{ic}=\frac{\pi T_{c0}}{2\gamma}\frac{1}{l_1^0}, \tag{35}$$

where

$$T_{c0}=\frac{2\gamma}{\pi}\sqrt{D_1D_{c1}}\exp\left(-\frac{1}{N_1V_{11}f_1}\right), \quad l_1^{0\prime}=l_1'|_{f_2=0}.$$

Formulas (34) and (35) agree with the corresponding expressions in Ref. 16 for $D_1=D_{c1}=\omega_D$, $f_1=1$, $l_1^{0\prime}=\alpha$ (α is defined in Ref. 16). It is easy to see on the basis of (32) that for a system with overlapping energy bands the value of T_{c0} and the values of the intraband and interband impurity-scattering potentials will have a substantial influence on the value of n_{ic}.

4. NUMERICAL CALCULATIONS AND DISCUSSION OF THE RESULTS

Let us obtain the explicit dependence of the superconducting transition temperature on the impurity concentration, taking into account the influence of the impurity on the chemical potential and also the electron scattering processes, both intraband and interband.

Equations (10) and (26) obtained above, which determine the value of T_c, must be supplemented by the equation determining the chemical potential:

$$n_0\pm n_i(z_B-z_A)=\sum_{m\mathbf{k}\omega} e^{i\omega 0^+}\overline{G}_m(\mathbf{k}\omega). \tag{36}$$

Here n_0 is the charge carrier density in the pure substance, and z_B-z_A is the difference between the valences of the impurity atom and host substance. The plus and minus signs correspond to electronic and hole conduction, respectively.

Substituting expression (4) for $T=T_c$ into (36) and doing the integration over energy and frequency, we reduce the latter equation to the form

$$\begin{aligned}
&n_0+n_i(z_B-z_A)\\
&=\sum_m\Big[\zeta_{cm}+x_m-\mu-(\zeta_m+x_m-\mu)-|\zeta_{cm}+x_m-\mu|\\
&\quad+|\zeta_m+x_m-\mu|\Big]+\frac{1}{\pi}\sum_m\left\{y_m\ln\frac{y_m^2+(\zeta_{cm}+x_m-\mu)^2}{y_m^2+(\zeta_m+x_m-\mu)^2}\right.\\
&\quad-2(\zeta_{cm}+x_m-\mu)\left[\arctan\frac{\zeta_{cm}+x_m-\mu}{y_m}\right.\\
&\quad\left.-\frac{\pi}{2}\operatorname{sgn}\frac{\zeta_{cm}+x_m-\mu}{y_m}\right]+2(\zeta_m+x_m-\mu)\\
&\quad\times\left.\left[\arctan\frac{\zeta_m+x_m-\mu}{y_m}-\frac{\pi}{2}\operatorname{sgn}\frac{\zeta_m+x_m-\mu}{y_m}\right]\right\},
\end{aligned} \tag{37}$$

where the quantities $x_m=\mathrm{Re}M_n(0)$ and $y_m=\mathrm{Im}M^*(0)$ satisfy the system of equations ($n,m=1,2$)

$$x_n=-\frac{1}{4\pi}\sum_m\frac{1}{\tau_{nm}}\ln\frac{y_m^2+(\zeta_{cm}+x_m-\mu)^2}{y_m^2+(\zeta_m+x_m-\mu)^2},$$

$$y_n=\sum_m\frac{1}{2\pi\tau_{nm}}\left[\arctan\frac{\zeta_{cm}+x_m-\mu}{y_m}+\arctan\frac{\mu-(\zeta_m+x_m)}{y_m}\right]. \tag{38}$$

We introduce the quantities

$$\tilde{n}_i=\frac{n_i}{2N_1}, \quad \tilde{n}_0=\frac{n_0}{2N_2},$$

and use the definitions

$$\begin{aligned}
&\frac{1}{2\tau_{nm}}=\tilde{n}_i\eta_{nm};\\
&\eta_{nm}=\frac{N_1N_m}{2}\int_0^{2\pi}d\varphi|u(\mathbf{p}_{F_n}-\mathbf{p}_{F_m})|^2|\chi(n\mathbf{p}_{F_n},\ m\mathbf{p}_{F_m})|^2.
\end{aligned} \tag{39}$$

The system of equations (10), (37), and (38) for the case of s symmetry of the order parameter and the system of equations (26), (37), and (38) for $d_{x^2-y^2}$ symmetry are solved self-consistently with allowance for the definitions $D_{cm}=\zeta_{cm}+x_m-\mu$ and $D_m=\zeta_m+x_m-\mu$. Here we choose the following values of the parameters of the theory:

$$\begin{aligned}
&\eta_{22}=\eta_{11}\frac{N_2}{N_1}; \quad \frac{N_2}{N_1}=0.2; \quad \eta_{12}=\eta_{21}\frac{N_2}{N_1};\\
&N_1V_{11}=0.2; \quad N_2V_{22}=0.4; \quad N_2V_{12}=0.018;\\
&N_1V_{21}=N_2V_{12}\frac{N_1}{N_2}.
\end{aligned} \tag{40}$$

Figure 1 shows the dependence of T_c on the impurity concentration for the case of $d_{x^2-y^2}$ symmetry of the order parameter. For an isovalent impurity ($z_B=z_A$) (see Fig. 1a) the rapid drop in T_c in the absence of interband scattering (curve *1*, $\eta_{21}=0$) is due to the destruction of electron pairs as a result of intraband scattering on impurities and the presence of a critical impurity concentration n_{ic}, above which superconductivity does not occur ($T_c=0$). As the interband scattering is increased (curve *2*, $\eta_{21}=0.05$, and curve *3*, $\eta_{21}=0.1$) the superconductivity is suppressed even faster. We note that the suppression of superconductivity occurs in the region of overlap of the energy bands.

Figure 1b shows the dependence of T_c on $\tilde{n}_i$ for $z_B-z_A=1$: curve *1′* corresponds to the case of no scattering of electrons on the impurity potential, and curve *1* corresponds to the absence of interband scattering on impurities ($\eta_{21}=0$). As the interband scattering increases (curve *2*, $\eta_{21}=0.05$, and curve *3*, $\eta_{21}=0.1$) a change in curvature of the curves is clearly seen in the region where the energy bands overlap, and there is a ''plateau'' (or ''step'') on the curve of T_c versus $\tilde{n}_i$. This behavior is a clear demonstration of the role of the filling factor of the energy bands (with increasing impurity concentration there is growth of the chemical potential, leading to a decrease in T_c) and of the scattering of electrons on the impurity potential. The formation of a ''plateau'' on the T_c versus $\tilde{n}_i$ curve is due to a decrease in the interband scattering near the boundary of the first effective energy band.

The foregoing analysis of the dependence of T_c on the impurity concentration was done with allowance for processes of electron scattering (intra- and interband) on the

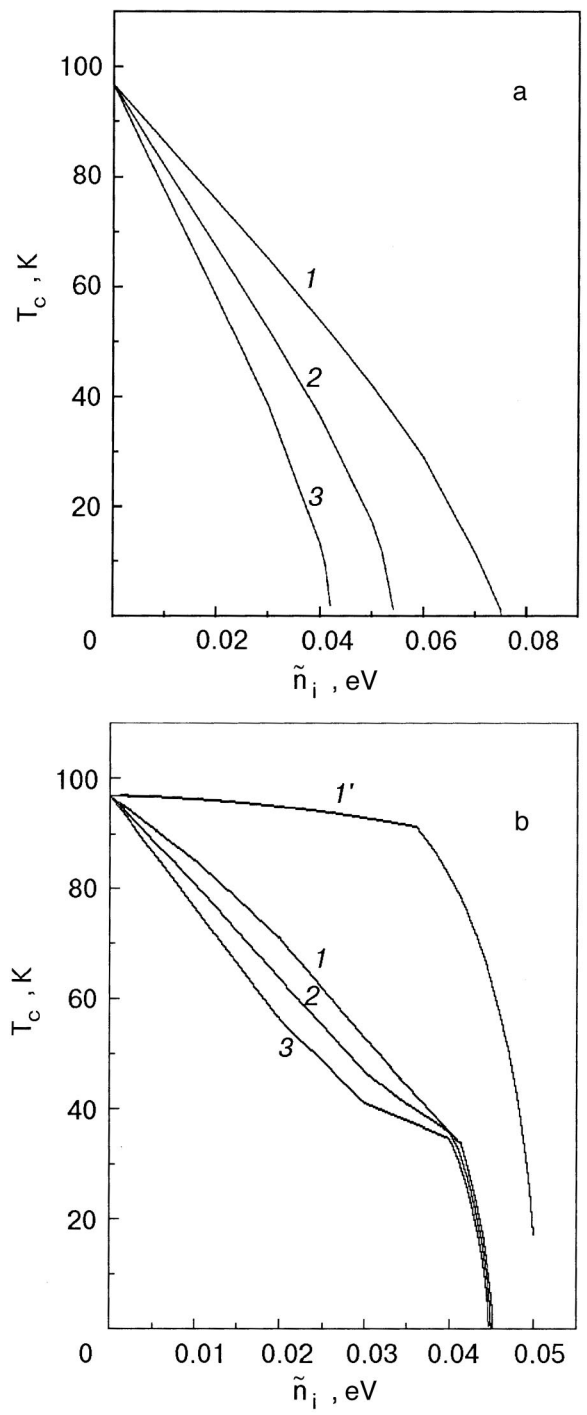

FIG. 1. Superconducting transition temperature T_c versus the impurity concentration $\tilde{n}_i$ for $z_B = z_A$ (a) and $z_B - z_A = 1$ (b) for the case of $d_{x^2-y^2}$ symmetry of the order parameter at $\eta_{11} = 0.5$, $\eta_{21} = 0$ (curve *1*), $\eta_{11} = 0.5$, $\eta_{21} = 0.05$ (curve *2*), and $\eta_{11} = 0.5$, $\eta_{21} = 0.1$ (curve *3*). Curve *1′* corresponds to $\eta_{11} = \eta_{21} = 0$.

impurity potential and in the absence of such scattering processes, in which case the impurity affects only the chemical potential. The onset of these processes in highly anisotropic superconductors is determined by the position of the substitutional impurity in the crystal.

Let us use these results to explain the experimental data on the dependence of T_c on the impurity concentration in HTSCs.

Figure 2 shows the experimental results on the dependence of T_c on the concentration of zinc as a substituent for

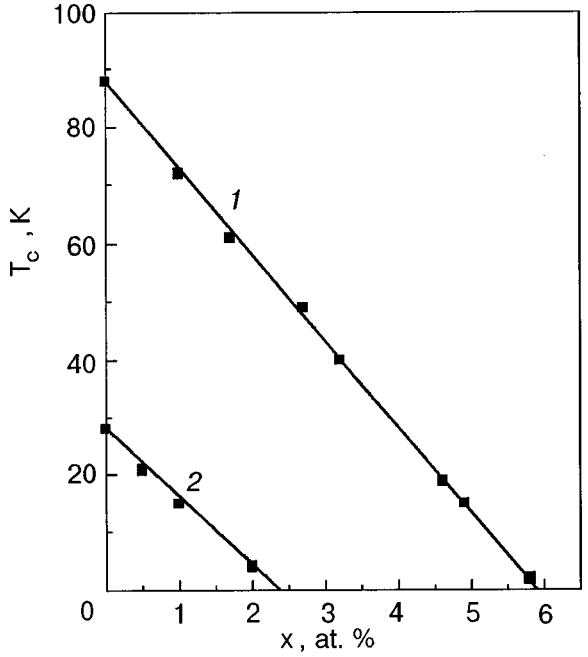

FIG. 2. Experimental dependence of the superconducting transition temperature T_c on the impurity concentration x in $YBa_2(Cu_{1-x}Zn_x)_3O_{7-\delta}$ (*1*) and $La_{1.8}Sr_{0.2}Cu_{1-x}Zn_xO_4$ (*2*) (Ref. 37), with substitution for the Cu atoms in the CuO_2 plane.

copper in the CuO_2 plane in yttrium and lanthanum ceramics.[9,43] Here the isovalent impurity Zn replaces Cu in the CuO_2 plane, which is responsible for the superconductivity. In this case processes of intra- and interband scattering on the impurity arise. A qualitative picture of the suppression of superconductivity, corresponding to Fig. 2, is given by the theoretical curves in Fig. 1a. In the case considered, that of $d_{x^2-y^2}$ symmetry of the order parameter (Fig. 1a), the superconductivity is completely suppressed by a nonmagnetic impurity, in agreement with the experimental data.

Figure 3 shows the experimental dependence of T_c on the impurity concentration in $YBa_2Cu_{3-x}M_xO_{7-y}$ when the Cu in the CuO_2 plane is replaced by the substitutional impurity M = Zn (curve *1*) and when the Cu in the chain is replaced by Al and Ga (curves *2* and *3*).[3,9] Figure 4 shows the theoretical curves of T_c versus the concentration of an isovalent impurity, e.g., Zn, for the cases of $d_{x^2-y^2}$ and *s* symmetry of the order parameter (curves *1* and *1′*, respectively), and curves *2* and *3* are for nonisovalent impurities (e.g., Al and Ga). In the first case the substitutional impurity is found in the CuO_2 plane, and its introduction gives rise to scattering of electrons on an impurity potential, which leads to a rapid decline of T_c with increasing impurity concentration. The introduction of Al or Ga in place of Cu in the chain, on the other hand, leads only to a change in the effective valence of the Cu in the CuO_2 plane and, hence, to a change in the chemical potential. We have a more rapid suppression of the superconductivity when the copper is replaced by zinc than for the substitution of aluminum or gallium, in qualitative agreement with the experimental data of Fig. 3.

Figure 1 shows the dependence of T_c on the impurity concentration in the metallic phase ($n_0 \neq 0$). In the case of an insulator ($n_0 = 0$) upon doping with $z_A \neq z_B$, superconductivity can arise in the system at rather high values of the superconducting transition temperature. The dependence of T_c on

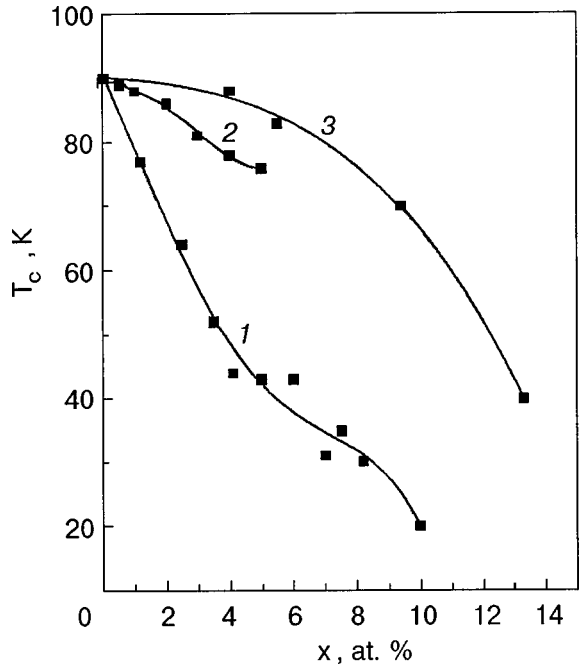

FIG. 3. Experimental dependence of the superconducting transition temperature T_c on the impurity concentration x in $YBa_2Cu_{3-x}M_xO_{7-y}$ in the orthorhombic phase. Curve *1* corresponds to the substitution of zinc for copper in the CuO_2 plane,[2] and curves *2* and *3* to the substitution of Ga and Al, respectively, for copper in the chain.

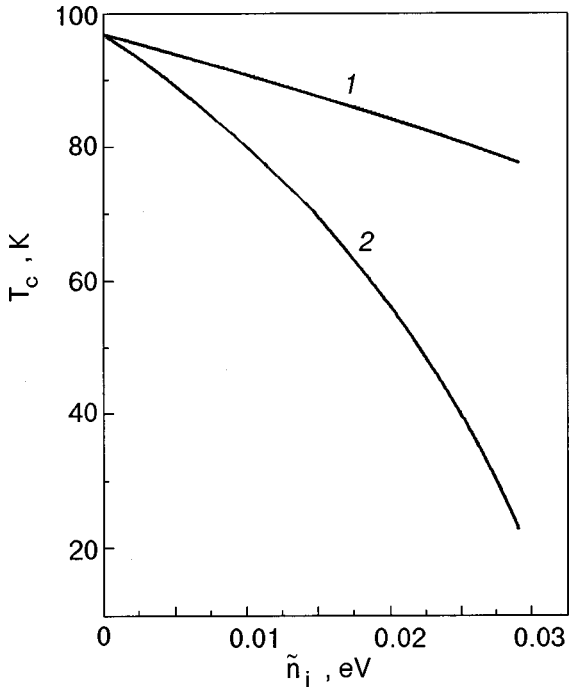

FIG. 5. Theoretical dependence of the superconducting transition temperature T_c on the impurity concentration $\tilde{n}_i$ for $\tilde{n}_0=0.22$ eV (metal) with $d_{x^2-y^2}$ symmetry of the order parameter for $\eta_{11}=0.2$, $\eta_{21}=0.02$, $z_B-z_A=-1$ (curve *1*) and $\eta_{11}=0.5$, $\eta_{21}=0.05$, and $z_B-z_A=-3$ (curve *2*).

the impurity (charge carrier) concentration is a bell-shaped curve for both the cases of s and $d_{x^2-y^2}$ symmetry of the order parameter, provided that one does not take into account the scattering on the impurity potential ($1/\tau_{nm}=0$); see also Ref. 21. These results are in qualitative agreement with the dependence of T_c on the carrier concentration in the CuO_2 plane for $(La_{1-x}Sr_x)_2CuO_4$ (Refs. 9 and 44) and certain copper-oxide superconductors,[9,45] when the impurity is introduced outside the CuO_2 plane and, hence, there is no scattering on the impurity. Taking the scattering processes into account ($1/\tau_{nm}\neq 0$) in the doping of an insulator preserves the bell-shaped dependence of T_c on the carrier concentration in the case of s symmetry of the order parameter, lowering it and narrowing the region of impurity concentrations in which superconductivity can occur. Consequently, the superconducting phase is determined by the concentration of charge carriers and the parameters of the impurity scattering ($1/\tau_{nm}\neq 0$). This result is in qualitative agreement with those obtained in Ref. 22, where a single-band model with s pairing and the concept of a disordered localized impurity was used. In the doping of an insulator in the case of $d_{x^2-y^2}$ symmetry of the order parameter it is impossible to achieve high values of T_c because of the rapid destruction of Cooper pairs by the intra- and interband scattering on impurities. Consequently, the introduction of a substitutional impurity in the CuO_2 plane in systems of that kind does not give rise to high-T_c superconductivity.

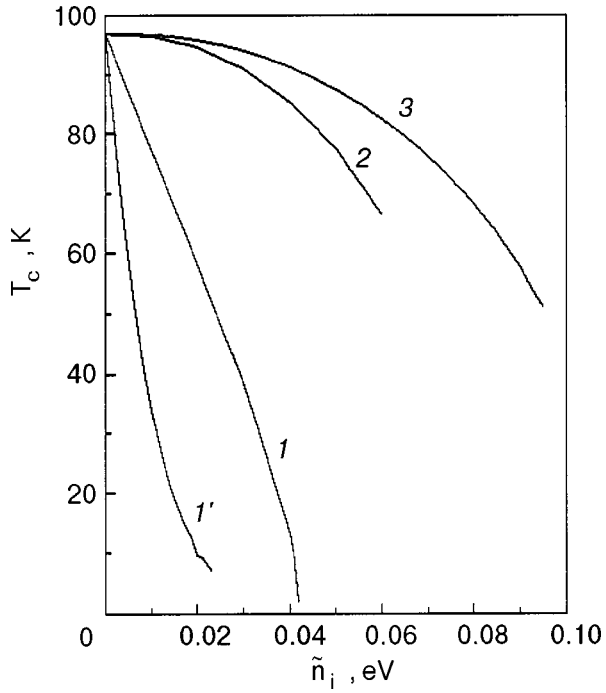

FIG. 4. Theoretical dependence of the superconducting transition temperature T_c on the impurity concentration $\tilde{n}_i$ for $\tilde{n}_0=0.22$ eV (metal): curves *1* and *1′* are for an isovalent impurity in the case of $d_{x^2-y^2}$ symmetry of the order parameter for $\eta_{11}=0.5$ and $\eta_{21}=0.1$ and for s symmetry of the order parameter for $\eta_{11}=3.5$ and $\eta_{21}=0.1$, respectively; curves *2* and *3* are for a nonisovalent impurity at $\eta_{11}=\eta_{21}=0$ and $z_B-z_A=-1.5$ and -1.0, respectively.

The theoretical curves in Fig. 5 describe the dependence of T_c on the concentration of a nonisovalent substitutional impurity in the metallic phase when it is substituted for copper in the CuO_2 plane or in the plane and chain. In this case both a mechanism of filling of the energy bands and processes of electron scattering on the impurity potential will come into play.

5. CONCLUSION

Characteristic features of HTSCs include an overlap of the energy bands at the Fermi surface, which is due to the

layered structure of the substance, and a variable charge carrier density, which is related to the oxygen or impurity content. In this paper these features have been taken into account in an attempt to explain the existing experimental data on the dependence of the superconducting transition temperature on the impurity concentration in these materials.

The particular form of the nonphononic mechanism of superconductivity was not precisely specified, but it was assumed that it involves some electron–boson interaction. If retardation is ignored, the description of the two-band system with such an interaction reduces to the BCS model generalized to the two-band case with a cutoff of the integrals over energy in the basic equations in accordance with the dispersion relation (2). Starting from the two-band Hamiltonian (1), which takes into account the interaction of the electrons with randomly distributed nonmagnetic impurities, we apply perturbation theory[41] and perform an averaging over the randomly distributed nonmagnetic impurities.

We have investigated systems having s and $d_{x^2-y^2}$ symmetry of the order parameter. To obtain the explicit dependence of the superconducting transition temperature T_c on the impurity concentration n_i, it is necessary, for a specified n_i, to solve self-consistently the system of equations (10), (37), and (38) and also (26), (37), and (38), which determine T_c, $\mathrm{Re}M_n(\omega)$, $\mathrm{Im}M_n(\omega)$, $n=(1,2)$ (M_n is the mass operator corresponding to the nth energy band).

When a substitutional impurity is introduced, there are two possible mechanisms by which it can influence T_c: through a change in the chemical potential on account of the valence effect and the scattering (inter- and intraband) of electrons on randomly distributed impurities, and by an explicit dependence on the impurity concentration. The effect of these mechanisms individually or jointly is determined by the position of the substitutional impurity in the highly anisotropic systems. In addition, the behavior of T_c depends radically on the initial state of the system (metal or insulator). In the case when the valences of the impurity and host atoms are the same (an isovalent impurity $z_B=z_A$), for a system with a metallic initial state the superconducting transition temperature T_c decreases on doping.

We note that for an isovalent impurity the curvature of the curves in the case of s symmetry of the order parameter is positive, whereas for $d_{x^2-y^2}$ symmetry we observe a negative curvature (see curves *1* and *1′* in Fig. 4). This is one of the important ways that the symmetry of the order parameter is manifested. Because of the characteristic electron–hole asymmetry (as a manifestation of anisotropy) in the systems under study with a nonphononic mechanism of superconductivity, only the intraband scattering of electrons on impurities makes the value of T_c depend substantially on the impurity concentration n_i. Thus for systems with s symmetry of the order parameter, the electron–hole asymmetry and also the scattering (inter- and intraband) of electrons on impurities leads to violation of the Anderson theorem.[12] We note that for systems with $d_{x^2-y^2}$ symmetry of the order parameter in the two-band case the critical impurity concentration n_{ic} is proportional to T_{c0} and inversely proportional to the total value of the scattering potentials for impurity scattering and can turn out larger than in the one-band case because of the higher value of T_{c0}, in spite of the fact that the intra- and interband scattering is an additional factor that decreases T_c [see Eqs. (32) and (35)].

An important role in the dependence of T_c on the impurity concentration n_i is played by the difference of the valence of an impurity atom and the atom it replaces ($z_B \neq z_A$). In particular, we have shown that a weak dependence of T_c on n_i can arise (a ''plateau''). The onset of the ''plateau'' is due to the interband scattering on impurities and to the decrease of this scattering near the boundary of the first effective energy band ($\mu=\zeta'_{c1}$) (Fig. 1b). We note that an alternative explanation of the steplike dependence mentioned above might be the presence of a so-called extended van Hove singularity arising on account of topological electronic transitions[14,28] or the overlap of three bands at the Fermi surface[29] In the region where the energy bands overlap, the curvature of the curves will change from negative to positive, regardless of the type of symmetry of the order parameter, as the interband scattering on impurities increases (Fig. 1b). Such a change in the curvature of the curves of T_c versus n_i is inherent only to systems with overlapping energy bands and is due to interband scattering of electrons on impurities. In the case when $z_B \neq z_A$, for a system initially in a metallic state (see Fig. 1b) the superconducting transition temperature T_c decreases on doping, and a ''plateau'' is formed. In the case of $d_{x^2-y^2}$ symmetry T_c goes to zero at $n_i=n_{ic}$.

It should be noted that the proposed theory of superconductivity with a nonphononic mechanism can also be applied to the case of a phonon-mediated mechanism with a lowered (or small) charge carrier density, where the electron–hole asymmetry is also clearly manifested. In that case one should make the substitutions $D_{cl}\to\omega_{Dl}$, $D_l\to\mu-\zeta_l$ (Ref. 26).

The two-band model proposed in this paper incorporates the basic features of HTSC materials (layered structure and variable carrier density) and can be used to study the behavior of T_c as a function of impurity concentration in these materials. Here it must be kept firmly in mind that under these conditions it is necessary to take into account the mechanism of electron scattering on impurities or the change in the chemical potential, or both simultaneously. For example, if the isovalent impurity Zn is substituted for Cu in the CuO_2 plane of an yttrium ceramic, then the intra- and interband scattering of electrons on the impurity potential must be taken into account, since this plane is responsible for the superconductivity and in it the periodicity of the crystal structure is disrupted on account of the random distribution of the substitutional impurity. We obtain a rapid drop in T_c with increasing impurity concentration (curves *1* and *1′* in Fig. 4). The replacement of Cu by the nonisovalent impurity Al or Ga in the chain in the same ceramic leads only to a change in the effective valence of the Cu in the CuO_2 plane[9] and, hence, only to a change in the chemical potential and to the dependence of T_c shown by curves *2* and *3* in Fig. 4. This approach makes it possible to obtain a strong decline in T_c with increasing Zn concentration and a weak decline with increasing Al concentration, as is observed in the experimental studies.

This model also contains other possibilities for describing the experimental data. For example, if a nonisovalent substitutional impurity is introduced in the CuO_2 plane, then

all of the mechanisms considered above for the influence of impurities on T_c will be manifested (Fig. 5).

In this paper the influence of impurities was investigated in a two-band model[19,20] in which the transfer of Cooper pairs from one band to the other takes place by whole pairs. The case of pure superconductors, with allowance for the various interband processes, was considered by the present authors in Ref. 26, where the problem reduces to an effective three-band model (with order parameters Δ_{11}, Δ_{22}, and Δ_{12}), which leads to an increase in T_c in comparison with the case considered in the present paper in the limit of a pure substance. The introduction of an impurity into that ''three-band'' model will lead to additional interband scattering on the impurity potential and will promote a more rapid suppression of the ratio T_c/T_{c0} with increasing impurity concentration. These additional effects can only lead to quantitative differences from the results obtained above, without altering the picture as a whole.

As we have said, here we have considered a quasi-two-dimensional system at charge carrier concentrations that are not too small and have used the mean field approximation. The fluctuation of the phase of the order parameter for the two-dimensional system with impurities was taken into account on the basis of a simple one-band model with *s* pairing in Ref. 46. It was found that the temperature T_{BKT} (the Berezinskiĭ–Kosterlitz–Thouless temperature) in the dirty limit differs weakly (by an amount $\sim 1/\tau_{tr}\varepsilon_F \ll 1$) from T_c^{MF}, which, according to the Anderson theorem,[12] does not depend on the impurity concentration. We note that in this model, in the presence of the electron–hole symmetry that exists in systems with a lowered density of charge carriers, the Anderson theorem[12] is violated, and the value of T_c^{MF} does depend on the impurity concentration, through the dependence of T_{c0} on the renormalized chemical potential (14), (17), (37) for $1/\tau_{12}=1/\tau_{21}=0$.

Here we have considered a more complicated model that incorporates such features of HTSC materials as the overlap of the energy bands, the symmetry of the order parameter, and the electron–hole asymmetry. In this case the Anderson theorem does not hold, and T_c^{MF} depends substantially on the impurity concentration (a nonmagnetic impurity can completely suppress the superconductivity). It is not ruled out that T_{BKT} for this model (in the purely two-dimensional case) will contain additional impurity dependence (besides the impurity dependence of T_c^{MF}).

*E-mail: statphys@asm.md

[1] R. Dupree and A. Gencten, and D. McK. Paul, Physica C **193**, 81 (1992).
[2] G. Xiao, M. Z. Ciepak, A. Garvin, F. H. Streitz, A. Bakhshai, and C. L. Chieh, Phys. Rev. Lett. **60**, 1446 (1988).
[3] J. M. Taracson, P. Barboux, P. F. Miceli, L. H. Greene, G. W. Hull, M. Eibshutz, and S. A. Sunshine, Phys. Rev. B **37**, 7458 (1988).
[4] T. R. Chien, Z. Z. Chang, and N. R. Ong, Phys. Rev. Lett. **67**, 2088 (1991).
[5] D. Goldshmidt, Y. Direktovich, A. Knizhnik, and Y. Eckstein, Phys. Rev. B **54**, 13348 (1996).
[6] S. K. Tolpygo, J. Y. Lin, M. Gurvitch, S. Y. Hou, and J. M. Philirs, Phys. Rev. B **53**, 12454 (1996).
[7] C. Panagopoulos, J. R. Coorer, N. Athanassoroulou, and J. Chrosch, Phys. Rev. B **54**, 12721 (1996).
[8] B. Bardi and U. V. Varadaraju, Phys. Rev. B **52**, 10507 (1995).
[9] N. M. Plakida, *High-Temperature Superconductivity* [in Russian], International Education Program, Moscow (1996).
[10] R. E. Walstedt, R. F. Bell, L. F. Schnermeyer, and I. V. Waszczak, Phys. Rev. B **48**, 10646 (1993).
[11] A. A. Abrikosov and L. P. Gor'kov, Zh. Éksp. Teor Fiz. **39**, 1781 (1960) [Sov. Phys. JETP **12**, 1243 (1961)].
[12] P. W. Anderson, J. Phys. Chem. Solids **11**, 26 (1959).
[13] V. A. Moskalenko and M. E. Palistrant, Dokl. Akad. Nauk SSSR **162**, 539 (1965) [Sov. Phys. Dokl. **10**, 457 (1965)]; Zh. Éksp. Teor. Fiz. **39**, 770 (1965) [Sov. Phys. JETP **12**, 509 (1966)].
[14] V. A. Moskalenko, M. E. Palistrant, and V. M. Vakalyuk, Usp. Fiz. Nauk **161**, 155 (1991) [Sov. Phys. Usp. **34**, 717 (1991)]; Solid State Commun. **69**, 747 (1989).
[15] V. A. Moskalenko, L. Z. Kon, and M. E. Palistrant, *Low-Temperature Properties of Metals with Band-Spectrum Features* [in Russian], Shtiintsa, Kishinev (1989).
[16] R. Fehrenbacher and R. M. Norman, Phys. Rev. B **50**, 3495 (1994).
[17] J. Bang, Phys. Rev. B **52**, 1279 (1995).
[18] J. M. Wheatley, T. C. Hsu, and P. M. Anderson, Phys. Rev. B **37**, 5897 (1988).
[19] V. A. Moskalenko, Fiz. Met. Metalloved. **8**, 503 (1959).
[20] H. Suhl, B. T. Mathias, and L. K. Walker, Phys. Rev. Lett. **3**, 552 (1959).
[21] M. Franz, C. Kollin, A. J. Berlinsky, and M. J. Salkola, Phys. Rev. B **56**, 7882 (1997).
[22] V. M. Loktev and Yu. G. Pogorelov, Physica C **272**, 151 (1996).
[23] H. Kim, G. Preosti, and P. Muzikar, Phys. Rev. B **49**, 3544 (1994).
[24] P. Konsin, N. Kristoffel, and T. Ord, Phys. Lett. **129**, 399 (1988).
[25] M. E. Palistrant and F. G. Kochorbe, Physica C **198**, 351 (1992).
[26] F. G. Kochorbé and M. E. Palistrant, Zh. Éksp. Teor Fiz. **104**, 3084 (1993) [JETP **77**, 442 (1993)]; Teor. Mat. Fiz. **96**, 459 (1993).
[27] E. V. Gorbar, V. P. Gusynin, and V. M. Loktev, Sverkhprovodimost' (KIAE) **6**, 483 (1993); Fiz. Nizk. Temp. **19**, 1171 (1993) [Low Temp. Phys. **19**, 832 (1993)].
[28] M. E. Palistrant and V. M. Vakalyuk, Sverkhprovodimost' (KIAE) **3**, 1805 (1990) [Superconductivity **3**, S215 (1990)].
[29] M. G. Kalalb, F. G. Kochorbé, and M. E. Palistrant, Teor. Mat. Fiz. **91**, 483 (1992).
[30] P. Konsin, N. Krisstoffel, and T. Ord, Nuovo Cimento **17**, 1 (1994).
[31] V. Z. Kresin and S. A. Wolf, Phys. Rev. B **41**, 4278 (1990); **35**, 8716 (1987).
[32] J. E. Hirsch and E. Marsiglo, Phys. Rev. B **43**, 424 (1991); X. Q. Hong and J. E. Hirsch, *ibid.* **45**, 12556 (1992).
[33] É. V. Gorbar, V. M. Loktev, and S. G. Sharapov, Fiz. Nizk. Temp. **21**, 421 (1995) [Low Temp. Phys. **21**, 713 (1995)].
[34] M. Helm, F. Forsthofer, and J. Keller, Phys. Rev. B **53**, 14481 (1996).
[35] F. G. Kochorbé and M. E. Palistrant, Zh. Éksp. Teor Fiz. **114**, 195 (1998) [JETP **87**, 570 (1998)].
[36] H. Krakauer and W. E. Pickett, Phys. Rev. Lett. **60**, 1665 (1988).
[37] J. F. Herman, R. V. Kasowski, and W. J. Hsau, Phys. Rev. B **36**, 6904 (1987).
[38] V. P. Gusynin, V. M. Loktev, and S. P. Sharapov, JETP Lett. **65**, 182 (1997); Fiz. Nizk. Temp. **23**, 180 (1997) [Low Temp. Phys. **23**, 132 (1997)]; Fiz. Nizk. Temp. **23**, 816 (1997) [Low Temp. Phys. **23**, 612 (1997)]; Zh. Éksp. Teor Fiz. **115**, 1243 (1999) [JETP **88**, 685 (1999)].
[39] V. P. Gusynin, V. M. Loktev, and S. P. Sharapov, JETP Lett. **69**, 141 (1999); Zh. Éksp. Teor Fiz. **117**, 1132 (2000) [JETP **90**, 993 (2000)]; Preprint cond-mat/9811207.
[40] E. V. Gorbar, V. M. Loktev, and S. G. Sharapov, Physica C **257**, 355 (1996).
[41] A. A. Abrikosov, L. D. Gor'kov, and I. E. Dzyaloshinskiĭ, *Methods of Quantum Field Theory in Statistical Physics* [Prentice-Hall, Englewood Cliffs, NJ (1963); Moscow, Nauka (1962)].
[42] V. A. Moskalenko, Dokl. Akad. Nauk SSSR **176**, 301 (1967) [Sov. Phys. Dokl. **12/**, 877 (1968)]; Fiz. Met. Metalloved. **23**, 585 (1967).
[43] A. V. Narlikar, C. V. N. Rao, and S. K. Agarual, *Studies of High Temperature Superconductors*, edited by A. Narlikar, Nova Science Publishers (1989), Vol. 1, p. 341.
[44] H. Takayi, T. Ido, S. Ishibashi, M. Uota, S. Uchida, and Y. Tokura, Phys. Rev. B **40**, 2254 (1989).
[45] J. Takura, *Physics of High-Temperature Surerconductors*, S. Maekawa and M. Sato (eds.), Heidelberg, Springer, Berlin (1992), p. 191.
[46] V. M. Loktev, R. M. Quick, and S. G. Sharapov, Preprint cond-mat/9904126.

Translated by Steve Torstveit

Optical evidence for compatibility of antiferromagnetism and superconductivity in $YBa_2Cu_3O_{6+x}$

V. V. Eremenko,* V. N. Samovarov, V. L. Vakula, M. Yu. Libin, and S. A. Uyutnov

B. Verkin Institute for Low Temperature Physics and Engineering, National Academy of Sciences of Ukraine, pr. Lenina 47, 61164 Kharkov, Ukraine

(Submitted April 18, 2000)
Fiz. Nizk. Temp. **26**, 1091–1103 (November 2000)

The evolution of the spectral composition of the absorption in the 1.25–2.6 eV region for metallic films of $YBa_2Cu_3O_{6+x}$ with superconducting transition temperatures of $T_c=51$ and 74 K is measured as the films are cooled from 180 to 20 K. Particular attention is paid to the temperature effects in two absorption bands: the A band ($\simeq 1.8$ eV), which reflects the appearance of holes dressed in antiferromagnetic (AFM) fluctuations, and the $(A+J)$ band ($\simeq 2.15$ eV), which reflects an additional (magnon) excitation of the short-range AFM order. It is found that the changes of these bands begin in the normal phase at $T<T^*$ in the temperature region corresponding to the opening of the pseudogap state, and the $(A+J)$ magnon band arises in the pseudogap state even in the case when it is absent at room temperatures. At the superconducting transition the parameters of the bands stop changing, and the $(A+J)$ magnon band is preserved in the superconducting state. The results are interpreted as evidence of a magnetic nature of the pseudogap state and for the compatibility of AFM short-range order with superconductivity. © *2000 American Institute of Physics.* [S1063-777X(00)00511-9]

INTRODUCTION

It is now established that as cuprate high-T_c superconductors (HTSCs) are cooled, a transition first occurs to a state with a pseudogap in the electronic excitation spectrum and then a transition to the superconducting (SC) state. The pseudogap state, being a precursor to superconductivity, is attracting increased attention and is widely studied, for example, by the methods of spin echo, nuclear relaxation, and angle-resolved photoemission spectroscopy (see reviews[1–3]). In particular, these experiments show that the maximum value of the pseudogap corresponds to the neighborhood of the point $(\pi,0)$ in the two-dimensional (2D) Brillouin zone. In the direction of the diagonal of the zone the pseudogap is absent. The influence of the pseudogap is registered at temperatures below T^*, which, depending on the doping level of the cuprate HTSC, is close to or noticeably higher than the critical temperature T_c. Near the optimal doping level the maximum values of the SC gap Δ_s and pseudogap Δ^* are approximately equal, $\Delta\approx 40$ meV,[1] and both of the gap features apparently have a spatial symmetry of the d type.[1–3]

Altogether, one can assume that in cuprate HTSCs the formation of the SC phase ''starts'' at $T=T^*$ and that the SC gap does not vanish at the critical point itself, unlike that of classical superconductors. The theoretical studies of the pseudogap state take two alternative approaches: an approach based on the formation of Cooper pairs above T_c,[4] and an approach in which fluctuations of the short-range antiferromagnetic (AFM) order play a decisive role[5] (a pseudogap in the spectrum of spin excitations). In any case the experimental and theoretical study of the problem of high-T_c superconductivity in cuprate HTSCs must include a joint treatment of the pseudogap anomalies at $T_c<T\leqslant T^*$ and the SC state proper at $T\leqslant T_c$.

The goal of the present study is to investigate the behavior of the absorption spectra in the visible region at 1.25–2.6 eV for $YBa_2Cu_3O_{6+x}$ films as the temperature passes through both the pseudogap and SC states. In the general scheme of things this experimental goal is extremely unusual, since the photon energy in our working frequency region is much greater than either of the gap features ($\hbar\omega \gg \Delta_s,\Delta^*$). In classical superconductors the range of optical absorption (reflection) that is informative for investigating superconductivity lies, as we know, near the SC gap energy $\hbar\omega\simeq\Delta_s$. If in the electronic spectrum of the normal phase an energy gap of a different nature, e.g., a quantity $\Delta_{\rm mag}$ for magnetic excitations, forms as the temperature is lowered, then the optical response to these changes will also be manifested at frequencies close to $\Delta_{\rm mag}$. For example, in U_2RuSi_2 $\times(T_c\simeq 1.5$ K) at $T<T^*\simeq 20$ K the opening of the magnetic gap leads to a decrease in the values of the optical conductivity in the low-frequency region of the spectrum, $\hbar\omega \simeq\Delta_{\rm mag}\simeq 10$ meV, while at higher energies the optical conductivity (reflection) does not change.[6] This picture of the ''suppression'' of the optical conductivity is observed in cuprate HTSCs (YBCO, Bi2212, LSCO) in the low-frequency region $\hbar\omega<2\Delta^*\approx 100$ meV,[1] where a pseudogap arises in these compounds at $T<T^*$.

In designing a spectroscopic study of the pseudogap and SC states in $YBa_2Cu_3O_{6+x}$ with the aid of high-energy photons $\hbar\omega\gg\Delta_s,\Delta^*$, we worked on the basis of two important findings of previous optical studies. First, it was shown quite some time ago that at fixed frequencies in the visible and infrared regions there are sharp kinks in the absorption signal at the SC transition on cooling of $YBa_2Cu_3O_{6+x}$ films.[7,8] Anomalies in the temperature dependence of the absorption intensity at $\hbar\omega=2$ eV in $YBa_2Cu_3O_{6+x}$ films with different doping have also been noted near $T^*\simeq 110$ K (for $T_c\simeq 90$ K)

and $T^* \simeq 160$ K (for $T_c \simeq 50$ K).[9] However, detailed studies of the temperature evolution of the spectral composition of the multicomponent absorption contour of $YBa_2Cu_3O_{6+x}$ at energies near $\hbar\omega \geqslant 1.25$ eV were not carried out. Second, we were guided by the results of our previous paper[10] on the study and analysis of the absorption spectra of $YBa_2Cu_3O_{6+x}$ films as a function of the doping level at 300 K. We had shown[10] that in the region $\hbar\omega = 1.25$–3 eV the multicomponent absorption spectrum contains features (optical ''markers'') which track the degree of pd hybridization (covalency) and the interaction of the heavy charge carriers with the magnetic subsystem as the sample is doped. For example, the degree of pd hybridization affects the parameters of the B_d^1 absorption band ($\simeq 1.5$ eV), which is due to the transition $d_{xy} \rightarrow d_{x^2-y^2}$ in the spectrum of the Cu^{2+} ion. At the same time, the absorption bands A ($\simeq 1.8$ eV) and $(A+J)$ ($\simeq 2.1$ eV) are sensitive to the AFM ordering (AFM fluctuations). In particular, the $(A+J)$ band reflects the probability of two-magnon excitation upon interband transitions involving charge transfer. As the doping is increased at 300 K in the metallic phase, the covalent and magnetic (correlation) contributions to the spectrum of charge carriers compete with each other: the A and $(A+J)$ bands decrease in intensity and broaden, but the B_d^1 band is enhanced on metallization.

As the films are cooled from 300 K the behavior of these bands must necessarily follow the same scenario as it does during doping. One expects several versions of the mutual changes in the A, $(A+J)$, and B_d^1 absorption bands in $YBa_2Cu_3O_{6+x}$ as the pseudogap state and then the SC state are passed. For example, for some of these absorption bands there may be no change with temperature at all. Behind each of these scenarios are certain mechanisms for the onset of the pseudogap state, and alternative possibilities for the competition (coexistence) of AFM magnetic ordering and superconductivity. The experimental data obtained in the present study show that the spectral composition of the absorption of light in $YBa_2Cu_3O_{6+x}$ on cooling evolves in such a way that one can assert that antiferromagnetism and superconductivity are mutually compatible in this material. For example, the A absorption band, due to AFM fluctuations, and the $(A+J)$ absorption band, which reflects the excitation of magnons in the metal, are enhanced in the pseudogap state and conserved in the superconducting phase. On the whole, analysis of the available data suggests that high-T_c superconductivity is of a spin-wave nature.

GENERAL APPROACH TO THE ANALYSIS OF THE SPECTRA. THE EXPERIMENT

Before we present and discuss the experimental results, let us state our approach to the identification of the absorption spectra.

In the energy region $\hbar\omega = 1$–3 eV the absorption spectrum of $YBa_2Cu_3O_{6+x}$ for light with polarization $\mathbf{E} \| ab$ is a multicomponent spectrum. In this spectral interval fall optical transitions of different natures: intraband, interband, and local dd transitions in the Cu^{2+} ions. For identification of the transitions we consider the structure of the density of states $N(E)$, which is common to copper-oxide HTSCs. It is shown in Fig. 1 together with the scheme of splitting of the

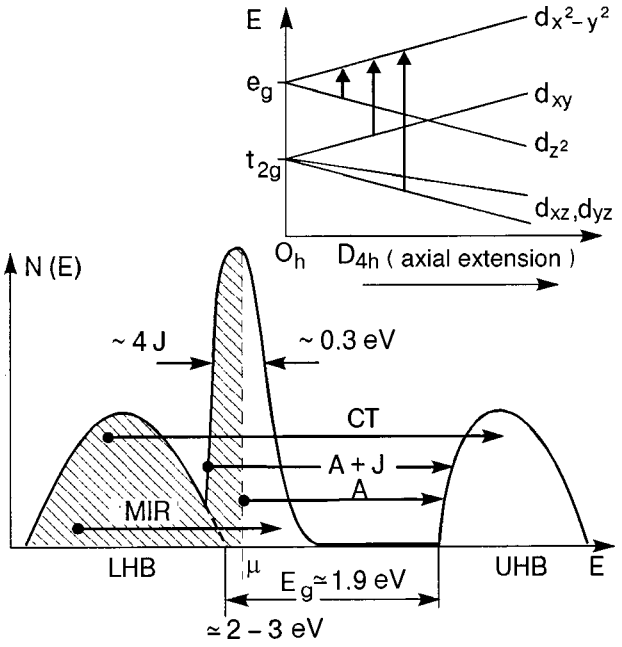

FIG. 1. Schematic illustration of the splitting of the d levels of the Cu^{2+} ion in a crystalline field of tetragonal symmetry D_{4h} and the distribution of the density of states $N(E)$ in copper oxide HTSCs with a hole type of doping. The arrows indicate the optical transitions considered in the analysis of the measured absorption spectra. The energy levels are indicated without adherence to a scale.

Cu^{2+} levels in the tetragonal field of the oxygen p ligands. The arrows denote the possible transitions in the metallic phase.

The picture of the distribution of the density of states in cuprate HTSCs is determined by electronic (Hubbard) correlations and the features of the copper–oxygen interactions. The lower, pd-hybridized Hubbard band (LHB) is separated from the upper Hubbard band (UHB), which is formed predominantly by the d orbitals of copper, by an optical gap with a value of E_g. The gap owes its origin to the transfer of charge from the oxygen ions to the copper. For insulating compounds of $YBa_2Cu_3O_{6+x}$ with $x \simeq 0.3$ this gap has a value $E_g \simeq 1.7$ eV.[11] At the top of the lower Hubbard band in the metallic phase a quasiparticle peak arises in the density of states, the chemical potential lying within this peak. For a model of the interaction of hole carriers with AFM fluctuations the quasiparticle peak characterizes heavy carriers dressed in AFM fluctuations.[3,12,13] In the 2D Brillouin zone the strongest interaction of the charge carriers with the AFM fluctuations is realized along the Γ–M direction, but along other directions of the quasimomentum this interaction is weaker. The characteristic width of the quasiparticle (coherent) A peak is approximately $(3-4)J$, where $J \simeq 10^3$ K is the exchange interaction energy in the CuO_2 plane for $YBa_2Cu_3O_{6+x}$.[2] The total width of the lower Hubbard valence band is $\simeq 2$ eV.

The next four types of optical transitions in the metallic phase arise naturally in the framework of the proposed $N(E)$. In the region above the absorption threshold, $\hbar\omega \geqslant E_g$, a continuum component of interband transitions involving charge transfer, which will be called charge transfer (CT) transitions, arises. Near the threshold E_g there are two possible types of electronic transitions, which involve the qua-

siparticle A peak in the density of states (see Fig. 1). The first are transitions across the optical gap without excitation of the magnetic degrees of freedom (henceforth called the A transitions), and the second are higher-frequency transitions involving the simultaneous transfer of charge and excitation of the magnetic subsystem (henceforth called $(A+J)$ transitions). All of these transitions should be manifested in the spectra in the form of comparatively narrow-band spectral contours with widths on the scale of the energy J. Finally, there are intraband transitions from the interior of the valence band into the hole-state region that opens up with doping. Their spectral weight is concentrated mainly in the mid-infrared region (MIR transitions). The red boundary of the MIR transitions must have a value close to the width of the A peak, i.e., $\simeq 0.3$–0.4 eV, but the short-wavelength wing can extend in energy to the entire width of the valence band and can even span the visible region. In experiments with metallized $YBa_2Cu_3O_{6+x}$ films ($x>0.4$) the asymmetric MIR absorption contour has a maximum near 0.6 eV and a slowly falling short-wavelength wing that extends all the way to 3 eV.[8,10]

For the dd transitions in $YBa_2Cu_3O_{6+x}$ in the case of polarization $\mathbf{E}\|ab$ the largest contribution to the absorption is from the transitions $d_{xy}\rightarrow d_{x^2-y^2}$ and $d_{yz,xz}\rightarrow d_{x^2-y^2}$. In the case of weak pd hybridization (degree of covalency) the dd transitions, by virtue of the symmetry selection rule, give rise to low-intensity bands with absorption coefficients having a value of $\alpha\simeq 10^4$ cm^{-1} in the insulator phase.[10,14] In this case the dd transitions are clearly manifested in the Raman scattering spectra. For example, in the Raman spectra the transition $d_{xy}\rightarrow d_{x^2-y^2}$ is clearly expressed in the insulator phase of $YBa_2Cu_3O_{6+x}$ ($x\leqslant 0.4$) in the form of a band centered around 1.5 eV.[15] As the pd hybridization is enhanced in the metal, the absorption coefficient for the dd transitions grows to values comparable to the coefficients for the CT transitions, $\alpha\simeq 10^5$ cm^{-1} (Ref. 10), but in the Raman scattering spectra these transitions are strongly greatly weakened upon metallization.[15]

The ideas set forth above had been used previously in an analysis of the evolution of the spectral composition of the absorption of $YBa_2Cu_3O_{6+x}$ thin films ($\mathbf{E}\|ab$) as the samples are doped.[10] It was shown that the six transitions indicated (CT, A, $(A+J)$, $d_{xy}\rightarrow d_{x^2-y^2}$, $d_{yz,xz}\rightarrow d_{x^2-y^2}$, and MIR) describe the multicomponent absorption spectrum of $YBa_2Cu_3O_{6+x}$ films to an accuracy of 5% or better, both in the insulator phase ($x\simeq 0.35$) and in the metallic phase in the region $x=0.5$–0.9.

The simplest spectrum is the absorption spectrum of $YBa_2Cu_3O_{6+x}$ in the insulator phase at 300 K. For example, at the boundary of the transition to the metal at $x\simeq 0.35$ in the spectral region 1.25–3 eV the spectrum is dominated by the Gaussian contours from the A transition, the $(A+J)$ transition, and the CT continuum component. Band A is centered at $\simeq 1.8$ eV, and the $(A+J)$ band at $\simeq 2.1$ eV is separated from it by an energy equal to the two-magnon excitation energy $\hbar\omega_{2\mathrm{mag}}$. For $YBa_2Cu_3O_{6+x}$ ($x\leqslant 0.6$) the two-magnon maximum in the Raman scattering spectra has an energy $\hbar\omega_{2\mathrm{mag}}\simeq 3J\simeq 0.33$ eV.[16] At the temperature of the transition of the $YBa_2Cu_3O_{6+x}$ insulator film ($x\simeq 0.35$) to the AFM phase, both the A and $(A+J)$ bands are noticeably narrowed.[10] The narrowing of the bands is due to the fact that, as the temperature decreases below the Néel point ($T_N\simeq 170$ K) a spin gap appears, the value of which is 3–5 meV in the weakly metallized phase of YBCO.[17] It has also been shown[10] that the reduction of the absorption in the wings of the A contour arises as a result of the narrowing effect, which in turn is dictated by a decrease in the number of magnons as the temperature is lowered in the region $T<T_N$, in accordance with the Bose–Einstein temperature factor.

Experiment. In this paper the absolute absorption spectra and the changes with temperature are measured for two metallized $YBa_2Cu_3O_{6+x}$ films, which will be designated as VN604 and VN608. They belong to a series of single-crystal VN films grown at the Physics Institute of the University of Erlangen, Germany, in Prof. G. Saemann-Ischenko's department. Films of this series have been used previously for studying the absorption spectra at 300 K as a function of doping.[10] The films were prepared on $SrTiO_3$ substrates by the laser sputtering of targets. They are c-oriented and have a thickness $l=2300$ Å. For the VN604 film the parameter $c=11.722$ Å and the start of the transition is $T_c^{\mathrm{on}}=51$ K, and for the VN608 films, $c=11.705$ Å and $T_c^{\mathrm{on}}=74$ K. The total widths of the SC transitions, according to the results of the magnetic measurements, are around 1.5 K. According to the calibration data[18] for $YBa_2Cu_3O_{6+x}$ films, these values of T_c^{on} correspond to doping indices of $x\simeq 0.45$ (VN604) and $x\simeq 0.7$ (VN608). The measurements were made in unpolarized light with the $\mathbf{E}$ vector of the light wave in the CuO_2 plane, $\mathbf{E}\|ab$.

The experimental procedure for the measurements of the absorption spectra [the absorption coefficients $\alpha(\omega)$] is set forth in detail in Ref. 10. Here we mention only the key points. For 300 K we represent the absolute absorption spectra in dimensionless units of optical density, αl. These data are obtained by comparative measurements of the transmission spectra of the films and clean substrates. The data obtained on cooling of the films is represented for each temperature in the form of a difference spectrum $\Delta(\alpha l)=[\alpha(T)-\alpha(T_0)]l$ as a function of the photon energy, where T_0 is the upper boundary of the temperature interval of the measurements. The value of $\Delta(\alpha l)$ is determined from the relation $\Delta(\alpha l)=\ln[t_{T_0}(\hbar\omega)/t_T(\hbar\omega)]$, where $t(\hbar\omega)$ is the measured transmission spectrum of the film at the given temperature. The above relation holds well without allowance for temperature-related changes of the reflection coefficient $R(\omega)$. In the energy region $\hbar\omega\geqslant 1.25$ eV on cooling of the metallic phase of $YBa_2Cu_3O_{6+x}$ the temperature-related changes of R per degree are small, $\delta R/\delta T\simeq 10^{-4}$ K^{-1} (Ref. 19; the absolute level of the reflection is also low, $R\simeq 10\%$). Here the growth of the transmission turns out to be substantially larger (by at least an order of magnitude), $\delta t/\delta T\gg\delta R/\delta T$. Therefore, the use of the relation given above to determine $\Delta(\alpha l)$ in our working frequency region is entirely justified. (Taking the temperature dependence of R into account is necessary for finding $\alpha(T)$ in the energy region $\hbar\omega\simeq 0.5$ eV, where $R\simeq 60\%$ and $\delta t/\delta T\simeq\delta R/\delta T$.[20])

EXPERIMENTAL RESULTS AND DISCUSSION

1. Let us consider the data for the VN604 film. with $T_c^{\mathrm{on}}\simeq 51$ K. Figure 2a shows the absorption spectrum $(\alpha l)_{\mathrm{exp}}$

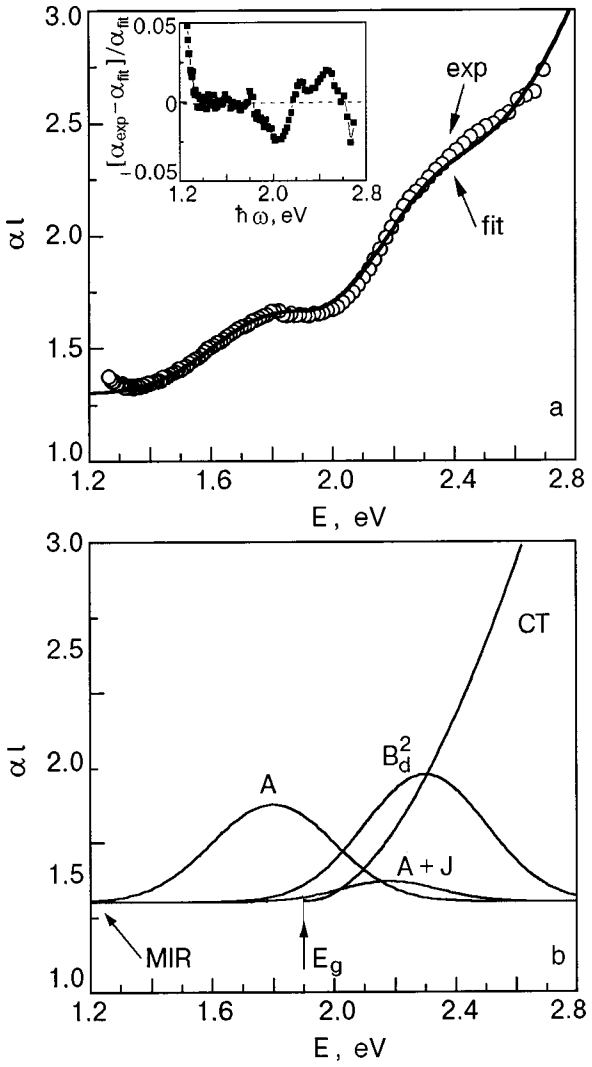

FIG. 2. Absorption spectrum $\alpha l(E)$ measured at 300 K for the VN604 film, with $T_c^{on}=51$ K (○), in comparison with the model spectrum (————) (a). The inset shows the relative difference of these spectra $(\alpha_{exp}-\alpha_{fit})/\alpha_{fit}$. The decomposition of the model spectrum into components (b). A constant MIR absorption level $(\alpha l)_{MIR}=2.3$ was taken as the zero level for the A, B_d^1, B_d^2, and CT components.

of this film at 300 K in the spectral region 1.25–2.8 eV. Here the solid curve shows the model dependence $(\alpha l)_{fit}$, which is the sum of five components into which the measured spectrum was decomposed. These components are shown individually in Fig. 2b. They are described by Gaussian contours centered at E_0 with a standard deviation σ and an amplitude coefficient μ_0:

$$(\alpha l)_n=\frac{\mu_0}{\sigma\sqrt{\pi}}\exp\left[-\frac{(E-E_0)^2}{2\sigma^2}\right],$$

and also by continuum frequency dependences $\alpha l(E)$. In accordance with the general approach to the analysis of absorption spectra which was discussed above, the spectral composition is made up of the following components:

1) a Gaussian contour $(\alpha l)_A$ for an electronic transition from the correlation maximum of the density of states — the A band;

2) a Gaussian contour $(\alpha l)_{A+J}$ for a transition from the correlation maximum with simultaneous excitation of the magnetic subsystem — the $(A+J)$ band;

3) a Gaussian contour $(\alpha l)_{2B}$ for the transition $d_{xz,yz}\rightarrow d_{x^2-y^2}$ in the Cu^{2+} ion — the B_d^2 band;

4) a continuum component of interband transitions $(\alpha l)_{CT}$ involving charge transfer from the oxygen to the copper — the CT component. This component of the spectrum, according to an analysis of the data, is best described by a dependence of the form $(\alpha l)_{CT}=\mu_0^{CT}(E-E_g)^2/E$. Such a dependence is typical for direct allowed transitions, when there are tails of the densities of states of the lower and upper bands extending into the optical gap,[21] and also in the case of heavy doping, when electron scattering effects are appreciable.[22] In the case when there are tails of the densities of states, this dependence has been verified, for example, in the optical experiments of Ref. 23 on YBCO;

5) a continuum component of the short-wavelength wing of the MIR absorption band, $(\alpha l)_{MIR}$. We have assumed a constant level for this absorption in the region $\hbar\omega>1.2$ eV (the curve labeled MIR in Fig. 2b). Choosing the frequency dependence of this component in the form $(\alpha l)_{MIR}\propto 1/\omega$, for example, would have only a weak effect on the parameters of the other components.

Thus the total multicomponent absorption contour is described in the form

$$(\alpha l)_{fit}=\sum_{n=1}^{3}\frac{\mu_{0n}}{\sigma_n\sqrt{\pi}}\exp\left[-\frac{(E-E_{0n})^2}{2\sigma_n^2}\right]+\frac{\mu_0^{CT}(E-E_g)^2}{E}+(\alpha l)_{MIR}.$$

Let us now give the quantitative characteristics of this decomposition by which the experimental spectrum $(\alpha l)_{exp}$ can represented with an accuracy of 4% or better over the energy energy interval by the sum $(\alpha l)_{fit}=(\alpha l)_A+(\alpha l)_{A+J}+(\alpha l)_{2B}+(\alpha l)_{CT}+(\alpha l)_{MIR}$. The relative difference $(\alpha l)_{exp}$ from the model $(\alpha l)_{fit}$ is shown in the inset in Fig. 2b. Thus the model parameters are as follows:

Gaussian A band: $E_0^A=1.8$ eV, $\sigma_A=0.19$ eV, $\mu_0^A=0.11$ eV;

Gaussian $(A+J)$ band: $E_0^{A+J}=2.18$ eV, $\sigma_{A+J}=0.19$ eV, $\mu_0^{A+J}=0.02$ eV;

Gaussian B_d^2 band: $E_0^{2B}=2.3$ eV, $\sigma_{2B}=0.2$ eV, $\mu_0^{2B}=0.15$ eV;

continuum CT component: $E_g=1.9$ eV, $\mu_0^{CT}=6$ eV^{-1};

absorption level of the MIR band: $(\alpha l)_{MIR}=1.3$.

If we compare this model decomposition for the metallized film with the decomposition of the absorption spectrum at 300 K for a $YBa_2Cu_3O_{6+x}$ insulating film ($x\simeq 0.35$),[10] we can draw the following conclusions. Upon metallization the A and $(A+J)$ absorption bands behave in the same way, demonstrating a broadening of their Gaussian contours and a lowering of their amplitude coefficients. The $(A+J)$ band is most strongly diminished in the metal: for the VN604 film its area decreases by more than a factor of 20 (and the coefficient μ_0^{A+J} decreases by the same factor). The substantial decrease in the contribution of this band indicates that the magnons arising upon the excitation of the $(A+J)$ transition simultaneously with the creation of a heavy-hole charge car-

rier are strongly damped in the metal. As we shall show below, in the even more metallized VN608 film the $(A+J)$ absorption band is completely absent by 300 K, while the A band, although weakened, nevertheless still exists. These changes of the A and $(A+J)$ absorption bands occur at 300 K after a transition to the metallic phase, where the AFM correlations of the short-range order are conserved. For cuprate HTSCs the correlation length of the AFM fluctuations in the metallic phase is $\xi \simeq 10$ Å,[2] which is approximately an order of magnitude smaller than in the insulator phase.

In regard to the local dd transitions we must note the following. In the spectra of the insulator phase at $x \simeq 0.35$ and 300 K the contribution from the dd transitions does not exceed a few percent.[10] At the same time, in the VN604 film in the spectral region 1.2–2.8 eV only the second of the two possible transitions $d_{xy} \rightarrow d_{x^2-y^2}$ and $d_{xz,yz} \rightarrow d_{x^2-y^2}$ is clearly manifested in the absorption, in the form of the B_d^2 band. The appearance of the B_d^2 peak in the weakly metallized BN604 film can be attributed to the circumstance that the mixing of the oxygen and copper orbitals occurs mainly for the $d_{xz,yz}$ states, i.e., the covalent bonding is enhanced in the direction transverse to the CuO_2 plane. We note that in $YBa_2Cu_3O_{6+x}$ in the ortho-II phase the distance between the CuO_2 plane and the apical oxygen O(4) decreases sharply (by about 0.1 Å) at the insulator–metal transition, and this promotes the leakage of electrons into the CuO_x chain plane and, hence, hole metallization of the CuO_2. The appearance of the B_d^1 band (derived from the transition $d_{xy} \rightarrow d_{x^2-y^2}$) at 1.5 eV, i.e., the advent of covalency enhancement directly in the CuO_2 active plane, is clearly seen at 300 K for the highly metallized VN608 film.

Let us now consider the behavior of the absorption spectra on cooling for the VN604 film with $T_c^{on} = 51$ K. Figure 3 shows the difference spectra $\Delta(\alpha l) = \alpha l(T) - \alpha l(T_0)$ measured in the region 1.2–2.6 eV, relative to $T_0 = 184$ K. As we see in Fig. 3, for the interval 168–184 K only the continuum weakening of the absorption is observed $(\Delta(\alpha l) < 0)$. For clarity, the frequency behavior of this background component is indicated qualitatively by the dashed curves. This wide-band change in the absorption spectrum is due primarily to the temperature-related weakening of the intensity of the short-wavelength wing of the MIR component at visible frequencies for temperatures $T \geqslant 168$ K. When the $YBa_2Cu_3O_{6+x}$ films are cooled, there is an increase in the absorption coefficient at frequencies $\hbar\omega < 1$ eV within the contour of the maximum of the MIR absorption band.[8,10,20] Therefore, near $\hbar\omega \simeq 1$ eV, where $\Delta(\alpha l)_{exp} \simeq 0$, there is a change in sign of the temperature dependence of the continuum absorption for the MIR component. We will not discuss this effect of the temperature-induced redistribution of the intensities within the MIR absorption contour itself[24] but will instead concentrate on the temperature behavior of the narrow-band features due to the A and $(A+J)$ bands. For the temperature region $T \geqslant 168$ K it can be stated that the A and $(A+J)$ absorption contours are independent of temperature. At 138 K, however, the spectral features due to the temperature transformation of the A and $(A+J)$ bands are already noticeable against the continuum background. As the temperature is lowered further from 138 to 59 K these spectral features become more pronounced, taking the form of individual bands centered at the maxima of the A band (1.8 eV) and $(A+J)$ band (2.15 eV). At the superconducting transition with $T_c^{on} = 51$ K and in the superconducting phase itself at 25 K both the continuum and the narrow-band spectral variations practically cease. In this regard we note that, according to the data of an earlier-mentioned paper,[9] the intensity of the absorption signal at a frequency of 2 eV ceases to depend on temperature in the SC phase.

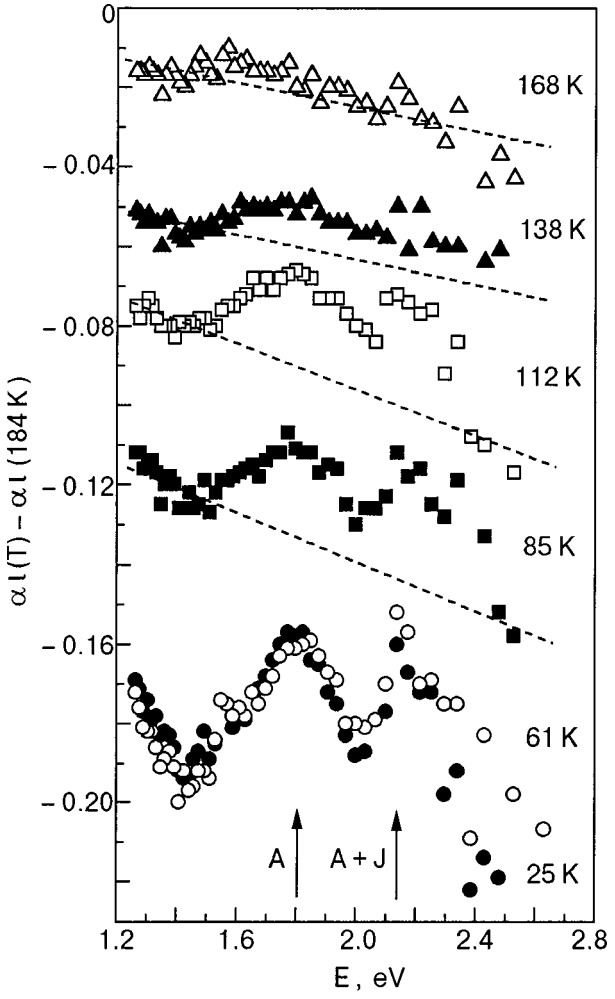

FIG. 3. Difference spectra of the absorption $[\alpha l(T) - \alpha l(T_0)]$ measured relative to the initial temperature $T_0 = 184$ K in the VN604 film, with $T_c^{on} = 51$ K, at film temperatures T [K]: 168 (△), 138 (▲), 112 (□), 85 (■), 61 (○), 25 (●). For clarity the data for 112 K have been shifted downward along the vertical axis by -0.01, the data for 85 K by -0.03, and the data for 61 and 25 K by equal amounts -0.06.

It is straightforward to conclude that the appearance of narrow-band features on the difference spectra of the absorption occurs because of a narrowing of the A and $(A+J)$ bands and growth of their amplitudes. To illustrate what we have said, in Fig. 4 we present the experimental data on $\Delta(\alpha l)_{exp} = \alpha l(25\,\mathrm{K}) - \alpha l(184\,\mathrm{K})$ and the model dependence $\Delta(\alpha l)_{fit}$ (solid curve), from which one can obtain quantitative characteristics of the spectral components at low temperatures. With allowance for the temperature effects in the MIR component and of the A and $(A+J)$ bands, the model dependence has the form $\Delta(\alpha l)_{fit} = \Delta(\alpha l)_{fit}(25\,\mathrm{K}) - \Delta(\alpha l)_{fit}(184\,\mathrm{K}) = \Delta(\alpha l)_A^{fit} + \Delta(\alpha l)_{A+J}^{fit} + \Delta(\alpha l)_{MIR}^{fit}$. Since for $T > 184$ K the temperature dependence is insignificant, we took the parameters of the model decomposition of the

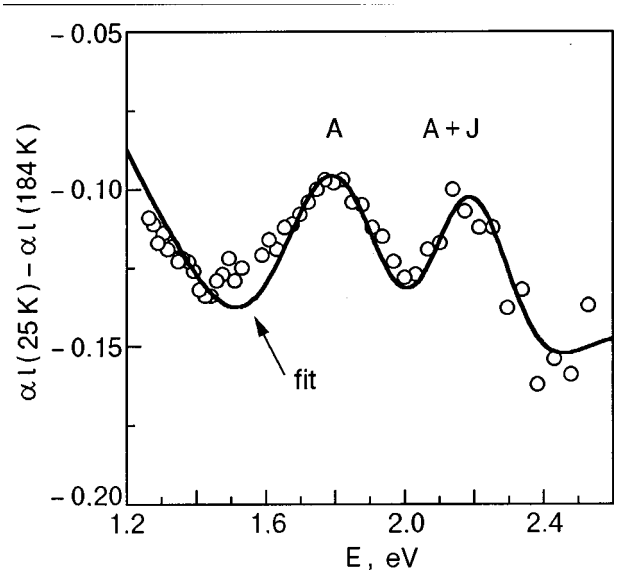

FIG. 4. The difference spectrum of the absorption $[\alpha l(25\,\mathrm{K})-\alpha l \times(184\,\mathrm{K})]$ of the VN604 film measured in the superconducting state at 25 K relative to that at the initial temperature $T_0=184$ K (○). The solid curve is the model difference spectrum including the temperature effects in the MIR, A, and $(A+J)$ components (see text).

spectrum at 184 K the same as at 300 K: $(\alpha l)_{\mathrm{fit}}(184\,\mathrm{K})=(\alpha l)_{\mathrm{fit}}(300\,\mathrm{K})$ (see above). The model curve in Fig. 4, which describes the experiment well, was obtained for the following parameters of the spectrum at low temperatures:

— for the MIR component $\Delta(\alpha l)^{\mathrm{fit}}_{\mathrm{MIR}}=-0.148+0.13/E^4$, i.e., in the region $E\leqslant 1$ eV the intensity of the MIR component increases as the temperature is lowered $(\Delta(\alpha l)^{\mathrm{fit}}_{\mathrm{MIR}}>0)$, as was discussed above, but in our working frequency region this component suffers temperature-related weakening $(\Delta(\alpha l)^{\mathrm{fit}}_{\mathrm{MIR}}<0)$;

— for the A and $(A+J)$ absorption bands the parameters of the Gaussian contours of $(\alpha l)_{A,A+J}$ change upon cooling to 25 K: the standard deviation of the A contour decreases from $\sigma_A=0.19$ eV (300 K) to 0.165 eV (25 K), i.e., by 10%, while the amplitude coefficients are conserved ($\mu_0^A=0.11$ eV (300 K), $\mu_0^A=0.11$ eV (25 K)); the standard deviation of the $(A+J)$ contour decreases from $\sigma_{A+J}=0.19$ eV (300 K) to 0.13 eV (25 K), i.e., by 30%, and the amplitude coefficient μ_0^{A+J} increases by just as large a factor (from 0.02 eV at 300 K to 0.027 eV at 25 K, i.e., by 35%).

Thus the temperature effects in the A and $(A+J)$ bands occur between 184 and 168 K. The bands narrow, and their area increases, mainly for the $(A+J)$ band. At the superconducting transition the spectral composition and parameters of the absorption bands cease to change, and for the superconducting phase one can say that the absorption spectrum is ''frozen.''

It is straightforward to associate the start of these temperature effects in the region 138–168 K with the temperature T^* at which the pseudogap state is formed. For example, the temperature dependence of the spin–lattice relaxation time of the copper nuclei, $1/T_1T\propto \mathrm{Im}\chi(\mathbf{q},\omega)/\omega|_{\omega\to 0}$ ($\mathrm{Im}\chi(\mathbf{q},\omega)$ is the imaginary part of the magnetic susceptibility for wave vector $\mathbf{q}$), is characterized by pseudogap behavior below $T^*=150$ K in $YBa_2Cu_3O_{6+x}$ with $T_c\approx 60$ K.[2] At temperatures below T^* the values of $1/T_1T$ decrease rather

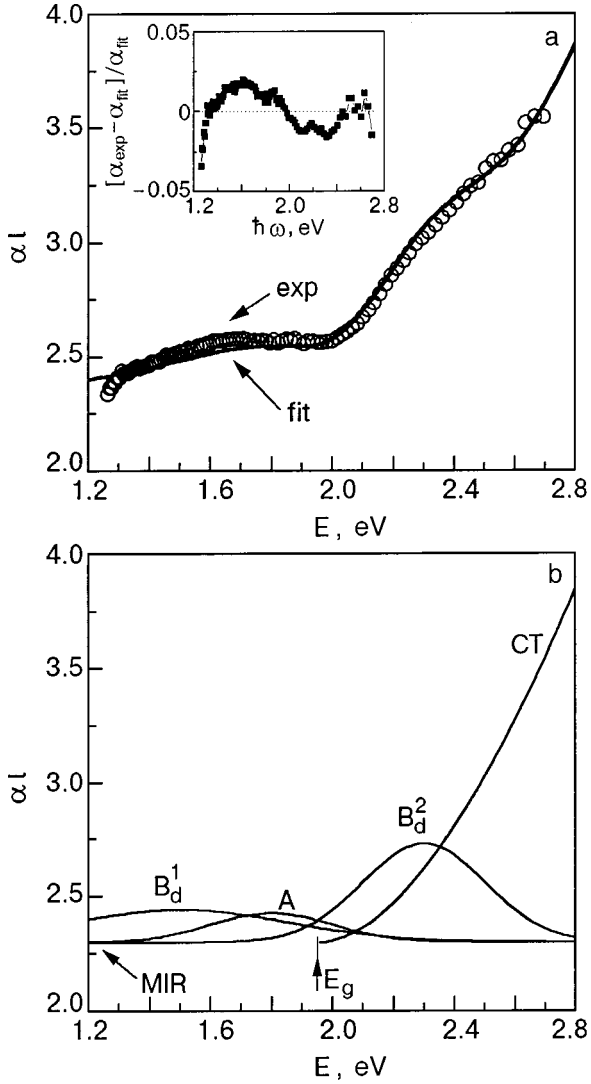

FIG. 5. Absorption spectrum $\alpha l(E)$ of the VN608 film, with $T_c^{\mathrm{on}}=74$ K (○), measured at 300 K, in comparison with the model spectrum (———) (a). The inset shows the relative difference of these spectra $(\alpha_{\mathrm{exp}}-\alpha_{\mathrm{fit}})/\alpha_{\mathrm{fit}}$. The decomposition of the model spectrum into components (b). A constant MIR absorption level $(\alpha l)_{\mathrm{MIR}}=2.3$ was taken as the zero level for the B_d^1, A, B_d^2, and CT components.

sharply as the temperature is lowered, demonstrating a lowering of the spectral weight of the low-frequency magnetic excitations. Neutron scattering data for $YBa_2Cu_3O_{6+x}$ with $T_c=59$ K also attest to the strong decrease of $\mathrm{Im}\chi(\mathbf{q},\omega)$ below $T^*=150$ K in the low-frequency interval $\hbar\omega<16$ meV.[25] Before discussing the microscopic nature of the behavior of the A and $(A+J)$ bands upon the formation of the pseudogap and superconducting states, let us consider the temperature evolution of the spectra for the more highly metallized film VN608.

2. Figure 5a shows the measured absorption spectrum $(\alpha l)_{\mathrm{exp}}$ of a VN608 film ($T_c^{\mathrm{on}}=74$ K) at 300 K, the solid curve representing the total model spectrum $(\alpha l)_{\mathrm{fit}}$, and Fig. 5b shows the model decomposition of this spectrum into components.

This decomposition allows one to describe the spectral curve $(\alpha l)_{\mathrm{exp}}$ to an accuracy of 4% or better throughout the entire spectral interval 1.2–2.7 eV (inset in Fig. 5a). The spectrum contains five components.

1. A Gaussian absorption component B_d^1 for the transition $d_{xy} \rightarrow d_{x^2-y^2}$, with the parameters $E_0^{1B} = 1.5$ eV, $\sigma_{1B} = 0.36$ eV, and $\mu_0^{1B} = 0.09$ eV.

2. A Gaussian absorption component A for transitions from the correlation maximum of the density of states, with the parameters $E_0^A = 1.8$ eV, $\sigma_A = 0.2$ eV, and $\mu_0^A = 0.045$ eV.

3. A Gaussian absorption component B_d^2 for the transition $d_{xz,yz} \rightarrow d_{x^2-y^2}$, with the parameters $E_0^{2B} = 2.3$ eV, $\sigma_{2B} = 0.2$ eV, and $\mu_0^{2B} = 0.15$ eV. This absorption band is the same as in the BN604 film.

4. A component due to interband transitions involving charge transfer — the CT component of the spectrum. Its frequency dependence did not change (see above), but the value of the optical gap increased somewhat, to $E_g = 1.95$ eV, because of the shift of the Fermi level upon metallization; $\mu_0^{CT} = 6\ \text{eV}^{-1}$.

5. A MIR absorption level $(\alpha l)_{\text{MIR}} = 2.3$. The contribution of the short-wavelength wing increased on account of the increase of the entire MIR absorption band as the doping level was raised.

In choosing the decomposition we strove to minimize the number of parameters to be varied in the spectral decomposition in comparison with the parameters of the VN604 film. It is easily seen that for the VN608 film the band B_d^1 appears in the decomposition of the spectrum, reflecting an enhancement of the covalency in the CuO_2 plane, while the area of the A band decreases, attesting to a decrease in the number of heavy hole carriers, and the ''magnon'' absorption band $A+J$ vanishes entirely.

The difference spectra $\Delta(\alpha l) = \alpha l(T) - \alpha l(T_0)$ of the absorption for this film relative to the temperature $T_0 = 170$ K are presented in Fig. 6. We see that for the temperature region 130–170 K only the weakening of the continuum absorption with decreasing temperature is observed, which is due to the decrease of the intensity of the short-wavelength wing of the MIR component (the picture is completely analogous to the temperature-related changes for the BN604 film on cooling in the interval 168–184 K). The narrow-band spectral features appear in the temperature interval 84–130 K, i.e., at lower temperatures than for the VN604 film. In this connection we point out immediately that as the doping of the $YBa_2Cu_3O_{6+x}$ increases, the temperature of formation T^* of the pseudogap state decreases, approaching T_c (Ref. 1).

Even in a qualitative approximation the difference spectra have three distinguishable narrow-band features, corresponding to the B_d^1, A, and $(A+J)$ absorption bands. Of particular interest, of course, is the fact that the absorption band $(A+J)$, which is absent at room temperatures, appears on cooling below T^*. As in the case of the VN604 film, there are practically no temperature-related changes of the spectra in the superconducting phase between 50 and 19 K (see Fig. 6). Incidentally, by comparing the data at 50 and 19 K one can nevertheless conclude that a certain spectral redistribution occurs in the SC phase, tending to enhance the $(A+J)$ maximum and narrow the B_d^1 component.

For a quantitative description of the difference spectrum of VN608, Fig. 7a presents a comparison of the experimental data at 19 K and the model dependence $\Delta(\alpha l)_{\text{fit}}$ (solid curve). The model curve was obtained with allowance

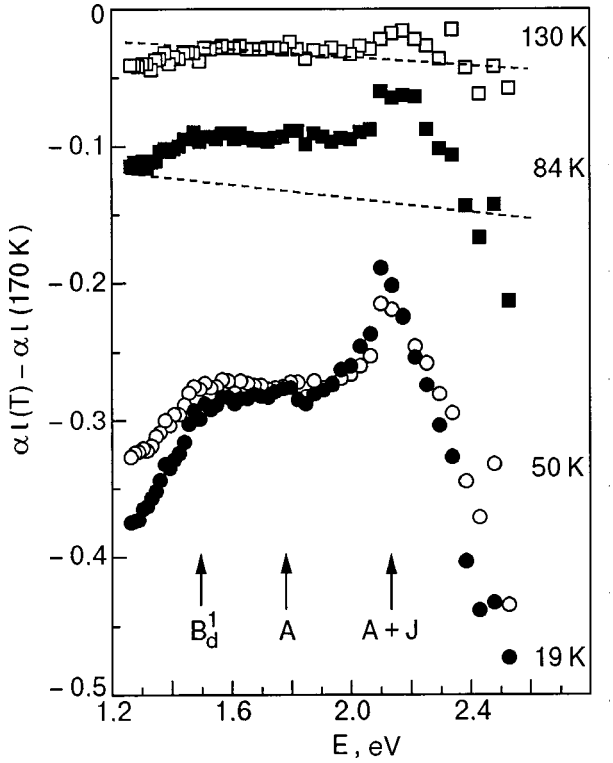

FIG. 6. Difference spectra of the absorption $[\alpha l(T) - \alpha l(T_0)]$ measured for the VN608 film, with $T_c^{\text{on}} = 74$ K, relative to the initial temperature $T_0 = 170$ K. The film temperatures were $T = 130$ K (□), 84 K (■), 50 K (○), 19 K (●). For clarity the data for $T = 84$ K have been shifted downward along the vertical axis by an amount -0.03, and the data for $T = 50$ K and $T = 19$ K by equal amounts -0.20.

for the change of the following components: $\Delta(\alpha l)_{\text{fit}} = (\alpha l)_{\text{fit}}(19\,\text{K}) - (\alpha l)_{\text{fit}}(170\,\text{K}) = \Delta(\alpha l)_{1B}^{\text{fit}} + \Delta(\alpha l)_A^{\text{fit}} + \Delta(\alpha l)_{A+J}^{\text{fit}} + \alpha(\alpha l)_{\text{MIR}}^{\text{fit}}$. The parameters of the model decomposition at 170 K were taken equal to those at 300 K, since the temperature effects in the absorption spectrum in the interval 170–300 K are insignificant. It should be noted that one can set $(\alpha l)_{A+J}^{\text{fit}}(170\,\text{K}) = 0$ in this model decomposition, since the $(A+J)$ band does not appear in the absolute spectra. The four components of the model difference spectrum $\Delta(\alpha l)_i^{\text{fit}}$ ($i \equiv 1B$, A, $A+J$, MIR) are shown in Fig. 7b. It should be noted that the B_d^1, A, and $(A+J)$ components are constructed in such a way that the zero level for them is the MIR component (the curve labeled MIR in Fig. 7).

The following quantitative changes characterize the experimental difference spectrum at 19 K to sufficient accuracy.

For the MIR component: $\Delta(\alpha l)_{\text{MIR}}^{fit} = -0.28 + 0.17/E^4$ (curve MIR in Fig. 7b) and, hence, a change in direction of the temperature dependence for the component occurs near 0.9 eV.

For the covalent band B_d^1 at 1.5 eV the standard deviation of the contour decreased from $\sigma_{1B} = 0.36$ eV (300 K) to 0.23 eV (19 K), i.e., by 35%, while the amplitude coefficient remained nearly unchanged ($\mu_0^{1B} = 0.09$ eV at 300 K and 0.107 eV at 19 K). The conservation of the μ_0^{1B} value indicates that the degree of pd mixing, which reaches the doping level at 300 K, is practically unchanged on cooling.

For the A contour centered at 1.8 eV the standard deviation decreased from $\sigma_A = 0.2$ eV (300 K) to 0.18 eV (19 K),

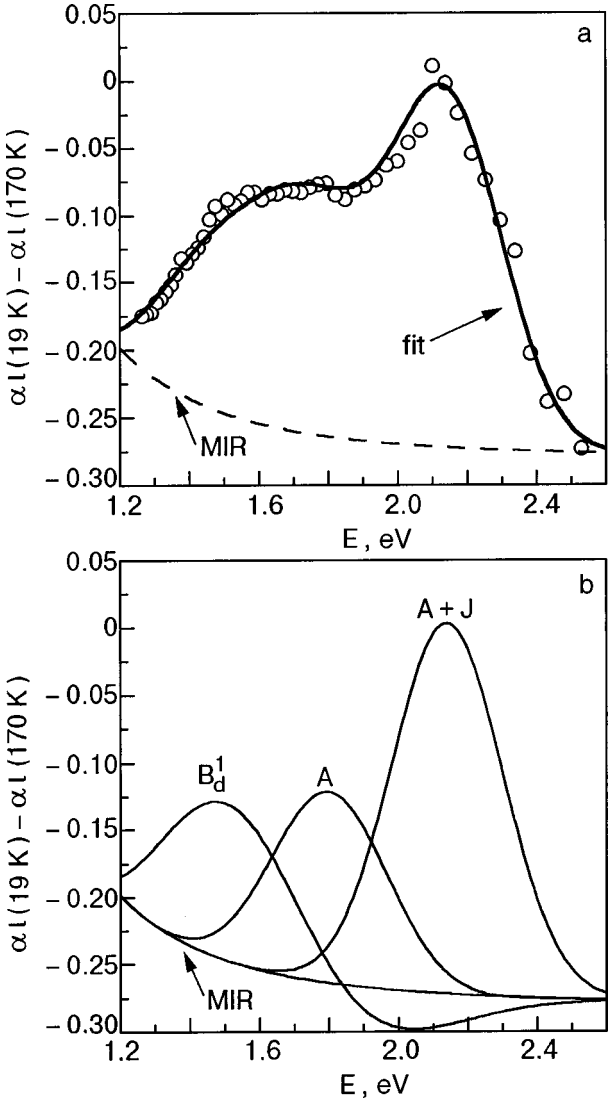

FIG. 7. Difference spectrum of the absorption $[\alpha l(19\,\mathrm{K}) - \alpha l(170\,\mathrm{K})]$ measured in the superconducting state of the VN608 film at $T = 19$ K relative to the initial temperature $T_0 = 170$ K (○). The solid curve labeled ''fit'' shows the model difference spectrum (a). The spectral composition of the model difference spectrum (b). The frequency dependence $\Delta(\alpha l)_{\mathrm{MIR}} = [(\alpha l)_{\mathrm{MIR}}(19\,\mathrm{K}) - (\alpha l)_{\mathrm{MIR}}(170\,\mathrm{K})$, labeled in the figure as MIR, was taken for the zero level of the spectral components (see text).

i.e., by 10%, while the amplitude coefficient increased by nearly a factor of two, from $\mu_0^A = 0.045$ eV (300 K) to 0.086 eV (19 K). In comparison with the VN604 film the amplitude coefficient (the area of the band) increased significantly while maintaining the same scale of decrease in the standard deviation.

For the $(A+J)$ contour, since it is absent at 300 K, the difference spectrum $\Delta(\alpha l)_{A+J}^{\mathrm{fit}}$ at 19 is a pure Gaussian with the parameters $\sigma_{A+J} = 0.16$ eV and $\mu_0^{A+J} = 0.07$ eV. The standard deviation of this contour at 19 K has practically the same value as in the insulator phase for $x \simeq 0.35$, where $\sigma_{A+J} = 0.17$ eV.[10] Here the amplitude coefficient of the $(A+J)$ contour in the VN608 film is more than three times its value at low temperatures in the VN604 film, with the lower T_c.

3. Comparing the temperature effects in the spectra for the two superconducting films VN604 and VN608, we see that they have some basic things in common:

— the temperature effects in the parameters of the covalent band B_d^1, the correlation band A, and the ''magnon'' band $(A+J)$ on cooling of $YBa_2Cu_3O_{6+x}$ from room temperatures begins below T^* in the existence region of the pseudogap state and takes place in the temperature interval $T_c \leqslant T \leqslant T^*$;

— the highest sensitivity to the formation of a pseudogap state is manifested by the ''magnon'' band $(A+J)$, which appears or is enhanced in the spectra of that state. All of the absorption bands are narrowed as the films are cooled in the region of the pseudogap state;

— in the superconducting phase the rate of the temperature evolution of all the spectral parameters of these bands decreases sharply. We note in particular that the ''magnon'' absorption band $(A+J)$ is conserved in the existence region of the superconducting phase.

In analyzing the microscopic causes of the temperature evolution of the spectral composition of the absorption in $YBa_2Cu_3O_{6+x}$, we must first discuss the behavior of the absorption bands A and $(A+J)$, which are related to the magnetic degrees of freedom. It is noteworthy that for $T < T^*$ there occurs a temperature-related narrowing of the A and $(A+J)$ absorption contours (after an enhancement of these bands at $T = T^*$). This picture is completely analogous to the behavior of these absorption bands in the insulating phase of $YBa_2Cu_3O_{6+x}$ at $x \simeq 0.35$, where they, being temperature-independent above T_N, begin to narrow in the AFM phase at $T < T_N \simeq 170$ K.[10] The narrowing effect in the pseudogap state of the films is also observed in the B_d^1 band: the amplitude coefficient of absorption for this dd transition remains practically unchanged as the temperature is lowered $(\mu_0^{1B} \simeq \mathrm{const})$, indicating that the level of pd mixing is conserved at low temperatures, but the B_d^1 contour itself is strongly narrowed. It is known[26,27] that in AFM crystals the dd absorption bands for ions with an unfilled d orbital, e.g., for Mn^{2+} in three-dimensional, two-dimensional, and quasi-one-dimensional magnetic structures, exhibit a noticeable narrowing as the temperature is lowered at $T \leqslant T_N$. The temperature-related narrowing of the dd absorption bands at $T < T_N$ is dictated by a decrease in the number of magnons in accordance with the Bose–Einstein factor. In the temperature region $T < \Delta_N / k_B$ the width of the dd absorption bands becomes weakly dependent on temperature. The sensitivity of the dd bands to the formation of an AFM state is particularly pronounced in the presence of an energy gap Δ_N in the spin-wave spectrum.[27]

In developing an analogy between the behavior of these absorption bands in the AFM insulator phase and in the metallized phase of $YBa_2Cu_3O_{6+x}$, we must recognize that the formation of a quasigap at $T \leqslant T^*$ occurs specifically in the spectrum of magnetic excitations. In such a case the nature of the pseudogap state is due to the decisive role of AFM fluctuations of the short-range order. The value of the spin gap for the correlation length ξ of the AFM fluctuations is $\Delta^* = c/\xi$ (Refs. 13 and 28), where $c \simeq 0.5$ eV·Å (Ref. 25) is the characteristic spin-wave velocity in $YBa_2Cu_3O_{6+x}$. Then for $\xi \simeq 10$ Å we get a gap of $\Delta^* \simeq 50$ meV. For wave vectors $q > \xi^{-1}$ the spin waves remain the same as in the presence of long-range magnetic order and are insensitive to the absence of AFM correlations at distances greater than

ξ.[28,29] According to Refs. 28 and 29, spin waves in the metallized states of HTSCs carry spin $S=1$ and are uncharged.

The effect wherein the $(A+J)$ band is preserved in the superconducting state is worthy of attention, as is the whole spectral composition of the absorption formed in the pseudogap state. This experimental result is nontrivial. It is completely possible to realize a situation in which the $(A+J)$ band would vanish in the SC phase, while the parameters of the B_d^1 and A contours change in the opposite direction in comparison with their values for the AFM pseudogap state. The conservation of the spectral composition of the absorption in the SC phase is, in our opinion, quite convincing evidence of the compatibility of short-range AFM ordering and superconductivity in $YBa_2Cu_3O_{6+x}$.

In discussing this question let us call attention to the following result. We have seen that the increase in T_c in the VN608 film is accompanied by enhancement of the degree of pd mixing, i.e., the intensity of the covalent B_d^1 absorption band is enhanced by doping. The simultaneous observation of the B_d^1 band and the A correlation band in the absorption spectra of $YBa_2Cu_3O_{6+x}$ was regarded in Ref. 10 as proof of the existence of a correlation polaron in the metallic phase. A correlation polaron is a mobile hole charge carrier around which is formed a region of predominantly covalent bonding and weakened Hubbard correlations (a region of strong metallization), while outside this region the matrix of strong Hubbard correlations is preserved.[30] The simultaneous observation of the A and B_d^1 absorption peaks at low temperatures in our experiments can serve as evidence that regions of AFM ordering coexist with more highly metallized regions, which, strictly speaking, become superconducting. In other words, in the CuO_2 plane the compatibility of antiferromagnetism and superconductivity is realized between spatially separate regions (domains) with different concentrations of doped holes. The possibility of a spatially separate pattern of coexistence of AFM ordering and superconductivity in HTSCs has been investigated experimentally in a number of studies (see, e.g., Refs. 1,3, and 16).

It is also of interest to compare directly the temperature behavior of the A and $(A+J)$ absorption bands and the temperature dependence of the homogeneous part of the magnetic susceptibility $\chi_0(T)$. According to the spin-wave model,[28,29] the susceptibility $\chi_0(T)$ in cuprate HTSCs, being weakly dependent on temperature for $T>T^*$, begins to decrease sharply as the spin gap opens for $T<T^*$, while in the SC phase at $T<T_c$ it again becomes independent of temperature. It is easy to see that such a trend of $\chi_0(T)$ corresponds to the temperature behavior of the A and $(A+J)$ absorption bands. Therefore, in view of what we have said above, one can assume that the results obtained in this paper are consistent with a spin-wave mechanism of high-T_c superconductivity.

CONCLUSION

The main result of this study is the experimental evidence supporting the view that the pseudogap state is due to AFM ordering of the short-range order, which is conserved in the SC phase. The many nonstandard properties of copper-oxide HTSCs in the normal and SC phases are apparently a manifestation of a fundamental feature of low-dimensional systems, in which scalar (charge) correlations and vector (magnetic) correlations are well developed.[2] In the final analysis these correlations are what give cuprate HTSCs their unique optical properties properties that are not encountered in classical metals or doped semiconductors. We mention, e.g., a sensitivity of the absorption of high-energy photons to the superconducting transition, as discussed in the present paper, a significant redistribution of the oscillator strengths of the interband transitions in favor of the intraband transitions in response to very low doping levels $\simeq 1\%$ (Ref. 2), and various kinds of nonequilibrium optical phenomena in the normal and SC states.[24] Our optical results can be regarded as a manifestation of the temperature-dependent contribution of the Hubbard correlations to the electronic spectrum.

It is also completely logical to assume that the results of the experiments on $YBa_2Cu_3O_{6+x}$ are of an extremely general character and are valid for other cuprate HTSCs with an active CuO_2 plane. The fundamental features of the electronic structure of cuprate HTSCs (the distribution of the density of states with a correlation A peak, the conservation of the AFM fluctuations of the short-range order in the metallic phase, the formation of a pseudogap state) can be obtained in the framework of a general one-band 2D Hubbard model (or its modifications) for the CuO_2 plane.

The first, key result of this paper, in our opinion, is that measurement of the temperature evolution of the spectral composition of the absorption in the 1–3 eV region, where the optical features of the CuO_2 plane are located, is an informative diagnostic tool for the normal and SC states. Studies done in this region have shown the following:

— the cooling of metallized $YB_2Cu_3O_{6+x}$ films from room temperatures leads not only to quantitative but also to qualitative changes of the spectral composition of the absorption of the films. Such changes are suffered by the dd absorption band ($d_{x,y}\rightarrow d_{x^2-y^2}$, $\hbar\omega\simeq 1.5$ eV), by the correlation band of absorption with charge transfer, which reflect the existence of the correlation maximum of the density of states (the A band, $\hbar\omega\cong 1.8$ eV), and by the ''magnon'' absorption band (the $(A+J)$ band, $\hbar\omega\simeq 2.1$ eV) due to additional excitation of the magnetic degrees of freedom;

— all of the temperature-related changes of these narrow-band spectral features occur at $T\leqslant T^*$ in the existence region of the pseudogap in the density of electronic excitations in the normal state of $YBa_2Cu_3O_{6+x}$;

— in the temperature region of the pseudogap state, $T_c \leqslant T\leqslant T^*$, the A, $(A+J)$, and dd absorption bands narrow, and the ''magnon'' band $(A+J)$ arises even when it is absent in the spectral composition of the absorption in the temperature region $T>T^*$;

— the character of the temperature effects in the A, $(A+J)$, and dd absorption bands in the pseudogap state is analogous to what is seen in an AFM insulator, a fact which undoubtedly indicates that the formation of the pseudogap state in a system of AFM fluctuations of the short-range order is of a magnetic nature;

— in the superconducting phase the quantitative and qualitative changes in the spectral composition of the absorption that have accumulated by the point of the transition to the SC phase practically cease, and in the superconducting

phase the spectral composition of the absorption, including the ''magnon'' band $(A+J)$, is conserved;

— the data obtained in this study and the analysis performed demonstrate the compatibility of superconductivity with antiferromagnetism of the short-range order and suggests a spin-wave nature of the high-T_c superconductivity in cuprate HTSCs.

The authors thank V. I. Fomin for a helpful discussion of the results, and S. V. Shevtseva for assistance in the preparation of the manuscript.

*E-mail: eremenko@ilt.kharkov.ua

[1] T. Timusk and B. Statt, Rep. Prog. Phys. **62**, 61 (1999).
[2] M. Imada, A. Fujimori, and Y. Tokura, Rev. Mod. Phys. **70**, 1039 (1998).
[3] G. G. Sergeeva, Yu. P. Stepanovskiĭ, and A. V. Chechkin, Fiz. Nizk. Temp. **24**, 1029 (1998) [Low Temp. Phys. **24**, 771 (1998)].
[4] V. Emery, S. A. Kivelson, and O. Zachar, Phys. Rev. B **56**, 6120 (1997).
[5] D. Pines, Turk. J. Phys. **20**, 535 (1996).
[6] D. A. Bonn, J. D. Garrett, and T. Timusk, Phys. Rev. Lett. **61**, 1305 (1988).
[7] I. Fugol, G. Saemann-Ischenko, V. Samovarov, Yu. Rybalko, V. Zhuravlev, Y. Ströbel, B. Holzapfel, and P. Berberich, Solid State Commun. **80**, 201 (1991).
[8] H. L. Dewing and E. K. H. Salje, Supercond. Sci. Technol. **5**, 50 (1992).
[9] I. Fugol, A. Ratner, V. Samovarov, M. Libin, B. Holzapfel, and G. Saemann-Ischenko, Physica C **235–240**, 1081 (1994).
[10] V. V. Eremenko, V. N. Samovarov, V. N. Svishchev, V. L. Vakula, M. Yu. Libin, and S. A. Uyutnov, Fiz. Nizk. Temp. **26**, 739 (2000) [Low Temp. Phys. **26**, 541 (2000)].
[11] G. Yu, C. H. Lee, D. Mihailovic, A. J. Heeger, C. Fincher, N. Herron, and E. M. McCarron, Phys. Rev. B **48**, 7545 (1993).
[12] N. Bulut, Turk. J. Phys. **20**, 548 (1996).
[13] V. Barzykin and D. Pines, Phys. Rev. B **52**, 13585 (1995).
[14] J. D. Perkins, R. J. Birgeneau, J. M. Graybeal, M. A. Kastner, and D. S. Kleinberg, Phys. Rev. B **58**, 9390 (1998).
[15] D. Salamon, P. Abbamonte, Ran Liu, M. V. Klein, W. C. Lee, D. M. Ginsberg, I. I. Tartakovkskii, and B. W. Veal, Phys. Rev. B **53**, 886 (1996).
[16] A. A. Maksimov, D. A. Pronin, S. V. Zaĭtsev, I. I. Tartakovskiĭ, M. V. Kleĭn, and B. U. Vil, Zh. Éksp. Teor. Fiz. **116**, 684 (1999) [JETP **89**, 366 (1999)].
[17] V. L. Aksenov and V. V. Kabanov, Phys. Rev. B **49**, 3524 (1994).
[18] J. Ye and K. Nakamura, Phys. Rev. B **48**, 7554 (1993).
[19] M. J. Holcomb, C. L. Perry, J. P. Collman, and W. A. Little, Phys. Rev. B **53**, 6734 (1996).
[20] Y. Yagil, F. Baudenbacher, M. Zhang, J. R. Birch, H. Kinder, and E. K. H. Salje, Phys. Rev. B **52**, 15582 (1995).
[21] V. V. Sobolev and V. V. Nemoshkalenko, *Electronic Structure of Solids near the Fundamental Absorption Edge* [in Russian], Naukova Dumka, Kiev (1992).
[22] E. F. Gross (Ed.), *Optical Properties of Semiconductors* [in Russian], Mir, Moscow (1970).
[23] V. D. Okunev and Z. A. Samoĭlenko, Fiz. Tverd. Tela (Leningrad) **33**, 2811 (1991) [Sov. Phys. Solid State **33**, 1588 (1991)].
[24] I. Ya. Fugol, V. N. Samovarov, and M. Yu. Libin, Fiz. Nizk. Temp. **25**, 459 (1999) [Low Temp. Phys. **25**, 335 (1999)].
[25] J. Rossat-Mignod, L. P. Regnault, C. Vettier, P. Bourge, P. Burlet, J. Bossy, J. Y. Henry, and G. Lapertot, Physica C **185–189**, 86 (1991).
[26] V. V. Eremenko, N. F. Kharchenko, Yu. G. Litvinenko, and V. M. Naumenko, *Magneto-Optics and Spectroscopy of Antiferromagnets*, Springer Verlag, Berlin (1992).
[27] A. V. Eremenko, V. V. Slavin, I. S. Kachur, and V. G. Piryatinskaya, Fiz. Nizk. Temp. **18**, Supplement No. S1, 137 (1992).
[28] A. Sokol, J. Phys. Chem. Solids **56**, 1679 (1995).
[29] S. Sachdev, A. V. Chubukov, and A. Sokol, Phys. Rev. B **51**, 14874 (1995).
[30] J. B. Goodenough and J. C. Zhou, Phys. Rev. B **42**, 4276 (1990); **49**, 4251 (1994).

Translated by Steve Torstveit

Light-induced reversible optical absorption in single-crystal slabs of yttrium iron garnets

R. A. Doroshenko* and M. D. Nadezhdin

Institute of Physics of Molecules and Crystals Ufa Science Center, Russian Academy of Sciences, 450075 Ufa, Russia

(Submitted October 4, 1999; revised May 4, 2000)
Fiz. Nizk. Temp. **26**, 1104–1107 (November 2000)

An additional increase of the optical absorption is observed when light of intensity greater than 1 W/cm^2 acts on single-crystal slabs of yttrium iron garnets. When a sample is subsequently subjected briefly to illumination by IR light of low intensity ($\sim$10 mW/cm^2) this effect is partially diminished or vanishes completely. © *2000 American Institute of Physics.* [S1063-777X(00)00611-3]

The change of the optical absorption coefficient α in iron-garnet ferrites under illumination at low temperatures was investigated in Refs. 1–6. In yttrium iron garnets (YIG) under illumination the optical absorption can increase or decrease, depending on the type of doping impurity.[1] The character of the change in the optical absorption depends on the spectral composition of the light.[5] At relatively low intensities that do not cause heating of the sample, the changes of the optical absorption reach equilibrium values that are preserved after the light is shut off.

Light affects the physical parameters of photomagnetic crystals in a complicated way. In addition to the photoinduced changes in the parameters, it is quite likely that there will also be a thermally induced change in the elastic (magnetoelastic) state as a result of the surface heating.[7] In turn, the modified elastic state of the sample can lead to new manifestations of the photoinduced effect. For example, the presence of elastic stresses in an iron garnet film due to the lattice misfit of the film and substrate leads to a high-temperature photoinduced effect.[8] In the present paper we investigate the change in the optical absorption under intense illumination that leads to heating of the sample. Here the time that the light acts is dosed in order to avoid overheating of the sample above the temperature attained. The source of illumination was a KGM-12/250 tungsten lamp (''white light''). To select irradiation in the infrared region an IKS-2 light filter was used. The temperature of the sample was monitored by a copper–Constantan thermocouple with a wire thickness of 0.05 mm, the junction of which was glued to the surface to be illuminated. The diameter of the focused light beam on the surface was $\approx$2 mm, which made it possible to obtain a high density of radiation and to illuminate part of the sample without heating the junction of the thermocouple by the beam. The measurement of the absorption coefficient α was done at a fixed wavelength $\lambda_m = 1.1$ μm at an intensity of the measuring beam of $\sim$50 μW/cm^2. The samples for the study were prepared in the form of disks 0.05 cm thick and 3.6 mm in diameter, consisting of single-crystal $Y_3Fe_5O_{12}$ grown from a $BaO–B_2O_3$ solution. In the absence of illumination the sample, which was glued to the cold finger of the vacuum cryostat, had a temperature of 80 K. The change of the absorption coefficient $\Delta\alpha$ at 1.1 μm was calculated according to the formula $\Delta\alpha = (1/h)\ln(I_d/I_l)$ (Ref. 1), where h is the thickness of the sample (in cm), I_d and I_l are the intensities of the measuring beam before and after the illumination, respectively. The use of this expression presupposes a uniform distribution of photoinduced changes over the thickness of the sample.

Figure 1 shows the time dependence of the change in the absorption coefficient $\alpha(t)$ upon illumination of the sample after cooling in darkness. Curve *1* was obtained at an irradiation intensity of $P \approx 0.5$ W/cm^2, for which no noticeable heating of the sample occurred during the illumination. The illumination brought about an increase in α to a value α_{eq}, and this state persisted for a long time. We note that in the single crystals under study the photoinduced changes of the magnetic parameters also persist over time.[11] At an intensity of $\sim$3 W/cm^2 the action of the light is accompanied by heating of the sample and causes an additional increase in the absorption coefficient α to a value α_{rel}, which is much higher than the value α_{eq} (segment AB of curve *2* in Fig. 1). The absorption level α_{rel} attained at 80 K is metastable, and after the illumination is turned off, it slowly relaxes to the value α_{eq} (the dashed curve in Fig. 1). It is found that the

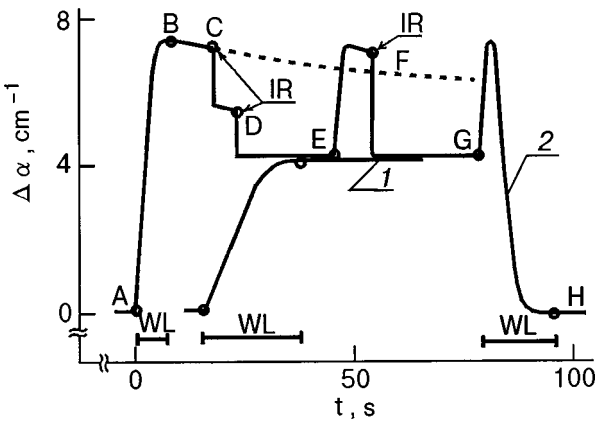

FIG. 1. Time dependence of the change $\Delta\alpha$ in the absorption coefficient under illumination by light of intensity 0.5 W/cm^2 (curve *1*) and 3 W/cm^2 (curve *2*); WL indicates intervals of illumination by ''white light'' (the continuous spectrum of a tungsten lamp). At the points *C*, *D*, and *F* the sample was briefly illuminated by infrared (IR) light with an intensity 10 mW/cm^2.

relaxation process is sharply accelerated under brief (around 1 s) illumination of the sample by IR light ($\lambda_{IR} > 0.9$ μm) of low intensity, ~ 10 mW/cm^2 (points C, *D*, and *F* on curves *2* in Fig. 1). We see that α_{rel} can vanish completely or undergo a partial or multistage decrease. No effect of the measuring beam ($\lambda = 1.1$ μm) on the relaxation process was detected in a check done by turning it on briefly at extended (~ 25–30 s) time intervals. After α has decreased to the level α_{eq} the IR illumination did not affect the level of optical absorption. Repeated illumination by an intense light beam (point *E* on curve *2* in Fig. 1) increased the absorption coefficient to the value α_{rel}. Light in the visible region (0.4–0.8 μm) did not cause a decrease of the additional absorption, a circumstance that attests to the bulk character of the observed effect.

Figure 2 shows the temperature dependence of the change $\Delta\alpha$ in the absorption coefficient on illumination (curves *AB*, *AC*, *AD*, and *AE*). The maximum effect is observed if the surface temperature of the sample under illumination does not exceed 120 K. When the light is turned off (curves *B*–*E*) there is a rapid (taking place over 7–10 s) decrease of the temperature to the initial value and a return of the $\Delta\alpha$ values along curves *1*–*4*, respectively. The level of optical absorption attained corresponds to the number of photoinduced centers at the temperature of the sample at the time the illumination is turned off. Curves *1*–*4* were obtained at a constant intensity but for different illumination times, i.e., the thickness of the photoinduced layer remains constant. A brief illumination (to preclude heating) with light of the same or higher intensity did not produce any additional discernable effect.

The curves of the temperature dependence in Fig. 2 and curve *2* in Fig. 1 were obtained with light of intensity $P \approx 3$ W/cm^2. For light of lower intensity the value of the effect in the initial illumination decreases. Increasing the intensity to $P > 3$ W/cm^2 leads initially to a slight increase and then to a decrease of the observed photoinduced effect on account of the stronger growth of the thermal effect of the light as the intensity is increased. We see from the curves in Fig. 2 (curves *2*–*4*) that heating the sample above $T_{max} \approx 120$ K at the time of the illumination leads to a decrease in the value of the effect. When the temperature is increased to ~ 200 K and the illumination is prolonged (curve *4* in Fig. 2) the photoinduced optical effect vanishes completely (segment *GH* of curve *2* in Fig. 1). In this case the sample undergoes a transition to its initial state, and the entire cycle can repeat. Thus by varying the spectral composition and intensity of the illumination, one can reversibly alter the optical absorption in the samples.

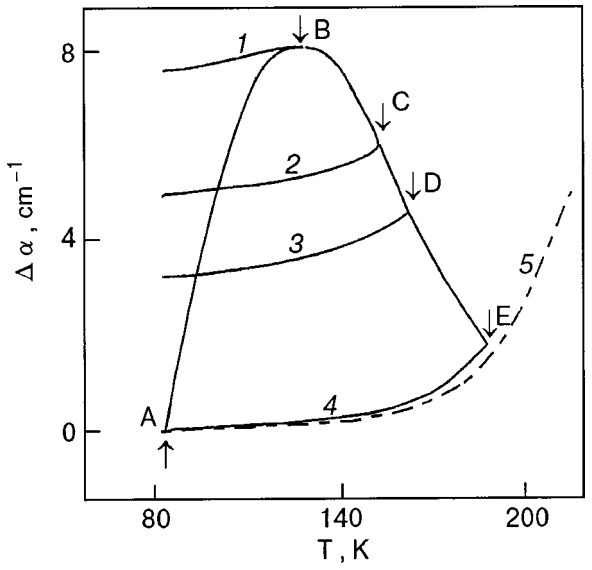

FIG. 2. Temperature dependence of the change $\Delta\alpha$ of the optical absorption coefficient under illumination by light with an intensity $P \approx 3$ W/cm^2. The arrows ↑ and ↓ denote the times at which the light is turned on and off, respectively. Curves *1*–*4* show the return of the values of $\Delta\alpha(T)$ on cooling after the illumination is turned off at points *B*–*E*, respectively. The dashed curve *5* shows the change $\Delta\alpha$ of the optical absorption with temperature on cooling in darkness.

The value of the photoinduced optical effect was measured at a wavelength of 1.1 μm, at which the level of optical absorption increases as the concentration of Fe^{4+} ions increases.[9,10] It can be assumed that the photoinduced equilibrium growth of α (to the value α_{eq}) is due to the formation of Fe^{4+} ions in octahedral sites. The formation of long-lived Fe^{4+} ions occurs through the photoexcitation of the electronic transitions ${}^6A_{1g}({}^6S) \rightarrow {}^4T_{1g}({}^4G), {}^4T_{2g}({}^4G)$, as has been observed experimentally in a discrete scanning of the illumination over the spectrum. The maximum value of the equilibrium effect is determined by the concentration of photoactive centers — that fraction of the iron ions that change their valence on illumination on account of the transition of an electron to free acceptor levels. The photoinduced changes of the magnetic properties of the given samples due to the formation of Fe^{4+} ions provide additional evidence in support of this conclusion.[11]

The additional photoinduced absorption α_{rel} observed under intense illumination causing photothermal deformations can be attributed to the formation of an additional quantity of nontrivalent iron ions or to an increase in the optical absorption on the part of the existing photoinduced nontrivalent iron ions. The features of the onset of additional optical absorption (the fact that it occurs only in the presence of elastic stresses arising in the photothermal heating of the surface of the sample on the cold finger and not when the sample is placed in liquid nitrogen) and its quenching argue in favor of the second mechanism. We note that quenching of the photoinduced effect is not observed under IR illumination (curve *1* in Fig. 1), even when that effect is reversible at higher temperatures.

The additional optical absorption in the samples under study is due to the change in the orbital state of the Fe^{4+} ions and is determined by the increase in the probability of excitation of the electrons. For Fe^{4+} ions the degenerate ground state e_g is split by the Jahn–Teller effect into levels of the type d_{z^2} and $d_{x^2-y^2}$. For elongated octahedra (tetragonal distortions of the elongation) the orbital ground state is a state of the type d_{z^2} (Ref. 12). The presence of elastic stresses affects the filling sequence of the levels. In the photoexcitation of the Fe^{4+} ions in elastically deformed octahedra the orbital state with the reverse sequence of level positions becomes more favorable ($d_{x^2-y^2}$ is the ground state and d_{z^2} is

the upper orbital state). The capture cross sections of the wave functions for photons are different in this case. After the illumination is stopped, the state becomes metastable, and, in the absence of elastic strains, photoexcitation by IR light is sufficient for the transition of the Fe^{4+} ions to the initial orbital state (from the ground state of the type d_{z^2}). The important role of nonuniform elastic stresses is also indicated by the light-induced rearrangement of the domain structure at room temperature in the samples studied.[7]

Further studies are needed for justification of the mechanism for the change in the orbital state of the Fe^{4+} ions under the combined action of light and elastic stress. Additional confirmation of the proposed mechanism might be obtained from studying the magnetic and magnetooptic properties of the samples under analogous conditions. The effect of IR quenching of the additional absorption, quantitative estimates of the rate of this quenching and the spectral characteristics of the effect merit further study.

This study was carried out with the financial support of the Russian Foundation for Basic Research.

*E-mail: dar@anrb.ru

[1] E. M. Gyorgy, J. F. Dillon, and J. P. Remeika, J. Appl. Phys. **42**, 1454 (1971).
[2] N. G. Nakhodkin and V. V. Voznyuk, Fiz. Tverd. Tela (Leningrad) **31**, 114 (1989) [Sov. Phys. Solid State **31**, 610 (1989)].
[3] K. Hisatake, I. Matsubara, K. Maeda, H. Yasuoka, H. Mazaki, and K. Uematsu, J. Magn. Magn. Mater. **140–144**, 2127 (1995).
[4] K. Hisatake, I. Matsubara, K. Maeda, H. Yasuoka, H. Mazaki, and K. Uematsu, J. Magn. Soc. Jpn. **19**, Suppl S1, 263 (1995).
[5] R. A. Doroshenko and M. D. Nadezhdin, Fiz. Tverd. Tela (St. Petersburg) **38**, 3075 (1996) [Phys. Solid State **38**, 1682 (1996)].
[6] V. A. Bedarev, S. L. Gnatchenko, R. A. Rupp, and B. Sugg, Fiz. Nizk. Temp. **24**, 281 (1998) [Low Temp. Phys. **24**, 212 (1998)].
[7] V. G. Veselago, R.A. Doroshenko, M. S. Setchenkov, and M. D. Nadezhdin, Fiz. Tverd. Tela (Leningrad) **30**, 2863 (1988) [Sov. Phys. Solid State **30**, 1653 (1988)].
[8] V. P. Sokhatskiĭ and V. F. Kovalenko, JETP Lett. **61**, 1021 (1995).
[9] D. L. Wood and I. P. Remeika, J. Appl. Phys. **17**, 1232 (1966).
[10] D. L. Wood and I. P. Remeika, J. Appl. Phys. **38**, 1038 (1967).
[11] Fotomagnetizm, Trudy IOFAN **44**, Nauka, Moscow (1992).
[12] K. I. Kugel' and D. I. Khomskiĭ, Usp. Fiz. Nauk **136**, 621 (1982) [Sov. Phys. Usp. **25**, 231 (1982)].

Translated by Steve Torstveit

Phase diagram and the spectra of coupled magnetoelastic waves of a biaxial ferromagnet with a biquadratic interaction in an external magnetic field

Yu. A. Fridman,* O. A. Kosmachev, and G. É. Baĭramalieva

V. I. Vernadskiĭ Tavricheskiĭ National University, ul. Yaltinskaya 4, 95007 Simferopol, Ukraine
(Submitted March 6, 2000)
Fiz. Nizk. Temp. **26**, 1108–1114 (November 2000)

The spectra of coupled magnetoelastic waves of a biaxial ferromagnet with a biquadratic interaction are investigated as a function of the external magnetic field. It is shown that the dynamic properties of magnetoelastic waves and the phase states of the system are determined by the relation between the Heisenberg and biquadratic exchange constants. A three-dimensional phase diagram is constructed for the system. © *2000 American Institute of Physics.* [S1063-777X(00)00711-8]

1. INTRODUCTION

There is great interest at the present time in the study of magnets with non-Heisenberg exchange interactions of a more complex nature between the magnetic ions.[1–4] From a practical standpoint it is of interest to study the characteristics of the spectrum of excitations of these magnets as the external magnetic field is changed. Studies of this kind are important because of the existence of a number of singlet magnets,[5,6] which, as we know, can be found in a nonmagnetic state for $H=0$ (in the so-called quadrupolar (QP) phases), which undergo a transition to a magnetic phase upon imposition of a sufficiently strong external magnetic field.

This metamagnetic transition can be of various natures. In particular, the singlet ground state of the magnet may be conditional on a large value of the one-ion anisotropy (OA).[3,4,7] Another mechanism leading to a nonmagnetic phase at $H=0$ might be the presence of a biquadratic interaction.[1,2] In highly anisotropic Heisenberg magnets these two factors can act simultaneously, giving rise to peculiarities of the ground state and features in the spectral properties.

In addition to the indicated factors the spectral characteristics of magnets (especially in the neighborhood of orientational phase transitions the magnetoelastic (ME) interaction has a large influence.[8,9]

The study of the phase states and spectra of highly anisotropic ferromagnets of both the Heisenberg and non-Heisenberg types has been the subject of many papers (see, e.g., the review in Ref. 2). For example, in Ref. 3 the magnon spectra in a highly anisotropic non-Heisenberg ferromagnet was investigated in the case of zero external magnetic field. In Ref. 4 the same system was investigated but with allowance for the ME interaction. It was shown in these papers that those systems can have phase transitions with respect to the material constants of the system. These transitions occur along the magnon branch of excitations; they are not reorientational but take place through a decrease in the modulus of the magnetization vector.[3] Taking the ME interaction into account leads to a narrowing of the existence region of the ferromagnetic phases and a widening of the existence region of the quadrupolar phases.[4]

In Ref. 7 a highly anisotropic biaxial ferromagnet in an external magnetic field was investigated with allowance for the ME interaction. It was shown that the phase transitions in such a system are reorientational, the soft mode being a quasielastic branch of excitations. However, the biquadratic interaction was not taken into account in the model of Ref. 7.

By studying the field dependence of the spectra of magnetic and sound-wave excitations for various regions of interaction parameters, one can acquire additional information about the nature of singlet magnets and metamagnetic transitions.

2. DISPERSION RELATION FOR COUPLED MAGNETOELASTIC WAVES

Let us consider a ferromagnetic crystal having biaxial one-atom anisotropy and a biquadratic exchange interaction and located in an external magnetic field $\mathbf{H}\|0X$. The Hamiltonian of such a system can be written in the form

$$\mathcal{H}=-H\sum_n S_n^x-\frac{1}{2}\sum_{n,n'}\{J(n-n')\mathbf{S}_n\mathbf{S}_{n'}+K(n-n')\times(\mathbf{S}_n\mathbf{S}_{n'})^2\}-B_2^0\sum_n (3(S_n^z)^2-S(S+1))-B_2^2\sum_n \frac{1}{2}\{(S_n^+)^2+(S_n^-)^2\}+\nu\sum_n S_n^i S_n^j u_{ij}(n)+\int dr\left\{\frac{\lambda+\eta}{2}\sum_i u_{ii}^2+\eta\sum_{i,j} u_{ij}^2+\lambda\sum_{i\neq j} u_{ii}u_{jj}\right\}, \tag{1}$$

where S_n^i is the spin operator at site n, $J(n-n')$ and $K(n-n')$ are the Heisenberg and biquadratic interaction constants, respectively, B_2^0 and B_2^2 are the OA constants, ν is the ME coupling constants, λ and η are elastic moduli, and $u_{ij}(n)$ are components of the elastic strain tensor $(i,j=x,y,z)$.

The first term in (1) is the Zeeman interaction, the second, third, and fourth terms describe the magnetic sub-

system, the fifth is the ME interaction, and the last term describes the elastic subsystem in the continuum approximation.

Without loss of generality we can assume that $B_2^2>0$, since the half plane $B_2^2<0$ is only a mirror reflection of the other, with interchanged indices x and y. For example, if $B_2^2<0$, after rotating the coordinate system about the $0Z$ axis by an angle of $\pi/2$, we would obtain Hamiltonian (1) with the substitution $B_2^2\to|B_2^2|$. Imposing an external field directed along the $0X$ axis breaks the symmetry of the problem, and therefore in the calculations below we shall make use of the condition that $B_2^2>0$.

In the most general case Eq. (1) must be written in a rotationally invariant form.[10] Rotational invariance leads to a number of interesting effects, in particular, to the appearance of a new mechanism of ME coupling which is directly due to the OA. However, for the spectral characteristics of massive free samples the rotational invariance leads only to a renormalization of the coefficients in the spectrum of ME waves.[11] Rotational invariance becomes important in the study of magnetic films, wires, or clamped samples.[12] We shall therefore ignore the rotational invariance when considering a massive sample in this paper.

To simplify the calculations we shall assume that the magnetic ion has spin $S=1$.

The OA and ME coupling can be taken into account exactly by using the technique of Hubbard operators[9,13,14] constructed on a complete basis of one-ion states.

Separating out the mean field $\langle S^x\rangle$ and the additional fields q_2^p $(p=0,2)$ in the exchange part of (1), we obtain the following expression for the one-site Hamiltonian $\mathcal{H}_0(n)$:

$$\mathcal{H}_0(n)=-\overline{H}S_n^x-\tilde{B}_{2n}^0O_{2n}^0-\tilde{B}_{2n}^2O_{2n}^2+\nu S_n^iS_n^ju_{ij}(n), \quad (2)$$

where

$$\overline{H}=H+\sum_n\left(J(n-n')-\frac{1}{2}K(n-n')\right)\langle S^x\rangle;$$

$$\tilde{B}_{2n}^0=B_{2n}^0+\frac{1}{6}\sum_{n'}K(n-n')q_{2n}^0;$$

$$\tilde{B}_{2n}^2=B_{2n}^2+\frac{1}{2}\sum_{n'}K(n-n')q_{2n}^2;$$

$$q_{2n}^0=\langle O_{2n}^0\rangle,\quad q_{2n}^2=\langle O_{2n}^2\rangle;$$

$$O_{2n}^0=3(S_n^z)^2-2;\quad O_{2n}^2=\frac{1}{2}\{(S_n^+)^2+(S_n^-)^2\}.$$

Solving the one-ion problem $\mathcal{H}_0\Psi_n(M)=E_M\Psi_n(M)$ with the Hamiltonian (2), we obtain the eigenfunctions of the one-site Hamiltonian and the energy levels of the magnetic ion with allowance for the ME interaction:

$$E_+=\frac{\tilde{B}_2^0-\tilde{B}_2^2}{2}+\nu\left(u_{xx}^{(0)}+\frac{u_{yy}^{(0)}+u_{zz}^{(0)}}{2}\right)-\frac{\chi}{2};$$

$$E_0=\frac{\tilde{B}_2^0-\tilde{B}_2^2}{2}+\nu\left(u_{xx}^{(0)}+\frac{u_{yy}^{(0)}+u_{zz}^{(0)}}{2}\right)+\frac{\chi}{2};$$

$$E_-=\tilde{B}_2^2-\tilde{B}_2^0+\nu(u_{yy}^{(0)}+u_{zz}^{(0)}); \quad (3)$$

$$\chi^2=4\overline{H}^2+[3\tilde{B}_{2n}^0+\tilde{B}_{2n}^2+\nu(u_{yy}^{(0)}-u_{zz}^{(0)})]^2;$$

$$\Psi_n(+)=\cos\theta|+\rangle+\sin\theta|0\rangle;$$

$$\Psi_n(0)=-\sin\theta|+\rangle+\cos\theta|0\rangle;\quad \Psi_n(-)=|-\rangle, \quad (4)$$

where

$$\cos 2\theta=\frac{3\tilde{B}_{2n}^0+\tilde{B}_{2n}^2+\nu(u_{yy}^{(0)}-u_{zz}^{(0)})}{\chi},$$

$$\sin 2\theta=\frac{2\overline{H}}{\chi};\quad |\pm\rangle=\frac{1}{\sqrt{2}}(|1\rangle\pm|-1\rangle),$$

$|0\rangle$, $|1\rangle$, $|-1\rangle$ are the eigenfunctions of the operator S^z, and the spontaneous strains $u_{ij}^{(0)}$, which are determined from the condition that the free energy density be minimum, have the following form at low temperatures:

$$u_{xx}^{(0)}=-\frac{\nu(\lambda+\eta)}{\eta(\eta+3\lambda)};\quad u_{yy}^{(0)}=-\frac{\nu(\eta-\lambda)}{\eta(\eta+3\lambda)}\sin^2\theta;$$

$$u_{zz}^{(0)}=-\frac{\nu(\eta-\lambda)}{\eta(\eta+3\lambda)}\cos^2\theta.$$

We should mention that the eigenfunctions (4) are obtained in general form (for $S=1$) in Ref. 14.

We use the eigenfunctions (4) of the one-site Hamiltonian $\mathcal{H}_0$ as a basis for constructing the Hubbard operators[9,13] $X_n^{M'M}\equiv|\Psi_n(M')\rangle\langle\Psi_n(M)|$ describing the transition of a magnetic ion from the state M' to the state M. In terms of the Hubbard operators the Hamiltonian (2) can be put in the form

$$\mathcal{H}_0(n)=\sum_M P_MH_n^M+\sum_\alpha P^\alpha X_n^\alpha,$$

where $H_n^M\equiv X_n^{MM}$ are the diagonal Hubbard operators, and α are the root vectors.

The coupling of the spin operators with the Hubbard operators is determined in the standard way, and in the case under discussion it has the form

$$S_n^+=(H_n^+-H_n^0)\sin 2\theta+(X_n^{+0}+X_n^{0+})\cos 2\theta$$
$$+(X_n^{-+}-X_n^{+-})\sin\theta+(X_n^{-0}-X_n^{0-})\cos\theta;$$

$$S_n^-=(S_n^+)^+; \quad (5)$$

$$S_n^z=(X_n^{+-}+X_n^{-+})\cos\theta-(X_n^{0-}+X_n^{-0})\sin\theta.$$

The dynamical properties of magnets have a number of features in the neighborhood of the phase transition. It is well known that taking the ME interaction into account leads to hybridization of the elementary excitations, and even though the ME coupling is very weak, in the neighborhood of an orientational phase transition this parameter plays an important role in the dynamics of the system.[8,9] To study this question we write the strain tensor in the form of two terms: the spontaneous strains $u_{ij}^{(0)}(n)$, defined above, and a dynamic term $u_{ij}^{(1)}(n)$, which describes lattice vibrations. This term is related to the phonon annihilation (creation) operators $b_{k,\lambda}$ $\times(b_{k,\lambda}^+)$ by the well-known relation[15]

$$u_{ij}^{(1)}=\frac{i}{2}\sum_{k,\lambda}\frac{\exp(i\mathbf{k}\cdot\mathbf{n})}{[2mN\omega_\lambda(k)]^{1/2}}(b_{k,\lambda}+b_{-k,\lambda}^{+})(e_\lambda^i(k)k_j + e_\lambda^j(k)k_i),$$

where $\mathbf{e}_\lambda(k)$ is the phonon polarization unit vector, $\lambda = l,t,\tau$ is the polarization index, m is the mass of the magnetic ion, N is the number of sites in the lattice, $\omega_\lambda(k) = c_\lambda k$ is the dispersion relation for free phonons, and c_λ is the velocity of λ-polarized sound.

Separating out in the one-site Hamiltonian (2) the part proportional to $u_{ij}^{(1)}(n)$ and quantizing it in accordance with the formula given, we obtain a Hamiltonian describing processes of conversion of magnons into phonons and back:

$$\mathcal{H}_{\rm tr}=\sum_n\left\{\sum_M \mathcal{P}_M H_n^M+\sum_\alpha \mathcal{P}_\alpha X_n^\alpha\right\}, \tag{6}$$

where

$$\mathcal{P}_{M(\alpha)}=\frac{1}{N^{1/2}}\sum_{k,\lambda}(b_{k,\lambda}+b_{-k,\lambda}^{+})T_n^{M(\alpha)}(k,\lambda),$$

with $T_n^{M(\alpha)}(k,\lambda)$ being the transformation amplitudes.

It is well known that the spectrum of elementary excitations is determined by the poles of the Green function. The Green function for the system under study has the form

$$G^{\alpha\alpha'}(n,\tau;n',\tau')=-\langle\hat{T}\tilde{X}_n^\alpha(\tau)\tilde{X}_{n'}^{\alpha'}(\tau')\rangle.$$

Here $\hat{T}$ is the Wick operator, $\tilde{X}_n^\alpha(\tau)$ is the Hubbard operator in the Heisenberg representation, and the average is done using the total Hamiltonian $\mathcal{H}=\mathcal{H}_{\rm int}+\mathcal{H}_{\rm tr}+\mathcal{H}_0$.

From here on we shall do the calculation in the mean field approximation, and we shall therefore need only the ''transverse'' part of the exchange Hamiltonian, which can be written in the form

$$\mathcal{H}_{\rm int}=-\frac{1}{2}\sum_{\substack{n,n'\\ \alpha,\beta}}\{\mathbf{c}(\alpha)\hat{A}_{nn'}\mathbf{c}(\beta)\}X_n^\alpha X_{n'}^\beta,$$

where the eight-dimensional vector $\mathbf{c}(\alpha)$ has the following components:

$$\mathbf{c}(\alpha)=\{\gamma_1^{\parallel}(\alpha),\gamma_1^{\perp}(\alpha),\gamma_1^{\perp}{}^*(-\alpha),\gamma_2^{\parallel}(\alpha),\gamma_2^{\perp}(\alpha),\gamma_2^{\perp}{}^*\times(-\alpha),\gamma_3^{\perp}(\alpha),\gamma_3^{\perp}{}^*(-\alpha)\},$$

while the 8×8 matrix $\hat{A}_{nn'}$ decomposes into a direct sum of two matrices:

$$\hat{A}_{nn'}=\hat{A}_{nn'}^{(3)}\oplus\hat{A}_{nn'}^{(5)};$$

$$\hat{A}_{nn'}^{(3)}=\left\{J(n-n')-\frac{1}{2}K(n-n')\right\}\begin{pmatrix}1&0&0\\0&0&1/2\\0&1/2&0\end{pmatrix},$$

$$\hat{A}_{nn'}^{(5)}=\frac{K(n-n')}{2}\begin{pmatrix}1&0&0&0&0\\0&0&1/2&0&0\\0&1/2&0&0&0\\0&0&0&0&1/2\\0&0&0&1/2&0\end{pmatrix}. \tag{7}$$

The functions $\gamma_i^{\parallel(\perp)}(\alpha)$ are determined from the relation between the spin operators and the Hubbard operators (5).

Turning on the biquadratic interaction formally has the effect of increasing the dimension of the vectors $\mathbf{c}(\alpha)$ and the matrix $\hat{A}_{nn'}$ in comparison with the case when only the Heisenberg exchange is taken into account. The eight-dimensionality of the vectors $\mathbf{c}(\alpha)$ is due to the fact that for biquadratic exchange the number of linearly independent operators is equal to five, while in the case when both the biquadratic and Heisenberg interactions are present (the structure of the latter is determined by three independent spin operators S_n^i) it is necessary to use an eight-dimensional basis.

The equation for the Green function has the form of Larkin's equation.[16] Solving it, we obtain the dispersion relation for the coupled ME waves:

$$\det\|\delta_{ij}+x_{ij}\|=0; \tag{8}$$

where

$$x_{ij}=G_0^\alpha(\omega_n)b(\alpha)c_{ij}(\alpha) + B^0(k,\lambda,\lambda')T^{-\alpha}(k,\lambda)G_0^\alpha(\omega_n)b(\alpha)T^\beta \times(-k,\lambda')G_0^\beta(\omega_n)b(\beta)c_{ij}(\alpha,\beta).$$

Here

$$B^0(k,\lambda,\lambda')=\frac{D_\lambda(k,\omega_n)}{1-Q_{\lambda\lambda'}D_{\lambda'}(k,\omega_n)};$$

$$Q_{\lambda\lambda'}=T^\alpha(-k,\lambda)G_0^\alpha(\omega_n)T^{-\alpha}(k,\lambda')b(\alpha);$$

$$c_{ij}(\alpha,\beta)=a_{ik}(\alpha,\beta)A_{kj};\quad a_{ik}=c_i(\alpha)c_k(-\beta),$$

$$b(\alpha)=\langle\boldsymbol{\alpha}\mathbf{H}\rangle_0;$$

$D_\lambda(k,\omega_n)=(2\omega_\lambda(k))/(\omega_n^2-\omega_\lambda^2(k))$ is the Green function of a free λ-polarized phonon, and $G_0^\alpha(\omega)=\{\omega+(\boldsymbol{\alpha}\cdot\mathbf{E})\}^{-1}$ is the zeroth Green function. Equation (8) is valid at arbitrary temperatures and for arbitrary relationships among the material constants.

3. SPECTRA OF COUPLED MAGNETOELASTIC WAVES AND THE PHASE DIAGRAMS OF A BIAXIAL FERROMAGNET

Let us analyze Eq. (8) for different relationships between the constants of the Heisenberg and biquadratic exchange ($J_0>K_0$ and $J_0<K_0$). To simplify the calculations we restrict discussion to the low-temperature case ($T\ll T_C$, where T_C is the Curie temperature).

We consider the most interesting case, when the direction of the wave vector coincides with the direction of the external field ($\mathbf{k}\|0X$). In this geometry the nonzero components of the polarization unit vector are e_l^x, e_t^z, and e_τ^y, and the nonzero transformation amplitudes have the form

$$T^{-+}(k,t)=T^{+-}(k,t)=i\frac{\nu}{2}T_0(k,t)e_t^z k\sin\theta,$$

$$T^{-+}(k,\tau)=-T^{+-}(k,\tau)=\frac{\nu}{2}T_0(k,\tau)e_\tau^y k\cos\theta, \tag{9}$$

$$T_0(k,\lambda)=\frac{\exp(i\mathbf{k}\cdot\mathbf{n})}{(2m\omega_\lambda(k))^{1/2}}.$$

As was shown in Refs. 3 and 4, in the absence of external field, four phases can be realized in the system: two magnetic (the FM_x phase with $\langle S\rangle \| 0X$, and the FM_z phase, with $\langle S\rangle \| 0Z$), and two quadrupolar.

For $H \neq 0$ (H is large, higher than a certain H_c), analysis of the order parameters of the system

$$\langle S^x\rangle = \sin 2\theta; \quad q_2^0 = \langle O_2^0\rangle = \frac{3}{2}(1+\cos 2\theta) - 2;$$

$$q_2^2 = \langle O_2^2\rangle = \frac{1}{2}(1+\cos 2\theta)$$

shows that the quadrupolar phases cannot exist at any values of the material constants B_2^0, $B_2^2 > 0$, K_0, and J_0, since turning on the magnetic field gives rise to a nonzero magnetic moment in the system, i.e., the appearance of quadrupolar–ferromagnetic QFM_x phase ($\langle S^x\rangle \to 1$ for $H \to \infty$). For $H \leqslant H_c$ the system undergoes a transition to a canted QFM_{zx} phase, in which both $\langle S^x\rangle$ and $\langle S^z\rangle$ components of the magnetization vector exist simultaneously. The transition field H_c is determined from the spectra of coupled ME waves. To determine it, we use the dispersion relation for $H \geqslant H_c$, i.e., we assume that the system is found in the QFM_x phase, near the line of the QFM_x–QFM_{zx} phase transition.

In this case Eq. (8) ''decouples'' with respect to polarizations, and its solutions have the following form:

$$\omega_1(k) = \omega_l(k); \quad \omega_2(k) \approx \omega_\tau(k); \quad \varepsilon_1(k) \approx \chi;$$

$$\varepsilon_2^2(k) = [E_{+-} + J(k)]^2 - [J(k) - K(k)]^2 \cos 2\theta - \frac{a_0[E_{+-} + J(k) - (J(k) - K(k))\cos 2\theta]\omega_t^2(k)(1-\cos\theta)}{(E_{+-} J(k))^2 - (J(k) - K(k))^2 \cos^2 2\theta}; \tag{10}$$

$$\omega_3^2(k) = \omega_t^2(k)\left\{1 + \frac{[E_{+-} + J(k) - (J(k) - K(k))\cos 2\theta]a_0(1-\cos 2\theta)}{(E_{+-} + J(k))^2 - (J(k) - K(k))^2 \cos^2 2\theta}\right\};$$

where

$$E_{+-} = E_+ - E_- = \frac{3}{2}(B_2^0 - B_2^2) - \frac{K_0}{2} - a_0 - \frac{\chi}{2};$$

$$a_0 = \frac{\nu^2}{2\eta}.$$

It follows from the solutions (10) of the dispersion relation that the l- and τ-polarized phonons do not interact with the magnetic subsystem; the high-frequency magnon branch $\varepsilon_1(k)$ likewise does not interact with the elastic subsystem. The low-frequency quasimagnon branch $\varepsilon_2(k)$ and the t-polarized sound wave (the quasiphonon branch $\omega_3(k)$) interact with each other, forming a hybridized ME wave.

It should be noted that in the given geometry, a decrease of the magnetic field to the value H_c is accompanied by a decrease in the modulus of the magnetization vector to the value $\langle S^x\rangle_{H=H_c}$. For $H = H_c$ the system undergoes a transition to the QFM_{zx} phase, while for $H = 0$ the component $\langle S^x\rangle$ goes to zero, and the system undergoes a transition to the FM_z phase.[3,4] We interpret the field H_c as the field of a phase transition; it is determined from the condition of ''softening'' of the spectrum of t-polarized quasiphonons. Here the quasiphonon spectrum has the form

$$\omega_3^2(k) = \omega_t^2(k)\,\frac{\alpha k^2 + H - H_c}{\alpha k^2 + H - H_c + a_0},$$

where $\alpha = J_0 R_0^2$, with R_0 the interaction radius. The phase transition field is

$$H_c = \left\{\frac{3B_2^0 - B_2^2}{2}[\xi - B_2^2 - 3B_2^0 - 2(J_0 - K_0 - a_0)]\right\}^{1/2},$$

$$\zeta = \{[3(B_2^2 - B_2^0) + 2(J_0 - K_0 - a_0)]^2 + 16(3B_2^0 - B_2^2)(J_0 - K_0 - a_0)\}^{1/2}.$$

Thus for $H = H_c$ in the long-wavelength limit ($\alpha k^2 \ll a_0$) the quasiphonon spectrum ''softens,'' while the quasimagnon spectrum exhibits a ME gap given by

$$\varepsilon_2(0) = \sqrt{a_0(1-\cos 2\theta_c)[a_0(1-\cos 2\theta_c) + 2(J_0 - K_0)\cos 2\theta_c]}.$$

Here

$$\cos 2\theta_c = \cos 2\theta_{H=H_c} = \frac{3(B_2^2 - B_2^0) - 2(J_0 - K_0 - a_0) + \xi}{4(J_0 - K_0 - a_0)}.$$

The modulus of the magnetization vector for $H = H_c$ is equal to

$$\langle S^x\rangle_{H=H_c} = \sqrt{1 - \cos^2 2\theta_c}.$$

Thus the QFM_x–QFM_{zx} phase transition occurs through a decrease in the modulus of the magnetization vector, i.e., it is not reorientational with respect to the vector order parameter. However, at the phase transition point the soft mode is a t-polarized quasiphonon mode, as is typical for reorientational phase transitions.[8] Consequently, the reorientation in this case reduces to a rotation of the principal axes of the quadrupole moment tensor. Behavior of this kind has been observed in the system under discussion, for $H = 0$ and $K_0 > J_0$ (Ref. 4).

The phase diagram in the variables

$$\left(\frac{B_2^2}{J_0 - K_0}, \frac{B_2^0}{J_0 - K_0}, \frac{H}{J_0 - K_0},\right)$$

corresponds to the situation considered, which is illustrated in Fig. 1. The figure shows a few cross sections of the phase

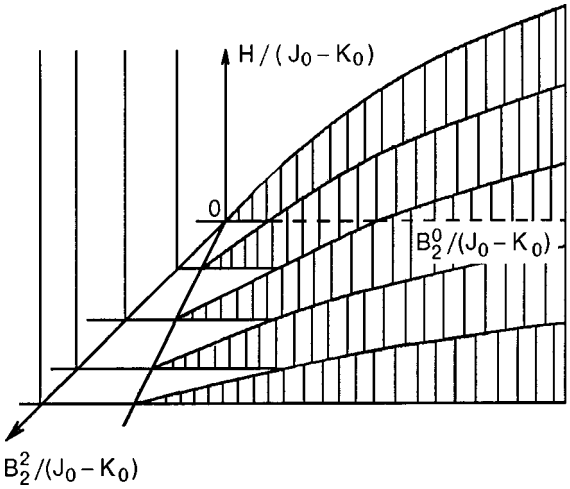

FIG. 1. Phase diagram of a biaxial ferromagnet with a biquadratic interaction in the case $J_0>K_0$.

diagram for $J_0>K_0$. For example, the region $B_2^2<3B_2^0$, $B_2^2<J_0-K_0-a_0$ for $H=0$ corresponds to the FM_z phase ($\langle S\rangle \| 0Z$). Imposing a field H along the $0X$ axis gives rise to a magnetic moment in the $Z0X$ plane, i.e., to the QFM_{zx} phase (the shaded regions of the phase diagram). When the critical field H_c is reached, the system undergoes a transition to the QFM_x phase through growth of the modulus of the magnetization vector.

If the biquadratic exchange exceeds the Heisenberg interaction, then only the two quadrupolar phases, QP_1 and QP_2, can be realized in the system in the absence of magnetic field.[3,4] Imposing a field will make it impossible for the QP_1 and QP_2 phases to exist, since $\langle S^x\rangle \neq 0$ for $H\neq 0$. Analysis of the spectra of elementary excitations shows that the magnetization component $\langle S^z\rangle$ does not arise for any values of the magnetic field. Thus for $K_0>J_0$ and $H\neq 0$ the system is found in the QFM_x phase and does not undergo a phase transition.

*E-mail: man@expl.cris.crimea.ua

[1] É. L. Nagaev, *Magnets with Complicated Exchange Interactions* [in Russian], Nauka, Moscow (1988).
[2] V. M. Loktev and V. S. Ostrovskiĭ, Fiz. Nizk. Temp. **20**, 983 (1994) [Low Temp. Phys. **20**, 775 (1994)].
[3] V. V. Val'kov, G. N. Matsuleva, and S. G. Ovchinnikov, Fiz. Tverd. Tela (Leningrad) **31**, 60 (1989) [Sov. Phys. Solid State **31**, 948 (1989)].
[4] Yu. N. Mitsaĭ, Yu. A. Fridman, O. V. Kozhemyako, and O. A. Kosmachev, Fiz. Nizk. Temp. **25**, 690 (1999) [Low Temp. Phys. **25**, 513 (1999)].
[5] R. Aleonard and P. Morin, Phys. Rev. **19**, B3868 (1979).
[6] P. Morin, J. Rouchy, and D. Schmitt, Phys. Rev. **17**, B3684 (1978).
[7] Yu. N. Mitsay, Yu. A. Fridman, O. V. Kozhemyako, and M. S. Kochmanski, Acta Phys. Pol. A **96**, 363 (1999).
[8] E. A. Turov and V. G. Shavrov, Usp. Fiz. Nauk **140**, 429 (1983) [Sov. Phys. Usp. **26**, 593 (1983)].
[9] Yu. N. Mitsaĭ and Yu. A. Fridman, Teor. Mat. Fiz. **81**, 263 (1989).
[10] V. G. Bar'yakhtar and E. A. Turov, in *Electronic Structure and the Electronic Properties of Metals and Alloys* [in Russian], Naukova Dumka, Kiev (1988), p. 37.
[11] I. M. Vitebskiĭ, N. M. Lavrinenko, A. N. Maĭorova, Yu. N. Mitsaĭ, and Yu. A. Fridman, Ukr. Fiz. Zh. (Russ. Ed.) **39**, 597 (1994).
[12] V. G. Bar'yakhtar, V. M. Loktev, and S. M. Ryabchenko, Zh. Éksp. Teor. Fiz. **88**, 1752 (1985) [Sov. Phys. JETP **61**, 1040 (1985)].
[13] R. Z. Zaĭtsev, Zh. Éksp. Teor. Fiz. **68**, 207 (1975) [Sov. Phys. JETP **41**, 100 (1975)].
[14] V. M. Loktev and V. S. Ostrovskiĭ, Fiz. Tverd. Tela (Leningrad) **20**, 3086 (1978) [Sov. Phys. Solid State **20**, 1779 (1978)].
[15] L. D. Landau and E. M. Lifshitz, *Statistical Physics*, 3rd ed., Part 1 [Pergamon Press, Oxford (1980); Nauka, Moscow (1976)].
[16] Yu. A. Izyumov and Yu. N. Skryabin, *Statistical Mechanics of Magnetically Ordered Systems* [in Russian], Nauka, Moscow (1987).

Translated by Steve Torstveit

ELECTRONIC PROPERTIES OF METALS AND ALLOYS

Manifestation of the band structure of the semimetal in the tunneling conductance of a metal–insulator–semimetal junction

A. I. Khachaturov*

A. A. Galkin Donetsk Physics and Engineering Institute, National Academy of Sciences of Ukraine, ul. R. Lyuksemburg 72, 83114 Donetsk, Ukraine

E. Hatta and V. M. Svistunov

Nanoelectronics Laboratory Graduate School of Engineering, Hokkaido University, Sapporo 060-8628, Japan

(Submitted March 2, 2000; revised April 17, 2000)
Fiz. Nizk. Temp. **26**, 1115–1120 (November 2000)

The contribution of the electron band of the semimetal to the differential conductance of a metal–insulator–semimetal tunnel junction is found. It is established that the tunneling conductance depends substantially on the barrier parameters. The conductance curve exhibits a convexity with a maximum that in general does not correspond to the edges of the band or to a saddle point of the band, as has been proposed previously. It is shown that the band structure is well resolved in the second derivative of the current with respect to the voltage, d^2I/dV^2. © *2000 American Institute of Physics.* [S1063-777X(00)00811-2]

Back in the 1960s it was firmly established experimentally that the band structure of semiconductors and semimetals are reflected in the tunneling characteristics.[1–3] Subsequently attempts were made to develop a method of investigating the band structure of solids on the basis of these experiments.[3–6] If successful, such a method would permit one to study not only the bands directly adjacent to the Fermi level, as is the case for methods based on the de Haas–van Alphen, Shubnikov–de Haas, and cyclotron resonance methods, but also to obtain information about the bands lying considerable distances away from it. However, the results presented by different groups had disagreements far in excess of the experimental error limits. For this reason it was not possible to develop reliable rules for relating the features of the tunneling characteristics with the singular points of the band structure. As a result, research activity in this area fell off substantially, and at present there is hardly any attempt to use the tunneling effect to study the band structure of new materials such as metal-oxide compounds, for example. This is largely because of a lack of a suitable theory that would permit calculating the contribution of an individual band to the total tunneling current.[7]

In the present paper we propose a model approach to the analysis of electron tunneling in metal–insulator–semimetal junctions. We assume that the metallic electrode is an ordinary Fermi metal with a quadratic dispersion relation, while the counterelectrode is a hypothetical multiband semimetal with a cubic crystal lattice. To describe the insulating layer we use a trapezoidal model, according to which the application of a voltage V causes the shape of the potential barrier to change according to the law (Fig. 1)

$$\varphi(z,V)=\varphi_1+(\varphi_2-eV-\varphi_1)z/d, \tag{1}$$

where φ_1 and φ_2 are the barrier heights, d is the barrier thickness, and z is the coordinate perpendicular to the plane of the tunnel junction. In the WKB approximation the transparency of such a barrier can be determined from the formula[8]

$$P=\exp\left(-2\int_0^d |k_z^*(z)|dz\right), \tag{2}$$

where k_z^* is the wave-vector component perpendicular to the plane of the barrier in the insulator. We assume that the tunneling has an elastic and specular characteristic, i.e., that the total energy $E=E_z+E_\parallel$ of the tunneling electron and the parallel component of its quasimomentum $k_\parallel$ are conserved. The ''parallel'' $E_\parallel$ and ''normal'' E_z components of the kinetic energy under these conditions will in general not be conserved.

The formula for the tunneling current at $T=0$ K has the form[9]

$$J(V)=\frac{2e}{h}\int dE\int\int P(E_z,V)dk_x\,dk_y, \tag{3}$$

where the integration is over the area of overlap of the projections of the constant-energy surfaces of the electrons on the plane of the junction. Since in this paper we are primarily interested in band effects in the semimetal, we shall assume that its constant-energy projection lies completely inside the projection of the metallic electrode.

In that case, for finding the tunneling current it is sufficient to know only the ''transverse'' density of states $N(E_\parallel)$ of the semimetal:

$$J(V)=\frac{2e}{h}\int dE\int P(E-E_\parallel,V)N(E_\parallel)dE_\parallel. \tag{4}$$

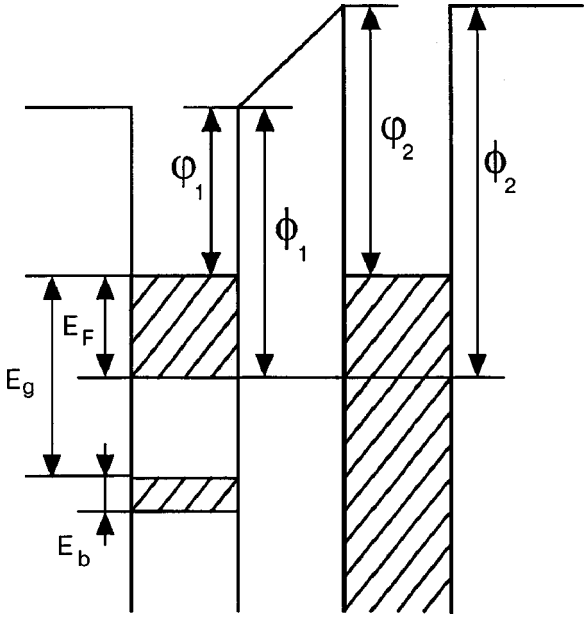

FIG. 1. Energy diagram of a metal–insulator–semimetal tunnel junction with a two-band semimetal.

In the tight-binding approximation the dispersion of the nth band is given by the expression

$$E_n(k)=E_n-2A_n[\cos(ak_x)+\cos(ak_y)+\cos(ak_z)], \quad (5)$$

where a is the lattice constant. The width of such a band is $E_b=12A$, and the distance from the bottom of the band to the saddle point is $E_s=4A$. The electronic density of states was calculated by the following procedure: the area S encompassed by the constant-energy curve $E_\parallel(k_x,k_y)=4A-2A[\cos(ak_x)+\cos(ak_y)]$ was multiplied by 2 (to take into account the spin degeneracy) and differentiated with respect to $E_\parallel$:

$$N(E_\parallel)=\frac{1}{2\pi^2}\frac{dS}{dE_\parallel}. \quad (6)$$

As we have said, in general the parallel component of the energy is not conserved, and the relation between its value $E_\parallel$ in the semimetal and its value $E_\parallel^*$ in the insulator can be rather complicated. Here, however, we shall assume for simplicity that the relation $E_\parallel^*(k_\parallel^*)$ is given by Eq. (5) and, hence, $E_\parallel^*=\alpha E_\parallel$, which is valid if the insulator layer is a cubic crystal with the same lattice constant a but a different parameter A^*, so that $\alpha=A^*/A$. This approach is justified by the fact that we are interested in the manifestation of band effects for the semimetal and not for the insulator layer. Assuming that the effective mass approximation is valid in the z direction in the insulator, we write the integrand in (2) as

$$|k_z^*(z)|=\sqrt{(\phi(z))-E_z^*}=\sqrt{2m^*\{\phi(z)-E+\alpha E_\parallel\}},$$

and after integration we obtain

$$P(V,E-E_\parallel)=\exp\left\{\frac{-A_d}{\phi_2-eV-\phi_1}\sqrt{(\phi_2-eV-\phi_1-E+\alpha E_\parallel^*)^3}-\sqrt{(\phi_2-\phi_1-E+\alpha E_\parallel^*)^3}\right\}, \quad (7)$$

where $A_d=4\sqrt{2m^*}d/3\hbar$, m^* is the effective mass of an electron in the conduction band of the insulator, and ϕ_1 and ϕ_2 are the barrier heights measured from the bottom of the band.

Let us consider the simplest case, when, in addition to the conduction band, the semimetal has a completely filled electron band that does not cross with it in energy (see Fig. 1). We assume that the position of the Fermi level is such that the Fermi surface does not touch the boundaries of the Brillouin zone, i.e., $E_F<4A_1$. As necessary the proposed scheme can easily be generalized to any number of arbitrarily located bands. Let a bias voltage V be applied to the junction, shifting the Fermi level of the semimetal upward relative to the Fermi level of the opposite metal electrode. The contribution to the tunneling current from the conduction band in this case can be found from the formula

$$J_1(V)=\frac{2e}{h}\int_{E_F-eV}^{E_F}dE\int_0^E P(E_\parallel,V)dE_\parallel, \quad eV<E_F, \quad (8)$$

$$J_1(V)=\frac{2e}{h}\int_0^{E_F}dE\int_0^E P(E_\parallel,V)dE_\parallel, \quad eV>E_F.$$

All of the energies in this formula are measured from the bottom of the conduction band (and, henceforth, all energies will be measured from the bottom of the band whose contribution is being determined at the time), so that the heights of the tunnel barrier for the conduction band are $\phi_1=\varphi_1+E_F$, $\phi_2=\varphi_2+E_F$ (for a completely filled band the barrier heights are $\phi_1=\varphi_1+E_g+E_b$ and $\phi_2=\varphi_2+E_g+E_b$, where E_g is the distance from the Fermi level to the upper edge of the band). Differentiating, we obtain an analytical expression for the contribution to the tunneling conductance from the Fermi band:

$$\sigma_1(V)=\frac{2e}{h}\left[\int_{E_F-eV}^{E_F}dE\int_0^E N(E_\parallel)P'(E-\alpha_1E_\parallel,V)dE_\parallel+\int_0^{E_F-eV}N(E_\parallel)P(E_F-eV-\alpha_1E_\parallel,V)dE_\parallel\right], \quad eV<E_F, \quad (9)$$

$$\sigma_1(V)=\frac{2e}{h}\left[\int_0^{E_F}dE\int_0^E N(E_\parallel)P'(E-\alpha_1E_\parallel)dE_\parallel\right], \quad eV>E_F,$$

where $\alpha_1=A^*/A_1$, and the derivative of the penetrability of the tunnel barrier with respect to the voltage, $P'(E-kE_\parallel^*,V)$, can be calculated analytically:

$$P'(E_z^*,V)=\frac{eA_d}{2}\frac{(\phi_2-3\phi_1-eV+2E_z^*)(\phi_2-eV+E_z^*)^{1/2}+2(\phi_1-E_z^*)^{3/2}}{(\phi_2-eV-\phi_1)^2}P(E_z^*,V). \tag{10}$$

The contribution to the tunneling current from an electron band lying a distance E_g below the Fermi level is given by

$$J_2(V)=0, \quad eV<E_g,$$

$$J_2(V)=\frac{2e}{h}\left(\int_{3E_s+E_g-eV}^{3E_s}dE\int_{E-E_s}^{2E_s}P(E-\alpha_2E_\parallel,V)N(E_\parallel)dE_\parallel\right), \quad E_g<eV<E_s+E_g,$$

$$J_2(V)=\frac{2e}{h}\left(\int_{2E_s}^{3E_s}dE\int_{E-E_s}^{2E_s}P(E-\alpha_2E_\parallel,V)N(E_\parallel)dE_\parallel+\int_{3E_s+E_g-eV}^{2E_s}dE\int_{E-E_s}^{E}P(E-\alpha_2E_\parallel,V)N(E_\parallel)dE_\parallel\right),$$
$$E_s+E_g<eV<2E_s+E_g,$$

$$J_2(V)=\frac{2e}{h}\left(\int_{2E_s}^{3E_s}dE\int_{E-E_s}^{2E_s}P(E-\alpha_2E_\parallel,V)N(E_\parallel)dE_\parallel+\int_{E_s}^{2E_s}dE\int_{E-E_s}^{E}P(E-\alpha_2E_\parallel)N(E_\parallel)dE_\parallel\right.$$
$$\left.+\int_{3E_s+E_g-eV}^{E_s}dE\int_{0}^{E}P(E-\alpha_2E_\parallel,V)N(E_\parallel)dE_\parallel\right), \quad 2E_s+E_g<eV<3E_s+E_g,$$

$$J_2(V)=\frac{2e}{h}\left(\int_{2E_s}^{3E_s}dE\int_{E-E_s}^{2E_s}P(E-\alpha_2E_\parallel,V)N(E_\parallel)dE_\parallel+\int_{E_s}^{2E_s}dE\int_{E-E_s}^{E}P(E-\alpha_2E_\parallel)N(E_\parallel)dE_\parallel\right.$$
$$\left.+\int_{0}^{E_s}dE\int_{0}^{E}P(E-\alpha_2E_\parallel,V)N(E_\parallel)dE_\parallel\right), \quad 3E_s+E_g<eV, \tag{11}$$

where $\alpha_2=A^*/A_2$.

Differentiating Eq. (11) with respect to V, we find analytical expressions for the contribution from the electron band to the tunneling conductance; they are rather awkward and will not be given here. The total tunneling current and the total conductance are equal to the sums of the contributions from the individual bands of the semimetal: $J(V)=J_1(V)+J_2(V)$ and $\sigma(V)=\sigma_1(V)+\sigma_2(V)$. In Fig. 2 we present the results of a calculation of the tunneling conductance for a tunnel junction whose semimetal electrode had the following parameters: Fermi energy $E_F=0.27$ eV; $A_1=75$ meV; distance between the Fermi level and the upper edge of the electron band $E_g=0.4$ eV; width of the electron band $E_b=12A_2=0.15$ eV; cubic lattice constant $a=2.5$ Å. The potential barrier heights φ_1 and φ_2 were assumed equal to 1.2 eV, and the thicknesses were varied: 8 Å (curve *1*), 12 Å (curve *2*), 14 Å (curve *3*), 16 Å (curve *4*), 20 Å (curve *5*). Up to $eV=E_F$ only the electrons of the conduction band contribute to the tunneling conductance. As expected, the term $\sigma_1(V)$ falls off with increasing voltage as a consequence of the small value of E_F in comparison with the height of the tunnel barrier. A similar result was obtained for a small group of free carriers in Ref. 10. Thus the first minimum on the curve of the tunneling conductance corresponds to the value of the Fermi energy. The authors of Ref. 3, from a comparison of the tunneling spectra with the optical absorption and transmission spectra came to the conclusion that the maximum of the differential conductance corresponds to the band edge. In Ref. 5 it was asserted that the maximum of the tunneling conductance corresponds to a saddle point, which in our case is located at $eV_{\text{saddle}}=E_g+8A_2$. Calculations show that, strictly speaking, the maximum of the contribution to the tunneling conductance from the electron band coincides with neither the edges of the electron band nor with the saddle point. As can be seen in Fig. 3, the singular points of the band structure are well resolved on the d^2I/dV^2 curve obtained by numerical differentiation of $\sigma(V)$. The beginning and end of the band are manifested as steplike jumps upward and downward at the voltages $eV=E_g$ and $eV=E_g+12A_2$, respectively. The curve has a sharp maximum at $eV=E_g+4A_2$ and a sharp minimum at $eV=E_g+8A_2$, which divide the band into three equal parts. As is seen in Fig. 2, the character of the manifestation of the band

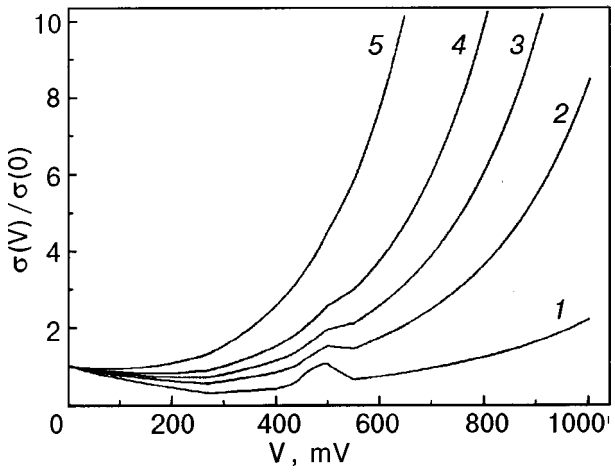

FIG. 2. Calculated curves of the differential conductance σ versus voltage V for a metal–insulator–semimetal tunnel junction with a two-band semimetal, for different thicknesses of the insulator layer, d [Å]: 8 (*1*), 12 (*2*), 14 (*3*), 16 (*4*), 20 (*5*). The height of the rectangular potential barrier is $\varphi_1=\varphi_2=1.2$ eV. The parameters of the hypothetical semimetal were assumed to have the values $a=2.5$ Å, $A_1=75$ meV, $E_F=0.27$ meV, $A_2=12.5$ meV, and $E_g=0.4$ meV.

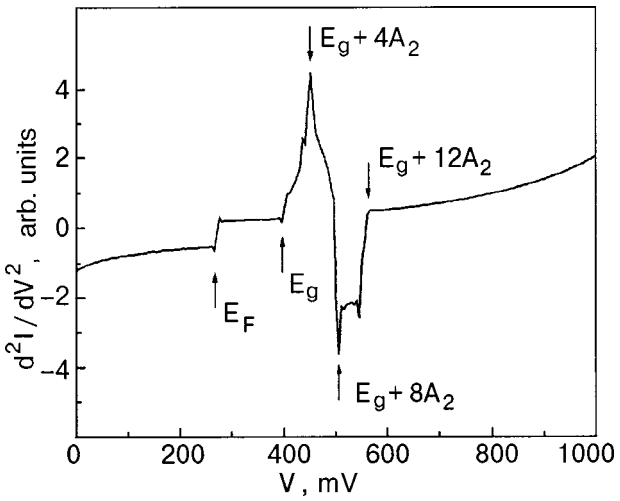

FIG. 3. Second derivative of the current with respect to the voltage, d^2I/dV^2, obtained by numerical differentiation of curve *1* in Fig. 2.

features of the semimetal depends strongly on the properties of the insulator layer. For example, a doubling of the thickness of the insulator layer, which would be entirely feasible in experiments being done by different research groups, would result in the nearly complete vanishing of these features (curves *1–5* in Fig. 2).

In our opinion, the results presented here confirm that electron tunneling is completely applicability for studying the band structure of semimetals in the case of noncrossing bands. The main difficulty lies in the fact that, in addition to the unknown band parameters sought, the problem contains additional parameters that substantially influence the measured tunneling characteristics.[7,11] The insulator layer has been and still remains the least studied and most poorly controllable element of a tunnel junction, and it is not surprising that it is the main factor hindering the study of the band structure. We believe that the proposed model offers hope of circumventing this difficulty. It opens up some factually grounded possibilities for detailed experimental study of the tunneling characteristics of semimetals and a subsequent reconstruction of the band structure.

The authors are grateful to Prof. M. Oda for helpful discussions. One of the authors (V.M.C.) thanks Prof. K. Mukasa for hospitality and the Ministry of Education, Science, and Culture of Japan for financing his stay at the University of Hokkaido.

*E-mail: khach@sts.dipt.donetsk.ua

[1] L. Esaki and P. J. Stiles, Phys. Rev. Lett. **4**, 902 (1965).
[2] L. Esaki and P. J. Stiles, Phys. Rev. Lett. **16**, 574 (1966).
[3] J. J. Hauser and L. R. Testardi, Phys. Rev. Lett. **20**, 12 (1968).
[4] H. T. Chu, N. K. Eib, P. N. Henriksen *et al.*, Phys. Rev. B **18**, 4546 (1979).
[5] Yu. Sawatari and M. Arai, J. Phys. Soc. Jpn. **360**, 360 (1970).
[6] M. A. Belogolovskiĭ, A. A. Galkin, and V. M. Svistunov, Zh. Éksp. Teor. Fiz. **69**, 1795 (1975) [Sov. Phys. JETP **42**, 912 (1975)].
[7] Yu. F. Komnik, *Physics of Metal Films* [in Russian], Atomizdat, Moscow (1979).
[8] W. A. Harrison, Phys. Rev. **123**, 85 (1961).
[9] R. Stratton, in *Tunneling Phenomena in Solids*, edited by E. Burstein and S. Lundqvist [Plenum Press, New York (1969); Mir, Moscow (1973)].
[10] A. I. Khachaturov, V. M. Svistunov, and M. A. Belogolovskii, Czech. J. Phys. **46**, Suppl. Part S2, 1031 (1996).
[11] E. Hatta and K. Mukasa, Solid State Commun. **103**, 235 (1997).

Translated by Steve Torstveit

LOW-DIMENSIONAL AND DISORDERED ALLOYS

Impedance of a thin metal film in the regime of strong magnetodynamic nonlinearity

S. A. Derev'anko, G. B. Tkachev, and V. A. Yampol'skiĭ

*A. Ya. Usikov Institute for Radio Physics and Electronics, National Academy of Sciences of Ukraine, ul. Akad. Proskury 12, 61085 Kharkov, Ukraine**

(Submitted April 25, 2000)
Fiz. Nizk. Temp. **26**, 1121–1129 (November 2000)

The nonlinear response of a metallic film to the self-magnetic field of an ac transport current is investigated theoretically. The nonlinearity is due to a magnetodynamic mechanism which derives from the influence of the magnetic field of the current on the dynamics of the conduction electrons and is most typical for pure metals at low temperatures. The nonlinearity leads to a dependence of the surface impedance on the amplitude of the ac current. It is shown that the real part of the surface impedance, which is responsible for the Joule losses, has a smooth maximum as a function of the amplitude. The imaginary part of the surface impedance is also a nonmonotonic function of the amplitude and has a minimum. © *2000 American Institute of Physics.* [S1063-777X(00)00911-7]

1. INTRODUCTION

It is known that pure metals at low temperatures have a number of peculiar nonlinear properties. The nonlinearity is due to the influence of the magnetic component of the wave or the self-magnetic field of the transport current on the dynamics of the current carriers in the metal and, consequently, on the conductivity of the sample. This nonlinearity mechanism is called magnetodynamic. The phenomena deriving from this mechanism have been the subject of a number of publications (see, e.g., the review[1,2] and the references cited therein). An example of these phenomena is the generation of the so-called current states — a peculiar hysteretic rectification effect for radio-frequency current and the excitation of the intrinsic magnetic moment of the sample.[3] The effects of magnetodynamic nonlinearity are clearly manifested in thin samples having a thickness d that is much smaller than the mean free path l of the current carriers, $d \ll l$.

It was shown in Ref. 4 that the magnetodynamic mechanism leads to an increase in the static conductivity of a metal film and, hence, to a deviation of the current–voltage (I–V) characteristic from Ohm's law to the side of lower resistance. The interaction of an external low-frequency electromagnetic wave, with a dc transport current flowing along a metal film, was analyzed in Ref. 5. It was found that the interaction arising as a result of the magnetodynamic nonlinearity leads to unusual nonanalytic behavior of the electric field on the surface of the metal and to a peculiar sort of amplification effect for an electromagnetic signal in comparison with the signal in the absence of current.

In this paper we present a theoretical analysis of the situation in which a low-frequency ac transport current $I(t)$ is flowing along a film. As was shown in Ref. 4, the main features of the nonlinear response of the film in the presence of a high transport current are due to the fact that the self-magnetic field of the current is distributed antisymmetrically over the thickness of the sample. In the center of the film it is equal to zero, while at the boundaries it takes on values which are equal in magnitude and opposite in sign. This sign-varying distribution of the magnetic field gives rise to particles of a new type in terms of the character of their motion — trapped particles, whose trajectories wind around the plane of alternation of the sign of the magnetic field of the current. We assume that the magnitude of the current is such that the characteristic radius of curvature $R(I)$ of the electron trajectories in the self-field $H(I)$ of the current is much larger than the thickness of the film:

$$d \ll R(I), \quad R(I) = cp_F/eH(I) \propto I^{-1} \tag{1}$$

($-e$ and p_F are the charge and Fermi momentum of the electron, and c is the speed of light in vacuum). Then the relative number of trapped electrons, which is equal in order of magnitude to the angle $(d/R)^{1/2}$ of their approach to this plane, is small. However, these particles do not suffer collisions with the boundaries of the sample and interact with the ac field in the metal over the whole length of the mean free path l. According to the concept of ineffectiveness,[1,6,7] their conductivity $\sigma_{\rm tr}$ can be estimated as follows:

$$\sigma_{\rm tr} \sim \sigma_0 (d/R)^{1/2} \propto I^{1/2}, \tag{2}$$

where σ_0 is the conductivity of a massive sample. At the same time, under conditions of diffuse reflection of electrons from the surface of the sample the so-called ''fly-through'' particles, which collide with the boundaries of the film, have a conductivity of the order of $\sigma_0(d/l)$. From this we see that there exists a high-current regime in which the equation

$$[dR(I)]^{1/2} < 1 \tag{3}$$

holds and the principal contribution to the conductivity is given by the trapped group of electrons. This causes a deviation of the I–V characteristic from Ohm's law and leads to a square-root dependence of the voltage on the current. Inequality (3) means that the characteristic arc length of the trajectory of a trapped electron is much smaller than the

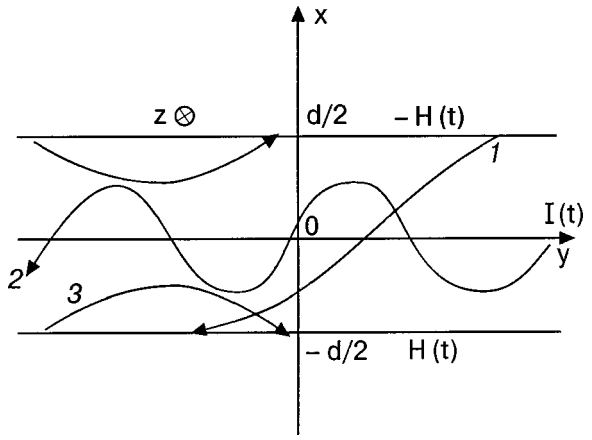

FIG. 1. Geometry of the problem: trajectories of the fly-through (*1*), trapped (*2*), and surface (*3*) electrons.

mean free path, and the electron, before scattering, is able to complete many oscillations about the plane on which the magnetic field changes sign (Fig. 1).

If an alternating current is flowing along the film, then the conductivity of the sample can change appreciably over the period of the current oscillations. This is because there is a regime of strong nonlinearity at high currents due to the dominant contribution of the trapped particles. In this paper we investigate theoretically the time dependence of the voltage in a film carrying a transport current consisting of a dc component and a low-frequency ac component and satisfying conditions (1) and (3). Here the dc component pushes the system into the nonlinear regime, and the ac component governs the dynamic response. We will show that the nonlinearity leads to nonmonotonic dependences of the real and imaginary parts of the surface impedance on the amplitude of the ac component of the current on account of the emergence of the I–V characteristic onto a nonlinear segment. At large values of the dc component of the current the real part of the surface impedance, which is responsible for the Joule losses, has a smooth maximum as a function of the amplitude of the ac offset, this maximum falling at values of the amplitude close to the value of the dc component of the current. As the value of the dc component is decreased, the curve becomes more complicated, and a minimum appears on it in addition to the maximum. The imaginary part of the surface impedance has one minimum as a function of the amplitude of the ac current; this minimum varies slightly as the dc component is decreased and lies in the same region of amplitude values as the maximum of the real part. In this paper we also obtain asymptotic expressions describing the different stages of the emergence onto the nonlinear I–V characteristic.

2. STATEMENT OF THE PROBLEM

Let us consider a metal film carrying an ac current $I(t)$ which is the sum of a dc component and a harmonically alternating component:

$$I(t)=I_0+I_1\cos\omega t. \tag{4}$$

We introduce a coordinate system whose x axis is directed along the normal to the boundaries of the film. The plane $x=0$ corresponds to the center of the sample (see Fig. 1). The y axis is chosen collinear with the current, and the z axis is chosen parallel to the magnetic field vector $\mathbf{H}(x,t)$. The dimensions of the film along the y and z axes (L and D, respectively) are assumed to be much larger than the thickness d.

In this geometry Maxwell's equations have the form

$$-\frac{\partial H(x,t)}{\partial x}=\frac{4\pi}{c}j(x,t),\quad \frac{\partial E(x,t)}{\partial x}=-\frac{1}{c}\frac{\partial H(x,t)}{\partial t}. \tag{5}$$

Here $j(x,t)$ and $E(x,t)$ are the y components of the current density and electric field. Equation (5) must be solved jointly with the boundary conditions

$$H(\pm d/2,t)=\mp 2\pi I(t)/cD\equiv\mp H(t). \tag{6}$$

We are interested in the quasistatic case, when the frequency ω of the wave is much less than the relaxation frequency ν of the charge carriers, $\omega\ll\nu$.

In addition, we assume that the characteristic radius of curvature of the electron trajectories $R(x,t)$ is much greater than the film thickness d:

$$d\ll R(x,t),\quad R(x,t)=cp_F/e|H(x,t)|. \tag{7}$$

3. MAIN GROUPS OF CURRENT CARRIERS. THE I–V CHARACTERISTIC OF THE FILM

Let us consider the dynamics of electrons in a magnetic field $H(x,t)$ that is sign-varying in space. The gauge of the vector potential is conveniently chosen in the form

$$\mathbf{A}(x,t)=\{0,A(x,t),0\},\quad A(x,t)=\int_0^x dx'H(x',t). \tag{8}$$

The integrals of motion of an electron in a nonuniform magnetic field $H(x,t)$ are the total energy (equal to the Fermi energy) and the generalized momenta $p_z=mv_z$ and $p_y=mv_y-eA(x,t)/c$ (m is the mass of the electron). The electron trajectory in a plane perpendicular to the magnetic field is determined by the velocities $v_x(x,t)$ and $v_y(x,t)$. For a Fermi sphere of radius $p_F=mV$ we have

$$\begin{aligned}&|v_x(x,t)|=(v_\perp^2-v_y^2)^{1/2},\quad v_\perp=(v^2-v_z^2)^{1/2},\\ &v_y(x,t)=[p_y+eA(x,t)/c]/m.\end{aligned} \tag{9}$$

The classically accessible regions of the electron motion along the x axis are found from the inequalities

$$-p_y-mv_\perp\leqslant eA(x,t)/c\leqslant -p_y+mv_\perp \tag{10}$$

which ensure that the radicand in the expression for $|v_x(x,t)|$ in (9) is positive.

Figure 2 shows the domains of motion of electrons in the plane of the variables (x,p_y). For specificity we have chosen a point in time when the total current $I(t)$ through the sample is positive. The upper boundary on the phase plane is described by the curve $p_y=mv_\perp-eA(x,t)/c$, and the lower boundary by the curve $p_y=-mv_\perp-eA(x,t)/c$. It is seen in Fig. 2 that, according to the character of the motion, the electrons are divided into several groups, depending on the magnitude and sign of the integral of the motion p_y.

1) *Fly-through electrons.* The existence region of these electrons is delimited by the inequalities

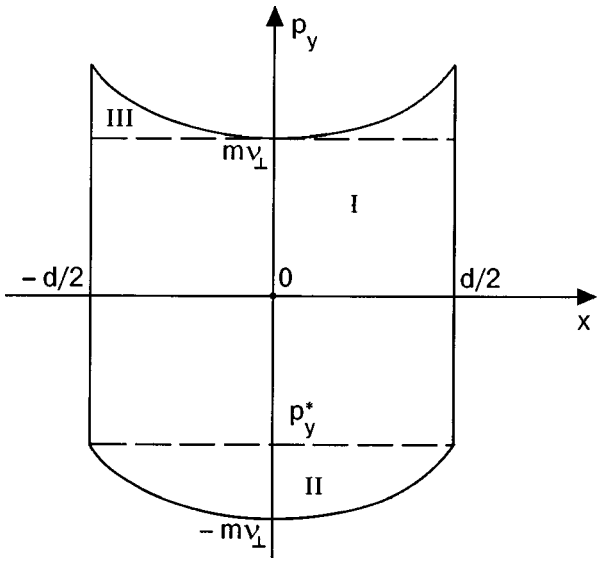

FIG. 2. Phase plane (p_y,x), showing the existence regions of the fly-through (I), trapped (II), and surface (III) particles.

$$p_y^* = -mv_\perp - eA(d/2,t)\operatorname{sgn} I(t)/c \leqslant p_y \operatorname{sgn} I(t) \leqslant mv_\perp . \tag{11}$$

The fly-through electrons undergo collisions with both boundaries of the film. By virtue of condition (7), their trajectories are hardly curved by the magnetic field of the current.

2) *Trapped electrons.* These exist in the region

$$-mv_\perp \leqslant p_y \operatorname{sgn} I(t) \leqslant p_y^* . \tag{12}$$

Their trajectories are nearly flat oscillatory curves that wind around the plane $x=0$ at which the sign of the magnetic field changes. The period of these oscillations is $2T$, where T is given by the relation

$$T = \int_{x_1(t)}^{x_2(t)} \frac{dx}{|v_x(x,t)|}. \tag{13}$$

The boundaries of the integration region are the turning points of the particle $[x_1(t)<0<x_2(t)=-x_1(t)]$, which are the roots of the equation

$$eA(x_{1,2},t)/c = -mv_\perp - p_y . \tag{14}$$

3) *Surface electrons.* The particles of this group undergo collisions with only one of the boundaries of the film. It can be shown that for diffuse reflection of electrons by the boundaries, their contribution to the conductivity of the metal determines an unimportant constant of the order of unity in the argument of the logarithm in the asymptotic expression for the conductivity of the fly-through electrons. These surface electrons will not be taken into account further.

The description of the electron groups given here is analogous to that given in Ref. 5. The difference is that in our case the plane at which the magnetic field changes sign exists at all times and coincides with the center of the sample. Because of this, the boundaries of the existence regions of the electron groups are changed.

To calculate the current density of the fly-through and trapped particles we employ the standard method using the Boltzmann transport equation. The transport equation is linearized in the electric field $E(x,t)$, which is the sum of a uniform potential component $E_0(t)$ and a nonuniform solenoidal component $\boldsymbol{\mathcal{E}}(x,t)$:

$$E(x,t) = E_0(t) + \boldsymbol{\mathcal{E}}(x,t),$$

$$\boldsymbol{\mathcal{E}}(x,t) = -\frac{1}{c}\left(\frac{\partial A(x,t)}{\partial t} - \frac{\partial \overline{A}(t)}{\partial t}\right). \tag{15}$$

The quantity $\overline{A}(t)$ is the vector potential averaged over the thickness of the sample:

$$\overline{A}(t) = \frac{1}{d}\int_{-d/2}^{d/2} A(x',t)\,dx'. \tag{16}$$

The nonlinearity in the problem is due to the nonuniform of the magnetic field of the current, $H(x,t)$, which appears in the Lorentz force. We consider a range of low frequencies for which the first term in (15) is dominant (the corresponding inequality will be given in the Conclusion). For this case (i.e., the case of a quasi-uniform electric field) the asymptotic expressions for the current density under conditions (3) and (7) can be taken from Ref. 4:

$$j_{\text{fl}} = \sigma_{\text{fl}} E_0(t), \tag{17}$$

$$\sigma_{\text{fl}}(t) = \frac{3}{8}\sigma_0 \frac{d}{l}\ln\frac{R(t)}{d}, \quad R(t) = \frac{cp_F}{e|H(t)|},$$

$$j_{\text{tr}} = \sigma_{\text{tr}} E_0(t), \tag{18}$$

$$\sigma_{\text{tr}}(t) = \frac{36\pi^{1/2}}{5\Gamma^2(1/4)}\sigma_0\left[\frac{e}{cp_F}|A(x,t)-A(d/2,t)|\right]^{1/2}.$$

These formulas clearly go over to the results of Ref. 4 in the limit $\omega \to 0$. These asymptotic expressions (17) and (18) must be substituted into Maxwell's equations (5). We introduce a dimensionless coordinate and a dimensionless vector potential:

$$\xi = 2x/d, \quad a(\xi,t) = A(x,t)/A(d/2,t). \tag{19}$$

The equation for $a(\xi,t)$ has the form

$$\frac{\partial^2 a(\xi,t)}{\partial \xi^2}\operatorname{sgn} I(t) = u\{r[1-a(\xi,t)]^{1/2}+1\}. \tag{20}$$

The quantity r appearing in (20) is the ratio of the maximum value of the conductivity of the trapped carriers to the conductivity of the fly-through particles:

$$r = \frac{\sigma_{\text{tr}}(0)}{\sigma_{\text{fl}}} = \frac{96\pi^{1/2}}{5\Gamma^2(1/4)}\frac{l}{d}\left[\frac{e}{cp_F}\left|A(d/2,t)\right|\right]^{1/2}\ln^{-1}(R/d), \tag{21}$$

and the parameter u is related to the voltage across the sample, $U=E_0L$, as

$$u = \frac{U\pi\sigma_{\text{fl}}d^2}{cL|A(d/2,t)|}. \tag{22}$$

The boundary conditions on Eq. (20) are the dimensionless forms of relations (6):

$$\left.\frac{\partial a}{\partial \xi}\right|_{\xi=1} = -\frac{d}{2}\frac{H(t)}{A(d/2,t)},$$
$$\left.\frac{\partial a}{\partial \xi}\right|_{\xi=-1} = \frac{d}{2}\frac{H(t)}{A(d/2,t)}, \quad a(1,t)=1. \tag{23}$$

The last, additional condition in (23) is a consequence of the normalization (19) of the vector potential.

The boundary-value problem (20), (23) is largely analogous to that considered in Ref. 5. The differences are that the magnetic field $H_0+H_1\cos\omega t$ at the surface of the film is due to the alternating self-field of the current [see Eqs. (4) and (6)] and not to the harmonic field of the incident wave. The sign-varying nature of the time dependence of the current in the film is taken into account in Eq. (20) by the factor $\operatorname{sgn} I(t)$. In addition, as we have said, the plane at which the sign of the magnetic field changes is fixed and at all time coincides with the center of the sample.

The solution of the boundary-value problem (20) is an even function of the dimensionless coordinate ξ and is given by the formula

$$|\xi| = \left(\frac{3}{4ru\,\operatorname{sgn} I(t)}\right)^{1/2}\int_0^{a(\xi,t)} d\zeta\,[1-(1-\zeta)^{3/2}+3\zeta/2r]^{-1/2}. \tag{24}$$

Although one cannot use Eq. (24) to obtain the explicit form of the function $a(\xi,t)$, one can determine the average value of the conductivity of the trapped electrons over the thickness of the sample:

$$\frac{\overline{\sigma}_{\rm tr}}{\sigma_{\rm fl}} = r\int_0^1 d\zeta(1-\zeta)^{1/2}[1-(1-\zeta)^{3/2}+3\zeta/2r]^{-1/2} \times\left(\int_0^1 d\zeta[1-(1-\zeta)^{3/2}+3\zeta/2r]^{-1/2}\right)^{-1}. \tag{25}$$

To determine the voltage U, we integrate both sides of Eq. (20) over ξ from -1 to 1 with allowance for the boundary conditions (23). After using formula (22) and doing some simple manipulations, we obtain

$$U(t) = \frac{cL}{2\pi d\sigma_{\rm fl}(t)}\frac{H(t)}{1+\overline{\sigma}_{\rm tr}/\sigma_{\rm fl}}. \tag{26}$$

The ratio of the conductivities $\overline{\sigma}_{\rm tr}/\sigma_{\rm fl}$ depends on the parameter r [see Eq. (25)]. Using Eq. (22) and the relation (21) between $A(d/2,t)$ and r, from the first boundary condition (23) with the use of (24) we arrive at an algebraic equation for r:

$$r^2(1+2r/3) = \operatorname{sgn} I(t)\left(\frac{H(t)}{\widetilde{H}}\right)^2\frac{\widetilde{U}}{U\ln^3(R/d)}. \tag{27}$$

Here we have introduced the notation

$$\widetilde{H} = \frac{25\Gamma^4(5/4)}{9\pi}\frac{cp_Fd}{el^2}, \quad \widetilde{U} = \frac{4clL\widetilde{H}}{3\pi\sigma_0d^2}. \tag{28}$$

The physical meaning of the quantities introduced consists in the fact that at such values of the magnetic field and voltage the characteristic arc length $(Rd)^{1/2}$ of the trajectories of the trapped electrons becomes of the same order as the mean free path l. It is also convenient to introduce a characteristic current $\widetilde{I}$ corresponding to the magnetic field $\widetilde{H}$. According to Eq. (7),

$$\widetilde{I} = \frac{cD\widetilde{H}}{2\pi}. \tag{29}$$

Strictly speaking, relations (26) and (27) describe the current–voltage characteristic only in the region of high currents, where the condition $H(t)\gg\widetilde{H}$ [i.e., condition (3)] is satisfied. However, an analysis shows that the expressions obtained are always good interpolating formulas, even when condition (3) is not met.

4. SURFACE IMPEDANCE OF A FILM IN THE UNIFORM APPROXIMATION

As we said in the previous Section, in this paper we investigate the case of low frequencies, when the potential term $E_0(t)$ is dominant in expression (15). In this Section we shall find the surface impedance of a film in the leading (homogeneous) approximation, in which the nonuniform solenoidal contribution $\boldsymbol{\mathcal{E}}$ in (15) is zero. To calculate the surface impedance one must know the time dependence of the electric field at the surface of the film. In the case under study, the electric field in the film is uniform and contains only the potential component $E_0(t)$, which is uniquely determined by the voltage U across the sample. In turn, the time dependence of the voltage [for a specified time dependence of the total current $I(t)$] is given by formulas (26) and (27). Thus with the aid of expressions (26) and (27) one can find the surface impedance of the film as the ratio of the Fourier harmonic of the electric and magnetic fields at the surface of the metal:

$$Z_\omega = \frac{4\pi}{c}\frac{E_{0,\omega}}{H_\omega}.$$

Going over from the fields to the voltage and current with the use of relation (6), we obtain

$$Z_\omega = 2\frac{D}{L}\frac{U_\omega}{I_\omega}, \tag{30}$$

where U_ω and I_ω are the Fourier harmonics of the voltage and current:

$$U_\omega = \frac{\omega}{2\pi}\int_0^{2\pi/\omega} dt\,U(t)e^{i\omega t}, \quad I_\omega = \frac{\omega}{2\pi}\int_0^{2\pi/\omega} dt\,I(t)e^{i\omega t}. \tag{31}$$

We see from formulas (4), (26), and (27) that the voltage depends on time only through $\cos\omega t$. Therefore the surface impedance is real-valued:

$$Z_\omega = R_\omega = \frac{4\omega}{\pi}\frac{D}{L}\frac{1}{I_1}\int_0^{\pi/\omega} U(t)\cos\omega t\,dt. \tag{32}$$

Figure 3 gives the result of a numerical calculation of the dependence of the surface impedance on the dimensionless amplitude of the ac component of the current, $I_1/\widetilde{I}$. The impedance is given in units of

$$\widetilde{R} = \frac{D}{L}\frac{\widetilde{U}}{\widetilde{I}} = \frac{8l}{3\sigma_0d^2}.$$

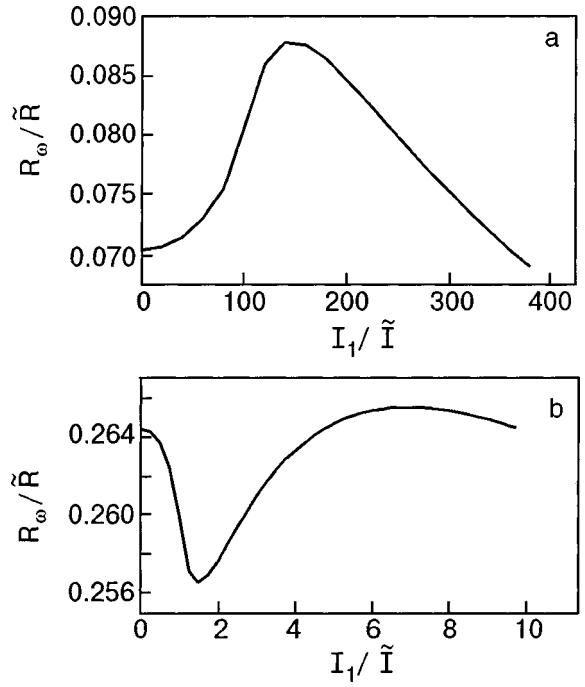

FIG. 3. Dependence of the real part R_ω of the surface impedance on the amplitude I_1 of the ac component of the current for $I_0/\tilde{I}=100$ (a) and 1 (b).

Figure 3a illustrates the case when the dc component of the current is rather large, $I_0/\tilde{I}=100\gg 1$, and the regime of strong nonlinearity arises right from the start. The nonmonotonic dependence of the impedance in this situation can be explained as follows. If the amplitude of the ac component I_1 of the current is small compared with the dc offset I_0, then the total current is not very different from I_0 at any time in the oscillation period. Therefore, the system will at all times be found in the highly nonlinear regime, when the total current is large and the radius of curvature R of the electron trajectories is so small that inequality (3) holds. Under these conditions the conductivity of the sample is always determined by the trapped group of electrons and is characterized by a large parameter $\overline{\sigma}_{\rm tr}/\sigma_{\rm fl}\sim r\sim I/\tilde{I}\sim l/(Rd)^{1/2}\gg 1$, for which reason the surface impedance is small. In the opposite limiting case, when the relative amplitude of the current is large, $I_1\gg I_0$, the contribution of the dc offset I_0 becomes unimportant, and we are actually dealing with a large-amplitude harmonic signal. Because of the large signal amplitude the sample is found in the highly nonlinear regime during the preponderance of the period, and the impedance is again small. Finally, in the region of intermediate amplitudes, $I_1\sim I_0$, when during much of the period the current corresponds to the linear part of the I–V characteristic, an appreciable contribution to the amplitude dependence of the signal comes from the linear region, with its relatively small conductivity. Therefore a smooth maximum appears on the $R_\omega(I_1)$ curve in the vicinity of $I_1\sim I_0$. Because the conductivity of the trapped electrons depends on the current in a weak, square-root manner [see Eq. (2)], the relative size of this maximum is not very large ($\sim$10–15% in Fig. 3a).

It is interesting to track the change in the dependence described above as the dc offset I_0 is decreased. Figure 3b shows a plot of the real part of the surface impedance at $I_0/\tilde{I}=1$. At small values of the amplitude $I_1\sim I_0\sim\tilde{I}$ one can discern a slightly nonlinear segment of the I–V characteristic. The parameter $\overline{\sigma}_{\rm tr}/\sigma_{\rm fl}$, which determines the relative contribution to the conductivity from trapped and fly-through electrons, turns out to be of the order of unity in this case (unlike the situation in Fig. 3a, which corresponds to $\overline{\sigma}_{\rm tr}/\sigma_{\rm fl}\gg 1$). At relatively large values of the amplitude, $I_1\gg I_0$, as in the case of a strong dc offset, the impedance begins to fall off on account of the emergence on the nonlinear part, but for all amplitudes smaller than or of the order of I_0, the contribution of the trapped electrons becomes small, and the nonlinearity is weak. In this case, as is seen in Fig. 3b, the $R_\omega(I_1)$ curve will have a minimum in addition to the maximum. As in the case $I_0\gg\tilde{I}$, the relative scale of changes in the impedance is small.

Equations (26) and (27) can be used to obtain useful asymptotic expressions for the voltage $U(t)$, the nonlinearity parameter $r(t)$, and the impedance $R_\omega(I_1)$ for the case of large currents $I(t)\gg\tilde{I}$. Expanding the I–V characteristic (26) in a series in powers of $\tilde{I}/I(t)$ with the use of (25) and (27), we get

$$U(t)/\tilde{U}=\mathrm{sgn}[I(t)]\frac{|I(t)/\tilde{I}|^{1/2}}{(3b_1^3/2)^{1/2}}+O(1), \tag{33}$$

$$r(t)=\frac{|I(t)/\tilde{I}|^{1/2}b_1^{1/2}}{\ln(R/d)}+O(1), \tag{34}$$

$$b_1=\frac{2}{\sqrt{\pi}}\frac{\Gamma(7/6)}{\Gamma(2/3)}\approx 0.77. \tag{35}$$

The asymptotic behavior (33), (34) is realized, for example, at a large dc offset $I_0\gg\tilde{I}$ (see Fig. 3a) under conditions such that the amplitude I of the ac component is either very large ($I_1\gg\tilde{I}_0$) or comparatively small ($I_1\ll\tilde{I}_0$). In the first case the impedance has the asymptotic behavior

$$\frac{R_\omega}{\tilde{R}}=\frac{64}{(27\pi^3 b_1^3)^{1/2}}\Gamma^2(5/4)\left(\frac{\tilde{I}}{I_1}\right)^{1/2}\approx 2.69\left(\frac{\tilde{I}}{I_1}\right)^{1/2}. \tag{36}$$

In the second case, in the limit $I_1\to 0$, we get

$$\left.\frac{R_\omega}{\tilde{R}}\right|_{I_1\to 0}=\left(\frac{2}{3b_1^3}\right)^{1/2}\left(\frac{\tilde{I}}{I_0}\right)^{1/2}. \tag{37}$$

5. NONUNIFORM COMPONENT OF THE ELECTRIC FIELD. IMAGINARY PART OF THE SURFACE IMPEDANCE

In the previous Section we obtained the behavior of the electric field at the surface of the sample without taking into account the nonuniform (solenoidal) component $\boldsymbol{\mathcal{E}}$. In that approximation the impedance turned out to be real-valued. To obtain a nonzero imaginary part of the impedance it is necessary to take into account terms of higher order in the frequency, and, specifically, the solenoidal component of the electric field in Eq. (15). Since the field $\boldsymbol{\mathcal{E}}(x,t)$ is distributed symmetrically over the thickness of the film, for finding the surface impedance it is sufficient to calculate the field $\boldsymbol{\mathcal{E}}$ only

on the upper boundary of the film, $x=d/2$. Using formula (15), we obtain the following expression for the correction ΔZ_ω to the impedance:

$$\Delta Z_\omega=\frac{4\pi}{c}\frac{\mathcal{E}_\omega(d/2)}{H_\omega}=-\frac{4\pi}{c}\frac{cD}{2\pi}\frac{2}{I_1}\frac{\omega}{2\pi c}\times\int_0^{2\pi/\omega}[\dot{A}(d/2,t)-\dot{\bar{A}}(t)]e^{i\omega t}\,dt$$

$$=i\frac{2D\omega^2}{\pi cI_1}\int_0^{2\pi/\omega}[A(d/2,t)-\bar{A}(t)]e^{i\omega t}\,dt. \qquad (38)$$

Just as in the previous Section, we can assume that, because the time appears in formula (38) only in the combination $\cos\omega t$, the integral on the right-hand side is a purely real quantity and reduces to the integral over a half period. Thus we ultimately get

$$\Delta Z_\omega=i\frac{4D\omega}{\pi cI_1}\int_0^{\pi}[A(d/2,\tau)-\bar{A}(\tau)]\cos\tau\,d\tau. \qquad (39)$$

Here we have made the change of variables $\tau=\omega t$. Thus the first correction to the impedance turns out to be purely imaginary. It wholly determines the imaginary part of the impedance.

According to Eq. (39), in order to calculate the corrections to the impedance one must know $A(d/2,\tau)$ and $\bar{A}(\tau)$. The value of $A(d/2,\tau)$ is easily found from Eq. (21):

$$A(d/2,\tau)=-\operatorname{sgn}I(\tau)\tilde{H}d\ln^2(R/d)r^2/4. \qquad (40)$$

Here r is the solution of the equation obtained from (27) by substituting U from the formula for the I–V characteristic (26).

To obtain $\bar{A}$, the average value of the vector potential over the thickness of the film, we must use the solution (24) of Maxwell's equations:

$$\bar{A}(\tau)=A(d/2,\tau)\frac{1}{2}\times\int_{-1}^{1}a(\xi,\tau)d\xi=A(d/2,\tau)\left(\frac{3}{4ru\operatorname{sgn}I(\tau)}\right)^{1/2}$$

$$\times\int_0^1\frac{\zeta d\zeta}{[1-(1-\zeta)^{3/2}+3\zeta/2r]^{1/2}}=A(d/2,\tau)f(\tau), \qquad (41)$$

where the function $f(\tau)$ is given by the expression

$$f(\tau)=\left(\int_0^1\frac{\zeta d\zeta}{[1-(1-\zeta)^{3/2}+3\zeta/2r(\tau)]^{1/2}}\right)\times\left(\int_0^1\frac{d\zeta}{[1-(1-\zeta)^{3/2}+3\zeta/2r(\tau)]^{1/2}}\right)^{-1}. \qquad (42)$$

The final formula for the impedance is found by using (40) and (41). It can be written in the form

$$X_\omega=-\operatorname{Im}\Delta Z_\omega=i\frac{2\omega d}{c^2}\frac{\tilde{I}}{I_1}\int_0^{\pi}\operatorname{sgn}[I(\tau)]r^2(\tau)\ln^2[R(\tau)/d]\times[1-f(\tau)]\cos\tau\,d\tau. \qquad (43)$$

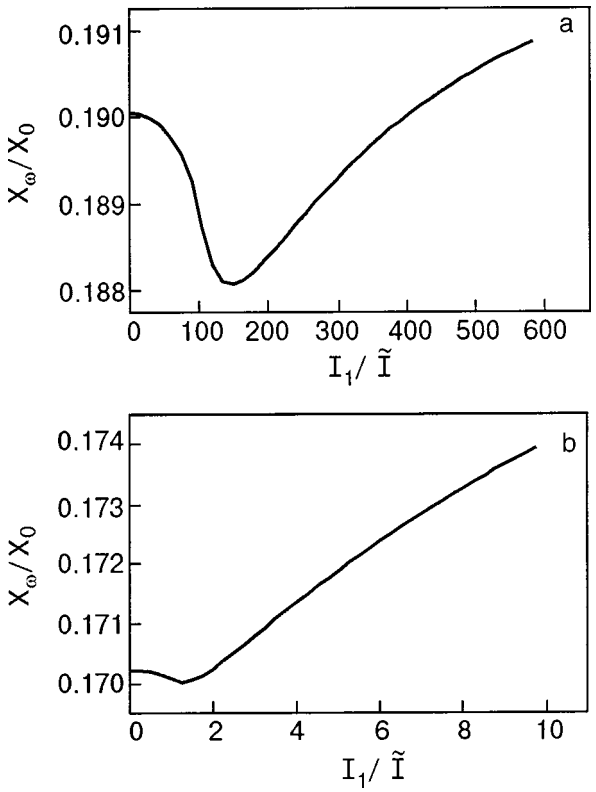

FIG. 4. Dependence of the imaginary part X_ω of the surface impedance on the amplitude I_1 of the ac component of the current for $I_0/\tilde{I}=100$ (a) and 1 (b). The impedance is normalized to the quantity $X_0\equiv(4\pi/c)(\omega d/c)$.

It is easy to obtain an asymptotic expression for X_ω at large values of the current amplitude $I_1\gg\tilde{I}$. Using formula (34), we obtain the following expression for the imaginary part of the impedance:

$$X_\omega=\frac{4\pi}{c}b_2\frac{\omega d}{c}, \qquad (44)$$

$$b_2=\frac{1}{60\pi^{1/2}}\left(\frac{\Gamma(1/6)\Gamma(1/3)}{2\pi}\right)^3\approx0.13.$$

Exactly the same formula is obtained for the case $I_0\gg\tilde{I}$, $I_1\to0$ as well. An interesting consequence of these results is that at large values of the dc component I_0, the imaginary part of the surface impedance at large and small amplitudes of the ac component I_1 turns out to be independent of the dc offset I_0 and is equal to the impedance of the vacuum attenuated by the parameter $\omega d/c$. A more exact numerical calculation, the result of which is presented in Fig. 4 for the cases of strong and weak nonlinearity (large and small values of I_0) shows that over a wide range of amplitudes the impedance agrees with formula (44) in order of magnitude. Furthermore, as can be seen from Fig. 4, the imaginary part of the impedance, like the real part, is a nonmonotonic function of the amplitude. We note that the scale of the relative variations of the imaginary part of the impedance is even smaller than that for the real part and amounts to only 1–2%.

6. CONCLUSION

We have investigated a new manifestation of the magnetodynamic nonlinearity in a film carrying an alternating

current. We have studied the nonlinear response of a sample to the self-magnetic field of a transport current of the form $I_0+I_1\cos\omega t$. We have shown that the magnetodynamic nonlinearity leads to nonmonotonic dependence of both the real and imaginary parts of the impedance on the amplitude I_1.

The results obtained are valid under the condition that the nonuniform component of the electric field in (15) is much less than the potential component. Let us estimate the two components of the electric field for the most interesting, highly nonlinear regime (when the total current in the system is much greater than $\tilde{I}$). For the potential component we obtain from formula (33)

$$E_0 \sim \frac{c l \tilde{H}}{\sigma_0 d^2}\left|\frac{I}{\tilde{I}}\right|^{1/2} \sim \frac{c l \tilde{H}}{\sigma_0 d^2}\,\frac{l}{(Rd)^{1/2}}. \tag{45}$$

For an estimate of the solenoidal field $\boldsymbol{\mathcal{E}}$ we make use of the fact that in the highly nonlinear regime the quantities $\overline{A}(\tau)$ and $A(d/2,\tau)$ differ only by a numerical factor. This follows from formulas (41) and (42). Using (15) and (40) and the asymptotic formula (34), we arrive at the estimate

$$\boldsymbol{\mathcal{E}} \sim \frac{\omega d}{c}\,\frac{I_1}{\tilde{I}}\,\tilde{H}. \tag{46}$$

Now the condition for applicability of the results obtained here can be written in the form the following inequality:

$$\frac{d^3}{l}\,\frac{I_1}{\tilde{I}}\,\frac{(Rd)^{1/2}}{l} \ll \delta_n^2(\omega), \quad \delta_n^2(\omega) = \frac{c^2}{4\pi\sigma_0\omega}, \tag{47}$$

where $\delta_n(\omega)$ is the penetration depth of the signal under conditions of the normal skin effect. At a fixed mean free path l, inequality (47) is actually a restriction on the frequency of the signal.

Let us estimate the characteristic frequencies for which the nonmonotonic amplitude dependence of the impedance can be observed experimentally. For a sample of thickness $d=10^{-2}$ cm and width $D=0.5$ cm, with a carrier mean free path $l=10^{-1}$ cm, an electron density $N=10^{23}$ cm^{-3}, and a Fermi momentum $p_F=10^{-19}$ g·cm/s, the highly nonlinear regime sets in at currents $I_0\sim I_1\sim 10$ A. It follows from (47) that for these parameter values the frequency ω must be smaller than 10^3 s^{-1}.

a)E-mail: stanislv@ire.kharkov.ua

[1] V. T. Dolgopolov, Usp. Fiz. Nauk **130**, 241 (1980) [Sov. Phys. Usp. **23**, 134 (1980)].
[2] N. M. Makarov and V. A. Yampol'skiĭ, Fiz. Nizk. Temp. **17**, 547 (1991) [Sov. J. Low Temp. Phys. **17**, 285 (1991)].
[3] G. I. Babkin and V. T. Dolgopolov, Solid State Commun. **18**, 713 (1976).
[4] É. A. Kaner, N. M. Makarov, I. B. Snapiro, and V. A. Yampol'skiĭ, Zh. Éksp. Teor Fiz. **87**, 2166 (1984) [Sov. Phys. JETP **60**, 1252 (1984)].
[5] S. A. Derevyanko, G. B. Tkachev, and V. A. Yampol'skiĭ, Fiz. Nizk. Temp. **26**, 86 (2000) [Low Temp. Phys. **26**, 64 (2000)].
[6] A. B. Pippard, Proc. R. Soc. London, Ser. A **191**, 385 (1947).
[7] A. B. Pippard, Proc. R. Soc. London, Ser. A **224**, 273 (1954).

Translated by Steve Torstveit

Electron transfer and vibrational modes in a finite molecular chain

E. Ya. Glushko*

Pedagogical University, pr. Gagarina 54, 50086 Krivoi Rog, Ukraine
(Submitted May 6, 2000)
Fiz. Nizk. Temp. **26**, 1130–1143 (November 2000)

A statistical quantum discrete model for a molecular bridge between metallic electrodes is proposed. A theory of conduction is developed on the assumption that the main contribution to the electron transfer is due to nonequilibrium-populated electron-affinity states of the molecule. It is shown that the field-induced modification of the states of the bridge molecule, together with the Coulomb blockade effect, leads to suppression of the electron transfer. Relations are obtained for the electron–vibron interaction, and the contribution of atomic vibrations to the conductance of the chain is discussed. The current–voltage characteristics of molecular bridges are calculated for different positions of the spectrum of the molecule with respect to the levels of the chemical potentials of the electrodes. Explanations are given for the stepped and asymmetric character of the current–voltage characteristic observed experimentally and for the fractional charging of the bridge molecule.
 [S1063-777X(00)01011-2]

1. INTRODUCTION

Molecular electronics, the physics of systems or devices whose basic functional units are molecules, has in the last few years been making successful progress toward the development of a technology for fabricating reliable contacts of molecules with metallic and semiconductor electrodes for the creation of molecular analogs of diodes and transistors.[1–8] Recent measurements[3] the conductance of molecular bridges between metallic electrodes, fabricated by the deposited microbridge technique of Ref. 9, revealed a number of interesting features. In particular, it was found that the current–voltage (I–V) curves have a stepped character and, under certain conditions, an asymmetry with respect to the sign of the applied voltage. Experiments[8] have revealed femtosecond electron transfer times between molecules adsorbed on the surface of semiconductors under various conditions. Transfer times with a similar order of magnitude have been observed for the tertiothene[3] and benzene-1,4 dithiol[4] molecules.

There are two main approaches to the theoretical analysis of the conductance of molecular bridges. The Landauer wave model[10,11] treats a molecular bridge between electrodes as a scattering center that reflects electron waves coming from the cathode. The current is proportional to the transmission coefficient of the molecule for the electron wave near the Fermi energy of the electrode or to a certain convolution of the transmission coefficient in this region.[3,11] However, calculations of the linear conductance in the wave model give values that are too high as compared to experiment.[3,4,6] We shall show below that the discrepancy can be attributed to the fact that the model did not tak into account the rearrangement of the electronic structure of the molecule in the electric field of the electrodes nor the contribution to the conductance from electron-affinity states of the molecule. The kinetic model of the conductance of molecular bridges[3,12,13] is based on the phenomenological rate Γ of a ternary vertex process — the tunneling hop of an electron from electrode k to the molecule,

$$\Gamma_{ij}^{k\pm}=\frac{2\pi}{\hbar}|T_{ij}|^2\rho_k f(E_i-E_j), \tag{1}$$

with the participation of a pair of molecular terms, with energies E_i and E_j. The tunneling matrix element T_{ij} is determined in the quasiclassical approximation, with the height and width of the effective tunnel barrier at the contact of the molecule with electrode k being chosen by a fitting procedure and without taking into account the dependence of T_{ij} on the indices. The function f in (1) is given by the Fermi–Dirac distribution with the difference E_i-E_j appearing in place of the usual difference between the energy of the state and the Fermi energy, and ρ_k is the density of states near the Fermi level and is assumed constant. Calculation of the conductance in the kinetic model for a bisthioltertiophene molecule adsorbed on gold electrodes[3] gave the correct order of magnitude and reflected the basic features of the I–V characteristics of molecular bridges, but the theoretical justification for the model remains unclear on account of the undefined physical meaning of Γ and of the distribution function f. Another shortcoming is the failure to take into account the contribution to the conductance from electron-affinity states, which always lie above the states of excitation of the neutral molecule and, accordingly, are closer to the Fermi surface of the metallic contacts.

Molecular bridges between macroscopic electrodes can be treated as quantum sections incorporated in an ordinary electrical circuit. The current flowing through the molecule is determined by the energy spectrum of the molecule, the discrete electronic spectrum of which is manifested in a stepped character of the I–V characteristic. An important role in this effect is played by the relationship between the chemical potentials of the electrodes and the electron-affinity spectrum of the molecule and also by the field-induced modification of the spectrum of the molecule and of the distribution of the

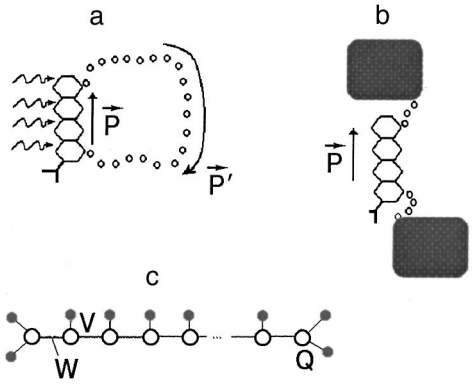

FIG. 1. A molecule as a quantum element of an electrical circuit: a complete circuit with a quantum emf in the form a photoexcited noncentrosymmetric molecule (a); a bridge molecule between macroscopic electrodes (b); a model of a linear hydrocarbon molecule (c). The transfer amplitudes are W for between carbon atoms, V for within the unit cell, and Q for the boundary cells.

electron density in its states. As a result of the field broadening of the energy band, the the electron-affinity levels successively pass near the chemical potentials of the left and right electrodes. The effect also depends on the density of states of the left and right electrodes, and this dependence is especially significant in the case of high fields or semiconductor contacts. The intramolecular phonons (vibrational modes) have a weak influence on the electron transfer and on the nonequilibrium population of the states that is established in the current-carrying system, and the Peltier effect can be neglected on account of the good heat removal. A complete molecular quantum circuit is presented in Fig. 1a. The role of the source of brief emf can be played by a polar molecule incorporated in the molecular circuit. The polarization of the quantum source can be controlled by an external resonant electromagnetic field, which switches the molecule into a long-lived triplet excited state. The current pulse flowing in the quantum circuit is due to the difference of the dipole moments of the molecule in the ground and excited states. Stabilization of the excited state can be achieved by applying a suitable bias voltage to the ends of the molecule (Fig. 1b). Then the transition to the excited state will rearrange the electron-affinity spectrum of the molecule, thus affecting the electron transfer through the molecule.

In this paper we investigate theoretically the conductance of molecular bridges in a model which combines an exact solution of the problem of the electronic and vibrational states of a finite chain of general form in a static electric field, taking into account the quantum interaction of the electronic subsystem with the metallic or semiconductor electrodes, which are reservoirs of electrons, and also with the phonon subsystem. The proposed model is based on the assumption that affinity states of the molecular bridge play an important role in the passage of current along it. The dispersion relations and the distributions of the electron density and the amplitudes of the characteristic vibrational modes are obtained here by the transfer matrix method without using the approximations of translational invariance and periodic boundary conditions. The current–voltage characteristics of a simple molecular chain at different temperatures are calculated in the nearest-neighbor approximation with allowance for the influence of the field on the interatomic barriers. The experimentally observed asymmetry of the I–V characteristics is given an explanation, and it is shown that the field modification of the electron-affinity spectrum plays a governing role in the conductance of molecular bridges. The nonequilibrium populations of the states and the current charging of the chain are calculated.

2. ELECTRONIC STRUCTURE OF A CHAIN IN AN EXTERNAL FIELD

In the adsorption of a molecule on an electrode, a thermodynamic equilibrium population of the molecular electron-affinity states is established. The ''extra'' electrons are drawn from an unlimited reservoir of particles in the left and right electrodes, while the ''inherent'' electrons occupy deep-lying states of the unexcited molecule and do not take part in the transfer processes. For example, according to the data of Ref. 3 for the bisthioltertiophene molecule the excited states occupy the energy region from -9.5 eV to -8 eV, whereas the Fermi energy of the gold electrodes lies 4.3 eV below the vacuum level. The intramolecular electrons begin to contribute to the conductance upon excitation and ionization of the molecule, but that situation is not considered here. In the proposed model the spectrum of the electron affinity of the molecule is formed on the basis of the ''bare'' atomic electron-affinity levels with allowance for the resonance interatomic transfer of electrons. The value of the matrix element of the resonant hopping is determined from the condition that the bottom of the affinity band coincides the electron affinity of the whole molecule. We note that for a rather long chain the affinity spectrum approaches the one-electron spectrum of excited states, while the electron affinity begins to be determined by the bottom of the band of excited states. Justification for this assertion comes from the fact that the effective one-electron potential of a large system for an individual valence electron is indistinguishable from the effective potential in which an ''extra'' electron moves after being injected into the system.

Let us write the Hamiltonian of the problem for an N-period linear chain (Fig. 1c) in the absence of electric field in the second-quantized representation:

$$\hat{H}_0=\sum_{l,j}^{N}\varepsilon_j a_{lj}^{+}a_{lj}+\sum_{l,j,m,i}V_{lm}^{ij}a_{lj}^{+}a_{mi}, \tag{2}$$

where l enumerates the unit cells and j the atoms within the unit cell, ε_j specifies the bare atomic levels of the affinity states, and the Hermitian matrix V_{nm}^{ij} governs the transfer of an electron between atoms. The Hamiltonian matrix (2) for an adsorbed molecular chain of the polyacetylene type, R–$(CH)_n$–R, in the nearest-neighbor approximation is given in Table I. In the model adopted, electron transfer between cells can occur only via the carbon atoms; W is the amplitude of this process, and V is the amplitude of the hops within the unit cell (Q is that for the end atoms).

The solution of the eigenvalue problem for a finite chain in the absence of field leads to a dispersion relation of the form[12,13]

$$(\lambda_l,-\nu_l)\hat{\Lambda}^m\begin{pmatrix}\nu_r\\ \lambda_r\end{pmatrix}=0,\quad \hat{\Lambda}=\begin{pmatrix}\mu & \nu\\ \lambda & 0\end{pmatrix}, \tag{3}$$

TABLE I. Matrix of the eigenvalue problem.

1	1′	1″	2	2′	3	3′	…	−1	−1′	N	N′	N″
Δ_1	Q	0	0	0	0	0						
Q	Δ_1'	Q	0	W	0	0						
0	Q	Δ_1''	0	0	0	0						
0	0	0	Δ	V	0	0						
0	W	0	V	Δ'	0	W						
0	0	0	0	0	Δ	V						
0	0	0	0	0	V	Δ'						
							…					
								Δ	V	0	0	0
								V	Δ'	0	W	0
								0	0	Δ_N	Q	0
								0	W	Q	Δ_N'	Q
								0	0	0	Q	Δ_N''

where $m=N-2$; μ, ν, and λ are the minors of the dynamical matrix (see Table I); the subscripts l and r correspond to the left and right boundaries, and

$$\mu=(\varepsilon_0-E)(\varepsilon_1-E)-V^2; \quad \nu=-\lambda=W(\varepsilon_0-E);$$
$$\nu_r=\lambda_l=(\varepsilon_0-E)[(\varepsilon_0-E)(\varepsilon_1-E)-2Q^2]; \tag{4}$$
$$\nu_l=\lambda_r=-W(\varepsilon_0-E)^2.$$

Here ε_0 and ε_1 denote the atomic electron-affinity levels of the cell, and E stands for the energy eigenvalues. In the table $\Delta_1=\Delta_1'=\Delta_N=\Delta_N'=\varepsilon_1-E$, $\Delta=\varepsilon_0-E$. A power of the transfer matrix $\hat{\Lambda}$ is found with the aid of the canonical transformation $\hat{\Theta}$ that diagonalizes the matrix $\hat{\Lambda}$:

$$\hat{\Theta}=\frac{1}{D}\begin{pmatrix} x_{22} & -x_{21} \\ x_{12} & x_{11} \end{pmatrix}; \quad \hat{\Theta}^{-1}=\begin{pmatrix} x_{11} & x_{21} \\ x_{12} & x_{22} \end{pmatrix};$$
$$D=\det(\hat{\Theta}); \tag{5}$$
$$\hat{\Lambda}^m=\frac{1}{D}\begin{pmatrix} x_{11}x_{22}\lambda_1^m-x_{12}x_{21}\lambda_2^m & x_{11}x_{21}(\lambda_2^m-\lambda_1^m) \\ x_{22}x_{12}(\lambda_1^m-\lambda_2^m) & x_{11}x_{22}\lambda_2^m-x_{12}x_{21}\lambda_1^m \end{pmatrix},$$

where x_{ij} are the elements of the eigenvectors of the matrix $\hat{\Lambda}$,

$$\hat{X}_1^+=(x_{11}, x_{12}); \quad \hat{X}_2^+=(x_{12}, x_{22});$$
$$x_{11}=x_{21}=\nu; \quad x_{12}=-\lambda_2, \quad x_{22}=-\lambda_1,$$

and the eigenvalues of the transfer matrix $\hat{\Lambda}$ have the form

$$\lambda_j=\mu/2+(-1)^i(\lambda_\nu)^{1/2};$$
$$\lambda_\nu=\mu^2/4-\lambda^2; \quad j=1,2. \tag{6}$$

The substitution of (4) and (5) into (3) leads to a generalized dispersion relation for the electronic states of the chain:

$$\lambda_1^m(\nu_r x_{22}-\lambda_r x_{21})(\lambda_0 x_{11}-\nu_0 x_{12})$$
$$-\lambda_2^m(\nu_r x_{12}-\lambda_r x_{11})(\lambda_0 x_{21}-\nu_0 x_{22})=0, \tag{7}$$

which in the general case describes both itinerant and localized states. In the energy region where the discriminant λ_1, λ_2 is negative, the terms on the left-hand side of (7) are mutually conjugate, making it possible to write the solution in explicit form:[15]

$$E_{sj}=\frac{1}{2}\left\{\varepsilon_0+\varepsilon_1-2W\xi\cos\frac{\pi s+\varphi_{lr}}{m}+(-1)^j\right.$$
$$\left.\times\left[\left(\varepsilon_0-\varepsilon_1+2W\xi\cos\frac{\pi s+\varphi_{lr}}{m}\right)^2+4V^2\right]^{1/2}\right\}, \tag{8}$$

where $j=1,2$, $\xi=\mathrm{sgn}(E-\varepsilon_0)$, φ_{lr} is an additional phase due to the left and right boundaries of the chain:

$$\varphi_{lr}=\arccos\left(\frac{(\nu_r x_{22}-\lambda_r x_{21})(\lambda_0 x_{11}-\nu_0 x_{12})}{|(\nu_r x_{22}-\lambda_r x_{21})(\lambda_0 x_{11}-\nu_0 x_{12})|}\right), \tag{9}$$

and s takes on integer values such that the argument of the cosine in (8) is found within the interval $(0,\pi)$. The structure of (8) corresponds to two bands of electronic states. The value $j=1$ in (8) corresponds to transfer between main atoms (carbon) of the chain. The value $j=2$ corresponds to indirect transfer between side atoms (hydrogen), induced by a transfer between main atoms. The width of the induced band for $V\ll W$ is proportional to the product VW, and its center is situated near ε_0. The number of states in the bands is determined by the end radicals and can fluctuate from $N-2$ to N, depending on the relative sizes of the transfer parameters Q, V, and W in a particular case. From the diagrams in Fig. 2 showing the dependence of the spectrum on

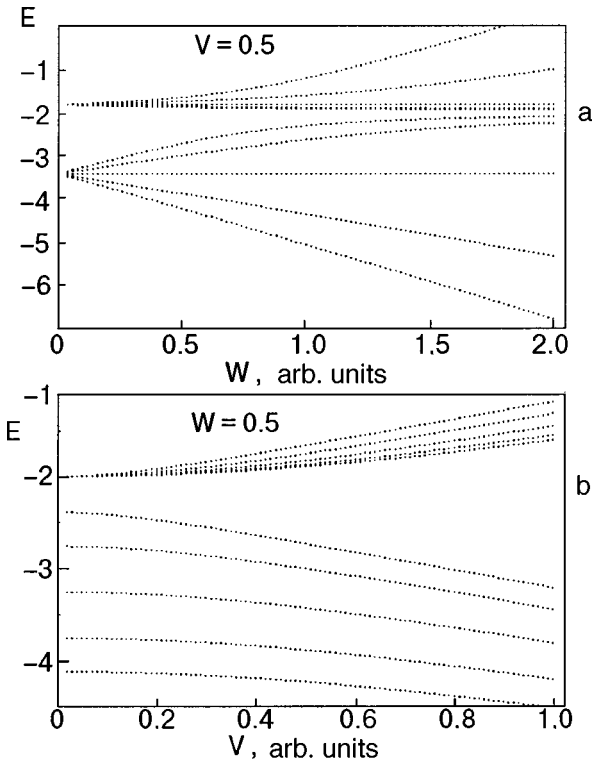

FIG. 2. Parametric diagram of the spectrum of a complex chain: the dependence on the amplitudes W (a) and V (b).

the indirect transfer amplitude V, one can conclude that the width of the energy band varies directly with the amplitude V.

In the region $\mu^2+4\lambda\nu>0$ the energy states, if they exist, have a localized character with amplitudes that fall off with distance from the ends of the chain.

In the case of a nonzero electric field $\boldsymbol{\mathcal{E}}$ the diagonal matrix elements in the first term on the right-hand side of (2) have the form

$$\varepsilon_j \to \varepsilon_j + \boldsymbol{\mathcal{E}}ekd + \boldsymbol{\mathcal{E}}ed_l, \tag{10}$$

and in the dispersion relation (3) the power of the transfer matrix is replaced by a product:

$$(\lambda_l, -\nu_l)\prod_{k=2}^{N-1}\hat{\Lambda}_k\begin{pmatrix}\nu_r'\\ \lambda_r'\end{pmatrix}=0, \quad \hat{\Lambda}_k=\begin{pmatrix}\mu_k & \nu_k\\ \lambda_k & 0\end{pmatrix}, \tag{11}$$

$$\mu_k=(\varepsilon_0-E+\boldsymbol{\mathcal{E}}ekd+\boldsymbol{\mathcal{E}}ed_l)(\varepsilon_1-E+\boldsymbol{\mathcal{E}}ekd+\boldsymbol{\mathcal{E}}ed_l)-V^2;$$

$$\nu_k=-\lambda_k=W(\varepsilon_0-E+\boldsymbol{\mathcal{E}}ekd+\boldsymbol{\mathcal{E}}ed_l);$$

$$\nu_r'=(\varepsilon_0-E+U-\boldsymbol{\mathcal{E}}ed_r)[(\varepsilon_0-E+U-\boldsymbol{\mathcal{E}}ed_r)\times(\varepsilon_1-E+U-\boldsymbol{\mathcal{E}}ed_r)-2Q^2];$$

$$\lambda_r'=-W(\varepsilon_0-E+U-\boldsymbol{\mathcal{E}}ed_r)^2,$$

where k enumerates the cells, d denotes the distance between atoms in the chain, d_r and d_l are the lengths of the adsorption bonds on the right and left ends of the molecule, and $U=\boldsymbol{\mathcal{E}}(Nd-d+d_r+d_l)$ is the potential difference between the ends of the chain. Equation (11) is reduced by a canonical transformation to the form (7)

$$e^{f_1}(\nu_r y_{22}-\lambda_r y_{21})(\lambda_0 y_{11}-\nu_0 y_{12}) - e^{f_2}(\nu_r y_{12}-\lambda_r y_{11})(\lambda_0 y_{21}-\nu_0 y_{22})=0 \tag{12}$$

with the use of the the matrix operations of logarithmification and exponentiation:

$$\ln\left(\prod_{k=2}^{N-1}\hat{\Lambda}_k\right)=\sum_k\frac{1}{D_k}\begin{pmatrix}x_{11}^k x_{22}^k\ln\lambda_1^k-x_{12}^k x_{21}^k\ln\lambda_2^k & x_{11}^k x_{21}^k\ln\dfrac{\lambda_2^k}{\lambda_1^k}\\ x_{12}^k x_{22}^k\ln\dfrac{\lambda_1^k}{\lambda_2^k} & x_{11}^k x_{22}^k\ln\lambda_2^k-x_{12}^k x_{21}^k\ln\lambda_1^k\end{pmatrix}, \tag{13}$$

$$\prod_{k=2}^{N-1}\hat{\Lambda}_k=\exp\left(\sum_k\begin{pmatrix}\dfrac{\lambda_1^k\ln\lambda_1^k-\lambda_2^k\ln\lambda_2^k}{\lambda_1^k-\lambda_2^k} & \dfrac{1}{\lambda_2^k-\lambda_1^k}\ln\dfrac{\lambda_2^k}{\lambda_1^k}\\ \dfrac{1}{\lambda_2^k-\lambda_1^k}\ln\dfrac{\lambda_2^k}{\lambda_1^k} & \dfrac{\lambda_1^k\ln\lambda_1^k-\lambda_2^k\ln\lambda_2^k}{\lambda_2^k-\lambda_1^k}\end{pmatrix}\right), \tag{14}$$

where $\lambda_i^k=[\mu_k+(\mu_k^2+4\lambda_k\nu_k^{1/2})]/2$ are the eigenvalues of the transfer matrices that appear in the product, f_1 and $f_2=-f_1$ are the eigenvalues of the matrix $\hat{F}$ in the argument of the exponential function in (14). The condition $\mu_k^2+4\lambda_k\nu_k=0$ determines the boundary between extended (delocalized) states, which are distributed over the entire length of the chain, and the states localized by the external field. Another cause of localization may be structural defects, including the ends of the chain. Calculations show that as the electric field increases, the region of extended states narrows from the edges of the band toward the center, while the width of the band increases by an amount equal to the applied potential difference U. The last extended states are converted to localized states when U exceeds the initial width of the band. The distribution of the amplitudes of the electron density in the chain is specified by the eigenvectors of the eigenvalue problem solved above. Our model for the chain allows us to obtain analytical expressions for the eigenvectors, which are determined by the coefficients C_{kj} of the canonical transformation:

$$a_s^+=\sum_{k,j}C_{kj}(s)a_{kj}^+, \quad a_s=\sum_{k,j}C_{kj}^*(s)a_{kj}. \tag{15}$$

The summation is over all cells k of the chain and atoms j within the unit cell. The index $s=1,2,\ldots,N$ enumerates the electronic affinity states. The explicit form of C_{kj} can be obtained using Cramer's rule, expanding out the determinants corresponding to each of the variables:

$$C_{k1}=d_{k-1}QV\prod_{i=k+1}^{N}(-\varepsilon_{0i}W); \quad C_{k2}=C_{k1}\frac{V}{E_s-\varepsilon_0}; \tag{16}$$

$$d_{k-1}=\frac{1}{\Theta_{k-3}}[e^{f_{k-3}}(\nu_r y_{22}-\lambda_r y_{21})(\lambda_0 y_{11}-\nu_0 y_{12}) - e^{-f_{k-3}}(\nu_r y_{12}-\lambda_r y_{11})(\lambda_0 y_{21}-\nu_0 y_{22})]. \tag{17}$$

The kth-order determinants Θ_k are determined by the upper left-hand corner of the matrix given in Table I. A calculation of the electron density $|C_{kj}(s,i)|^2$ both with and without allowance for the field dependence of the resonant-transfer matrix element V is done in Ref. 15. As the applied voltage is increased, the standing waves $C_{kj}(s,i)$ become more and more symmetric (or antisymmetric) with respect to the center of the linear molecule. Meanwhile, at sufficiently high fields ($\approx 10^9$ V/m) the interatomic barriers are lowered and the transfer amplitudes increase, tending to restore the symmetry of the electron density distribution.

3. VIBRATIONAL SPECTRUM AND MODE AMPLITUDES OF THE ATOMIC CHAIN

Let us consider the problem of small vibrations of the atoms in a bounded adsorbed chain. If the system has finite dimensions, it is necessary to take into account the translational invariance of the vibrational modes. While having a weak effect on the eigenfrequencies and densities of itinerant states, translational invariance is manifested substantially in the distribution of the mode amplitudes along the chain and, furthermore, has an appreciable influence on the amplitudes and frequencies of the localized vibrations.[17]

In the conduction phenomenon, vibrations give rise to a scattering channel of the injected carriers in addition to resonant transfer. Furthermore, the phonon or vibron mechanism, against the background of the resonant interaction, by which the current carriers hop between sites of the chain, leads to the onset of a finite width of the electronic states. We shall assume that the electric field does not act on the elastic constants of the interatomic bond.

The classical expression for the vibrational energy of the complex chain whose electronic structure was considered above,

$$E_{cl}=\sum_{l,j}\frac{m_j\dot{U}_{l,j}^2}{2}+\sum_{l,j}\frac{k_j(U_{l,0}-U_{l+1-j,j})^2}{2}+\frac{k_fU_{1,f}^2}{2}+\frac{k_tU_{N,t}^2}{2} \tag{18}$$

contains a summation over the unit cells l of the linear chain; the index $j=0,1$ enumerates the atoms within a cell (Fig. 1c), and for the end cells $j=0,1,1'$. The nearest-neighbor approximation is used; k_f and k_t are the elastic constants of the adsorption bond of the end atoms f and t of the molecular bridge with the electrodes. The system of dynamical equations for the vibrations,

$$\begin{cases} m_1\omega^2U_{11}=k'(U_{11}-U_{10}); \\ m_0\omega^2U_{10}=k_0(U_{10}-U_{20})-k_1(U_{11}-U_{10})-k'(U_{1,1'}-U_{10})-k_fU_{1,0}; \\ m_{1'}\omega^2U_{11'}=k'(U_{11'}-U_{10}); \\ \cdots\cdots\cdots\cdots\cdots\cdots\cdots\cdots\cdots\cdots\cdots\cdots\cdots\cdots\cdots\cdots\cdots\cdots\cdots\cdots\cdots\cdots\cdots\cdots \\ m_1\omega^2U_{N1'}=k'(U_{N1'}-U_{N0}) \end{cases} \tag{19}$$

describes a dynamical matrix that coincides with the matrix of the electronic problem considered in the case of a polyacetylene chain (see Table I), where one must set

$$\begin{aligned} &\Delta_1=\Delta_N=k'-m_1\omega^2; \quad \Delta_1''=\Delta_N''=k'-m_{1'},\omega^2; \\ &\Delta_1'=k_0+k_f+2k'-m_0\omega^2; \quad \Delta=k_1-m_1\omega^2; \\ &\Delta'=2k_0+k_1-m_0\omega^2; \\ &\Delta_N'=k_0+k_t+2k'-m_0\omega^2; \quad Q=-k'; \\ &W=-k_0; \quad V=-k_1. \end{aligned} \tag{20}$$

Taking into account the formal equivalence of the electronic and vibrational problems, we can use the results obtained in (3)–(9) for the spectrum, with the following substitution in (8):

$$\begin{aligned} &E_{sj}=\omega_{sj}^2; \quad \varepsilon_0\Rightarrow\frac{2k_1}{m_1}; \quad \varepsilon_1\Rightarrow\frac{2k_0+k_1}{m_0}; \\ &W\Rightarrow\frac{k_0}{m_1}; \quad V\Rightarrow\frac{k_1}{(m_1m_0)^{1/2}}. \end{aligned} \tag{21}$$

Similarly, for the distribution of amplitudes along the chain A_{kj} $(k=1,2,\ldots,N)$ we have, with allowance for (16) and (17),

$$A_{k0}=d_{k-1}kk_1\prod_{i=k+1}^{N}(\Delta_ik_0); \quad A_{k1}=-A_{k0}\frac{k_1}{\Delta'}, \tag{22}$$

$$d_{k-1}=\frac{1}{\Theta_{k-3}}[\lambda_1^{k-3}(\nu_rx_{22}-\lambda_rx_{21})(\lambda_0x_{11}-\nu_0x_{12})-\lambda_2^{k-3}(\nu_rx_{12}-\lambda_rx_{11})(\lambda_0x_{21}-\nu_0x_{22})]. \tag{23}$$

The characteristic features of the amplitude distribution, which were studied for a simple chain in Ref. 17, are also present in the case of a complex adsorbed chain with two atoms per unit cell: the set of functions A_{ij} for the different modes $q=1,\ldots,N$ form a system of localized and delocalized standing waves which satisfy the theorem concerning the zeros of the eigenfunctions.[18] In particular, it follows from (22) that the vibrations of the atoms in the unit cell are 180° out of phase if $\Delta'>0$ and in phase if $\Delta'<0$.

4. ELECTRON–PHONON INTERACTION IN A LINEAR ATOMIC CHAIN

The results obtained in the classical approach are used in making the transition to the quantum vibrational problem. The Hamiltonian of the phonon subsystem

$$\hat{H}_{\rm ph}=\sum_{q,j}\hbar\omega_{qj}(b_{qj}^+b_{qj}+1/2) \tag{24}$$

is expressed in terms of the creation b_{qj}^+ and annihilation b_{qj} operators for a phonon of the jth branch of the qth mode, which are related by a canonical transformation A_{ki} (22) with

the bare operators b_{kj} of the vibrations of the jth atom of the kth unit cell:

$$b_{qj}^{+}=\sum_{k,i} A_{ki}(q,j)b_{ki}^{+}, \quad b_{qj}=\sum_{k,i} A_{ki}^{*}(q,j)b_{ki}. \tag{25}$$

The creation (annihilation) operators for vibrations at the sites, b_{ki}^{+} (b_{ki}) are related to the displacements U_{ki} of the atoms from the equilibrium positions by the relation $U_{ki} \rightarrow \Xi(b_{ki}^{+}+b_{ki})/\sqrt{2}$. Small displacements modify the resonant interaction, inducing interatomic electron transfer, which gives rise to an additional term in the Hamiltonian (2):

$$V_{nm}^{ij} \Rightarrow V_{nm}^{ij}+\tilde{V}_{ij}(U_{ni}-U_{mj}). \tag{26}$$

In the nearest-neighbor approximation the initial electron–phonon interaction (EPI) operator in the site representation has the form

$$\begin{aligned}\hat{H}_{ep}^{(1)}=&\frac{\tilde{V}_0\Xi_0}{\sqrt{2}}\sum_{n}^{N-1}(a_{n,0}^{+}a_{n+1,0}-a_{n+1,0}^{+}a_{n,0})\\ &\times(b_{n,0}^{+}+b_{n,0}-b_{n+1,0}^{+}-b_{n+1,0})+\frac{\tilde{V}_1\Xi_1}{\sqrt{2}}\\ &\times\sum_{n}^{N}(a_{n,0}^{+}a_{n,1}-a_{n,1}^{+}a_{n,0})(b_{n,0}^{+}+b_{n,0}-b_{n,1}^{+}-b_{n,1}),\end{aligned} \tag{27}$$

where $\tilde{V}_0=\partial V_{nm}^{00}/\partial x$ is the derivative of the amplitude for transfer along the chain, taken about $x=d(n-m)=d$. The first term in (27) corresponds to processes of hopping between the unit cells, with the absorption or emission of vibrational quanta of the site, and the second corresponds to vibronic processes within the cells. Only the longitudinal vibrations with respect to the direction of electron transfer are taken into account.

In an electric field another electron–phonon scattering channel appears, due to vibrational modulation of the atomic affinity levels ε_0 and ε_1 as a result of the dependence of their absolute values on the positions of the atom:

$$\hat{H}_{ep}^{(2)}=\frac{ed}{\sqrt{2}}\sum_{n,j}^{N}(\Xi_j\boldsymbol{\mathcal{E}})a_{n,j}^{+}a_{n,j}(b_{nj}^{+}+b_{nj}). \tag{28}$$

The scalar product under the summation sign in (28) ensures that only the longitudinal vibrations contribute under the condition that the molecule is oriented along the field.

An electron injected into the chain occupies one of the affinity states. The time of formation of such a state with an energy E_{sj} and an electron density distribution $|A_{ki}(s,j)|^2$ is of the order of 10^{-14}–10^{-15} s, which is much shorter than the time of transition of an electron across the molecular bridge, 10^{-12} s, at currents of $\approx 10^2$ nA or less. If the electron–phonon interaction time is also of the order of 10^{-12} s, then the phonon contribution is due to scattering of standing waves of electron density on standing waves of vibrational modes. In that case, by taking into account the orthogonality of the transformation matrices from the site representation to the eigenvector representation, we obtain

$$\hat{H}_{ep}^{(1)}+\hat{H}_{ep}^{(2)}=\sum_{s,s'j,j',q,i} V_{s,s'}^{j,j'}(q,i)a_{s,j}^{+}a_{s',j'}(b_{qi}^{+}+b_{qi}), \tag{29}$$

$$\begin{aligned}V_{s,s'}^{j,j'}(q,i)=&\frac{1}{\sqrt{2}}\sum_{n=1}^{N}\{[\tilde{V}_0\Xi_0(C_{n,0}(s,j)C_{n+1,0}^{*}(s',j')\\ &-C_{n0}^{*}(s,j)C_{n+1,0}(s',j'))(1-\delta_{nN})(A_{n,0}(q,i)\\ &-A_{n+1,0}(q,i))+\tilde{V}_1\Xi_1(C_{n,0}(s,j)C_{n+1,0}^{*}(s',j')\\ &-C_{n0}^{*}(s,j)C_{n+1,0}(s',j'))(A_{n,0}(q,i)-A_{n,1}(q,i))]\\ &+ed\varepsilon_{jj'}(\Xi_j\boldsymbol{\mathcal{E}})C_{n,j}(q,i)C_{n,j}^{*}(q,i)A_{n,j}(q,i)\}.\end{aligned} \tag{30}$$

It follows from (30) that the interaction of the electron and phonon subsystems is determined by finding the distributions of the electron and phonon densities along the chain.

The question of the contribution of the EPI to the conductance of linear molecular bridges is not altogether clear at present because of a lack of experimental data on the electron–vibrational coupling constants $\tilde{V}$ in linear molecules. Owing to the discreteness of the electronic and vibrational states in a mesoscopic system, an additional factor influencing the phonon contribution to the conductance arises: the commensurability of the electron and phonon bands. In particular, if the distance between electronic levels reaches values of the order of or smaller than the energy of a thermal phonon, then the phonons participate in the scattering of electrons, while otherwise the phonon mechanism is suppressed. The width of the phonon bands also plays a role, particularly the most populated acoustical band. In rigid finite systems with wide bands the density of states is small, and this also lowers the probability of absorption or emission of a phonon by an electron. Qualitative estimates[17–19] give for the width of the acoustical band of a linear –C = C– chain a value of the order of 0.1 eV. In that case, for a chain of length $N=30$ at room temperature only the lowest vibrational mode falls in the kT region. As we shall show below, the passage of current in a molecular bridge disrupts the thermodynamic equilibrium in the electronic subsystem, and that leads to disequilibrium in the phonon subsystem on account of the electron–phonon coupling. Analysis of expression (30) for the matrix element of the EPI shows that for translationally noninvariant phonons of a finite chain the role of the quasimomentum conservation laws is played by a less strict relation between the quantum numbers of the states s, s', and q. For example, for a simple chain the summation over the lattice in the matrix element $\hat{H}_{ep}^{2}$ gives

$$\tilde{V}^{(2)}_{s,s',q}=\frac{\Xi\mathcal{E}ed}{2(N+1)^{3/2}}\begin{cases}0, & s+s'+q=2k,\\ \dfrac{\sin\dfrac{\pi s}{N+1}\sin\dfrac{\pi s'}{N+1}\sin\dfrac{\pi q}{N+1}}{\sin\dfrac{\pi(s+s'+q)}{2(N+1)}\sin\dfrac{\pi(s+s'-q)}{2(N+1)}\sin\dfrac{\pi(s-s'-q)}{2(N+1)}\sin\dfrac{\pi(s-s'+q)}{2(N+1)}}, & s+s'+q=2k+1.\end{cases} \tag{31}$$

Thus we find that scattering processes for which the sum of the mode index of the vibrational mode taking part in the scattering plus the quantum numbers of the initial and final states of the electron has an even value are forbidden. Any of their odd combinations that satisfy energy conservation are allowed.

5. STATIC CONDUCTIVITY OF A LINEAR MOLECULE

The coupling between the electronic subsystem of an adsorbed molecule chain and the electrodes is manifested in a nonzero probability amplitude for the transfer of an electron to the molecule. The corresponding addition to the Hamiltonian operator,

$$\hat{H}_{ad}=G_l(a_l^+a_{10}+a_{10}^+a_l)+G_r(a_r^+a_{N,0}+a_{N,0}^+a_r) \tag{32}$$

contains the hopping amplitude of an electron between the ''banks'' and the end atoms of the chain, $G_{l,r}$. The indices l and r refer to the left and right banks, respectively. The electronic structure of the metallic electrodes in our model is determined by the density of states:

$$g(\varepsilon_{r,l})=\frac{4\pi H}{h^3}(2m)^{3/2}\varepsilon_{r,l}^{1/2}, \tag{33}$$

where H is the effective electrode volume that participates in the contact with the molecule, m is the effective mass of an electron, $\varepsilon_{r,l}=E_{Frl}-\chi_{r,l}+E_{sj}+U_{l,r}$ is the energy of the state E_{sj} measured from the start of the Fermi step of the right or left electrode, with allowance for the applied bias voltage $U_{l,r}$, and E_{Frl} denotes the corresponding Fermi energy. The chemical potential $\chi_{r,l}$ and the energy E_{sj} are measured from the vacuum level, which is taken as zero (Fig. 3). The ''banks'' play the role of infinite reservoirs of electrons which are found in thermodynamic equilibrium. The equilibrium populations of the electronic states of the thermal reservoirs are described by the Fermi distribution

$$N_{l,r}=\frac{1}{\exp((\varepsilon_{l,r}-E_F)/T)+1}, \tag{34}$$

where T is the temperature. In the model under consideration an injected electron occupies one of the electron-affinity states E_{sj} of the chain or one of the vibrational sublevels. The probability of such a process per unit time can be written in the second order of perturbation theory in the weak adsorption interaction according to the famous ''golden rule'':

$$W_{l\to sj}=\frac{2\pi}{\hbar}\int d\varepsilon g_l(\varepsilon)\Bigg\{N_l\Bigg[(1-N_{sj})|G_{lsj}|^2\delta(E_l-E_{sj})+\sum_{q,i,\xi}\left(N_{qi}+\frac{1+(-1)^\xi}{2}\right)(1-N_{sj,qi})|\tilde{G}_{l,sj}(q,i)|^2\times\delta(E_l-E_{sj}+(-1)^\xi\hbar\omega_{q,i})\Bigg]\Bigg\}. \tag{35}$$

The populations N_l and N_r for transfer at the right-hand boundary $W_{r\to sj}$ are determined according to Eq. (34) by substitution of the energies ε_l and ε_r. As to the populations of the electronic N_{sj} and vibronic $N_{sj,qi}$ states of the chain, they are governed by conservation of charge and the continuity of the flux of charge through the state sj.

The first term in (35) describes a resonant zero-phonon mechanism of bank–chain transfer, and the second term describes processes of transfer to the vibronic states of the molecule $E_{sj,qi}=E_{sj}+(-1)^\xi\hbar\omega_{qi}$ with absorption ($\xi=1$) and emission ($\xi=0$) of phonons of the ith branch of the qth mode. The probability of the reverse processes $W_{sj\to l}$ and $W_{sj\to r}$ is written in analogy with (35) with a suitable change of indices. The matrix elements of the transfer are determined from (32) as a result of a canonical transformation of the site operators for creation and annihilation and quantization of the displacements:

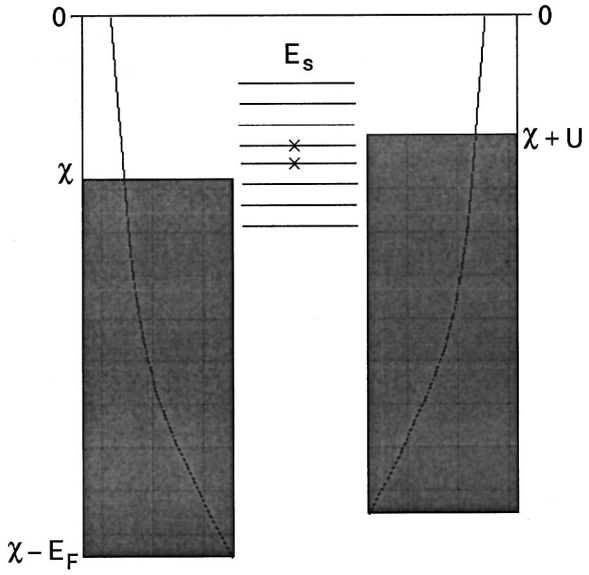

FIG. 3. Energy diagram of the problem: E_s are the electronic levels, E_F is the Fermi energy, χ is the chemical potential, and U is the potential difference. The solid curves show a plot of $g(\varepsilon)$.

$$|G_{l,sj}|^2=G_l^2|C_{sj}(1,0)|^2,$$
$$|\tilde{G}_{l,sj}(q,i)|^2=\tilde{G}_l^2|C_{sj}(1,0)A_{qi}(s,j)|^2,$$
$$|G_{r,sj}|^2=G_r^2|C_{sj}(N,0)|^2, \tag{36}$$
$$|\tilde{G}_{r,sj}(q,i)|^2=\tilde{G}_r^2|C_{sj}(N,0)A_{qi}(s,j)|^2.$$

Let us consider the zero-phonon contribution to the conductance, which is determined by the first term in (35). Assuming that the electron–phonon coupling is weak, we equate the electron flux of the sj state through the left and right boundaries of the chain,

$$I_{l\leftrightarrow sj}=\frac{2\pi e}{\hbar}|G_{l,sj}|^2 g_l(E_{sj}-\chi_l+E_{Fl}+U_l)(N_l-N_{sj}),$$
$$I_{r\leftrightarrow sj}=\frac{2\pi e}{\hbar}|G_{r,sj}|^2 g_r(E_{sj}-\chi_r+E_{Fr}+U_r)(N_{sj}-N_r), \tag{37}$$

and we obtain for the steady-state nonequilibrium population of the states of the chain

$$N_{sj}=\frac{|G_{l,sj}|^2 g_l(E_{sj}-\chi_l+E_{Fl}+U_l)N_l+|G_{r,sj}|^2 g_r(E_{sj}-\chi_r+E_{Fr}+U_r)N_r}{|G_{l,sj}|^2 g_l(E_{sj}-\chi_l+E_{Fl}+U_l)+|G_{r,sj}|^2 g_r(E_{sj}-\chi_r+E_{Fr}+U_r)}. \tag{38}$$

The total current through the molecule is written as a sum of the electron fluxes through all the states:

$$I=\frac{2\pi e}{\hbar}\sum_{s,j}|G_{l,sj}|^2|G_{r,sj}|^2 g_l(E_{sj}-\chi_l+E_{Fl}+U_l)g_r(E_{sj}-\chi_r+E_{Fr}+U_r)$$
$$\times\frac{N_l-N_r}{|G_{l,sj}|^2 g_l(E_{sj}-\chi_l+E_{Fl}+U_l)+|G_{r,sj}|^2 g_r(E_{sj}-\chi_r+E_{Fr}+U_r)}. \tag{39}$$

The dimensional part of the total current I_0, which is given by

$$I_0=\frac{e(2m)^{3/2}HG^2}{\pi\hbar^4}, \tag{40}$$

where G is the amplitude of the bank–molecule electronic transition, plays the role of the unit of current. The numerical value of I_0, if the energies in (39) are measured in eV and H is in Å^3, turns out to be $10.41HG^2$ μA. The relation obtained for the current allows for differences of the materials of the left and right banks and for the possibility of their asymmetric connection in the electrical circuit with respect to the vacuum level. In the symmetric case one has $U_r=-U_l=U/2$; then for the identical metal electrodes the I–V characteristic is antisymmetric with respect to the applied electrical bias. If, for example, the left electrode is grounded, than one must set $U_l=0$ and $U_r=U$ in Eq. (39), and the I–V characteristic loses symmetry with a change in sign of the applied voltage. Examples of symmetric and asymmetric molecular bridges are given in the experimental paper of Ref. 3. Calculations show that the value of the current as a function of voltage depends substantially on the electron density distribution $|C_{sj}(1,0)|^2$ and $|C_{sj}(N,0)|^2$ in the standing wave near the ends of the chain [see Eq. (36)] and on the difference in the populations of the banks. The square-root energy dependence of the densities of states g_l and g_r have a weaker effect on the value of the current. It is important for understanding the features of the current flow through a linear mesoscopic system that the characteristic temperatures $T\approx 0.02$–0.03 eV are ordinarily much smaller than the distances between levels of the electron-affinity band of the molecule. Therefore, as the applied bias voltage U is increased, the affinity levels pass one at a time through the region of effective transfer near the Fermi energies E_{Fl} and E_{Fr}. The entry of each new level into the active region corresponds to a sharply rising segment of the I–V characteristic, and the energy gaps, to the plateaus. The total charge trapped by the molecule behaves in a similar way. Below, for the example of a simple chain, we analyze the nature of the current through a molecular bridge, initially ignoring the Coulomb blockade effect. In the case of identical electrodes there are three possible arrangements of the affinity spectrum with respect to the Fermi surfaces of the banks.

1. We consider a system for which the lower edge of a narrow band of affinity states, of width ≈ 0.08 eV at $U=0$, lies above the chemical potential level χ by an amount δ. The corresponding I–V characteristic of a molecular bridge of length $N=20$ between copper electrodes ($\chi=-4.3$ eV, $E_F=7.0$ eV) for $\delta=0.01$ eV, a transfer amplitude $V=0.02$ eV, and a temperature $T=1.2$ K is presented in Fig. 4 (curve *1*). The fine-stepped structure of the left half of the characteristic corresponds to the successive passage of approximately one-half of the itinerant states through the fixed chemical potential of the left bank, which corresponds to a positive bias of $U\approx 50$ mV. Further growth of the potential difference weakens the transfer, because the field ''drains off'' electron density from the next states from the left bank. For short chains with $N\approx 8$–15 the falling part of the characteristic has large ''benches'' which mark the passage of the levels of the upper half of the band near the narrow (at the given temperature) active region of the left bank. The benches are smeared out as the temperature is increased and vanish completely at $T\approx 58$ K. The position of the first bench as $T\to 0$ is close to δ. As the length of the chain increases, the characteristic is smoothed out, and the value of the cur-

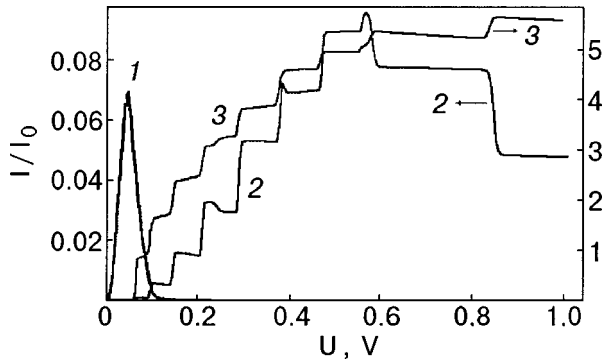

FIG. 4. The current–voltage (I–V) characteristic with allowance for allowance for charging. Configuration I: a narrow electronic band for $V=0.02$ eV, $N=20$, $T=1.2$ K (*1*), a band of intermediate width $V=0.2$ eV (*2*), and the dependence of the charging on the external field (*3*). $E_0=-3.8$ eV, $U_0=0.3$ eV, $T=22.2$ K, and $N=10$.

rent decreases slightly: $I_{\max}=0.06I_0$ for $N=8$ and $I_{\max}\approx 0.05I_0$ for $N=50$.

In the case of a wide band, with a width of ≈ 0.8 eV and $\delta\approx 0.1$ eV, the transfer is considerably more intense, and the I–V curve is shifted to higher voltages. Steps are observed even at room temperatures. As the temperature is lowered, these steps become sharper (curve *2* in Fig. 4). As in the case of a narrow band, the current rises when the band ''sinks'' below the level of the chemical potential of the left bank down to the center. Curve *3* in Fig. 4 shows the calculated dependence of the charging of the chain, $q=e\Sigma N_s$, on the applied voltage. It is seen that the charging of the chain and the jumplike increase in current are correlated processes. The regions of constant charge on curves *3* and constant charge on curve *2* are also correlated. Chaning in jumps, the charge of a 10-atom chain at a voltage of around 1 V across the molecule reaches a maximum value somewhat in excess of 5.4.

2. The center of the band of electron-affinity states in the absence of field coincides with the chemical potential of the banks. Figure 5 gives the calculated I–V characteristic of a 24-atom chain with a narrow band $V=0.01$ eV at a temperature $T=22$ K. For such a configuration the main contribution to the conductance comes from about one-fourth of all the

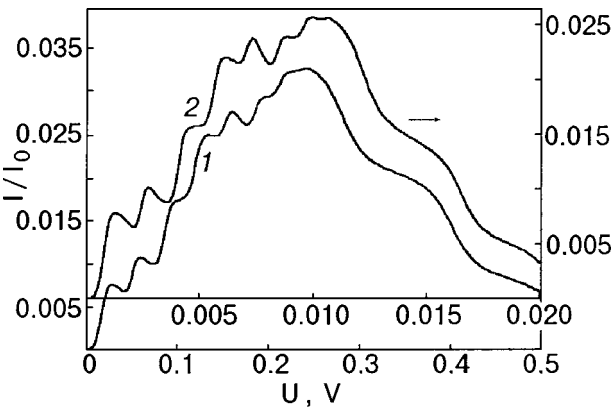

FIG. 5. I–V characteristic without allowance for charging. Configuration II: a band of intermediate width $V=0.2$ eV, $T=58$ K (*1*), and a narrow electronic band with $V=0.01$ eV, $T=22$ K (*2*). $E_0=-4.3$ eV, $U_0=0.08$ eV, $N=24$.

levels or one-half of the levels initially lying above the value of the chemical potential. As the length of the chain is increased, the benches associated with the gaps between levels are smoothed out, and the value of $I_{\max}$ decreases. The curve behaves in an analogous way as the temperature is raised. The interlevel oscillations vanish by $T=58$ K. In the case of a wide band (≈ 0.8 eV), as in the previous case, the I–V curve is shifted to higher voltages, and the value of the current increases. The steps are observed even at room temperatures. As the temperature is lowered, they become sharper (curve *2* in Fig. 5). As in the case of a narrow band, the increases in current occur when the band ''sinks'' below the level of the chemical potential of the left bank down to the center. A comparison of the cases of narrow and wide bands shows that the curves are similar under a scale transformation, confirming the above picture of successive passage of affinity levels near the Fermi surface of an electrode.

3. If the band of affinity states of the bridge molecule in the absence of field lies below the level of the chemical potential of the bands, then the conductance is strongly suppressed. The calculated I–V curves turn out to be structureless even at very low temperatures. As the temperature is raised, the maximum of the I–V curve increases and shifts to higher voltages. Numerical estimates show that the suppression of the conductance of a bridge in this case also is a consequence of the ''draining off'' of electron density from the ends of the chain by the field. However, as the electric field is increased further, in addition to the field-induced deformation of the electron density distribution, an opposing tendency begins to operate: the transfer amplitude V increases on account of the decrease of the effective thickness of the intersite potential barriers in the external field. The field-induced stimulation of transfer was taken into account in the model by the phenomenological relation

$$V=V_0e^{U/NU_0}, \tag{41}$$

where U_0 is the effective height of the potential barrier between neighboring atoms in the chain. In the examples considered above it was assumed that $U_0=0.2$ eV. The field-induced stimulation gives rise to a slight slope of the ''shelves'' on the I–V curve at low applied bias voltages. For $U>NU_0$ the current increases sharply on account of the broadening of the band of electronic states.

The conditions of contact can be such that a molecular bridge carrying a current is found in a negligibly weak external field. Such a situation arises if an extended linear molecule bridges the tips of thin electrodes. The voltage drop in this case occurs near the ends of the molecule, and the electric field has practically no influence on the electronic states. The solid curve in Fig. 6 shows the calculated I–V curve for a chain with four initial affinity states at $E_0=-4.25$ eV, $V=0.23$ eV, $U_0=0.5$ eV, and $T=0.03$ eV for gold electrodes. The dots show the corresponding dependence of the charge trapped by the molecule. There is a clear tendency to trap fractional charge — a consequence of the thermodynamic nonequilibrium population of the states of the current-carrying chain. The half-integer charge on the molecule through which current is flowing arises at low temperatures $T\ll V$ if there is an odd number of affinity states in the region $(\chi,\chi+U)$ (Fig. 3). The states lying above this region are not

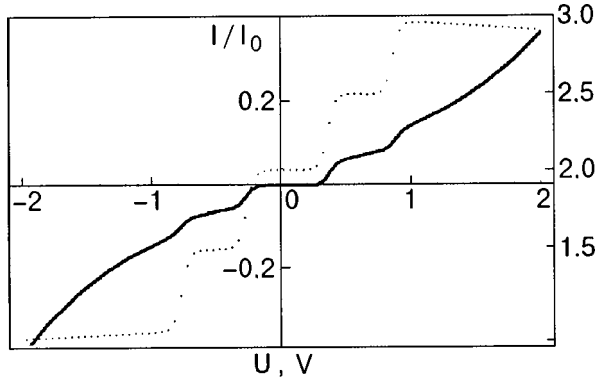

FIG. 6. Current–voltage characteristic without allowance for the field-induced modification. The solid curve is a band of intermediate width, $T=348$ K; the dots represent the trapped charge. $E_0=-4.25$ eV, $V_0-0.23$ eV, $U_0=0.08$ eV, $N=24$.

populated ($n_s=0$), while those lying below are completely occupied ($n_s=1$). For the states indicated by an asterisk in Fig. 3 it follows from Eq. (38) that $n_s\approx 1/2$ under conditions of symmetric contact of the molecule with the dislocations. It should be kept in mind that for the small bias voltages U considered here, the densities of states of the banks are approximately equal, $g_r\approx g_l$.

6. CONCLUSION

Molecular bridges carrying a current are examples of multiparticle parametric systems with a steady-state nonequilibrium distribution. The number of electrons trapped from outside the affinity states of the molecule is regulated by the external conditions. The discrete chain model of electron transfer studied in this paper is one of the simplest , and it also can take into account the main features of the passage of current through molecular bridges in a unified formalism. In another, the potential approach, the molecular bridge is associated with a system of adjacent potential wells along which the electrons pass from the cathode to the anode. Initially there is one electron-affinity level in each atomic potential well. In the system of wells the initial affinity level generates a band of states whose structure and position determine the character of the flow of current as a function of the applied voltage until the charge of the molecular bridge exceeds unity. Further increase in the charge creates a Coulomb barrier which modifies the affinity spectrum. The features of the electron spectrum of the neutral molecule M^0 are manifested in the conductance if the molecule is ionized. In that case the states are partially filled by an electron passing over from the electrode. As the applied voltage increases, the total population can exceed unity. At that time the charge state of the molecule changes, and the affinity spectrum of M^{-1} is turned on. In this paper we have not considered the influence of the change in charge on the state of the molecular bridge (Coulomb blockade). A phenomenological treatment of this effect was done in Refs. 3, 11 and 20–22 without taking the restructuring of the charge state into account and in Refs. 15 and 23 with these transitions included. A more rigorous approach requires solving the quantum many-body problem on a discrete chain with allowance for the dependence of the number of trapped particles on the applied potential difference.

A comparison of the results of the discrete chain model with the experimental data is difficult on account of a lack of reliable information about the electron affinity of the bridge molecules. Evidently, the results of Ref. 3 indicate that the bisthioltertiophene molecule adsorbed on an electrode has several affinity levels lying above the chemical potential by approximately 0.3 eV. The basic scheme of the electron transfer for the model remains as before if the molecule is bridging two semiconductors. In that case the density of states (33) takes into account the energy gaps of the electronic spectra of the banks. The model can also describe low-temperature electron transfer through atomic chains arising in the space between metallic electrodes. Structures of this kind have been investigated experimentally in Refs. 24–26 for monatomic bridges between Au, Pt, Al, Nb, Pb, K, and Na electrodes. The mechanism of transfer via affinity states of a monatomic bridge also lead to a stepped form of the conductance, with positive or negative slopes of the plateaus,[24] but the conductance can also vanish when the bottom of the conduction band of the chain rises above the chemical potential of the electrodes on account of the Coulomb blockade effect. The quantum parts of the circuit play an important role in single-electron transistors (SETs) and devices with a periodic dependence of the conductance on the bias voltage — electronic pawls and ratchets.[22] Although a linear treatment of the two-electrode model is not directly applicable to such systems, there is a fundamental similarity between molecular bridges and quantum dots (with their discrete spectra) in tunneling contact with several electrodes.

The author thanks Prof. A. M. Kosevich and the participants in seminar of the theoretical division of the B. Verkin Institute for Low Temperature Physics and Engineering at Kharkov, Ukraine for a discussion of the results of this study.

*E-mail: EYAGL@kpi.dp.ua

[1] R. H. Friend, Phys. Scr. **66**, 9 (1996).
[2] Y. Isono and H. Nakano, J. Appl. Phys. **75**, 4557 (1994).
[3] C. Kergueris, J.-P. Bourgoin, S. Palacin, D. Esteve, C. Urbina, M. Magoga, and C. Joachim, Phys. Rev. B **59** (19), 12505 (1999).
[4] M. A. Reed, C. Zhou, C. J. Muller, T. P. Burgin, and J. M. Tour, Science **278**, 252 (1997).
[5] A. Aviram, C. Joachim, and M. Pomerantz, Chem. Phys. Lett. **146**, 490 (1988).
[6] S. Datta, W. Tian, S. Hong, R. Reifenberger, J. I. Henderson, and C. S. Kubiak, Phys. Rev. Lett. **79**, 2530 (1997).
[7] R. M. Metzger, B. Chen, U. Hopfner, M. L. Lakshmikantham, V. Vuillaume, T. Kavai, X. Wu, H. Tashibana, T. V. Hughes, H. Sakurai, J. W. Baldwin, C. Hosch, M. P. Cava, L. Brehmer, and J. L. Ashwell, J. Am. Chem. Soc. **119**, 10455 (1997).
[8] F. Willig, in *Proceedings of the Symposium on Electronic Processes in Organic Condenced Matter, August 1998*, University of Rochester, Rochester, New York.
[9] J. N. van Ruttenbeek, A. Alvarez, I. Pineyro, C. Grachman, P. Joyez, M. H. Devoret, D. Esteve, and C. Urbina, Rev. Sci. Instrum. **67**, 108 (1995).
[10] M. Buttiker, Y. Imry, R. Landauer, and S. Pinhas, Phys. Rev. B **31**, 6207 (1985).
[11] S. Datta, *Electronic Transport in Mesoscopic Systems*, Cambridge Univ. Press, Cambridge (1995), Chapt. 3.
[12] E. G. Emberly and G. Kurczenov, Phys. Rev. B **58**, 10911 (1998).

[13] D. Porath, J. Levi, M. Tarabiah, and O. Millo, Phys. Rev. B **56**, 1 (1997).
[14] E. Ya. Glushko, Fiz. Tverd. Tela (St. Petersburg) **38**, 2051 (1996) [Phys. Solid State **38**, 1132 (1996)].
[15] E. Ya. Glushko, V. N. Evteev, and M. V. Moiseenko, ''Electronics and thermodynamics of molecular circuits'' [in Russian], Preprint KrDPU (1999).
[16] Fizicheskie velichiny. Spravochnik, I. S. Grigor'ev, and E. S. Meĭlikhov (red.), Atomizdat, Moscow (1991).
[17] E. Ya. Glushko and V. A. Khrisanov, Fiz. Nizk. Temp. **23**, 1215 (1997) [Low Temp. Phys. **23**, 910 (1997)].
[18] M. Poup and Ch. Svenberg, *Electron Processes in Organic Crystals* [in Russian], Vol. 2, Mir, Moscow (1985).
[19] A. Zewail, Physics Today **33**(11), 27 (November 1980).
[20] D. V. Averin and K. K. Likharev, in *Mesoscopic Phenomena in Solids*, edited by B. L. Altshuler, P. A. Lee, and R. A. Webb, Elsevier, Amsterdam (1991).
[21] C. Joachim, J. K. Gimzewski, R. R. Schlitter, and C. Chavy, Phys. Rev. Lett. **74**, 2102 (1995).
[22] S.-B. Carlsson, T. Junno, L. Montelins, and L. Samuelson, Appl. Phys. Lett. **75**, 1461 (1999).
[23] V. N. Evteev, M. V. Moiseenko, E. V. Zhuravel, E. Ya. Glushko, and V. A. Khrisanov, in *Proceedings of the 60 Annual APS Conference on Physical Electronics, June 18–21, 1997*, Eugene, Oregon, USA.
[24] A. I. Yanson, G. R. Bollingert, H. E. Brom, N. Agraight, and J. N. van Ruitenbeek, Nature (London) **395**, 783 (1998).
[25] A. I. Yanson, I. K. Yanson, and J. N. Ruitenbeek, Nature (London) **400**, 144 (1999).
[26] J. N. van Ruitenbeek, in *Metal Clusters on Surfaces: Structure, Quantum Properties, Physical Chemistry*, edited by K.-H. Meiwes-Broer, Springer-Verlag, Berlin (1999).

Translated by Steve Torstveit

QUANTUM EFFECTS IN SEMICONDUCTORS AND DIELECTRICS

Steep nonlinearity of the the forward-biased current–voltage characteristic of a system with a double-barrier resonant-tunneling structure built into a Schottky barrier

A. N. Korol'*

Ukrainian State University of Food Technologies, ul. Vladimirskaya 68, 03033 Kiev, Ukraine

O. V. Tretyak and D. I. Sheka

Taras Shevchenko Kiev University, ul. Vladimirskaya 64, 03033 Kiev, Ukraine

(Submitted February 7, 2000; revised June 22, 2000)
Fiz. Nizk. Temp. **26**, 1144–1149 (November 2000)

A contact between a metal and an *n*-type semiconductor with a double-barrier resonant-tunneling structure built into the space-charge region is investigated. Besides the well-known effect in which the current falls sharply, there is an additional possibilty: in this system there can also be a steep nonlinearity of the current–voltage (I–V) characteristic, specifically, an effect wherein the current increases precipitously. It is shown that the differential slope of the forward branch of the I–V characteristic can be considerably greater than e/kT — by more than an order of magnitude at optimum values of the parameters of the problem. The dependence of the I–V characteristic on the parameters of the structure is analyzed. © *2000 American Institute of Physics.* [S1063-777X(00)01111-7]

The intensive development of semiconductor technologies has brought particular attention to resonant-tunneling structures (RTSs). This is because, first, RTSs can serve as a basis for various novel semiconductor devices with speeds in the terahertz range.[1,2] This speed is based on the specific properties of the resonant tunneling of electrons through the structure. As we know, the resonant tunneling effect is responsible for a sharply nonlinear (resonance) dependence of the coefficient of tunneling transmittance of a RTS on the energy of the charge carrier, and the width of the resonance level depends on the parameters of the quantum-well system and can be adjusted over a rather wide range of values. A typical RTS is a double-barrier structure consisting of two tunnel-transparent potential barriers (thickness ~ 2 nm at a barrier height ~ 1 eV), separated by a quantum well (~ 3–5 nm wide) containing localized states. Such an RTS makes it possible to operate the structure in the ballistic regime, and the lifetime of an electron in the resonance state of the quantum well is of the order of 10^{-12} s (this value is given by a calculation according to Eq. (11) of this paper, for example). These features determine the domain of applicability of RTSs as elements with negative differential resistance of the current–voltage (I–V) characteristic, energy filters, etc. It should be noted that the performance of experimentally fabricated RTSs and devices based on them is generally inferior to the theoretical predictions. One notices that the discrepancy between theory and experiment is smallest at low temperatures.[1,2]

Interesting results have been obtained with the use of RTSs in combination with other semiconductor structures. In this paper we consider a combination of two structures — a resonant tunneling structure and a Schottky barrier — that is known in the literature. Schottky barriers are often used as a convenient instrument for studying the characteristics of various physical objects, including different types of RTSs. Besides, Schottky barriers can be used for other purposes, as well. For example, in Refs. 3 and 4 it was proposed to replace the usual collector of a standard double-barrier resonant tunneling diode (DBRTD) by a Schottky layer. It was shown that this could improve the frequency characteristics of RTSs. In the case considered in the present paper, however, the presence of the Schottky barrier plays a fundamentally more important role in the electronic processes under study.

We have shown that a Schottky barrier can be a blocking barrier for the resonant tunneling current in a system consisting of a metal and a semiconductor with a double-barrier RTS placed in the space-charge region; as a result, in some cases one can observe a very strong (jumplike) increase in the total current through the structure, while in other cases a jumplike decrease is observed. In other words, besides the usual sharp drop in current that is inherent in such a structure,[3] here we call attention to the additional possibility of realizing a steep nonlinearity in its I–V characteristic. It is clear from what follows that, depending on the parameters of the problem, the indicated nonlinearity can be manifested on both the forward and reverse branches of the I–V characteristic. Thus the Schottky barrier here plays the role of a kind of regulator of the electronic processes in the structure; in particular, it influences the observed shape of the I–V curves.

In this paper we restrict consideration to the case of forward biases ($U>0$) (the reverse branch of the I–V curve has features of its own and will be treated separately).

Let us take as our resonant tunneling structure a symmetric double-barrier RTS and place it in the space-charge

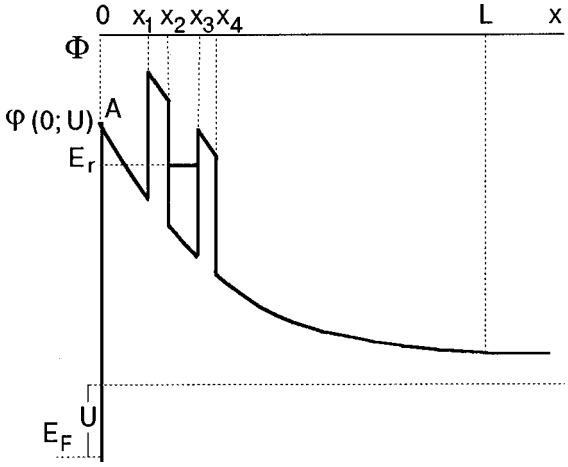

FIG. 1. Potential profile of the structure studied.

region of the Schottky contact (we shall refer to this as RTSC). The choice of a double-barrier structure is not fundamental — it is important only that the following conditions be met: the RTS chosen must have at least one resonance level, which can serve as a channel for current flow; the dimensions of the RTS must be considerably smaller that the width of the Schottky layer. The I–V characteristic of the system must depend substantially on the initial condition as to the supposed position of the resonance level E_r in relation to the top of the Schottky barrier at zero bias U; $\varphi(x=0, U=0)\equiv\varphi_0$ (Fig. 1). If $E_r-\varphi_0>0$, $U=0$, then the difference between the indicated levels increases monotonically, and the I–V characteristic has usual exponentially increasing form. A fundamentally different situation arises when $E_r-\varphi_0<0$, $U=0$. Now the resonant channel for the current flow (the resonance level of the quantum well) is initially blocked by the Schottky barrier, and the current is governed by the nonresonant tunneling of electrons and the above-barrier component of the current. As U is increased, the difference $|E_r(U)-\varphi(x=0,U)|$ decreases, and at a certain voltage $U=U_c$ a turning on of the resonant channel of current passage occurs. This turning on of the channel is accompanied by an exceedingly sharp rise of the current, and that is reflected in the shape of the I–V characteristic.

Thus there is a substantial difference in the functioning of a standard DBRTS and the system considered here. In the standard system, which is an initially (at $U=0$) symmetric structure, it is fundamentally impossible to have the conditions for resonant tunneling of the current arise only when an external voltage is applied, as is the case in a RTSC.

Let us call attention to some other differences reflected on the I–V characteristic between a standard DBRTS and the structure investigated here. First, the collector and emitter regions function somewhat differently. For example, in a standard DBRTS the collector plays the role of a reservoir capable of accepting electrons with any energies (which come from the emitter). In a RTSC the emitter (under forward bias, $U>0$) is a bulk semiconductor region, while the collector is the contact electrode, which can receive only an energy-restricted fraction of the electrons on account of the Schottky barrier.

Let us add that the main electron emission in a standard DBRTS takes place in the energy interval $[0, E_F]$, whereas in the RTSC structure electrons of high energies reach the collector, i.e., the ''working'' energy interval corresponds, in a certain comparative sense, to ''hot'' electrons.

Ultimately these differences give rise to certain features on the I–V characteristics of the structures.

It should be noted that calculating the I–V characteristic for a RTSC is a multiparameter problem. The parameters of the problem are: the thicknesses d_1 and d_3 of the left and right barriers, respectively, the width $d_2=w$ of the quantum well, the distance l between the RTS and the metal–semiconductor interface, the Schottky barrier height φ_0, the height V of the RTS barriers, the Fermi level E_F, the dopant concentration n, the temperature T, and the dielectric constant ε (10 parameters). This circumstance makes it advisable to obtain expressions for the I–V characteristic in analytical form — otherwise analysis of the I–V characteristic as a function of the many parameters would be extremely difficult. Furthermore, it turns out that detection of the effect we are looking for requires extremely precise optization of the parameters. This clearly makes a numerical computer analysis even more problematical. For these reasons we chose a modified WKB method, which can yield analytical formulas for the I–V characteristics.

We also note that the the main goal of this paper is to demonstrate the possibility of obtaining extraordinarily steep I–V characteristics in a modern semiconductor structure, and we have therefore omitted from consideration such factors as the accumulation of charge, roughness of the surface, nonparabolicity of the dispersion relation, etc., which cannot influence the effect under study in a qualitative way. We should also point out that the results obtained in this study are valid in cases when the resonant tunneling current can exceed the forward tunneling current and the above-barrier current; our comparison of these currents shows that the stated condition is well satisfied for a wide spectrum of parameters of the problem.

The current density in structures such as RTSCs is usually calculated using the formula (in atomic units)

$$j=j_0\int_0^\infty \frac{dE}{kT}D(E)\ln\frac{1+\exp[(E_F-E)/kT]}{1+\exp[(E_F-U-E)/kT]}, \tag{1}$$

$$j_0=m(kT)^2/2\pi^2, \tag{2}$$

where k is Boltzmann's constant, U is the external potential, and $D(E)$ is the transmittance, which depends on the electron energy E. In the general case it can be written in the form of a product, $D(E)=D_sD_r$, in which D_s and D_r the the coefficients of penetration of the electrons through the space-charge-region barrier and the DBRTS, respectively. A calculation of D_r by the modified WKB method[5] gives

$$D_r=[\cos h^2(\delta_1+\delta_3+\ln 4)\cos^2(\delta_2) + \cos h^2(\delta_1-\delta_3)\sin^2(\delta_2)]^{-1}, \tag{3}$$

$$\delta_i=\sqrt{2m}\int_{x_i}^{x_{i+1}}\sqrt{|E-\Phi(x)|}dx, \tag{4}$$

where the distances x_i are indicated in Fig. 1, $x_{i+1}=x_i+d_i$, $i=1,2,3$. Since ordinarily the conditions $\delta_1, \delta_3 \gg 1$ hold, we introduce the quantities D_i, $i=1,3$ (the transmittances of the left and right barriers) as

$$D_i = 0.25 \exp(-2\delta_i), \tag{5}$$

and for D_r we can write

$$D_r = \frac{4D_1D_3}{\sin^2(\delta_2-\nu)+(D_1+D_3)^2\cos^2(\delta_2-\nu)}. \tag{6}$$

This expression has sharp maxima as a function of energy E at values $E=E_n$ determined by the condition

$$\delta_2(E_n) = n\pi + \nu, \quad n = 1,2,\ldots \tag{7}$$

These maxima correspond to the resonant energy levels. The parameter ν in formula (6) depends on the shape of the potential well (and on the external field) and is determined by an exact calculation of the position of the resonance level, e.g., by the transfer matrix method,[6] with allowance for the differences in the effective masses of the electrons in the different regions of the structure.

For further analysis the coefficient D_r is conveniently written in the form of two terms, the first of which is a term of the Breit–Wigner type and the second is the result of an expansion of the remaining part in powers of $E-E_r$, i.e., in the neighborhood of the lowest resonance level $E_r \equiv E_1$:

$$D_r = D_t + D_v, \tag{8}$$

$$D_t = \frac{D_1D_3}{(D_1+D_3)^2}\frac{\Gamma^2}{(E-E_r)^2+0.25\Gamma^2}, \tag{9}$$

$$D_v = \frac{8}{3}D_1D_3\left[\frac{\sigma_2^2(E-E_r)^2+1.5(D_1+D_3)^2}{\sigma_2^2(E-E_r)^2+2(D_1+D_3)^2}+\ldots\right], \tag{10}$$

$$\Gamma = 2(D_1+D_3)/\sigma_2, \quad \sigma_2 = (0.5m)^{1/2}\int_{x_2}^{x_3}\frac{dx}{\sqrt{E_r-\Phi(x)}}. \tag{11}$$

The quantity Γ, as we see, plays the role of the half-width of the resonance level. For $E=E_r$ the coefficient D_t (9) has a sharp maximum and is thus responsible for the resonant tunneling current. The term D_v (10) is responsible for the nonresonant tunneling of electrons. (In the formulas given there is only one value of m, i.e., generally speaking, they are valid for systems with the same effective mass, e.g., systems of silicon with silicon carbide.[7] The corresponding expressions with different effective masses taken into account were obtained by the authors using a somewhat awkward method that had been proposed in Ref. 5; we can say that the refinement does not qualitatively alter the effect in question.)

In this same approximation[5] we can easily obtain the following expression for the transmittance of the upper barrier of the space-charge region with allowance for the effects of the image forces:

$$D_s = \left\{1+\exp\left[\frac{1.76(\overline{\varphi}-E)}{\gamma}\right]\right\}^{-1}, \tag{12}$$

$$\overline{\varphi} = \varphi(0)-(2\beta^2)^{-1}, \quad \beta = \left[\frac{\varepsilon}{4F(0)}\right]^{1/4},$$

$$\gamma = 0.5\varepsilon m^{1/2}\beta^{-3}, \tag{13}$$

where $F(0) = -d\varphi/dx|_{x=0}$ is the field of the space-charge region, and γ is the half-width of the derivative of the function $D_s(E)$ and is introduced for convenience in comparing the coefficients D_s and D_t. Thus the integrand in (1) includes the product of two rapidly varying functions: a δ-like function $D_t(E-E_r)$ (9) with a half-width Γ (11) and a θ-like function $D_s(\overline{\varphi}-E)$ (12) with a half-width of its derivative equal to γ (13), and also a function related to the electron energy distribution and which is smooth for $\Gamma, \gamma \ll kT$.

It is therefore clear that the result of the integration in (1) is a current with a jumplike dependence on the voltage, and the region of the jumplike change in $j(U)$ corresponds to values of the voltage at which the quantity $(\overline{\varphi}-E_r)$ changes sign.

To calculate the current it is also necessary to determine the quantity $\Phi(x)$ that appears in the formulas given; it is a sum of two terms: the potential $\varphi(x)$ of the space-charge region, and the potential of the DBRTS. The first potential is the solution of the equation

$$\nabla^2\varphi = -\frac{4\pi}{\varepsilon}\rho(x),$$

$$\rho = \begin{cases} n, & 0<x<x_1, \quad x_4<x<L \\ 0, & x_1<x<x_4, \quad x>L \end{cases} \tag{14}$$

with the boundary conditions $\varphi(0,U) = \varphi_0 + U$, $\varphi(L) = 0$, where L is the width of the Schottky layer. This solution has the form

$$\varphi(x) = \varphi_L + \frac{1}{2}\lambda n(x_4-x_1)(2x-x_4-x_1),$$

$$0<x<x_1, \tag{15}$$

$$\varphi(x) = \varphi_L - \frac{1}{2}\lambda n(x-x_4)^2, \quad x_1<x<x_4,$$

$$\varphi(x) = \varphi_L = \frac{1}{2}\lambda n(x-L)^2, \quad x_4<x<L,$$

$$L^2 = \frac{2\varphi(0)}{\lambda n}+(x_4^2-x_1^2), \quad \lambda = \frac{4\pi}{\varepsilon}. \tag{16}$$

The double-barrier resonant tunneling structure is located in the interval $x_1<x<x_4$, and the height of its potential barriers is V. In this interval the field of the space-charge region is given by

$$F = -\lambda n(L-x_4). \tag{17}$$

Once the potential $\Phi(x)$ is specified, one can find σ_2 and, hence, the half-widths Γ and γ.

Now all of the expressions needed for calculating the current density have been determined. Depending on the relative sizes of Γ and γ, we obtain two formulas for the I–V characteristic: for $\Gamma \gg \gamma$

$$j \simeq j_0 2\pi\frac{\Gamma}{kT}\frac{D_1D_3}{(D_1+D_3)^2}D_s(E_r)\exp\left(\frac{E_F-E_r}{kT}\right); \tag{18}$$

and for $\Gamma \ll \gamma$

$$j \simeq j_0 2\frac{\Gamma}{kT}\frac{D_1D_3}{(D_1+D_3)^2}\exp\left(\frac{E_F-E_r}{kT}\right)\left[\frac{\pi}{2}-\arctan\frac{2(\overline{\varphi}-E_r)}{\Gamma}\right]. \tag{19}$$

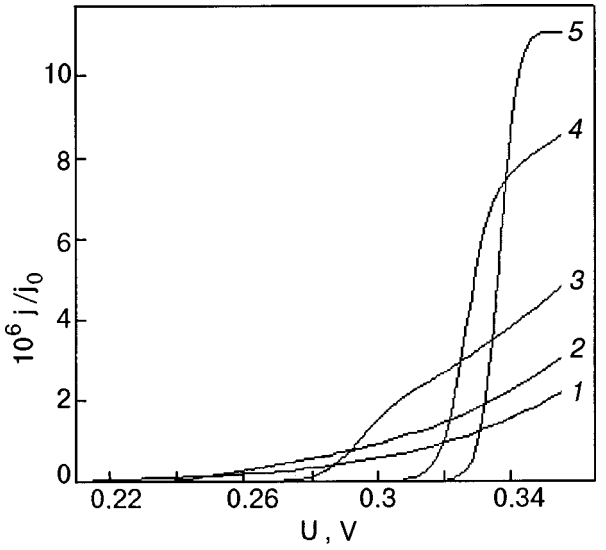

FIG. 2. Forward branch of the I–V characteristic for different values of l [Å]: 120 (*1*), 150 (*2*), 200 (*3*), 290 (*4*), and 380 (*5*); the values of the remaining parameters are given in the text; the energy position of the resonant level $E_r = 0.107$ eV.[3]

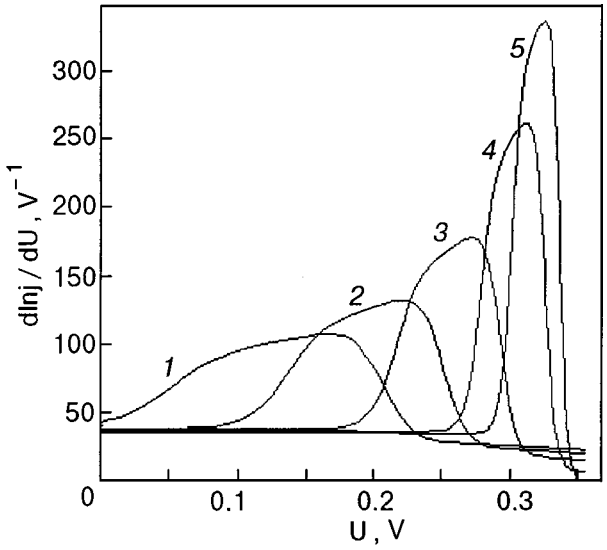

FIG. 3. Dependence of $\alpha = d \ln j/dU$ on the voltage; the parameters of the structure have the same values as for Fig. 2.

Thus we have obtained simple expressions for the current through the resonant tunneling structure under study, in a form convenient for further analysis.

Let us discuss the case $\gamma \gg \Gamma$, which is often encountered in practice. Figure 2 shows the voltage dependence of the current density calculated according to formula (19); the current density is normalized to j_0. The calculation was done for the following set of parameters: $T = 300$ K, $d_1 = d_3 = 20$ Å, $\omega = 50$ Å, $m(\mathrm{GaAs}) = 0.067 m_0$, $m(\mathrm{AlGaAs}) = 0.1 m_0$, $\varphi_0 = 0.44$ eV, and $n = 10^{17}$ cm^{-3}. Figure 3 shows the voltage dependence of the parameter $\alpha = d \ln j/dU$, which is often used to describe the I–V characteristic. The parameter values for Fig. 3 are the same as in Fig. 2.

The plotted functions completely confirm the assumptions made in this paper as to the character of the I–V curves. At voltages less than U_c the currents in the investigated RTSC structure are relatively small. Then, in the vicinity of $U = U_c$ there is a precipitous rise in the current. For example, for curve *5* the current increases by approximately a factor of 10 in response to a voltage change of 0.01 V. One is also struck by the large values of the parameter α describing the differential steepness of the I–V characteristic — they are much greater than the value e/kT typical for Schottky barriers. The values of U_c and α depend on many parameters of the structure: the height of the Schottky barrier, the dopant concentration, the distance from the DBRTS to the metal, the geometric parameters of the DBRTS, etc. For example, as the DBRTS is brought closer to the metal (with the other parameters fixed), the value of U_c decreases; e.g., the values of U_c for distances $l = 380$ Å and $l = 200$ Å (Fig. 2) differ by 0.05 V.

To explain the substantial growth of the current as the distance l from the metal to the DBRTS is increased, it is convenient to refer to Fig. 1. We see that at large l the opening of the channel for the resonant tunneling current (resonant energy E_r) occurs at a higher voltage $U = U_c$, which corresponds to a lower barrier height $\varphi\ (x = 0, U_c)$. Consequently, the distribution function makes for higher currents in this case.

Finally, we should say a few words about the possible advantages of the system investigated here from the standpoint of practical applications. We note first that it retains the advantage that motivated the proposal made in Ref. 3 to replace the conventional collector of the standard resonant-tunneling diode by a Schottky collector, namely: the possibility of reducing the emitter–collector capacitance. Here increasing the distance between the metal and the DBRTS leads not only to a decrease in capacitance but also to a simultaneous increase in the steepness of the I–V characteristic (see Figs. 2 and 3).

In addition, it should be noted that devices using the I–V characteristics given above (e.g., switches, rectifiers, amplifiers, etc.) can have good characteristics not only at low temperatures but even at room temperatures (the curves in Figs. 2 and 3 were calculated for $T = 300$ K).

*E-mail: korolam@usuft.kiev.ua

[1] Yu. Pozhela, *Physics of Fast Transistors* [in Russian], Mokslas, Vilnius (1989).
[2] I. N. Dolmanov, V. I. Tolstikhin, and V. G. Elenskiĭ, Zarubezhnaya Radioélektronika, No. 7, 66 (1990).
[3] Y. Konishi, S. T. Allen, M. Reddy, S. C. Martin, J. Liu, R. E. Muller, and M. J. Rodwell, Solid–State Electron. **36**, 1673 (1993).
[4] R. P. Smith, S. T. Allen, M. Reddy *et al.*, IEEE Electron Device Lett. **15**, 295 (1994).
[5] V. N. Dobrovolsky, D. I. Sheka, and B. V. Chernyachuk, Surf. Sci. **397**, 333 (1998).
[6] A. Ya. Azbel, Phys. Rev. B **28**, 4106 (1983).
[7] I. Pereira, M. P. Carreño, R. A. Onmori, D. R. T. Santos, and F. T. Gabriel, J. Non-Cryst. Solids **97–98**, 871 (1987).

Translated by Steve Torstveit

Static dielectric permittivity in gapless solid solutions $Hg_{1-x}Cd_xTe$

V. D. Prozorovskiĭ, I. Yu. Reshidova, and A. I. Puzynya

*A. A. Galkin Donetsk Physico-Technical Institute, National Academy of Sciences of Ukraine, ul. R. Lyuksemburg 72, 83114 Donetsk, Ukraine**

(Submitted February 25, 2000; revised May 31, 2000)
Fiz. Nizk. Temp. **26**, 1150–1154 (November 2000)

Results are presented from a comprehensive study of helicon interferometry, nonresonant cyclotron absorption, and the Shubnikov–de Haas effect at microwave frequencies in the compound HgTe and in $Hg_{1-x}Cd_xTe$ solid solutions. Analysis of the experimental results and the already existing theoretical concepts suggests that in the gapless semiconductor HgTe and its solid solutions the static dielectric permittivity ε_s depends on the concentration of conduction electrons and the band parameters. Anomalous behavior of $\varepsilon_s(x)$ is observed in the concentration interval $0.155 \leqslant x \leqslant 0.2$ and is attributed to a change in the structure of the edges of the conduction and valence bands in $Hg_{1-x}Cd_xTe$. © *2000 American Institute of Physics.* [S1063-777X(00)01211-1]

The compound HgTe and its solid solutions with cadmium telluride, $Hg_{1-x}Cd_xTe$, at a certain concentration x belong to the class of gapless semiconductors, since the bottom of the conduction band in them touches the top of the valence band.[1] A zero energy gap between these bands, which belong to the same representation Γ_8, makes for a dependence of the static dielectric permittivity ε on the wave vector $\mathbf{q}$ of the form[2]

$$\varepsilon(q)=\varepsilon_L+\frac{3\pi^2e^2m_n}{2\hbar^2q}, \tag{1}$$

where e is the charge of an electron, m_n is the mass of the electrons at the bottom of the conduction band, and ε_L is the contribution to the dielectric permittivity from all the bands other than Γ_8. The singularity in (1) for $\mathbf{q}\to 0$ is due to the anomalously high polarizability of the electron–hole vacuum. In the absence of conduction electrons this singularity leads to effective screening of the charge of the valence electrons on account of virtual transitions between the osculating valence and conduction bands. When the electrons go on to the conduction band from the donors or from the valence band, the singularity in (1) is suppressed, and the electron gas becomes degenerate.[1] Then, as a consequence of the Moss–Burstein effect, virtual transitions are possible only at energies $E \geqslant E_F$, where E_F is the Fermi energy. Therefore, in an impure gapless semiconductor the static dielectric permittivity ε_s has a finite value and grows with decreasing electron concentration according to the law:[3]

$$\varepsilon_s=\varepsilon_L+\frac{8e^2m_n}{\pi\hbar^2k_F}, \tag{2}$$

where the wave vector k_F corresponding to the Fermi energy is related to the electron concentration N in the usual way: $k_F^3=3\pi^2N$. This dependence leads to a weakening of the Coulomb interaction at large distances, and this is manifested, in particular, in a decrease in the bound-state energy[1] and in the scattering cross section at a Coulomb center.[4] It follows that the value of the static dielectric permittivity ε_s plays a role of some importance in the physics of gapless semiconductors. However, until now there have been no direct experimental studies of ε_s. We have therefore measured ε_s at liquid-helium temperature in HgTe samples with different concentrations N of free charge carriers and in samples of the solid solutions $Hg_{1-x}Cd_xTe$ with different mole fractions x of cadmium telluride. The most careful measurements of ε_s were made in the region of the zero-gap state of $Hg_{1-x}Cd_xTe$.

EXPERIMENT

To establish the relation between ε_s and N in single-crystal samples of n-type $Hg_{1-x}Cd_xTe$ with different values of x, it is necessary to determine N and the cyclotron effective mass m_c experimentally. This can be done by the methods of helicon interferometry, nonresonant cyclotron absorption (NCA),[5] and the Shubnikov–de Haas (SdH) effect at microwave frequencies.[6]

A study of the derivative of the reflection coefficient with respect to magnetic field, dR/dH, was done on a radio spectrometer having a design permitting measurements in the Faraday and Voigt configurations, respectively, with circular and linear polarizations of the microwave field in the resonant cavity. The coupling of the cavity with the sample was effected through an aperture in a diaphragm placed in front of the aperture coupling the cavity with the waveguide. As necessary a sample of a certain size could be placed in the cavity at an antinode of the microwave electric or magnetic field. Replaceable cylindrical cavities of the absorbing type for the TE_{112} mode, tuned to the frequencies $f_1=36.04$ GHz and $f_2=26.1$ GHz, were used. Changing from operation of the radio spectrometer in the Faraday configuration to operation in the Voigt configuration was done by rotating the electromagnet by 90°. The field H of the electromagnet was measured by a nuclear magnetometer and could be varied in the interval 0–16 kOe. The temperature of the sample during the studies was monitored to an accuracy of ± 0.05 K and stabilized to a precision of ± 0.02 K by means of a special apparatus.[7]

TABLE I. Physical parameters of the $Hg_{1-x}Cd_xTe$ samples.

№	x	ε_s, exp.	ε_s, calc.	N, 10^{15} cm^{-3}	m_c/m_0
1	0	115	70.3	0.80	0.0300
2	0	85	63.4	1.24	0.0300
3*	0	65	53.1	2.77	0.0300
4	0	47	40.1	13.00	0.0310
5	0	44	38.5	18.00	0.0320
6	0	33	28.0	200.00	0.0360
7	0.050	85	50.2	0.80	0.0181
8	0.110	87	51.0	0.08	0.0090
9*	0.110	60	33.5	0.65	0.0093
10	0.110	38	27.2	3.20	0.0096
11	0.110	27	22.0	20.00	0.0110
12*	0.140	50	23.3	0.65	0.0040
13*	0.150	47	21.1	0.58	0.0036
14	0.155	45	18.2	0.70	0.0032
15	0.160	45	18.1	0.80	0.0033
16	0.167	45	18.0	0.75	0.0032
17	0.175	45	17.9	0.80	0.0033
18	0.180	40	17.8	0.83	0.0037
19	0.200	21	17.6	0.83	0.0050
20	0.250	18	16.9	0.80	0.0172

Note: The asterisk indicates samples on which the Shubnikov–de Haas effect was observed.

The samples studied were in the form of disks 5–6 mm in diameter and 0.8–1.5 mm thick; their surfaces were mechanically polished and then immediately prior to the experiment were chemically polished in a 5% solution of bromine in methanol. The composition and uniformity of the samples were determined by means of a microanalyzer. The data for the samples studied are presented in Table I.

Measurements on sample No. 3 at 4.2 K in the Faraday configuration showed that for the extraordinary wave[1)] the curve dR/dH is an oscillatory function of the magnetic field (Fig. 1). The extrema of this curve are shifted to lower magnetic fields as the thickness of the sample is decreased; this is evidence that we are observing Fabry–Perot size resonances in this case. The position of the peak observed in a low magnetic field $H_1 \approx 460$ Oe does not depend on the thickness of the sample. When the direction of the external magnetic field is changed to the opposite, the extrema were not observed on the dR/dH curve. In the Voigt configuration the

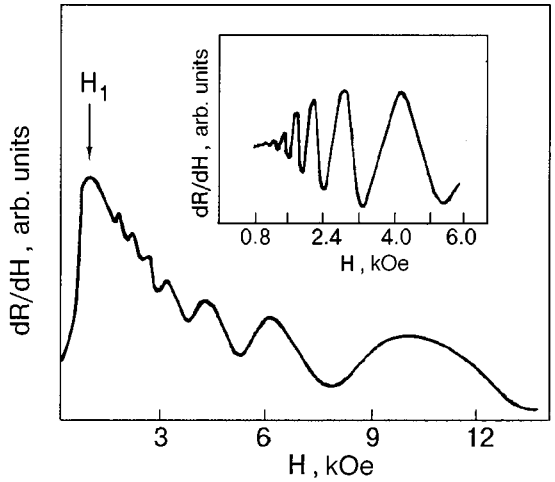

FIG. 1. Oscillations of the derivative of the reflection coefficient with respect to the magnetic field in sample No. 3, recorded in the Faraday and Voigt (inset) configurations at 4.2 K.

dR/dH curve is also oscillatory (inset in Fig. 1), and its extrema in the magnetic fields do not coincide with the extrema observed on the dR/dH curve in the Faraday configuration. The positions of these extrema in the magnetic field also remained unchanged as the sample thickness and the working frequency of the radio spectrometer were changed. In addition, analysis of the curve showed that the reflection coefficient is an oscillatory function of the magnetic field, with a period of $1/H$.

On the basis of the experimental data and in accordance with the theoretical ideas about the propagation of magnetoplasma waves in cold solid-state plasma,[8] we can state unequivocally that: 1) the peak observed on the dR/dH curve at a low magnetic field H_1 corresponds to the nonresonant cyclotron absorption (NCA), which is due to conduction electrons; 2) the oscillations of the dR/dH curve in the Faraday configuration are due to the propagation of a helicon wave in the sample and correspond to Fabry–Perot resonances; 3) the oscillations of dR/dH in the Voigt configura-

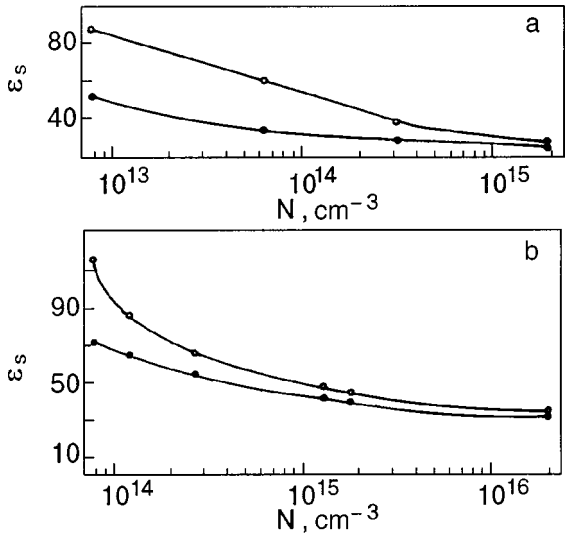

FIG. 2. Dependence of the static dielectric permittivity on the concentration of conduction electrons in samples of $Hg_{0.89}Cd_{0.11}Te$ (a) and HgTe (b). ○ — experiment, ● — calculation.

tion are due to the microwave SdH effect. The observation of quantum oscillations in this experiment is possible when the Fermi level is fixed at an acceptor level for this material.[1,6]

Thus, using our technique,[5] we determine ε_s, N, and m_c from the dR/dH curve, the oscillations of which correspond to Fabry–Perot resonances and are due to a change in the effective dielectric permittivity of the sample, $\varepsilon_{\text{eff}}=\varepsilon_s-[\omega_p^2/\omega(\omega\pm\omega_c-j/\tau)]$, with changing external magnetic field, where $\omega_p=4\pi e^2N/m_c$, $\omega_c=eH/m_cc$, c is the speed of light, ω is the working angular frequency of the radio spectrometer, $j=\sqrt{-1}$, and τ is the momentum relaxation time of the conduction electrons.

The reliability of the results obtained was confirmed by the fact that the values of N determined from the quantum oscillations observed in the Voigt configuration[6] agree within the experimental error limits with the values obtained by helicon interferometry.

The calculated values of ε_s were determined from the expression

$$\varepsilon_s=\varepsilon_L+\frac{8e^2}{\pi}\left[\frac{m_c}{\hbar^2(3\pi^2N)^{1/3}}-\frac{(3\pi^2N)^{1/3}}{E_g}\right], \tag{3}$$

which was obtained from relation (2) by substituting into it the expressions for k_F and m_n in the form:[1]

$$m_n=\frac{m_c}{1+2E/|E_g|}, \quad \text{where} \quad E=E_F=\frac{\hbar^2(3\pi^2N)^{2/3}}{2m_n}.$$

Here E_g is the width of the band gap, which was not determined experimentally but was calculated according to Ref. 1 as follows:

$$E_g(x,T)=-0.302+1.93x+5.35\times10^{-4}T(1-2x) \\ -0.81x^2+0.832x^3 \tag{4}$$

(all of the terms in formula (4) are given in electron-volts). In addition, ε_L was calculated by the formula[9]

$$\varepsilon_L=20.5-15.6x+5.7x^2. \tag{5}$$

The parameters of the samples necessary for finding and comparing the experimental and theoretical values of ε_s at different values of N and x were determined on the basis of the existing theoretical ideas and experimental data. The values of these parameters are given in Table I.

DISCUSSION AND CONCLUSIONS

The calculated and experimental curves of $\varepsilon_s(N)$ for HgTe and $Hg_{0.98}Cd_{0.11}Te$ are presented in Fig. 2. It is seen that the function $\varepsilon_s(N)$ is of the same character, i.e., $\varepsilon_s(N)$ decreases with increasing N in both cases, but there are quantitative differences. As we see from Fig. 2, the disagreement becomes large as N decreases. We attribute the quantitative difference in the calculated and experimental values of $\varepsilon_s(N)$ to the fact that expression (2) is of an extremely approximate nature and reflects only the qualitative variation without any claim to quantitative accuracy.[4]

Figure 3 shows the dependence of ε_s on the mole fraction of CdTe in $Hg_{1-x}Cd_xTe$. The concentration of conduction electrons in the samples in this case varied over the range $(5.8–8)\times10^{14}$ cm^{-3}. As we see from the figure, the experimental curve of $\varepsilon_s(x)$ in the interval $0<x<0.158$ has

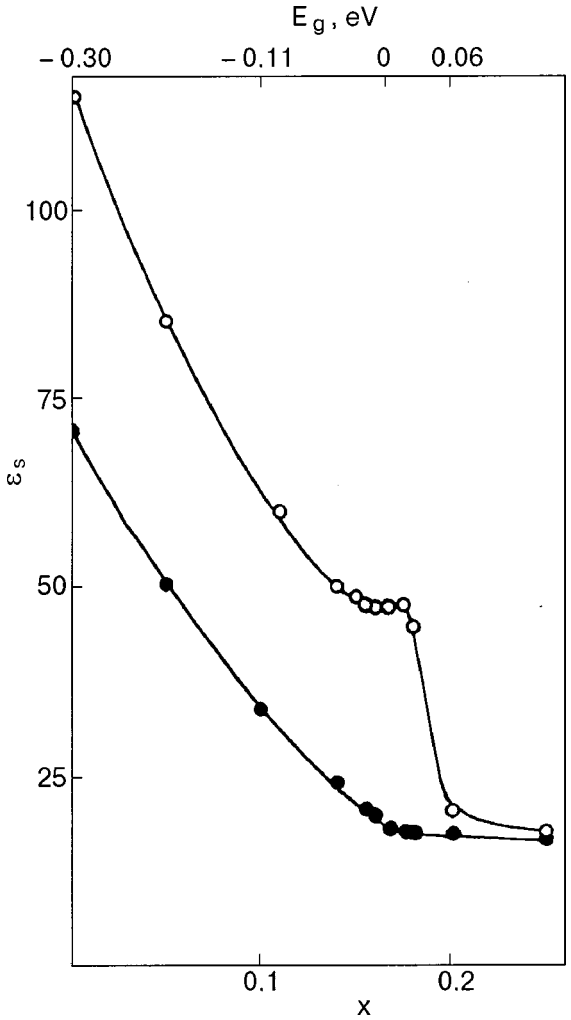

FIG. 3. Static dielectric permittivity in $Hg_{1-x}Cd_xTe$ as a function of the CdTe mole fraction at 4.2 K. ○ — experiment, ● — calculation.

the same character as the calculated curve. In the interval $0.158\leqslant x\leqslant0.178$ the experimental curve $\varepsilon_s(x)=\text{const}$. Then, for $x>0.178$ the experimental value of $\varepsilon_s(x)$ decreases sharply and approaches the calculated value, which is independent of N. The calculation of $\varepsilon_s(x)$ in the interval $0\leqslant x\leqslant0.16$ was done with the use of expressions (3)–(5), while for $x>0.16$ it was done using (5), since in that case, according to Refs. 1 and 4, ε_s is independent of N as $|E_g|\to0$. The fact that the calculated and experimental values of ε_s for $x\geqslant0.2$ are close is evidence that the static dielectric permittivity depends on the concentration of conduction electrons only in gapless semiconductors, and it confirms the reliability of our experimental data.

We attribute the difference in the character of the variation of the calculated and experimental curves of $\varepsilon_s(x)$ in the interval $0.155\leqslant x\leqslant0.2$ (corresponding to -17.6 meV$\leqslant E_g\leqslant59.6$ meV) to the change in the structure of the edges of the conduction and valence bands which, according to Refs. 10–12, occurs in solid solutions based on HgTe at values $E_g\approx\pm20$ meV. Those papers give evidence that at these values of E_g an inversion of the Γ_6 and Γ_8 bands occurs. This means that the equality $E_g=0$ does not hold in these solid solutions. Then, as a result of anomalous behavior of the structure of the edges of the Γ_6 and Γ_8 band as a function

of the value of E_g, an anomalous change of $\varepsilon_s(x)$ occurs at these values of E_g.

Thus it follows from what we have said that in gapless solid solutions $Hg_{1-x}Cd_xTe$ the static dielectric permittivity depends on the band parameters and on the concentration of free charge carriers, and the character of this dependence agrees with the theoretical predictions except in a region of values of E_g for which the structure of the edges of the conduction and valence band is disrupted.

*E-mail: prohorov@pr.fti.ac.donetsk.ua

[1)]The extraordinary wave in the Faraday configuration (**k**‖**H**) is the wave whose polarization direction corresponds to the direction of the cyclotron rotation of the free charge carriers.

[1] I. M. Tsidil'kovskiĭ, G. I. Kharus, and N. G. Shelushinina, *Impurity States and Transfer Phenomena in Gapless Semiconductors* [in Russian], UNTs AN SSSR, Sverdlovsk (1987).
[2] L. Liu and D. Brust, Phys. Rev. **173**, 777 (1968).
[3] L. Liu and E. Tosatti, Phys. Rev. Lett. **23**, 772 (1969).
[4] B. L. Gel'mont, V. I. Ivanov-Omskiĭ, and B. T. Kolomiets *et al.*, Fiz. Tekh. Poluprovodn. **5**, 266 (1971) [Sov. Phys. Semicond. **5**, 228 (1971)].
[5] V. D. Prozorovskiĭ and V. I. Ocheret'ko, Zh. Tekh. Phys. **60**(2), 192 (1990) [Sov. Phys. Tech. Phys. **35**, 253 (1990)].
[6] V. D. Prozorovskiĭ, I. Yu. Reshidova, S. Yu. Paranchich, and L. D. Paranchich, Fiz. Tverd. Tela (Leningrad) **32**, 3290 (1990) [Sov. Phys. Solid State **32**, 1904 (1990)].
[7] V. D. Prozorovskiĭ and Yu. M. Nikolaenko, Inventor's Certificate (USSR) No. 1319000; publ. Byull. Izobret., No. 23 (1987).
[8] J. D. Wiley, P. S. Peersy, and R. N. Dexter, Phys. Rev. **181**, 1173 (1969).
[9] A. V. Lyubchenko, E. A. Sal'kov, and F. F. Sizov, *Physical Principles of Semiconductor Infared Electronics* [in Russian], Naukova Dumka, Kiev (1984).
[10] E. A. Pashitskiĭ, Yu. A. Bratashevskiĭ, V. D. Prozorovskiĭ, and Yu. M. Nikolaenko, Fiz. Tverd. Tela (Leningrad) **29**, 3586 (1987) [Sov. Phys. Solid State **29**, 2055 (1987)].
[11] V. D. Prozorovskiĭ and I. Yu. Reshidova, Fiz. Tekh. Vys. Davlen. **2**, 66 (1992).
[12] V. D. Prozorovskiĭ and I. Yu. Reshidova, Fiz. Nizk. Temp. **25**, 1035 (1999) [Low Temp. Phys. **25**, 772 (1999)].

Translated by Steve Torstveit

Analog of the Grüneisen parameter for orientational excitations in the low-temperature phase of fullerite C_{60}

V. D. Natsik* and A. V. Podol'skiĭ

B. Verkin Institute for Low Temperature Physics and Engineering, National Academy of Sciences of Ukraine, pr. Lenina 47, 61164 Kharkov, Ukraine

(Submitted July 4, 2000; revised July 25, 2000)
Fiz. Nizk. Temp. **26**, 1155–1161 (November 2000)

A theoretical analysis of the heat capacity and thermal expansion of the low-temperature sc phase of fullerite C_{60} is made, based on the concepts of double-well orientational states of the molecules — the pentagonal and hexagonal configurations. To describe the coupling of the orientational states of the molecules with macroscopic deformations of the crystal lattice, it is assumed that the deformations contribute corrections to the energy parameters of the double-well states, and a parameter $g^{(\mathrm{or})}$ is introduced which is equivalent to the Grüneisen parameter in the theory of the thermal expansion of harmonic crystals. It is shown that this model can be used to obtain a qualitative description of the anomalies observed in the thermal properties of fullerite C_{60} near the orientational glass temperature $T_g \simeq 90$ K, and the possibilities for obtaining empirical estimates of the parameter $g^{(\mathrm{or})}$ are discussed.
 [S1063-777X(00)01311-6]

INTRODUCTION

It is known[1] that the contribution of lattice vibrations to the thermal properties of crystalline solids in the region of low temperatures and medium homologous temperatures can be described quite well by analyzing the thermal excitations of phonons in the harmonic approximation. In the case of molecular crystals a significant role can also be played by collective orientational vibrations (librons) and harmonic intramolecular modes. This approximation is also effective for describing the thermal expansion of crystals, which is by nature anharmonic. In that case, following the ideas of Mie[2] and Grüneisen,[3] it is sufficient to assume the existence of a linear dependence of the harmonic oscillation frequency ω_s on the components of the lattice strain tensor ε_{ik}. For crystals of the cubic system this dependence is conveniently written in the form $\omega_s^{(\varepsilon)} = \omega_s^{(0)}(1 - g_s \varepsilon_{ii})$, where $\omega_s^{(0)}$ and $\omega_s^{(\varepsilon)}$ are the eigenfrequencies of the harmonic oscillations of the undeformed and deformed crystal, respectively, $\varepsilon_{ii} = \varepsilon_{11} + \varepsilon_{22} + \varepsilon_{33}$ is the dilatation component of the strain, and g_s is a constant that has come to be called the Grüneisen parameter for the vibrational mode of index s. In those cases when the thermal motion of the crystal is determined by the excitation of oscillations of a single type with identical values $g_s = g$, the Grüneisen parameter is connected by simple thermodynamic relations with the temperature coefficient of volume expansion κ, the isothermal compressive bulk modulus $B^{(0)}$, and the heat capacity per unit volume measured at constant volume, C_V:

$$g = \frac{B^{(0)}\kappa}{C_V}. \tag{1}$$

In solid-state physics the Grüneisen parameter is regarded as be one of the most important characteristics of anharmonicity of crystal lattices. Since for most crystals the values of C_V, $B^{(0)}$, and κ can be independently measured by direct physical methods, one can use the thermodynamic relation (1) as an empirical check on the correctness of the Mie–Grüneisen approach to the description of the thermal expansion of a given crystal in a given temperature interval. The empirical value of the right-hand side of relation (1) is called the thermodynamic Grüneisen parameter of the crystal. The simplest criterion of correctness of the Mie–Grüneisen approximation is the absence of temperature dependence (or a sufficiently weak temperature dependence) of the thermodynamic Grüneisen parameter determined by relation (1). If the empirical values of the right-hand side of (1) have pronounced temperature anomalies, that would be evidence that an important role in the thermal motion of the crystal is being played by several different types of harmonic excitations with different values of g_s or by nonlinear excitations which are strongly coupled to the macroscopic deformations of the crystal lattice. An example are the anomalies detected near the critical temperatures of lattice phase transitions. These anomalies are the result of a loss of mechanical stability for a certain fraction of the collective vibrational degrees of freedom and the appearance of strong anharmonicity in the motion of the crystal with respect to these degrees of freedom.

In the experimental study of the thermal properties of the molecular crystal fullerite C_{60} in the low-temperature region, three pronounced anomalies of the thermodynamic Grüneisen parameter have been observed.[4–9] The first of these is observed near the phase transition from the high-temperature fcc phase to the low-temperature sc phase ($T_c = 260$ K), at which a partial orientational ordering of the C_{60} molecules occurs. The second anomaly is observed near the orientational glass temperature $T_g \simeq 90$ K and is due to the specifics of the thermally activated transitions between two orientational states of the molecules — the so-called pentagonal (p) and hexagonal (h) configurations. Finally, another anomaly is observed at liquid-helium temperatures; it is apparently

due to quantum effects in the anharmonic rotational motion of the molecules, although other mechanisms are possible.[10]

All of these low-temperature anomalies of the thermodynamic Grüneisen parameter of crystalline fullerite C_{60} are consequences of two main circumstances:

— the influence of the rotational degrees of freedom of the molecules on the thermodynamic characteristics of this crystal is rather large;

— the anharmonicity of the rotational motion of the molecules is extremely strong, and this has a substantial effect on the character of the thermal excitation of the rotational degrees of freedom at both moderately low and very low temperatures.

This means that in the analysis of the thermal expansion of fullerite C_{60} the Mie–Grüneisen approximation can be used only for describing the phonon contribution, while treating the influence of the lattice deformation on the thermal excitation of the rotational degrees of freedom will require developing some other approaches.

In this paper we carry out a semimicroscopic analysis of the anomaly observed in the thermal expansion of fullerite C_{60} near the orientational glass temperature T_g and which is due to the influence of the lattice deformations on the thermal excitation of the hexagonal configurations of the molecules. General thermodynamic relations linking the thermodynamic and rheological characteristics of fullerite with the concentration and parameters of the orientational excitations have been obtained by the authors in a previous paper.[11] Here we analyze in more detail the temperature dependence of the coefficient of thermal expansion of fullerite at temperatures near T_g and discuss the possibilities for obtaining empirical estimates of the lattice–orientation interaction parameter (an analog of the Grüneisen parameter).

1. CONTRIBUTION OF THE ORIENTATIONAL EXCITATIONS TO THE THERMODYNAMIC CHARACTERISTICS OF FULLERITE

Let us consider the sc phase of fullerite, which exists at temperatures $T<T_c$. In this phase the threefold symmetry axes of the C_{60} molecule are oriented along the space diagonals of the unit cube (directions of the $\langle 111\rangle$ type), but the molecules can execute relative rotations about these axes to large angles. These rotations are braked by the comparatively low potential barriers due to the noncentral part of the potentials of the intramolecular pair interaction. In the rotation of the molecules, two types of minima of the angle dependence of the intermolecular interaction energy are realized: global (the p configuration) and local (the h configuration). The pentagonal and hexagonal configurations are separated by an energy barrier: if the symbol U_p denotes the barrier for the $p\to h$ transition, then the barrier for the reverse transition $h\to p$ will have a value $U_h=U_p-\Delta$, where the symbol Δ denotes the difference of the energies of the p and h configurations.

Thus we single out a set of independent double-well states from the set of orientational states of the fullerite molecules. We denote by N_p and N_h the volume concentrations of pentagonal and hexagonal configurations, and by $N_0=N_p+N_h$ the volume concentration of the double-well configurations. Strictly speaking, at the present time there are only phenomenological ideas about the orientational states of the molecules in fullerite. It is clear that both librations of the molecules and their relative rotations by large angles must have a cooperative character, but there is no microscopic justification for the possibility of separating out the double-well states in the description of the collective dynamics of the molecules. For this reason the microscopic meaning of the quantities N_0, U_p, U_h, and Δ remain unclear, and they should be regarded as phenomenological parameters of the theory subject to experimental determination. On general grounds one can conclude only that if a is the length of the edge of the unit cell, then $4\leqslant N_0a^3\leqslant 24$: the left-hand side of this inequality corresponds to the number of molecules, and the right-hand side to the number of intermolecular bonds in the unit cell of the fcc structure.

In a state of thermodynamic equilibrium at temperature T the concentrations of the p and h configurations are described by the Boltzmann distribution and the balance relation:

$$\overline{n}_h=\frac{\overline{N}_h}{N_0}=\left(1+\exp\frac{\Delta}{kT}\right)^{-1},\quad \overline{n}_p=\frac{\overline{N}_p}{N_0}=1-\overline{n}_h, \tag{2}$$

where a bar over a symbol denotes the equilibrium state. One can also introduce average time for the thermally activated destruction of the p and h configurations, $\tau_{p,h}$, which are given by an activational formula of the form

$$\tau_{p,h}=\tau_0\exp\frac{U_{p,h}}{kT}, \tag{3}$$

where τ_0 is the characteristic period of the librations of the molecules, which should be regarded as yet another phenomenological parameter of the theory. Then time dependence of the nonequilibrium concentration of defect h configurations $n_h(t)$ (orientational relaxation) is described by the simple kinetic equation

$$\tau\frac{\partial}{\partial t}n_h+n_h=\frac{\tau}{\tau_p},\quad \tau=\frac{\tau_p\tau_h}{\tau_p+\tau_h}. \tag{4}$$

Here $\tau(T)$ plays the role of the average time for relaxation to the thermodynamic equilibrium distribution of the p and h configurations in the bulk of the fullerite crystal at a given temperature. If a certain laboratory time $t_{\rm lab}$ is specified, then one can introduce an orientational glass temperature T_g by defining it as a solution of the equation

$$\tau(T)=t_{\rm lab}. \tag{5}$$

For $T>T_g$ the thermally activated transitions between the p and h configurations occur relatively rapidly on the laboratory time scale, and the state of the fullerite can be regarded as a sort of orientational liquid; for $T<T_g$ there is insufficient time for thermodynamic equilibrium to be established in the double-well orientational states over standard laboratory times, and the the fullerite on cooling will enter an orientational glass state. Experiment shows that for $t_{\rm lab}\sim 10^4$ s the temperature $T_g\simeq 90$ K.[12]

The influence of orientational relaxation of the molecules on the thermal expansion of fullerite can be described in analogy with the Mie–Grüneisen approach: for this it is

necessary to introduce deformation corrections to the parameters of the double-well orientational states U_p, U_h, and Δ:[11]

$$U_{p,h}^{(\varepsilon)}=U_{p,h}-v_{p,h}\varepsilon_{ll}, \quad \Delta^{(\varepsilon)}=\Delta-v_\Delta\varepsilon_{ll}. \tag{6}$$

Here v_p, v_h and $v_\Delta=v_p-v_h$ are the constants of the deformation potential. Using the experimental results on the influence of hydrostatic pressure on the orientational glass transition of fullerite, one can obtain an empirical estimate for the values of the parameters v_p and v_h: $v_p\simeq v_h\simeq 2.0$ eV (with a relative accuracy of $\sim 10\%$).[11]

Relations (2) and (6) serve as the basis of a microscopic (or, more precisely, semimicroscopic) description of the contribution of the orientational excitations to the thermal characteristics of fullerite. Let us now turn to a description of this contribution in the framework of phenomenological thermodynamics. For this, in an analysis of the thermodynamic potentials of the crystal, in addition to the temperature T and strain ε_{ik} one should also consider the concentration n_h of the hexagonal excitations as a separate thermodynamic variable. Accordingly, the increment of the free energy of fullerite due to arbitrarily small increments of temperature Θ, strain ε_{ik}, and concentration of hexagonal excitations $\nu_h=n_h-\overline{n_h}$ can be written in the form of an expansion:[11]

$$\begin{aligned}\widetilde{F}(T+\Theta,\nu_h,\varepsilon_{ik})-F_0(T)&\\ =-\frac{1}{2}\xi(T)\Theta^2+\frac{1}{2}\eta(T)\nu_h^2+\frac{1}{2}\lambda_{iklm}(T)\varepsilon_{ik}\varepsilon_{lm}&\\ -\beta(T)\Theta\nu_h-\alpha(T)\Theta\varepsilon_{ik}\delta_{ik}-\gamma(T)\nu_h\varepsilon_{ik}\delta_{ik}+\ \ldots&\end{aligned} \tag{7}$$

This expansion takes into account the cubic symmetry of the crystal; δ_{ik} is the Kronecker delta, $F_0(T)$ is the free energy of the initial equilibrium state of the crystal at temperature T, and the expansion coefficients α, β, γ, ξ, η, and λ_{iklm} are temperature-dependent parameters of phenomenological thermodynamics; a summation over repeated coordinate indices is understood.

At specified strain ε_{ik} and temperature $T+\Theta$, minimization of the free energy (7) with respect to the variable ν_h will give the equilibrium distribution of hexagonal excitations:[11]

$$\overline{\nu_h}=\overline{n_h^{(\varepsilon)}}(T+\Theta)-\overline{n_h}(T)=\frac{\gamma}{\eta}\varepsilon_{ll}+\frac{\beta}{\eta}\Theta. \tag{8}$$

In the case of reversible thermodynamic processes, the condition of an extremum of the free energy implies the following expressions for the heat capacity per unit volume C_V, the volume coefficient of thermal expansion κ, and the bulk modulus defect $B^{(\infty)}-B^{(0)}$ ($B^{(\infty)}$ and $B^{(0)}$ are, respectively, the adiabatic and isothermal values of the bulk modulus):

$$\begin{aligned}&C_V=T\left(\xi+\frac{\beta^2}{\eta}\right), \quad \kappa=\frac{\alpha}{B^{(0)}}+\frac{\gamma\beta}{B^{(0)}\eta},\\ &B^{(\infty)}-B^{(0)}=\frac{\alpha^2}{\xi}+\frac{\gamma^2}{\eta}.\end{aligned} \tag{9}$$

In the phenomenological approach, the thermodynamic Grüneisen parameter g is given by the expression

$$g=\frac{B^{(0)}\kappa}{C_V}=\frac{\alpha\eta+\gamma\beta}{T(\beta^2+\xi\eta)}. \tag{10}$$

The explicit form of the temperature dependence of F_0 and the coefficients of the expansion (7) can be obtained only as the result of an analysis of the thermal motion of the crystal in the framework of statistical mechanics. Here the coefficients α, ξ, and λ_{iklm} will be determined by harmonic excitations (phonons, librons, intramolecular modes), while η, β, and γ will be determined by the double-well orientational states. It is seen from relations (9) that C_V, κ, and $B^{(\infty)}-B^{(0)}$ can be written as sums of additive contributions from oscillatory excitations and double-well orientational configurations (the first and second terms in (9), respectively), whereas in formula (10) for the thermodynamic Grüneisen parameter such a separation cannot be done. One can introduce the concepts of oscillatory $g^{(\mathrm{osc})}$ and orientational $g^{(\mathrm{or})}$ thermodynamic Grüneisen parameters, defined by the relations

$$g^{(\mathrm{osc})}=\frac{B^{(0)}\kappa^{(\mathrm{osc})}}{C_V^{(\mathrm{osc})}}=\frac{\alpha}{T\xi}, \quad g^{(\mathrm{or})}=\frac{B^{(0)}\kappa^{(\mathrm{or})}}{C_V^{(\mathrm{or})}}=\frac{\gamma}{T\beta}. \tag{11}$$

However, in the general $g\neq g^{(\mathrm{osc})}+g^{(\mathrm{or})}$.

Since the thermal excitation of an isolated h configuration is accompanied by an increase in the energy of the fullerite by an amount Δ, one can easily use Eq. (2) to obtain a microscopic expression describing the contribution of such excitations to the heat capacity per unit volume $C_V^{(\mathrm{or})}(T)$ for an infinitely slow change in temperature:

$$C_V^{(\mathrm{or})}(T)=N_0\Delta\left(\frac{d\overline{n_h}}{dT}\right)_V=\frac{N_0\Delta^2\overline{n_p}(T)\overline{n_h}(T)}{kT^2}. \tag{12}$$

Relations (2) and (6) can also be used to describe the microscopic analog of expression (8), which determines the equilibrium incremental contribution to the concentration of hexagonal excitations due to specified small increments of strain ε_{ij} and temperature Θ. In the linear approximation in ε_{ll} and Θ we get

$$\overline{n_h^{(\varepsilon)}}(T+\Theta)-\overline{n_h}(T)=\overline{n_p}(T)\overline{n_h}(T)\left(\frac{v_\Delta}{kT}\varepsilon_{ll}+\frac{\Delta}{kT^2}\Theta\right). \tag{13}$$

Comparing relations (8), (9) and (11)–(13), we obtain formulas which give the microscopic meaning of the parameters γ, β, η, and $g^{(\mathrm{or})}$:

$$g^{(\mathrm{or})}=\frac{v_\Delta}{\Delta}, \quad \gamma=N_0v_\Delta, \quad \beta=\frac{N_0\Delta}{T}, \quad \eta=\frac{kTN_0}{\overline{n_p}(T)\overline{n_h}(T)}. \tag{14}$$

From this we see that the analog of the Grüneisen parameter for orientational excitations is the dimensionless constant of the deformation potential, which contains the influence of the deformation on the difference between the local and global minima of the angle dependence of the intermolecular interaction energy.

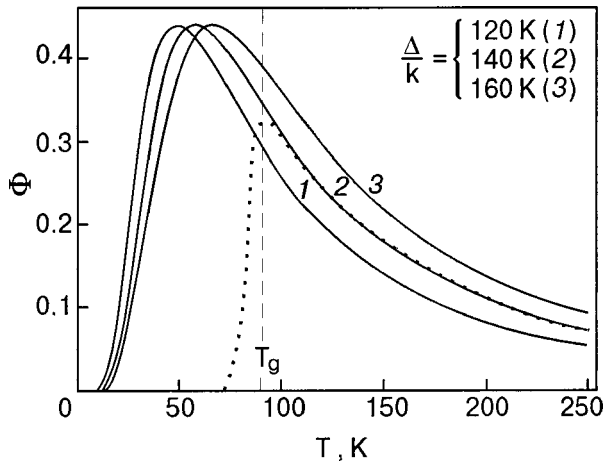

FIG. 1. Plots of the function $\Phi = C_V^{(or)}(T)/kN_0$ in Eq. (15) for several values of Δ close to the empirical values of this parameter.[13,15–18] The symbols (■) show schematically the temperature dependence of the heat capacity when the temperature is changed at a finite rate for $\Delta/k = 140$ K.

2. ANOMALIES OF THE HEAT CAPACITY AND THERMAL EXPANSION NEAR THE ORIENTATIONAL GLASS TEMPERATURE

In the previous Section we showed that the low-temperature heat capacity of fullerite is given by the sum

$$C_V = C_V^{(osc)} + C_V^{(or)},$$

where $C_V^{(osc)} = T\xi(T)$ is the total contribution of the harmonic excitations, and $C_V^{(or)}(T)$ is the contribution of the double-well orientational states. Using formula (12), we can write the temperature dependence of the heat capacity conveniently in the form

$$C_V(T) = C_V^{(osc)}(T) + kN_0\Phi\left(\frac{\Delta}{kT}\right),$$
$$\Phi(x) = \frac{x^2 e^x}{(1+e^x)^2}. \tag{15}$$

The function $\Phi(\Delta/kT)$ is plotted in Fig. 1 for several different values of the parameter Δ. It should be recalled that this function describes the orientational component of the heat capacity if it is measured for a sufficiently slow change in temperature. In any real experiment, however, the temperature is changed at a certain finite rate, and so the second term in formula (15) can be used for interpretation of experimental data only in the temperature interval $T_g < T < T_c$, while at lower temperatures (in the orientational glass state) one must assume that $\Phi \cong 0$ and $C_V^{(or)}(T < T_g) \equiv 0$.

The analysis done in Ref. 9 showed that the total rotational component of the heat capacity, consisting of the sum of $C_V^{(or)}$ and the librational contribution, turns out to be a rather small part of the total heat capacity. Therefore, our earlier conjecture[11] that the orientational excitations make the governing contribution to the thermodynamic characteristics of fullerite at $T > T_g$ must be incorrect (at least with regard to the heat capacity). However, precision measurements of the heat capacity near the orientational glass temperature $T_g \cong 90$ K have made it possible to extract this contribution.[13,14] This possibility arises because $C_V^{(or)}(T)$ has a nonmonotonic character in this region (Fig. 1), whereas the remaining components of the heat capacity near T_g are monotonic and relatively weak functions of temperature. Owing to the orientational glass effect, this nonmonotonicity is ''sharpened'' further: $C_V^{(or)} \simeq 0$ at temperatures below T_g, which gives rise to a smeared jump on the temperature dependence of the total heat capacity near the orientational glass temperature. The value of the temperature at which this anomaly is observed and the size of the jump depend on the rate of change of the temperature during the measurement of the heat capacity, and therefore the value $C_V^{(or)}(T_g)$ determined by formulas (15) gives an upper bound on the size of the jump.

The experimental values of the jump in the heat capacity $C^{(or)}(T_g) \cong 3.5$ J·mole^{-1}K^{-1} (Ref. 13), molar volume $V(T_g) \simeq 418$ cm^3·mole^{-1} (Ref. 9), and parameter $\Delta \simeq (11–13)\times 10^{-3}$ eV (Refs. 13 and 15–18) can be used to obtain a rough estimate for the phenomenological parameter N_0 in the theory of double-well orientational states:

$$N_0 = \frac{C_V^{(or)}(T_g)}{k\Phi(\Delta/kT_g)} \simeq (1.4-1.8)\times 10^{21}\ \text{cm}^{-3}. \tag{16}$$

This value corresponds to the lower bound $N_0 a^3 \simeq 4$ given in the Introduction.

The temperature dependence of the volume thermal expansion coefficient, according to formula (9), (14), and (15), is described by the relation

$$\kappa = \kappa^{(osc)}(T) + \frac{g^{(or)}C_V^{(or)}(T)}{B^{(0)}}$$
$$= \kappa^{(osc)}(T) + \frac{kN_0 v_\Delta}{B^{(0)}\Delta}\Phi\left(\frac{\Delta}{kT}\right). \tag{17}$$

It has been observed experimentally[9,13,14] that the anomalies of the coefficient of thermal expansion and of the thermodynamic Grüneisen parameter of fullerite at temperatures near T_g are considerably stronger than the anomaly of the heat capacity, and the assumption that the the orientational relaxation makes the predominant contribution to these characteristics does not seem unrealistic. This circumstance is evidence of an anomalously large absolute value of the parameter $g^{(or)}$.

We note that in the process of cooling fullerite at $T \to T_g$ one observes a rather sharp decrease in κ followed by a jumplike increase at the transition to the region $T < T_g$. According to formula (17), this means that the orientational Grüneisen parameter has a negative value. If we use the value measured in Ref. 13 for the jump in the thermal expansion coefficient, $\kappa^{(or)}(T_g) \simeq -4\times 10^{-5}$ K^{-1}, and the value $B \simeq 1.1\times 10^{11}$ dyne·cm^{-2} for the bulk modulus,[19] then we obtain the following empirical estimate for $g^{(or)}$:

$$g^{(or)} = \frac{v_\Delta}{\Delta} = \frac{\kappa^{(or)}(T_g)B^{(0)}(T_g)}{kN_0\Phi(\Delta/k/T_g)} \simeq -55. \tag{18}$$

We note that the experimental values of the parameters Δ, $B^{(0)}$, and especially $\kappa^{(or)}(T_g)$ have a rather large scatter, and therefore the estimate (18) for $g^{(or)}$ should be regarded as extremely rough, giving only an idea of the order of magnitude of this parameter. The values of v_Δ obtained here and in Ref. 11 differ not only in order of absolute magnitude but

also in sign. This discrepancy is due to the fact that in Ref. 11 we make use of the mistaken assumption mentioned above and also the data on the heat capacity of fullerite given in Ref. 20, which differ substantially from the data of other investigators.

Since the total heat capacity near the orientational glass temperature has a value $\simeq 80$ J·mole^{-1}K^{-1} (Ref. 9), which is considerably larger than its orientational component $C^{(\mathrm{or})}(T_g)\simeq 3.5$ J·mole^{-1}K^{-1} (Ref. 13), the anomalous temperature dependence of the total thermodynamic Grüneisen parameter of fullerite near T_g, noted in Ref. 9, is mainly due to the orientational component of the thermal expansion coefficient, $\kappa^{(\mathrm{or})}(T)$. According to (10), (11), and (17), we have

$$g = g^{(\mathrm{osc})} - \frac{kN_0}{C_V(T)}\left|\frac{v_\Delta}{\Delta}\right|\Phi\left(\frac{\Delta}{kT}\right). \tag{19}$$

This formula describes the jumplike ($\sim$2.5-fold) change in g at the transition through the temperature T_g.

Let us conclude this Section by discussing another possibility for obtaining empirical estimates for the parameters of the double-well model of the orientational states of fullerite, based on experimental study of the internal friction. The resonant interaction of elastic vibrations of the crystal with the double-well orientational states of the molecules leads to the existence of a peak on the temperature dependence of the internal friction Q^{-1}. The temperature T_m at which this peak is observed is determined by the equation $\omega\tau(T_m)=1$ [ω is the angular frequency of the vibrations, and τ is the orientational relaxation time (4)]. The height of the peak $Q^{-1}(T_m)$ is proportional to the value of the orientational component of the bulk modulus defect $[B^{(\infty)}-B^{(0)}]^{(\mathrm{or})}=\gamma^2/\eta$:[11]

$$Q^{-1}(T_m)=\frac{AN_0kT_m}{B^{(\infty)}}\left(\frac{v_\Delta}{\Delta}\right)^2\Phi\left(\frac{\Delta}{kT_m}\right). \tag{20}$$

Here $A\cong 0.5$ is a numerical coefficient whose exact value depends on the orientation of the wave vector of the vibrations. In Ref. 20 the peak $Q^{-1}(T_m)$ was observed at a temperature $T_m=215$ K and had a height of $\simeq 1\times 10^{-2}$. Substituting these values into formula (20), we obtain the estimate $|v_\Delta/\Delta|\simeq 21$, which is considerably smaller than the value in (18) obtained on the basis of thermal measurements. Thus the exact value of the parameter $g^{(\mathrm{or})}=v_\Delta/\Delta$ remains an open question.

CONCLUSION

This study is a continuation of our previous work.[11] Here we have separated out and analyzed in detail the components of the heat capacity and thermal expansion of the low-temperature phase of fullerite C_{60} due to thermal excitation of the double-well orientational states of the molecules — the pentagonal (p) and hexagonal (h) configurations. The relation between the orientation states of the molecules and the macroscopic strains of the crystal lattice is described in terms of renormalizations of the energy parameters of the p and h configurations in a linear approximation in the dilatation. The deformational contribution to the energy difference of the p and h configurations is characterized by a parameter $g^{(\mathrm{or})}$, which is equivalent to the Grüneisen parameter in the theory of the thermal excitation of harmonic vibrations of the crystal. It is shown that the orientational components of the heat capacity and thermal expansion of fullerite are proportional to a nonmonotonic function of temperature, and the orientational glass effect ''sharpens'' this nonmonotonicity and leads to an abrupt (jumplike) change in the thermal properties near the glass temperature $T_g\simeq 90$ K. This conclusion gives a qualitative explanation for the experimentally observed anomalies of the heat capacity, thermal expansion, and total thermodynamic Grüneisen parameter of fullerite at temperatures near T_g. A comparison of the results of the theory with the experimental data has yielded empirical estimates for the volume concentration of double-well orientational states and for the orientational Grüneisen parameter. We have also noted and corrected some inaccuracies in the estimates made in our previous paper.[11]

The authors are sincerely grateful to V. G. Manzhelii, V. M. Loktev, M. A. Strzhemechnyi, and A. I. Prokhvatilov for substantive and extremely helpful discussions of various aspects of the problem of the thermal properties of fullerite.

*E-mail: natsik@ilt.kharkov.ua

[1] G. Leibfried, in *Handbuch der Physik*, Vol. 7, Part 1 (edited by S. Flügge), Springer-Verlag, Berlin (1955), p. 104; *Microscopic Theory of Mechanical and Thermal Properties of Crystals* [Russian translation], Fizmatgiz, Moscow–Leningrad (1963).
[2] G. Mie, Ann. Phys. (Leipzig) **11**, 657 (1903).
[3] E. Grüneisen, Ann. Phys. (Leipzig) **26**, 393 (1908).
[4] A. Lundin, B. Sundqvist, P. Skoglund, A. Francsson, and S. Peterson, Solid State Commun. **84**, 879 (1992).
[5] L. A. Girifalco, J. Phys. Chem. **96**, 858 (1992).
[6] M. A. White, C. Meingast, W. I. F. David, and T. Matsuo, Solid State Commun. **94**, 481 (1995).
[7] A. N. Aleksandrovskii, V. B. Esel'son, V. G. Manzhelii, A. V. Soldatov, B. Sundqvist, and B. G. Udovidchenko, Fiz. Nizk. Temp. **23**, 1256 (1997) [Low Temp. Phys. **23**, 943 (1997)]; Fiz. Nizk. Temp. **26**, 100 (2000) [Low Temp. Phys. **26**, 75 (2000)].
[8] N. A. Aksenova, A. P. Isakina, A. I. Prokhvatilov, M. A. Strzhemechny, and V. N. Varyukhin, in *Recent Advances in the Chemistry and Physics of Fullerenes and Related Materials*, edited by K. M. Kadish and R. S. Ruoff, Electrochemical Society, Pennington (1994), p. 1543.
[9] N. A. Aksenova, A. P. Isakina, A. I. Prokhvatilov, and M. A. Strzhemechnyĭ, Fiz. Nizk. Temp. **25**, 964 (1999) [Low Temp. Phys. **25**, 724 (1999)].
[10] V. M. Loktev, Fiz. Nizk. Temp. **25**, 1099 (1999) [Low Temp. Phys. **25**, 823 (1999)].
[11] V. D. Natsik and A. V. Podol'skiĭ, Fiz. Nizk. Temp. **24**, 689 (1998) [Low Temp. Phys. **24**, 523 (1998)].
[12] O. Andersson, A. Soldatov, and B. Sundqvist, Phys. Rev. B **54**, 3093 (1996).
[13] F. Gugenberg, R. Heid, C. Meingast, P. Adelman, M. Braun, H. Wuhl, M. Haluska, and H. Kuzmany, Phys. Rev. Lett. **69**, 3774 (1992).
[14] C. Meingast and F. Gugenberger, Mod. Phys. Lett. B **7**, 1703 (1993).
[15] R. C. Yu, N. Tea, M. V. Salanon, D. Lorents, and R. Malhorta, Phys. Rev. Lett. **68**, 2050 (1992).
[16] M. I. F. David, R. M. Ibberson, T. J. S. Dennis, J. P. Hare, and K. Prassides, Europhys. Lett. **18**, 219 (1992).
[17] M. I. F. David, R. M. Ibberson, and T. Matsuo, Proc. R. Soc. London, Ser. A **442**, 129 (1993).
[18] W. Schranz, A. Fnith, P. Dolinar, H. Warhanek, M. Haluska, and H. Kuzmany, Phys. Rev. Lett. **71**, 1561 (1993).
[19] N. P. Kobelev, R. K. Nikolaev, Ya. M. Soĭfer, and S. S. Khasanov, Fiz. Tverd. Tela (St. Petersburg) **40**, 173 (1998) [Phys. Solid State **40**, 154 (1998)].
[20] N. P. Kobelev, Ya. M. Soifer, I. O. Bashkin, A. F. Gurov, A. P. Moravskii, and O. G. Rubchenko, Phys. Status Solidi B **190**, 157 (1995).

Translated by Steve Torstveit

SHORT NOTES

Absorption of electromagnetic field of the millimeter-wave band in perfect dielectric crystals

E. M. Ganapolskiĭ*

A. Ya. Usikov Institute of Radio Physics and Electronics, ul. Akad. Proskury 12, 61085 Kharkov, Ukraine
(Submitted June 7, 2000)
Fiz. Nizk. Temp. **26**, 1162–1165 (November 2000)

The dielectric losses in high-quality crystals of sapphire, ruby, fluorite, and quartz are measured at a frequency of 36 GHz in the temperature range 4.2–300 K by the spherical dielectric resonator method. The absorption coefficient of the electromagnetic field per unit wavelength Γ in the crystals is found to agree both in order of magnitude and in its temperature dependence with the Gurevich theory, which treats the absorption as being the result of an electrophonon interaction of the field with acoustical phonons as a result of the anharmonicity of the crystal lattice. It is found that the crystals studied have extremely low absorption in the millimeter-wave band even at moderately low temperatures (e.g., for sapphire $\Gamma \approx 10^{-8}$ at $T \approx 40$ K). Measurements are made of the residual absorption of the electromagnetic field at low temperatures, which is due to a single-phonon process of field absorption at defects of the crystal structure. It is found that the temperature dependence of the absorption of an electromagnetic field in a crystal is correlated with that for the absorption of hypersound.
 [S1063-777X(00)01411-0]

As we know, real nonconducting crystals have rather large dielectric losses at millimeter and submillimeter wavelengths. The nature of these losses is usually attributed to various charged defects, which serve as a source of conversion of the electromagnetic field into acoustical phonons, which constitute a heat bath. These charged defects, distributed randomly in the crystal, execute[4] periodic motion in the field of the electromagnetic wave. Since the charges are directly coupled to the crystal lattice, their motion is accompanied by emission of acoustical phonons. The conversion of electromagnetic field into phonons, from a quantum-mechanical point of view, can be treated as a single-phonon process, in which the absorption of a photon of frequency ω is accompanied by the creation of a single acoustical phonon of the same frequency.[1] (In ideal crystals this process is forbidden by the selection rules — energy and momentum conservation.) It is clear that such a direct conversion does not directly involve the phonon bath as a whole, and it is therefore independent of temperature. Multiphonon processes of electromagnetic field absorption on account of lattice defects are also possible; they are considered in Ref. 2. Since the charges created by these defects are directly coupled to the atoms of the lattice, their motion perturbs the phonon system, altering the phonon distribution function. The increase in entropy necessary for restoration of thermal equilibrium leads to absorption of the electromagnetic field. Multiphonon absorption of electromagnetic field, unlike the case of single-phonon absorption, can have a rather strong temperature dependence.

The absorption of electromagnetic fields at frequencies less than the Debye frequency can also occur in crystals not containing defects. As was shown in the papers by Gurevich,[3,4] the conversion of electromagnetic field into phonons can occur on account of the so-called electrophonon interaction. This interaction comes about because the alternating electric field, in polarizing the bound electrons, alters the interaction constants of the atoms with the lattice in nonpolar crystals. In polar crystals the field, in addition to this, also causes a relative displacement of the sublattices, which, on account of anharmonicity, leads to a change in the interaction between atoms. Here the most efficient process is three-phonon absorption, since the single-phonon process is forbidden by the conservation laws. The absorption mechanism is analogous to Akhiezer absorption of sound in crystals. The electric field of the wave in the electrophonon interaction alters the frequencies of the acoustical phonons on account of the anharmonicity of the lattice. Then a nonequilibrium state with a higher entropy is formed in the phonon gas, and the energy required for this is drawn from the electromagnetic field.

Gurevich absorption is extremely small and is strongly dependent on frequency and temperature. For example, for nonpolar, e.g., hexagonal, crystals, the absorption coefficient per unit wavelength $\Gamma \propto \omega T^5$, where T is the temperature; for cubic crystals $\Gamma \propto \omega^2 T^4$. For sapphire, e.g., at a frequency of 36 GHz, the absorption is 10^{-5} at room temperature and 10^{-13} at 15 K. For piezoelectric crystals the theory[3] predicts a substantially larger absorption.

In real crystals containing defects of the crystal structure, all of the aforementioned mechanisms contribute. Therefore, the identification of any one of them is a rather difficult problem in the general case.

The technological progress that has been achieved in the interests of quantum electronics has made it possible to syn-

thesize crystals of sapphire, ruby, and fluorite, as well as quartz, having extremely small numbers of structural defects. This makes it possible to investigate their dielectric losses in the millimeter-wave range and to estimate the relative efficiency of the absorption mechanisms indicated above. Here we describe the results of measurements of the temperature dependence of the absorption of an electromagnetic field at a frequency of 36 GHz in the temperature range from 4.2 to 300 K. For these measurements we have used the spherical dielectric resonator (SDR) method developed previously, which is capable of measuring extremely low dielectric losses in crystals in the millimeter-wave band.[5] Briefly, the essence of this method is as follows. A sphere made of the material to be studied is used as an open spherical dielectric microwave resonator. The diameter of the sphere is chosen such that the spherical dielectric microwave resonator is a quasioptical system, in which ''whispering gallery'' modes with radial index $n>30$, which have an ultrahigh quality factor Q, can be excited. Since the resonator is an open spherical dielectric microwave resonator, in which the field of the electromagnetic ''whispering gallery'' modes are concentrated in a thin layer near the spherical surface, the damping decrement for these modes is very sensitive to substances on the surface that absorb field energy. For this reason, particular care was taken to remove all foreign substances from the surface of the sphere. The resonators had a precise spherical shape (not more than 20 μm of ellipsoidal deviation) and an optical surface finish polished to a roughness of 0.1 μm or less.

For excitation of the electromagnetic oscillations in the SDR we used a dielectric-waveguide antenna, which was an end-radiating rectangular waveguide completely filled with a sapphire crystal. The antenna was placed near the surface of the sphere in such a way that its electromagnetic field was superposed with the ''whispering gallery'' modes in the SDR, the coupling coefficient lying in the range 0.3–0.5. The electric field in the antenna was oriented along the threefold crystallographic axis. In this arrangement the antenna excites *H* modes, which have the highest Q.

BRIEF DESCRIPTION OF THE SAMPLES

Sapphire. The samples of this crystal, which were flux grown by a hydrothermal method (the GOI method, named for the State Optical Institute, St. Petersburg), contained a comparatively small number of dislocations (10^2–10^3 cm $^{-2}$), and the angle of misorientation of the threefold crystallographic axis in the microtwin blocks of the structure did not exceed 1°. The diameter of the sapphire SDR was 28.5 mm.

Ruby. The ruby crystals were synthesized by the Verneuil method and contained a 0.05% chromium impurity. Since the Verneuil growth method is a substantially more nonequilibrium method than the GOI method, these crystals were inferior to the sapphire crystals in respect to the perfection of the crystal structure both in the number of dislocations and in the average angle of misorientation of the optic axis in the microtwin blocks. The diameter of the ruby SDR was 30.5 mm.

Quartz. We used high-quality natural crystals of Brazilian quartz of the ''extra'' type, with high transparency and a small number of dislocations. The diameter of the quartz SDR was 45 mm.

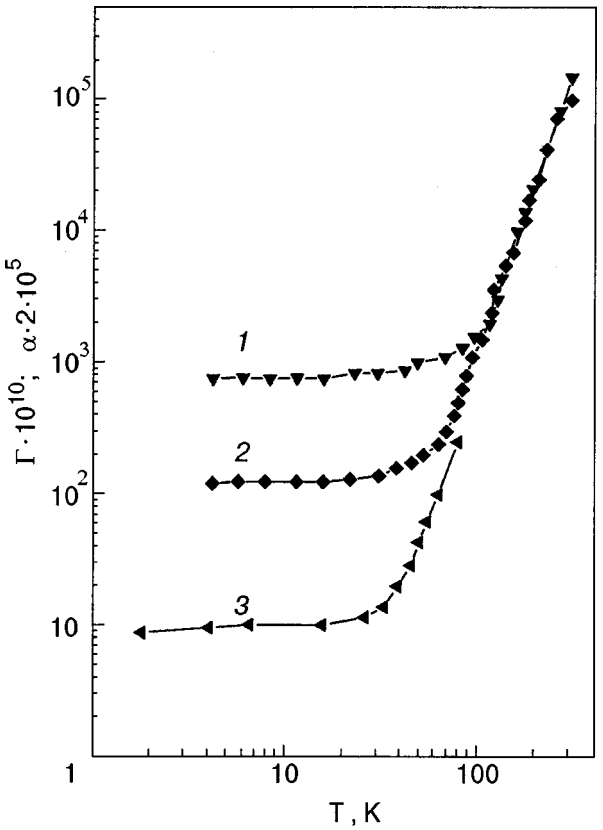

FIG. 1. Temperature dependence of the electromagnetic absorption coefficient γ in ruby (*1*) and sapphire (*2*). Curve *3* shows the temperature dependence of the hypersound absorption per unit wavelength, α, in sapphire at a frequency of 3 GHz.[9]

Fluorite. The fluorite crystals were synthesized by the hydrothermal method and had a high degree of uniformity and transparency. They contained a 0.01% europium impurity. The diameter of the fluorite SDR was 29 mm.

The Q of the SDRs, from which we determined the absorption coefficient of the electromagnetic field, was measured by a method described in Refs. 6 and 7. The results of the measurements are presented in Figs. 1 and 2. We note first of all that the experimental data are in qualitative agreement with the Gurevich theory. It was found (and this is one of the main results) that the crystals studied have extremely low absorption for millimeter-wave electromagnetic fields even at moderately low temperatures. For example, in sapphire the absorption, which is 10^{-5} at room temperature, reaches 10^{-8} when the crystal is cooled to 40 K.

On the whole, this agrees with the estimating formulas given in Refs. 3 and 4 and also with the data for sapphire[8] obtained by a less reliable method than that of Refs. 5 and 6. There is a total lack of existing experimental data on the dielectric losses in the millimeter-wave range in ruby, quartz, and fluorite crystals at low temperatures. This circumstance is due not so much to the low availability of perfect crystals as it is to the fact that it was only comparatively recently that an effective method was developed for measuring extremely low dielectric losses.[5,6]

The higher level of dielectric losses in quartz and fluorite as compared to sapphire can be explained by the lower De-

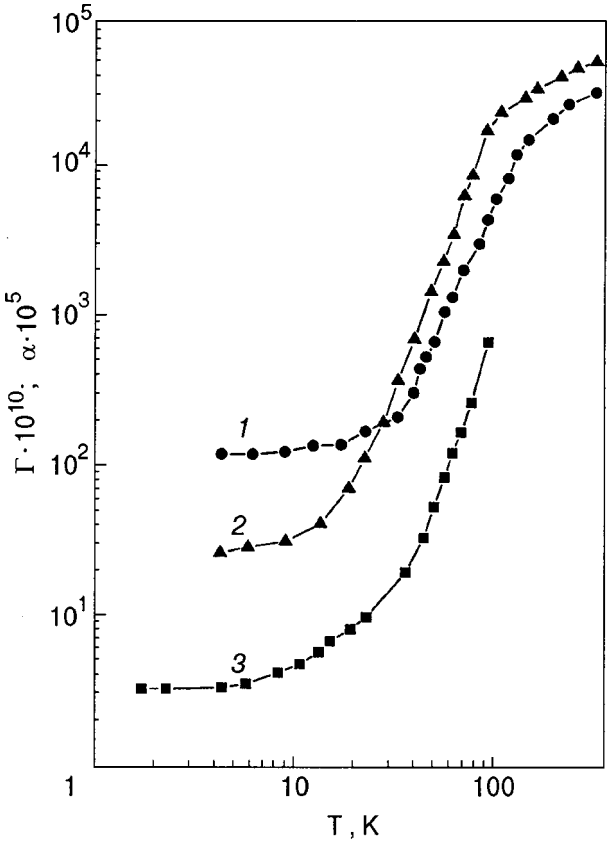

FIG. 2. Temperature dependence of the electromagnetic absorption coefficient Γ in fluorite (*1*) and quartz (*2*). Curve *3* shows the temperature dependence of the hypersound absorption α in quartz at a frequency of 3 GHz.[9]

bye temperature in these crystals. The higher loss in quartz as compared to fluorite is also in agreement with the conclusions of the theory as to the role of a center of symmetry in the absorption of electromagnetic fields.[3] The dielectric losses fall off sharply as the temperature of the crystals is lowered. The temperature dependence of the absorption for sapphire, ruby, and quartz is close to a T^5 law, while that of fluorite is close to $T^{3.5}$; these findings agree with the theory. The sharp decrease in the absorption of the electromagnetic field is observed only down to a certain temperature, which is 50–60 K in the case of sapphire and ruby, 40 K for fluorite, and 20 K for quartz. When the crystals are cooled below these temperatures the sharp decline in the absorption is slowed, and the curve of the temperature dependence goes out to a plateau. The temperature-independent absorption in the plateau region might be called the residual absorption of electromagnetic field. Since the absorption of a hypersonic wave in a dielectric crystal is directly due to a three-phonon process in which the phonons interact on account of anharmonicity, the temperature dependence of the absorption of an electromagnetic field due to the anharmonicity of the vibrations of the crystal lattice ought to be similar to the absorption of hypersound. This is demonstrated in Figs. 1 and 2, which show the corresponding curves for the temperature dependence of the absorption of longitudinal hypersound.[9]

The measured value of the residual absorption actually sets a minimum achievable level of electromagnetic loss occurring in perfect dielectric crystals. Since the residual absorption does not depend on the temperature, it can be assumed that it is due to a single-phonon process of absorption at impurities and other microscopic defects of the crystal. This view is supported by the fact that the level of residual absorption in ruby, which contains chromium impurity centers, is higher than that in sapphire.

*E-mail: ganap@ire.kharkov.ua

[1] B. M. Garin, Preprint No. 2 (477) [in Russian], Moscow, IRÉ AN SSSR (1988).
[2] H. Poulet and J. P. Mathieu, *Spectres de vibration et symetrie des cristaux*, Gordon and Breach, Paris–London–New York (1970); A. V. Galdetskiĭ and B. M. Garin, Preprint No. 17 (320), Moscow, IRÉ AN SSSR (1973).
[3] V. L. Gurevich, *Kinetics of Phonon Systems* [in Russian], Nauka, Moscow (1980).
[4] V. L. Gurevich, Fiz. Tverd. Tela (Leningrad) **21**, 3453 (1979) [Sov. Phys. Solid State **21**, 1193 (1979)].
[5] E. M. Ganapol'skiĭ, A. V. Golik, and A. P. Korolyuk, Fiz. Nizk. Temp. **19**, 1255 (1993) [Low Temp. Phys. **19**, 892 (1993)].
[6] E. M. Ganapolskii and A. V. Golik, Meas. Sci. Technol. (UK) **8**, 1016 (1997).
[7] E. M. Ganapolskii, A. V. Golik, and A. P. Korolyuk, Phys. Rev. B **51**, 11962 (1995).
[8] V. B. Braginsky, V. S. Ilchenko, and Kh. S. Bagdassarov, Phys. Lett. A **120**, 360 (1987).
[9] E. M. Ganapol'skiĭ, A. P. Korolyuk, and V. V. Tarakanov, Zh. Éksp. Teor. Fiz. **82**, 182 (1982) [Sov. Phys. JETP **55**, 108 (1982)].

Translated by Steve Torstveit

NEWS ITEMS

NATO Advanced Study Institute ''Modern Trends in Magnetostriction Study and Application''

V. V. Eremenko and V. A. Sirenko

Institute for Low Temperature Physics and Engineering, 47 Lenin Ave., 61164 Kharkov, Ukraine

M. R. J. Gibbs

Department of Physics and Astronomy, The University of Sheffield, Sheffield, S3 7RH, UK

H. Szymczak

Institute of Physics, Polish Academy of Sciences, 02-668 Warsaw, Poland
(Submitted June 27, 2000)
Fiz. Nizk. Temp. **26**, 1166-1169 (November 2000)

[S1063-777X(00)01511-5]

The NATO Advanced Study Institute ''Modern Trends in Magnetostriction Study and Application'' was held from May 22 to June 2, 2000, in Kiev, Ukraine. The co-directors and main organizers were V. G. Bar'yakhtar (Ukraine), V. V. Eremenko (Ukraine), M. R. J. Gibbs (UK), H. Szymczak (Poland), and V. A. Sirenko (Ukraine). The computer services were provided by L. D. Demchenko, N. I. Makedonskaya, and Yu. A. Shabakayeva (Ukraine); local administrators L. A. Chekal and T. N. Loshitskaya (Ukraine).

The objectives of the ASI were to determine the state of the art in basic and applied research on magnetostriction and related phenomena, to define and prioritize directions of investigation in the future, to consider new materials for common applications of magnetostriction-based devices, and to formulate new perspectives on magnetostriction phenomena and applications, using advances in materials design and technology. The specific topics included a general introduction to modern trends in magnetostriction study and application, the theory of magnetostriction and related phenomena, rare-earth magnetostriction study and application, magnetostriction of amorphous materials, CMR materials, giant magnetostriction in superconductors, structural study of magnetostriction, industrial applications, and magnetostriction of nanostructured materials.

The phenomenon of magnetostriction was discovered more than 150 years ago [J. P. Joule, Philos. Mag. **30**, 76 (1847)]. Since that time there has been study of both basic science and application in such areas as sound generators, magnetoacoustic transformers, actuators for opto-electronic systems, devices for nondestructive monitoring for quality control, and devices for remote detection and ranging. The recent development of modern technologies (e.g., microfabrication) and materials (e.g., rare-earth-based bulk materials and magnetic thin films) has created new opportunities for the study and application of magnetostriction. For example, the discovery of giant magnetostriction makes it possible, in particular, to generate ultrasound and to extend the application of nondestructive monitoring techniques; the development of cryogenic technologies gives new insight into forced magnetostriction, namely into its irreversible component, which is related to the magnetization-reversal and thermally activated processes involved in displacement of the domain walls and flux lines, i.e., into stability of magnetic and superconducting devices, as well as into the giant magnetostriction in rare-earth magnets (up to 10^{-2}). The new field of interest in magnetostriction as the strain derivative of the magnetic anisotropy is relevant to the magnetic recording industry, particularly as recorded densities go beyond 20 Gbits/in^2. As the physical dimensions of devices are reduced, the ratio of surface area to volume increases, and surface anisotropy (magnetostriction) effects may become significant in terms of ultimate switching speeds or noise floor. Miniaturization within the sensor/actuator sector can also lead to such complications, as a result of which magnetostrictive materials may now become competitive with piezoelectric materials. There has been a resurgence of interest in perovskite materials, particularly for their outstanding magnetoresistive properties. The fundamental mechanisms driving the observed effects are still being elucidated, but lattice distortion (Jahn–Teller) and significant magnetostrictions appear to play a part. There is an urgent need for coherent studies in this area.

Magnetic-field-induced giant magnetostriction has recently been discovered in high-temperature superconductors. The magnetoelastic strains may limit the technical applications of this important group of materials.

The spread of novel experimental techniques such as magnetic resonances, neutron scattering, and modern x-ray facilities into magnetostriction research allows high-resolution structural studies of magnetostriction and the differentiation of its surface and bulk components. It is timely to review and explore the various possibilities offered here, and attempt to coordinate the use of large-scale facilities to maximize the scientific output.

The goals of the proposed ASI were the delivery of lectures on new achievements and discussion of the prospects

for the study and application of the aforementioned magnetostriction effects among experts from the different branches of science and industry and representing the leading teams of the West and Eastern Europe. It is hoped that a more coordinated and focused approach at both the level of fundamental science and demonstration applications will advance the subject significantly. Wide dissemination of the meeting materials via publications will be an important outcome. The recent opening up of Eastern Europe makes such a meeting practical, whereas previously much expertise lay beyond the reach of Western scientists. This ASI was the first forum on modern trends in magnetostriction study and application. Only a meeting of this kind, which, with NATO support, brought together the worldwide acknowledged specialists in the related fields, would be capable of meeting the goals of expediting the solution of existing problems and assessing future prospects. Nearly 70 experts from 14 European countries and the USA participated in the ASI. Sixteen lectures were delivered by world-known experts on magnetostriction:

• J. I. Arnaudas (Universidad de Zaragoza, Spain), ''Magnetostriction of rare-earth based thin films and superlattices'';

• V. G. Bar'yakhtar (Institute of Magnetism, Ukraine), ''Magneto-acoustic resonance'';

• J. M. Barandiaran (Departamento de Electricidad y Electronica, Universidad del Pais Vasco (UPV/EHU), Spain), ''Magnetoelasticity in amorphous ferromagnets'';

• H. Chiriac (National Institute of R&D for Technical Physics, Romania), ''Giant magneto-impedance effect in amorphous wires'';

• B. Dabrowski, Z. Bukowski, S. Kolesnik, O. Chmaissem, J. Mais, and C. W. Kimball (Department of Physics, Northern Illinois University, USA), L. Gladczuk, A. Wisniewski, A. Szewczyk, M. Gutowska, and H. Szymczak (Institute of Physics; Polish Academy of Sciences, Poland), ''Spectacular magneto-related properties of complex oxides'';

• V. V. Eremenko and V. A. Sirenko (Institute for Low Temperature Physics & Engineering, Ukraine), ''Magnetostriction and spin-flopping of uniaxially compressed antiferromagnets. Comparison with superconductors'';

• A. Gerber (School of Physics and Astronomy, Tel-Aviv University, Israel), ''Magnetostriction in superconductors'';

• M. R. Gibbs (Department of Physics & Astronomy, The University of Sheffield, UK), ''Magnetostriction of multilayer systems'';

• M. Hirscher (Max-Planck-Institut fur Metallforschung, Germany) and T. Reininger (Festo AC & Co., Germany), ''Fundamental investigation and industrial applications of magnetostriction'';

• M. R. Ibarra, J. M. De Teresa, P. A. Algarabel, C. Marquina, and B. Garcia-Landa (Departamento de Física de la Materia Condensada and ICMA, University of Zaragoza-CSIC, Spain), ''Magnetostriction in colossal magnetoresistance manganese oxide perovskites'';

• A. Ludwig and E. Quandt (caesar, center of european advanced studies and research, Germany), ''Rare earth transition metal thin films and devices'';

• R. F. Pettifer (Department of Physics, University of Warwick, UK), ''Structural study of magnetostriction'';

• K. V. Rao (Department of Materials Science and Engineering (MSE), Royal Institute of Technology, Sweden), ''Local magnetostriction determination and mapping using atomic force microscopy'';

• H. Szymczak (Institute of Physics, Polish Academy of Science, Poland), ''Magnetostriction in heterogeneous magnetic systems'';

• Ruqian Wu (Department of Physics and Astronomy, California State University, USA), ''First principles determination of magnetostriction in surfaces, bulks, alloys and compounds.''

The following posters and progress reports were presented:

– A. I. Abramovich (Physics Department, Moscow State University, Russia), ''Giant volume magnetostriction in GMR manganites $Re_{1-x}Sr_xMnO_3$ (Re = Sm, Nd)'';

– G. E. Grechnev and A. Baranovskiy (Institute for Low Temperature Physics & Engineering, Ukraine), ''Origin of magnetovolume effect in $GdAl_2$ and $GdNi_2$ compounds'';

– A. B. Beznosov, E. L. Fertman, and V. V. Eremenko (Institute for Low Temperature Physics & Engineering, Ukraine), ''Electronic structure & magnetostrictive sensitivity of metallic glasses Fe–B'';

– C. Canalias, J. Wittborn, Ni. Polushkin, and K. V. Rao (Engineering Materials Physics Division, MSE, Royal Institute of Technology, Sweden), ''Magnetic studies of nanoscale laser patterned structures'';

– Chernyavsky Oleksandr (Department of Electron Structures, Charles University, Czech Republic), ''Field induced irreversibilities in an itinerant $5f$ electron UNiAl antiferromagnet'';

– Fergen Immanuel (Institute for Materials Research I, Forschungszentrum Karlsruhe, Germany), ''The influence of stress induced anisotropy on the hf properties of amorphous films'';

– Franco Victorino (Física de la Materia Condensada, Universidad de Sevilla), ''Magnetic anisotropy and devitrification of soft magnetic materials'';

– V. I. Gatalskaya, S. Barilo, G. L. Bychkov, and L. A. Kurochkin (Institute of Solid State & Semiconductor Physics, NASB, Belarus), H. Szymczak, R. Szymczak, and M. Baran (Institute of Physics, Polish Academy of Science, Poland), ''Magnetic properties of $La_{1-x}Li_xMnO_3$ single crystals'';

– L. I. Koroleva (Physics Department, Moscow State University, Russia), ''Peculiarities of volume magnetostriction in $La_{1-x}Sr_xMnO_3$ at Curie point region'';

– Kraus Ludek (Institute of Physics ASCR, Czech Republic), ''Stress dependence of giant magnetoimpedance and its potential applications'';

– K. V. Lamonova and A. L. Sukstanskii (DonFTI, Ukraine), ''Magnetoelastic interaction and a new type of domain walls in a magnetic sandwich structure'';

– Lupu Nicoleta (Magnetic Materials & Devices Laboratory, National Institute of R&D for Technical Physics, Romania), ''Melt spun amorphous magnetostrictive bimetal ribbons'';

– Minguez Pablo (Universidad del Pais Vasco, Spain),

''Magnetoelastic properties of $Fe_{73.5-x}Al_xSi_{13.5}B_9Cu_1Mo_3$ alloys ($x=0,2,4,6$)'';

– W. R. McCallum (Center for Rare Earths & Magnets, Iowa State University, USA), ''Composite magnetostrictive material for sensors and actuators'';

– S. Nikitin (Physics Department, Moscow State University, Russia), ''Magnetostriction, magnetocaloric and magnetoelastic effects in rare-earth compounds'';

– Yu. G. Pashkevich, V. A. Blinkin, V. P. Gnezdilov, V. S. Kurnosov, V. V. Tsapenko, V. V. Eremenko, P. Lemmens, M. Fischer, M. Grove, G. Gentherodt, L. Degiorgi, P. Wachter, J. M. Tranquada, and D. J. Butrey (DonFTI, Ukraine), ''Optical studies of the interaction of charge, magnetic & lattice subsystem in stripe ordered phase of $La_{1.775}Sr_{0.225}NiO_4$'';

– Oleksandr Prokhnenko (Institute of Physics ASCR, Czech Republic), ''Magnetovolume anomalies in $Ce_2Fe_{17-x}Mn_x$ compounds'';

– Sasso Carlo Paolo (Materials Department, IEN G. Ferraris, Italy), ''Analysis and optimization of the magnetomechanical properties of terfenol-D composites at audio frequencies'';

– Yu. Shabakayeva, V. V. Eremenko, V. A. Sirenko, N. I. Makedonskaya, V. Bruk, and M. Shvedun (Institute for Low Temperature Physics & Eng., Ukraine), H. Szymczak (Institute of Physics, Polish Academy of Science, Poland), ''About irreversible magnetostriction in perovskite-like structures'';

– I. V. Svechkarev, A. S. Panfilov, M. Kurisu, A. Fuse, and G. Nakamoto (Institute for Low Temperature Physics & Engineering, Ukraine), ''Effect of pressure on magnetic susceptibility of $CeCo_2$'';

– Irina Tereshina (Physics Department, Moscow State University, Russia), ''The effect of hydrogen on magnetostriction of rare-earth compounds $R_{1-x}R'_xFe_2$'';

– I. O. Troyanchuk, K. Baerner, and S. Trukhanov (Institute of Solid State & Semiconductor Physics, NASB, Belarus), H. Szymczak (Institute of Physics, Polish Academy of Science, Poland), ''Effect of oxygen content on magnetic and magnetotransport properties of the manganites'';

– S. A. Volokhov, P. N. Dobrodeev, A. V. Kildishev, and J. A. Nyenhuis (Department of Magnetism, Institute of Electrodynamics, NASU, Ukraine), ''Magnetic methods of monitoring microstructural changes in ferromagnetic pipelines'';

– J. Wittborn, F. Bros, K. V. Rao, J. Noques, A. Hottman, and Wan H. Sehuller (Engineering Materials Physics Division, MSE, Royal Institute of Technology, Sweden), ''Local magnetostrictive response using atomic force microscopy measurement and domain imaging of nanoscale magnetic dots on Si substrate'';

– A. A. Zvyagin, G. A. Zvyagina, and D. M. Apalkov (Institute for Low Temperature Physics & Engineering, Ukraine), ''Magnetic anisotropy of quantum low-dimensional magnets induced by the elastic subsystem of crystal.''

From the discussions on various classes of materials a number of themes emerged. Amorphous ferromagnets (ribbons, wires, or films) are quite well understood, and the reviews presented here demonstrate a mature subject. Thin film and multilayer materials present a number of challenges, and experimental and theoretical effort must still be expended to move the subject from a phenomenological to more mechanistic and predictive view of the effects of surfaces and interfaces. Work on manganites and superconductors can clearly benefit from magnetostriction studies, as the transport and magnetic properties are so intimately connected to lattice properties (Jahn–Teller distortions, polarons, etc.). The complimentarity of magnetostriction studies to more traditional magnetization measurements was clearly brought out. Measurement of magnetostriction remains somewhat contentious.

There remains a paucity of data on systems as common as NiFe, where the temperature and stress effects are almost unknown. It was exciting to see the possibilities which may come from the use of advanced light sources (ESRF) and diffraction studies, but other methods need further analysis of their accuracy and precision. It may be appropriate to organize a round-robin experiment. Applications of magnetostriction to sensing and actuation span from the very large (active vibration control) to the very small (MEMS). Note was made of cost and the conservatism of industry in moving to new materials and technologies, but it was again emphasized that the remote action possible through inductive drive or sensing can offer significant advantages, and the large figures of merit predicted for magnetoelastic sensors compared with semiconducting equivalents are being realized.

The Directors believe that the program served to bring together a geographically widespread community for a focused meeting. The views are clearly only a snapshot of the subject, but the accompanying book and the special issue of the Journal *Low Temperature Physics* (ILTPE–AIP) will act as a reference work in the field. New scientific links have been forged, and plans are being developed to maintain the momentum.

This article was published in English in the original Russian journal. Reproduced here with stylistic changes by the Translation Consultant.